OIL MANAGEMENT IN SYSTEMS RUNNING VAPOR COMPRESSION CYCLE

by

Vatsal M. Shah

A Dissertation

Submitted to the Faculty of Purdue University

In Partial Fulfillment of the Requirements for the degree of

Doctor of Philosophy

School of Mechanical Engineering

West Lafayette, Indiana

August 2021

THE PURDUE UNIVERSITY GRADUATE SCHOOL
STATEMENT OF COMMITTEE APPROVAL

Dr. Eckhard A. Groll, Co-chair
School of Mechanical Engineering

Dr. James E. Braun, Co-chair
School of Mechanical Engineering

Dr. W. Travis Horton, Committee Member
School of Civil Engineering

Dr. Peter H. Meckl, Committee Member
School of Mechanical Engineering

Approved by:
Dr. Nicole Key

To Devjibhai C. Shah and Nanjibhai C. Shah

ACKNOWLEDGMENTS

I am grateful to Prof. Eckhard Groll and Prof. James Braun for giving me an opportunity to work on this very interesting research project at the Herrick Laboratories. Their guidance and mentorship has played a big part in my learning experience throughout my graduate school journey. I thank Prof. Horton and Prof. Meckl for their valuable feedback and serving on my advisory committee. I also thank the shop staff, especially Frank Lee, for playing a major role in building the two experimental setups. Frank was always available with a smile and a helping hand to my never-ending requests of modifying the test setups. I also thank the PMS members of ASHRAE research project (RP:1721), particularly Dr. Ray Rite and Dr. Chris Seeton for providing a continuous technical feedback and support with the information needed for this research study. I also thank all the undergraduate and master students for their effort in building the test setups and running some of the tedious tests that were involved.

A special thanks to my friend, Abhinav, for encouraging me to pursue a PhD degree and believing in me, when I myself wasn't sure if I was capable of graduate school. To all my friends and lab-mates: Orkan, Parveen, Leon, Riley, Jon, Changkuan, Haotian, it was nice to have some great intellectual and inspirational conversations with you all and working with you on different projects. Whenever I needed you were always there to help without any hesitation. I am thankful to my parents, my brother Rushabh and his wife, Deepal for their support in pursuing education here in the US Lastly, I thank my wife, Tanvi. She was there to celebrate the good times with me, but was also there during the bad times to encourage me to keep going. I will forever remember her extraordinary sacrifice for this part of our journey.

TABLE OF CONTENTS

LIST OF TABLES

LIST OF FIGURES

NOMENCLATURE

Stratified Flow Model

A	$[m^2]$	Cross section area of pipe	α	[-]	Area Fraction
D	$[m]$	Hydraulic diameter of pipe	γ	$[rad]$	Angle of the wetted sector
f	[-]	Friction factor	ρ	$\left[\frac{kg}{m^3}\right]$	Density
h_L	$[m]$	Height of liquid level	μ	$\left[\frac{kg}{sm}\right]$	Dynamic viscosity
j	$\left[\frac{m}{s}\right]$	Superficial velocity	ν	$\left[\frac{m^2}{s}\right]$	Kinematic viscosity
L	$[m]$	Length of pipe	τ_W	$[Pa]$	Shear stress at pipe wall
$\dot{m}$	$\left[\frac{kg}{s}\right]$	Mass flow rate	τ_i	$[Pa]$	Shear stress at liquid-gas interface
m_{oil}	[g]	Oil retention	ω	[-]	Concentration
R	$[m]$	Hydraulic radius of pipe	$\left(\frac{\Delta P}{L}\right)_{TP}$	$\left[\frac{Pa}{m}\right]$	Two-phase pressure gradient
Re	[-]	Reynolds Number			
S	$[m]$	Perimeter			
u	$\left[\frac{m}{s}\right]$	Velocity			

Subscripts

L	Oil + liquid refrigerant	i	Liquid-Gas Interface
G	Refrigerant in gas phase	ref	Refrigerant

Annular Flow Model

A	$[m^2]$	Cross section area of pipe	α	[-]	Void Fraction
D	$[m]$	Hydraulic diameter of pipe	δ	[m]	Liquid film thickness
f_i	[-]	Interfacial Friction factor	δ^+	[-]	Dimensionless liquid film thickness
f_s	[-]	Friction factor of smooth pipe	ρ	$\left[\frac{kg}{m^3}\right]$	Density
g	$\left[\frac{m}{s^2}\right]$	Acceleration due to gravity	μ	$\left[\frac{kg}{sm}\right]$	Dynamic viscosity
j	$\left[\frac{m}{s}\right]$	Superficial velocity	ν	$\left[\frac{m^2}{s}\right]$	Kinematic viscosity
L	$[m]$	Length of pipe	τ_i	$[Pa]$	Shear stress at liquid-gas interface
m_{oil}	[g]	Oil retention	τ_W	$[Pa]$	Shear stress at pipe wall
$\dot{m}$	$\left[\frac{kg}{s}\right]$	Mass flow rate	$\left(\frac{dP}{dz}\right)$	$\left[\frac{Pa}{m}\right]$	Pressure gradient
R	$[m]$	Hydraulic radius of pipe	ω	[-]	Concentration
Re	[-]	Reynolds Number			
u	$\left[\frac{m}{s}\right]$	Velocity			

Subscripts

L	Oil + liquid refrigerant
G	Refrigerant in gas phase
ref	Refrigerant

ABBREVIATIONS

ASHRAE: American Society of Heating, Refrigerating and Air-Conditioning Engineers

CM3: Climate Master Heat Pump – 3ton

CM5: Climate Master Heat Pump – 5ton

COP: Coefficient of Performance

CRH: Chilled Water-glycol Re-heater

CWP: Chilled Water-glycol Pump

DAQ: Data Acquisition

EES: Engineering Equation Solver

HWP: Hot Water Pump

ID: Inner Diameter

PI: Proportional Integral

LFL: Lower Flammability Limit

LRP: Liquid Refrigerant Pump

OCR: Oil Circulation Ratio

OP: Oil Pump

PDPF: Pressure Drop Penalty Factor

PMS: Project Monitoring Subcommittee

RP: Research Project (contracted)

TRU: Transport Refrigeration Unit

Types of Oils

AB: Alkyle Benzene

MO: Mineral Oil

PAG: Polyalkylene Glycol

POE: Polyolester

PVE: Polyvinyl Ether

ABSTRACT

Most air conditioning and refrigeration systems that employ the vapor compression cycle rely on oil circulating with refrigerant to lubricate the bearings and other contact surfaces in the compressor. The lubricant acts as a sealant to reduce leakage losses during the compression process and it also helps to absorb some of the excess heat that is generated in the compression chamber. However, this oil circulation results in oil retention in various other components outside the compressor depending on the physical interaction between lubricant and refrigerant and their transport properties. Other factors, such as the geometry and orientation of connecting lines, and the system operating conditions, such as refrigerant flow rate and oil circulation ratio, also impact the oil retention. Because of oil retention, the oil level in the compressor reduces, which may ultimately affect its efficiency and life span. In addition, the effectiveness of heat exchangers (evaporators and condensers) decreases. The current line sizing rules reported in the ASHRAE Handbook on Refrigeration have only limited consideration of the effects of oil in the system. With the increasing development of variable-speed systems as well as future use of newer HFO refrigerants, there is a need in the industry for upgrading the line sizing recommendations, especially the connecting gas lines of unitary split systems, which consider the effects of oil retention. To develop these rules, measuring oil retention at different operating conditions is important. A test setup has been built to measure oil retention in horizontal and vertical lines of different diameters at different refrigerant and oil flow conditions. Based on the collected data, a physics-based semi-empirical model is developed which can predict oil retention in gas lines for some of the commonly used refrigerant-lubricant combinations in the HVAC&R industry.

Oil Circulation Ratio (OCR) is one of the input parameters to the model which predicts oil retention. A non-invasive, in-situ method to measure OCR in real time, which involves minimal human intervention, is developed. This method is based on oil separation and is implemented on the suction line. The approach has been validated with two different methods, one of which is an ASHRAE standard. The results of the study offer clear evidence that the method is as accurate as a standard method and it involves less human intervention as the measurement process is automated.

1. INTRODUCTION

1.1 Background

Oil has an important role in compressors of HVAC&R systems using the vapor compression cycle. Apart from the function of lubricating moving components of the compressor, the oil also acts as a sealant to reduce leakage losses from the compression chambers. Furthermore, it helps to absorb some of the excess heat generated during the compression of the refrigerant and reduce noise and vibration. Compressors are designed such that most of the oil gets separated from the refrigerant vapor before it leaves the compressor discharge port, however some amount of the oil is still discharged from the compressor along with the refrigerant vapor in the form of droplets. As this oil travels through the components of the vapor compression cycle, it is retained in the various components or worse, it is trapped in certain locations due to the inability to return with the refrigerant flow. Typically, the oil level in the compressor reduces, which may ultimately affect its efficiency and life span. Loss or lack of oil in the compressor sump due to improper oil management is one of the major reasons for a compressor failure. In addition, effectiveness of the heat exchangers (evaporators and condensers) decreases as a function of oil retention. Therefore, oil is essential for the compressors. However, its presence hurts in the remaining parts of the system. Although there is on-going research in the area of oil-free compression and a handful of oil-free compressors are commercially available, most of the HVAC&R systems running vapor-compression cycles still use oil-lubricated compressors. Industry needs design tools to develop oil management solutions that maintain the reliability and robustness of their products, while meeting newer energy-efficiency standards.

1.2 Motivation

There has been an aggressive push in the HVAC&R industry to improve system energy-efficiency from the U.S. Department of Energy. With tougher milestones, it is becoming challenging for the industry to maintain a good balance between the cost, energy-efficiency and reliability of their product. Transport refrigeration is one of the examples of this industry, where the refrigeration equipment is required to operate in harsh environments with a wide range of operating conditions. Most of these units typically have a compressor, which is driven directly through a diesel engine

or through a diesel generator, which supplies electricity to a hermetic compressor. Because of the space and weight constraints, these transport refrigeration units (TRU) have lower efficiencies compared to the stationary refrigeration equipment in supermarkets. With the increasing demand for refrigerated transport to maintain a cold chain, the energy consumption of this sector is substantially increasing. As the primary source of energy is diesel, there is a considerable pressure on the industry to reduce energy consumption. Therefore, designers have a challenging task to build reliable, energy-efficient solutions without compromising on the temperature control of the transported food items.

One of the possible solutions to increase the coefficient of performance (COP) of these transport refrigeration units is to use variable-speed or tandem compressors or a combination of both to achieve capacity modulation to meet part-load conditions. Having tandem compressors not only allows capacity modulation, it adds redundancy to maintain some cooling in case one of the compressors fails, which is vital in the food transport industry. This concept is widely used in the refrigeration systems in a supermarket, however it is more challenging to implement such a system in space and weight restricted transport refrigeration units. Implementing proper oil management in tandem or variable-speed compressors adds further design challenges as there is no space for components such as an oil separator and one needs to depend on passive solutions. Significantly, higher oil throws from the compressor can occur during transients due to on/off cycling or significant changes in compressor speed. In addition, depending on the amount of retention, oil return can be compromised at lower refrigerant flows associated with part-load operation.

With better information about the oil circulation ratio (OCR) and oil retention in a system, designers can find better solutions to improve system performance while maintaining reliability of the compressor. As an example, if a designer selects a refrigerant line size based on full load at a single point design condition, then at part load, the oil may not return through these lines due to lower refrigerant velocities. On the other hand, if the line size is selected too conservatively, by choosing the minimum mass flow rate as a design condition, the pressure drop may get too high at higher flow rates and may reduce COP. Therefore, a simulation tool would be useful as a means of predicting the amount of oil retention and minimum refrigerant mass flux required for oil return through suction risers in order to optimize line size for a particular refrigerant/lubricant pair and

set of operating conditions. Control strategies can also be designed that can trigger an oil return mode and prevent the compressor from oil starvation.

In recent years, research into alternative refrigerants has intensified due to environmental concerns. In the 1930s, chlorofluorocarbons (CFCs) were developed as refrigerants with great thermodynamic performance along with lack of flammability and toxicity. However, they were eventually phased out as they caused depletion of the ozone layer. CFCs and HCFCs have been replaced with HFC-based refrigerants and their blends such as R134a and R410A. However, due to their high Global Warming Potential (GWP) of more than 1100, recent efforts have focused on identifying alternative more environmentally friendly refrigerants. Researchers have been looking into many natural refrigerants, including carbon dioxide (CO_2). However, the use CO_2 requires system modifications due to higher operating pressures and the need to recover throttling losses. Alternatively, newly developed HFOs with low GWP such as R1234yf and R1234ze(E) can be considered as drop-in replacements which possess similar thermodynamic properties compared to R134a and have low toxicity and moderate flammability. Due to different chemistry, these newer refrigerant/lubricant combinations have different transport properties. So, it has become necessary to understand oil-refrigerant interaction for these upcoming combinations, which may have a high potential for use in the industry.

1.3 Research Objectives

Current tables in Chapter 1 of the 2014 ASHRAE Refrigeration Handbook provide design direction in the area of oil return. These design criteria mainly assure that there exists enough mass flux in the suction lines to ensure oil returns to the compressor at minimum operating conditions, thereby keeping oil from accumulating in the system at an unacceptable rate when traditional, fixed capacity systems are employed. The current tables consider only R-22 and R134a with mineral oil and POE oils. However, better design tools are needed for the rising applications of variable-speed and tandem compressors coupled with emerging refrigerant/oil combinations in order to determine appropriate line sizes for oil return and to estimate oil retention and pressure drop scenarios. A more robust, general-purpose predictive model could enable design of better oil management strategies and address the issues that have arisen due to progression of the current state-of-the-art. The need for better design tools to address component-level reliability will continue to become

more relevant as variable mass-flow rate capacity modulation schemes become more popular to meet increasing efficiency requirements. This thesis focuses on developing such a model that feeds information to a design tool that bridges the current ASHRAE design guideline knowledge gap. The objective is to build a user-friendly modeling tool and engineering design guidelines for sizing vapor compression refrigerant gas lines to ensure oil return to compressors and minimum oil retention in the gas lines. A corollary to this objective is to gain a better understanding with regard to oil retention in the refrigerant lines for both air-conditioning and refrigeration applications.

Oil Circulation Ratio (OCR) is usually one of the inputs to models that predict oil retention. Although OCR is dependent on various factors such as the refrigerant mass flow rate, properties of refrigerant etc., it mainly accounts for oil that is discharged from the compressor, which varies for different types of compressors operating at different conditions. Therefore, a compressor level research is needed to develop a model to predict OCR. As this study was focused on system level oil management rather than the compressor level, the objective here was not to develop a model to predict OCR. Instead, a non-invasive, in-situ method has been developed to measure OCR in real time, which involves minimal human intervention. This method was implemented in the suction line of a transport refrigeration unit and the details of this measurement technique are reported as a part of this thesis. In addition, a design of a low-cost OCR sensor is also shown where the developed measurement technique is implemented in a small form factor apparatus, which allows to measure real-time OCR in any equipment rather than just in a lab environment.

2. DEVELOPMENT AND VALIDATION OF MEASURING IN-FLOW OIL CIRCULATION RATIO (OCR)

As mentioned earlier, the growing applications of variable-speed and tandem compressors coupled with emerging refrigerant/oil combinations has elevated the importance of measuring oil retention. To predict oil retention, OCR is one of the important parameters needed as an input. Recently, Ossorio and Navarro-Peris (2020) studied OCR in a variable -speed scroll compressor with propane. They used the 'Discrepancy Method' to calculate the mass flow rate of oil from the discrepancy in the refrigerant mass flow rate from a meter and energy balance. In another study, Li et al., (2020) studied the effect of OCR on heat transfer in an evaporator and COP of a mobile air-conditioning system for an electric vehicle. They measured OCR using the sampling method recommended in ASHRAE (2015). Measuring OCR quantifies the problem and helps in the development of better oil management solutions. However, measuring OCR within a vapor compression cycle is challenging due to various factors, such as phase change of the working fluid at different locations, miscibility between the oil and refrigerant, and varying flow regimes. Therefore, a non-invasive, in-situ method has been developed to measure OCR in real time, which requires minimal human intervention, has minimal impact on cycle performance, and will work for any refrigerant and oil pair.

2.1 Literature Review

Various techniques have been proposed to measure OCR in the literature and many of them have been experimentally verified. A short description along with a few key advantages and disadvantages of these measurement techniques are listed in Table 2.1. A majority of these techniques measure the oil concentration in the liquid line where the refrigerant and oil are assumed to be homogenous, which is a good assumption if they are miscible. If they are homogenous and uniform, then measuring oil concentration in the refrigerant is the same as measuring OCR. However, this is not true in the gas line as there is a slip ratio between the refrigerant vapor and liquid oil. Gao et al., (2011) shows that oil concentration drastically differs from OCR in a system with immiscible oil (CO_2 and PAG). Therefore, if the refrigerant oil combination is not miscible or even partially miscible, the accuracy of these techniques to measure

OCR is questionable. Likewise, the sampling method suggested by ASHRAE (2015) may also be inaccurate if the refrigerant and lubricant sample that is collected from the liquid line is not homogenous.

The method discussed here is fundamentally different. Instead of using the liquid line, the measurement is implemented on the suction line where the oil is separated from the vapor refrigerant using an oil separator and the rate of oil separation is measured. This method fundamentally eliminates the issue of immiscibility, while still giving the advantage of a real time measurement. In addition, if the oil separator is sized correctly for the application, there is no need of calibration for different combinations of oil and refrigerant. The only calibration that is required is the oil level sensor which is fairly simple. In addition, the solubility of refrigerant in the oil as a function of temperature and pressure is needed, which may be obtained from the oil supplier.

Oil separation methods to measure OCR have been investigated and published in the literature by Min and Hwang, (2000) and Gao et al., (2011). Min and Hwang, (2000) used an oil separator in the discharge line to separate the oil from the refrigerant, whereas Gao et al., (2011) have developed an oil droplet generation device which is installed in the suction line for oil separation. To measure the flow rate of the separated oil, Min and Hwang, (2000) used a calibrated sight tube to visually record the change in height. Gao et al., (2011) developed two-methods, namely the ‘oil-droplet method’ and the ‘oil-volume method’, which are simultaneously used to determine the oil flow rate and can then be used to measure OCR. The method developed here to separate oil and measure the oil flow rate is described in detail in the following sections.

Table 2.1: Oil circulation ratio measurement methods

Basis of Measurement Method	**Description**	**Advantages/Disadvantages**	**Reference**
Sampling	Refrigerant and lubricant mixture sample from liquid line is collected in an evacuated cylinder. Amount of refrigerant and lubricant in the cylinder are then measured using gravimetric method to measure OCR	Advantages Low Cost Disadvantages Tedious, time consuming, not real-time, limited number of samples, charge removal	(ASHRAE, 2015)
Viscosity	(Baustian et al., 1988a) used experimental data to develop a correlation of viscosity as a function of temperature and oil concentration for R12 and R22 with naphthenic oil and R502/AB. With an inline viscometer in the liquid line and temperature measurement, OCR can be measured using the developed correlation.	Advantages Real time No need of charge removal Disadvantages Transient response of the viscometer is poor because of slow measurement speed Accuracy of ±1 to ±2% Calibration required Cannot work with immiscible refrigerant and lubricant	(Baustian et al., 1988a)
Acoustic velocity	Acoustic velocity sensor was developed to measure oil concentration in liquid line. Calibration curves relating oil concentration to acoustic velocity and temperature need to be generated for a particular oil/refrigerant pair.	Advantages Real time and inline No need of charge removal Can measure OCR in transient states Works even with low quality two-phase mixture. Disadvantages Requires time consuming calibration. Cannot work with immiscible refrigerant and lubricant	(Baustian et al., 1988b) (Meyer and Saiz Jabardo, 1994) (Navarro de Andrade et al., 1999) (Lebreton and Vuillame, 2001)

Table 2.1 continued

Basis of Measurement Method	Description	Advantages/Disadvantages	Reference
Ultraviolet Light absorption	The concentration of oil in liquid line is measured using an ultraviolet spectrophotometer. The absorbance of light is proportional to the concentration of oil, which then basically measures OCR. Temperature and pressure correction are required using calibration techniques	Advantages Can measure OCR in transient states Accuracy of ±0.1 % No need of charge removal Disadvantages Requires expensive instruments such as a spectrophotometer. Needs calibration and pressure/temperature compensation Complex and fragile measurement system Cannot work with immiscible refrigerant and lubricant	(Kutsuna et al., 1991) (Wada et al., 1992) (Suzuki et al., 1993) (Wujek et al., 2007)
Refractive index	The difference in the refractive index between the pure refrigerant and refrigerant oil mixture is large enough to detect concentration of oil in refrigerant. This principle is used to build a sensor that can measure OCR in liquid line.	Advantages Real time and inline Can measure OCR in transient states Accuracy of ±0.1 % No need of charge removal Can be implemented for field application, because of relatively inexpensive instrumentation. Disadvantages -Darkening of oil or any optical impurities may affect the measurement - Cannot work with immiscible refrigerant and lubricant - Needs calibration of refractive index and temperature.	(Baustian et al., 1986a) (Newell, 1996) (Fukuta et al., 2004) (Fukuta et al., 2006) (Wujek et al., 2007) (Yoon et al., 2011)

Table 2.1 continued

Basis of Measurement Method	Description	Advantages/Disadvantages	Reference
Density	An inline Coriolis-effect flow meter which can measure density in the liquid line, along with a developed correlation for OCR as a function of temperature, pressure and measured density can be used to determine OCR. This correlation requires compressibility correction, which has been provided by the researchers. This calibration can be avoided for refrigerant lubricant pair that are known to follow ideal mixing assumption.	Advantages Real time and inline No need of charge removal Can be implemented for field application, because of relatively inexpensive instrumentation. Disadvantages Needs calibration and compressibility correction May be inaccurate in certain temperature, pressure and OCR region depending on lubricant and refrigerant pair.	(Baustian et al., 1988c) (Bayani et al., 1995) (Wujek and Hrnjak, 2009) (Yan et al., 2015)
Capacitance	Using the dielectric constants of fluids, Hwang et al. (2003) showed that the concentration of oil in liquid refrigerant is related to temperature, pressure and capacitance for CO_2 and PAG. Using a capacitance sensor along with temperature and pressure in the liquid, OCR can be measured.	Advantages Real time Can measure OCR in transient states Accuracy of ±0.5 % Relatively inexpensive instrumentation No need of charge removal Disadvantages Sufficient difference in the dielectric constants of refrigerant and lubricant is required. Calibration required.	(Baustian et al., 1986b) (Fukuta et al., 1999) (Hwang et al., 2003) (Hwang et al., 2008)
Visualization	Visualizing images captured using high speed camera through a transparent section at the compressor discharge, OCR and oil retention is measured based on oil droplet size, oil droplet speed and mass flow rate.	Advantages Noninvasive method Distribution of OCR between the film and droplets can be evaluated Can measure immiscible oils No need of charge removal Disadvantages Error in measurement increases with higher flow velocities. Due to complex instrumentation, field measurement may not be practical	(Xu and Hrnjak, 2016) (Xu and Hrnjak, 2017)

Table 2.1 continued

Basis of Measurement Method	Description	Advantages/Disadvantages	Reference
Oil Separation	Oil is separated from the refrigerant vapor in the discharge line or the suction line. The separated oil flow rate is measured with respect to liquid refrigerant mass flow rate, which then gives the value of OCR.	Advantages Inline and real time measurement Can measure OCR for immiscible refrigerant/oil pair Does not require calibration No need of charge removal Disadvantages May have impact on the cycle performance, depending on the modifications made.	(Min and Hwang, 2000) (Gao et al., 2011)

2.2 Experimental Setup

A transport refrigeration unit (TRU) with a single fixed speed scroll compressor was set up in a psychrometric chamber simulating ambient conditions as shown in the schematic of Figure 2.1. An adjoining psychrometric chamber simulated the refrigeration box condition. The supply and return air ducts of the TRU were connected through a common wall between the psychrometric chambers and were insulated to minimize heat loss. A picture of the setup is shown in Figure 2.2. The TRU was charged with R404A and the compressor was pre-charged with POE32 lubricant. The TRU was instrumented with pressure and temperature sensors, mass flow meters and other sensors related to oil measurement. The location of these sensors is shown in a schematic in Figure 2.3. Data from all these sensors were collected at an interval of one second and stored in a database file for further analysis. Temperature in the psychrometric chambers was maintained based on the conditions described in the test matrix in Table 2.2. The TRU was equipped with a vapor injection system, however for the current study, the expansion valve in the vapor injection line was shut off.

Table 2.2: Test conditions at which OCR was measured

Test Condition at steady-state	Condition #1	Condition #2	Condition #3	Condition #4
Ambient Temperature	37.8 °C (100 °F)	37.8 °C (100 °F)	37.8 °C (100 °F)	37.8 °C (100 °F)
Refrigeration Box Temperature	1.7 °C (35 °F)	-3.9 °C (25 °F)	-9.4 °C (15 °F)	-15 °C (5 °F)

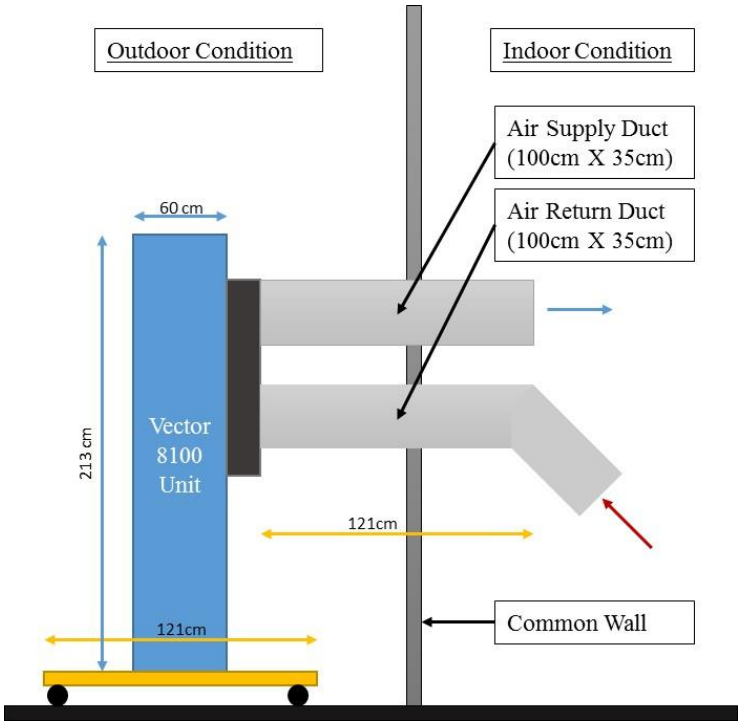

Figure 2.1: Schematic of the transport refrigeration unit inside the psychrometric chamber

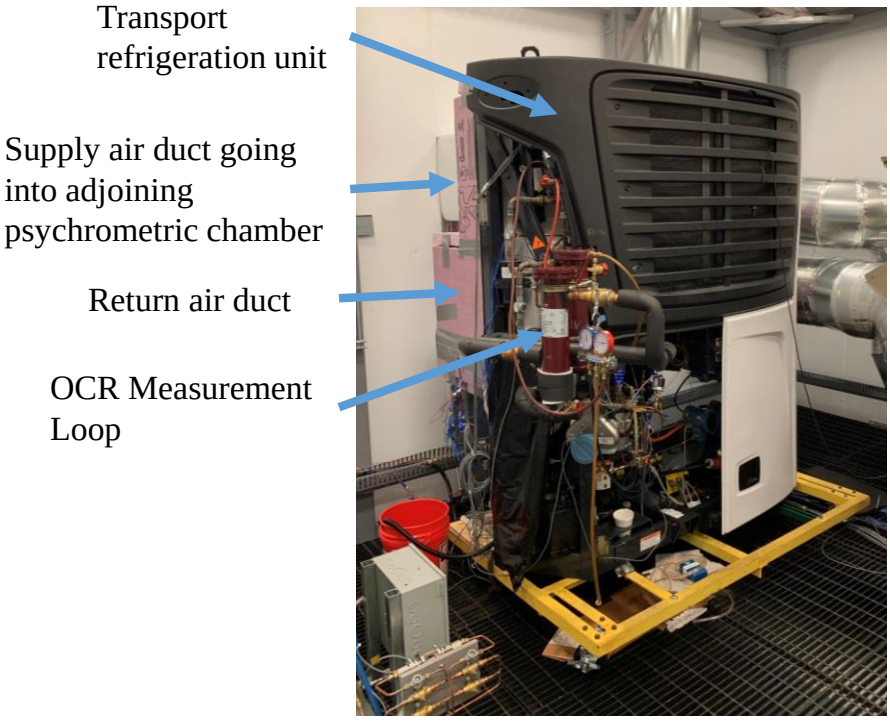

Figure 2.2: Picture of transport refrigeration unit installed in psychrometric chamber simulating ambient conditions

2.2.1 Oil Measurement Loop

An oil measurement loop was designed and built as per the schematic shown in Figure 2.3 in red. The loop consisted of an oil separator, a Coriolis-effect mass flow meter, an oil collector with liquid level probe, pressure sensor, and temperature probes as shown in Figure 2.4. When the oil loop was engaged, superheated gas in the suction line could be by-passed through the oil measurement loop through appropriate valves. When the loop was engaged, the oil was separated, and refrigerant flowed back to the system. Practically, some amount of oil flows along with the refrigerant and is bypassed through the separator. However, the coalescent type oil separators, used for measurement in this study, were considered highly effective over a wide range of operating condition as per the supplier. Therefore, it was assumed that 100% of the oil was separated from the refrigerant vapor. The oil from the separator flowed through the Coriolis-effect mass flow meter and into the oil collector. As shown in Figure 2.5, the liquid level probe in the oil collector continuously measured the level of oil in real time. A temperature-controlled heat tape was wrapped around the oil collector and was then insulated as shown in Figure 2.9. A solenoid valve was installed in the oil discharge line connecting the oil collector to the suction line. When the oil level in the collector increased more than the upper set point value, the solenoid valve automatically opened to drain the oil back into the compressor through the suction line. When the level in the oil collector reached the lower set point, the valve automatically closed to start collecting the oil again. The upper and lower set point values are user inputs.

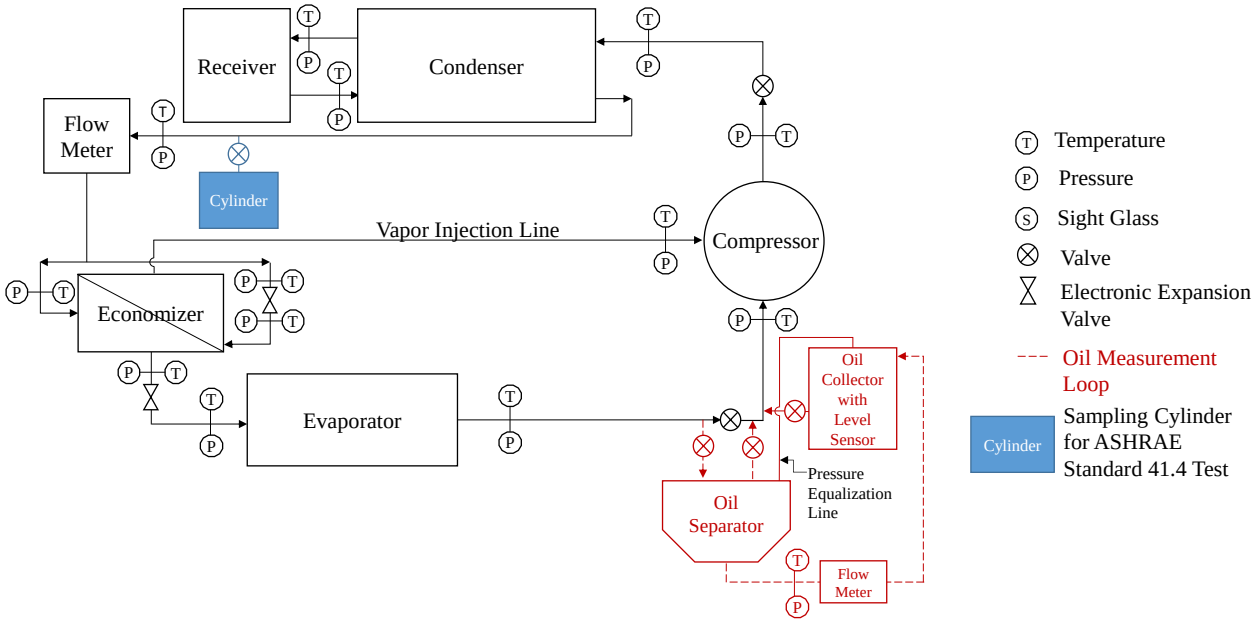

Figure 2.3: Schematic of test section showing the refrigeration unit and the modification for measuring OCR.

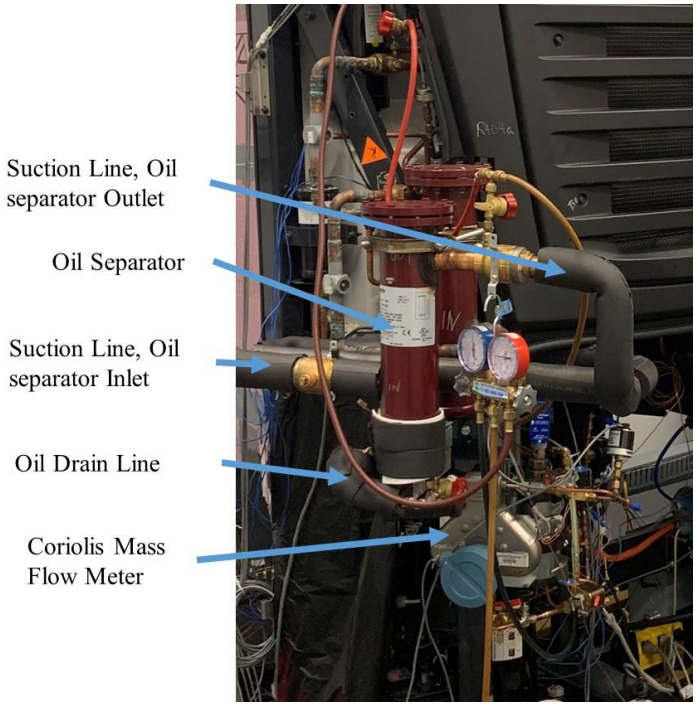

Figure 2.4: Picture of oil measurement loop in the suction line to measure OCR

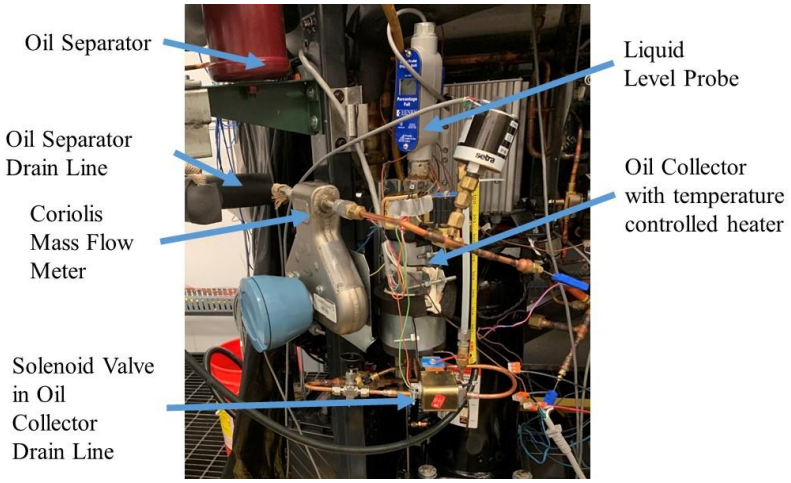

Figure 2.5: Picture of oil measurement loop consisting of oil collector with a liquid level probe

2.3 Experimental Procedures

Three different methods were used to measure the OCR for the purposes of validating the proposed measurement approach, and details of each of the methods are described in this section.

2.3.1 OCR Measurement Using Liquid Level Probe

The procedure for OCR measurement using a liquid level probe was carried out employing the following steps:

1. The system was first brought to steady state at a particular test condition described in the test matrix. At this initial stage, the oil measurement loop was disengaged from the system, by keeping the oil loop bypass valve open as shown in Figure 2.6.

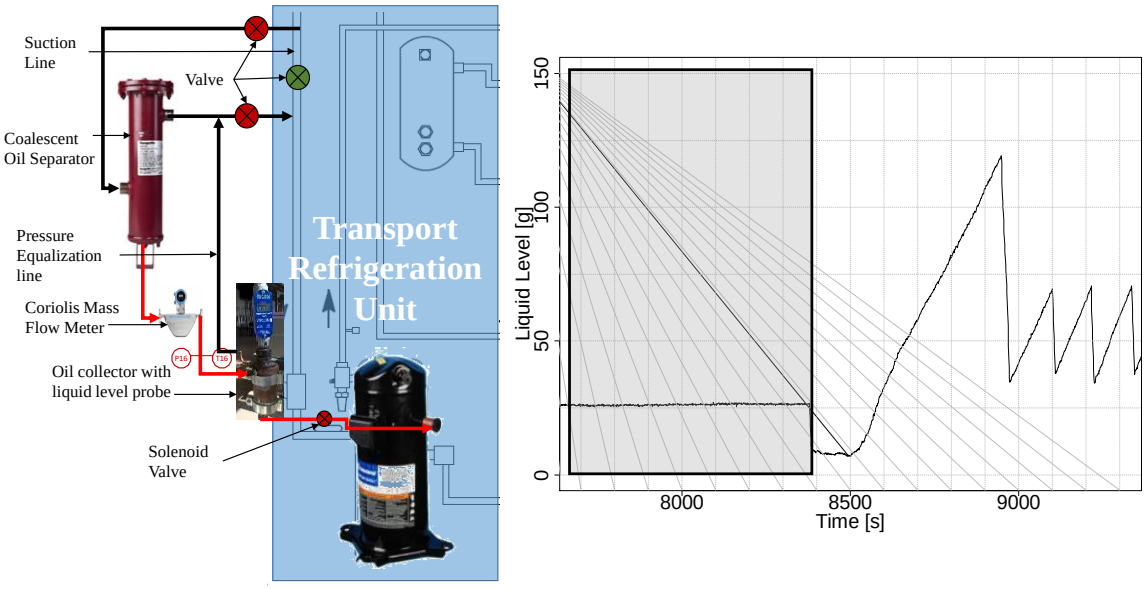

Figure 2.6: System running steady-state with OCR measurement loop disengaged

2. After one hour of steady-state operation, the oil measurement loop in the compressor suction line was engaged. Oil was separated and flowed into the collector, causing its level to rise. During this time the valve between the oil collector and the compressor suction line was kept shut, as shown in Figure 2.7. Before the oil loop was engaged, the oil collector was pre-charged with oil. The total capacity of the oil collector was approximately 450 g.

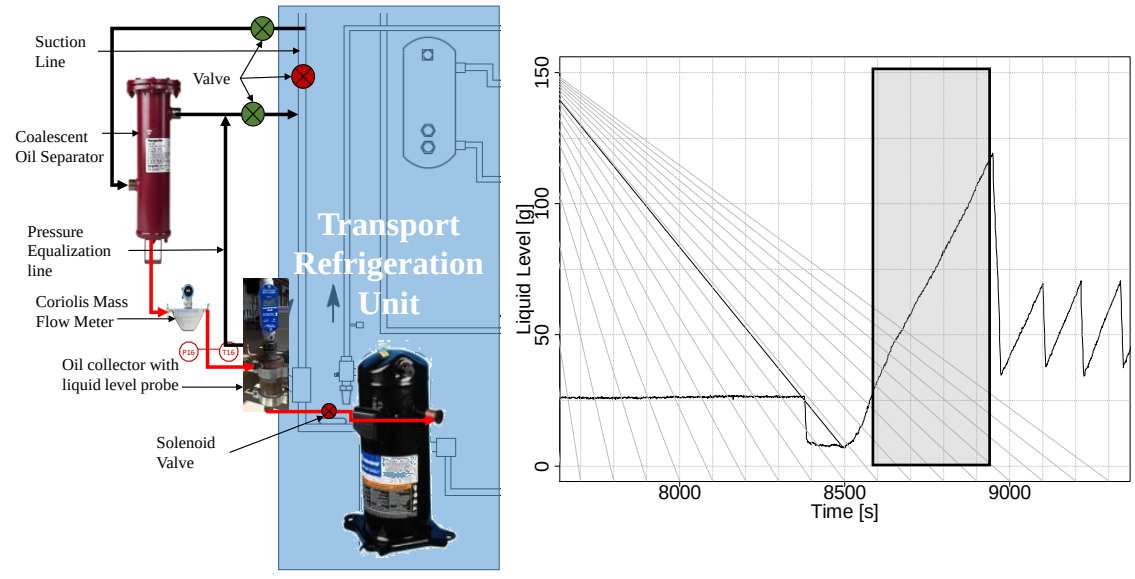

Figure 2.7: Oil getting collected as OCR measurement loop is engaged

3. An upper limit and a lower limit of the oil level was provided as an input from the test operator. Once the level reached its upper limit, the oil was drained back to the suction port of the compressor by automatically opening the solenoid valve between the compressor suction port and the oil collector as shown in Figure 2.8. When the lower limit was reached, the solenoid valve automatically closed so that the oil would start collecting once again.

4. Step 2 and Step 3 were repeated multiple times, and at each time the oil measurement loop was kept engaged. To accurately capture the OCR, it was important to maintain a steady flow of oil in the system. Therefore, to ensure that the measurement system was not impacting the dynamics of the oil circulation, less than 100 g of oil was collected in each cycle. To avoid large slugs of oil returning back to the compressor, oil was drained slowly by adjusting a manual needle valve installed before the solenoid valve in the collector drain line.

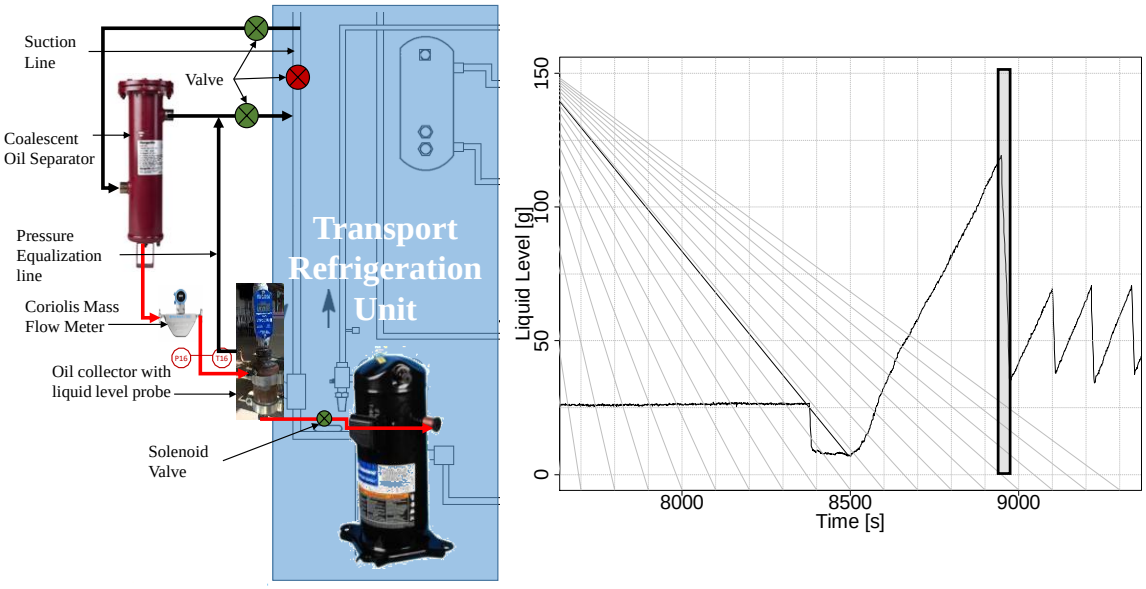

Figure 2.8: Oil being drained while OCR measurement loop is engaged

Solubility of R404A in POE of ISO VG 32 (Emkarate-RL32-3MAF)

Depending on the refrigerant-oil chemistry, there is some amount of liquid refrigerant dissolved in the oil. For a given refrigerant/oil pair, solubility of the refrigerant in the oil is a function of temperature and pressure. Cavestri, (1995) reports solubility charts of R404A with POE Oil

(Emkarate RL32S) as a function of pressure and temperature. The charts showing solubility at 40°C and 60°C are shown in APPENDIX B. The amount of oil in the collector was corrected based on this solubility.

To monitor the temperature of the oil and refrigerant inside the collector, five thermocouples were installed on the surface of the oil collector as shown in Figure 2.9. The temperature of the oil inside the collector was not measured. Using a temperature-controlled heat tape, the surface temperature of the oil collector was maintained at 70°C to prevent any refrigerant from condensing in the oil collector, while a pressure sensor monitored the pressure of the oil collector. Steady state readings of these temperatures and pressures are reported in Table 2.3. The average surface temperature was around 60°C. Considering there was a temperature gradient, the temperature of the oil was assumed to be 40°C for estimating the solubility. Using the chart for 40°C shown in APPENDIX B, the solubility for all four test conditions were estimated as shown in Table 2.3.

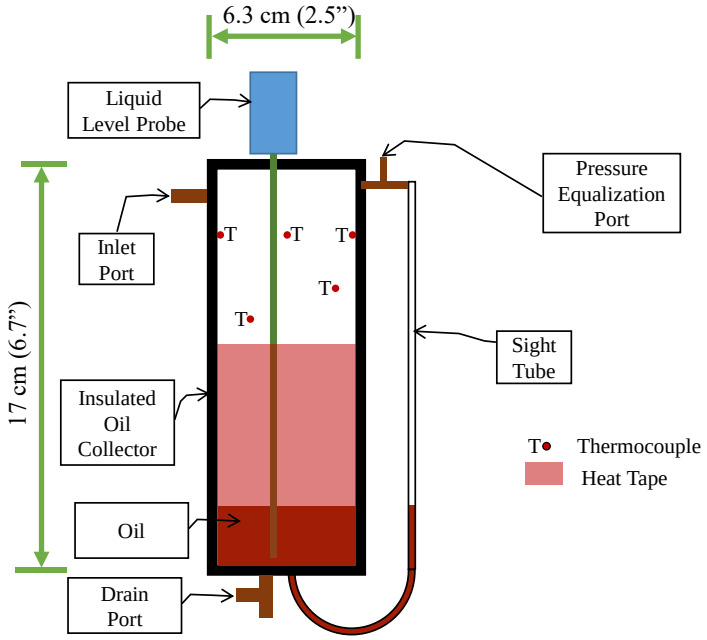

Figure 2.9: Schematic of oil collector used for level measurement

Table 2.3: Solubility of R404A in Emkarate RL32S oil at the collector temperature and pressure

Test Cond	Oil Collector Pressure [kPa]	Oil Collector Temperature						Percentage Refrigerant by Weight
		T17 [°C]	T18 [°C]	T19 [°C]	T20 [°C]	T21 [°C]	Average Temp [°C]	
1	414.3	56.5	61.0	69.9	57.0	55.3	59.94	6%
2	387.5	56.4	61.6	69.9	56.8	55.1	59.96	6%
3	360.5	55.9	61.2	69.9	56.4	54.7	59.62	4%
4	318.1	56.7	61.9	70 .0	57.0	55.5	60.22	3%

OCR Calculation from the Data Collected Using a Liquid Level Probe

As an example, Figure 2.10 shows a time-series plot of raw data of oil accumulation and discharge in the oil collector when the oil measurement loop was engaged in the suction line. Periods where the measured oil flow rates were relatively constant were selected for analysis and are highlighted in the transparent gray regions of the plots. During these periods, the slope of the oil accumulation over time was nearly linear. The amount of oil collected during each period was calculated by taking a difference of the amount of oil in the collector at the beginning and the end of each period. The mass of oil was corrected for the amount of refrigerant that was dissolved in the oil using the solubility listed in Table 2.3. This amount of oil was then divided by the number of seconds of the selected period to get mass flow rate of oil. (See Equation (2.1)). The OCR was calculated by dividing the mass flow rate of oil with the average refrigerant-oil mixture mass flow rate that is measured in the liquid line during each period (See Equation (2.2)). Similarly, OCR was calculated for all the periods at the same condition. Data of three of the periods is tabulated in Table 2.4 along with the measured refrigerant mass flow rates. The top plot of Figure 2.11 shows the raw data of all the samples and the bottom plot shows the calculated OCR values for all the samples. A major advantage of using this technique of measuring OCR is that multiple samples can be automatically

measured, which then helps to capture real-time dynamics of OCR in the system, except for the short discontinuity when the oil is being drained.

$$\dot{m}_{oil} = \frac{(m_{oil,end} - m_{oil,start})(1 - w_{ref})}{t_{end} - t_{start}} \quad (2.1)$$

$$OCR = \frac{\dot{m}_{oil}}{\dot{m}_{ref+oil}} \quad (2.2)$$

Table 2.4: Test data of oil measurement for suction line for operating condition #1

Sr.	**Description**	**Test 1**	**Test 2**	**Test 3**	**Units**
1.	Oil mass collected	70.6	68.59	72.51	g
2.	Duration of oil collection	97	92	92	s
3.	Oil mass flow rate	2.61	2.68	2.84	kg/h
4.	Refrigerant-oil mixture mass flow rate	457.3	456.3	456.3	kg/h
5.	Solubility of R404A in POE32 at operating condition #1 Cavestri, (1995)	6%	6%	6%	% Refrigerant by weight
6.	OCR	0.573	0.588	0.622	%

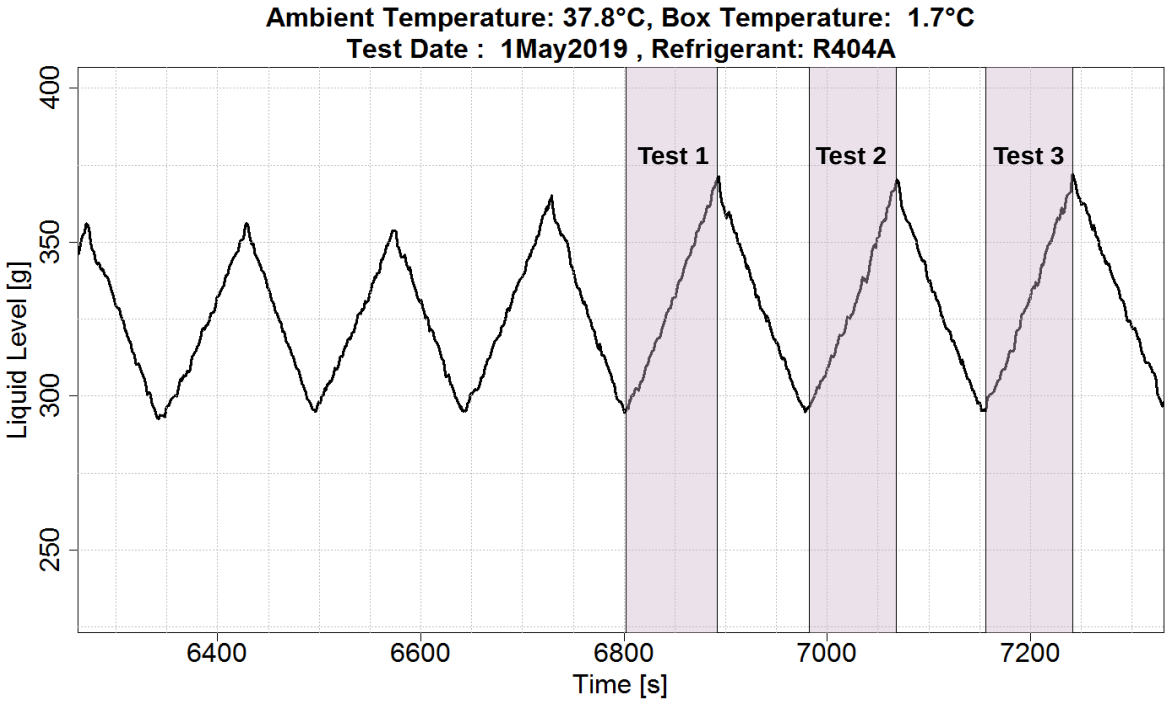

Figure 2.10: Time series plot of oil accumulation in oil level collector showing collection and discharge cycles for operating condition #1

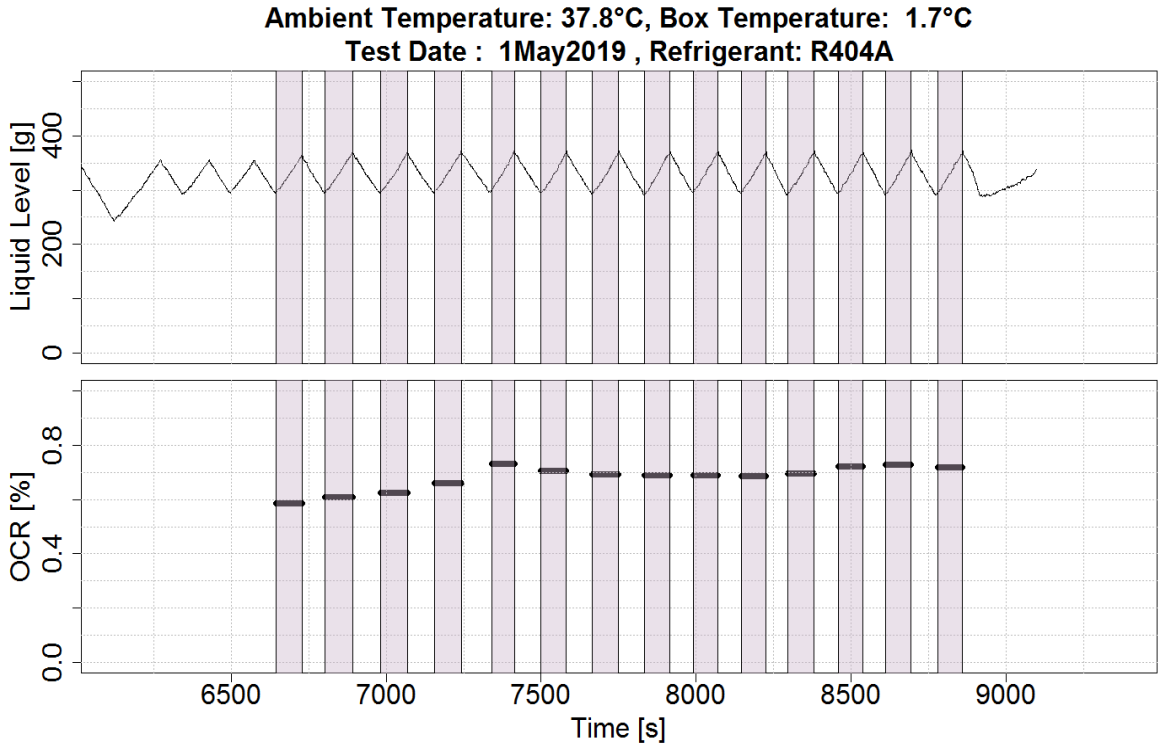

Figure 2.11: Time series plot of oil level in the collector (top) and calculated OCR (bottom) for test run in suction line for condition #1

2.3.2 OCR Measurement Using a Visual Method

The liquid level probe described in the previous sections is a capacitance-based sensor. To ensure that the probe was measuring the level correctly, an alternative method was needed for validation. A gravimetric method is usually considered a good primary method for validation and is considered in the next section. In order to independently validate the liquid probe measurement, a transparent sight tube attached in parallel with the oil collector was used to visually measure the level of oil in the collector as shown in Figure 2.12. Before charging the TRU with refrigerant, the level of the sight tube was calibrated by injecting a known amount of oil mass into the collector. The mass of oil injected was known by measuring the filled and empty glass syringe on a weighing scale with an accuracy of 0.01 g. With this calibration, the oil mass flow rate was calculated by measuring the time duration of the collection period and visually measuring the difference in the level of the oil in the sight tube at the beginning and the end of that duration. The time duration was measured using a stopwatch. These measurements were carried out simultaneously with the OCR measurement using the liquid level probe.

Figure 2.13 shows close agreement of OCR measurement results using the liquid level probe method and the visual method for one particular condition (Condition #4 in Figure 2.3). In addition, refer to

Table A.1 through Table A.4 in APPENDIX A for the data from the four different conditions that shows similar agreement.

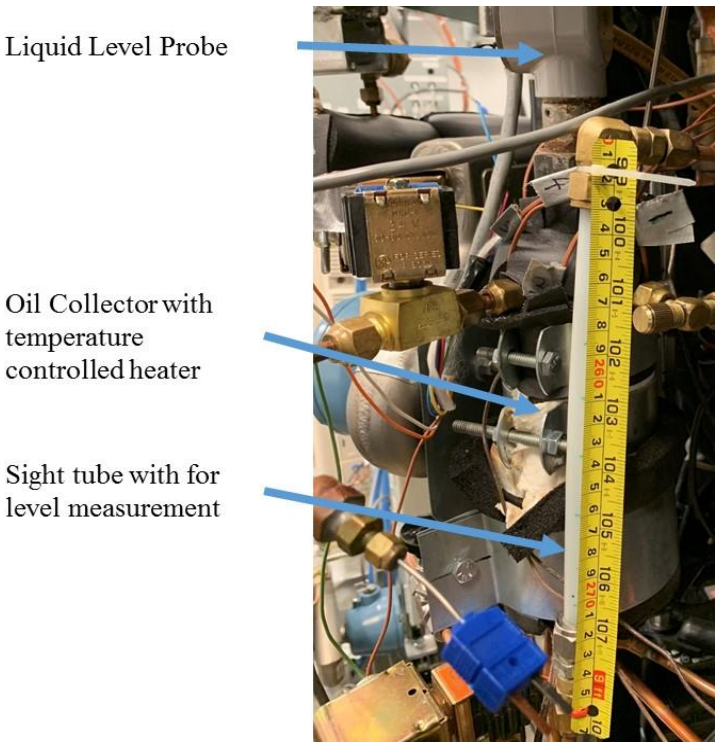

Figure 2.12: Visual measurement of liquid level in sight tube

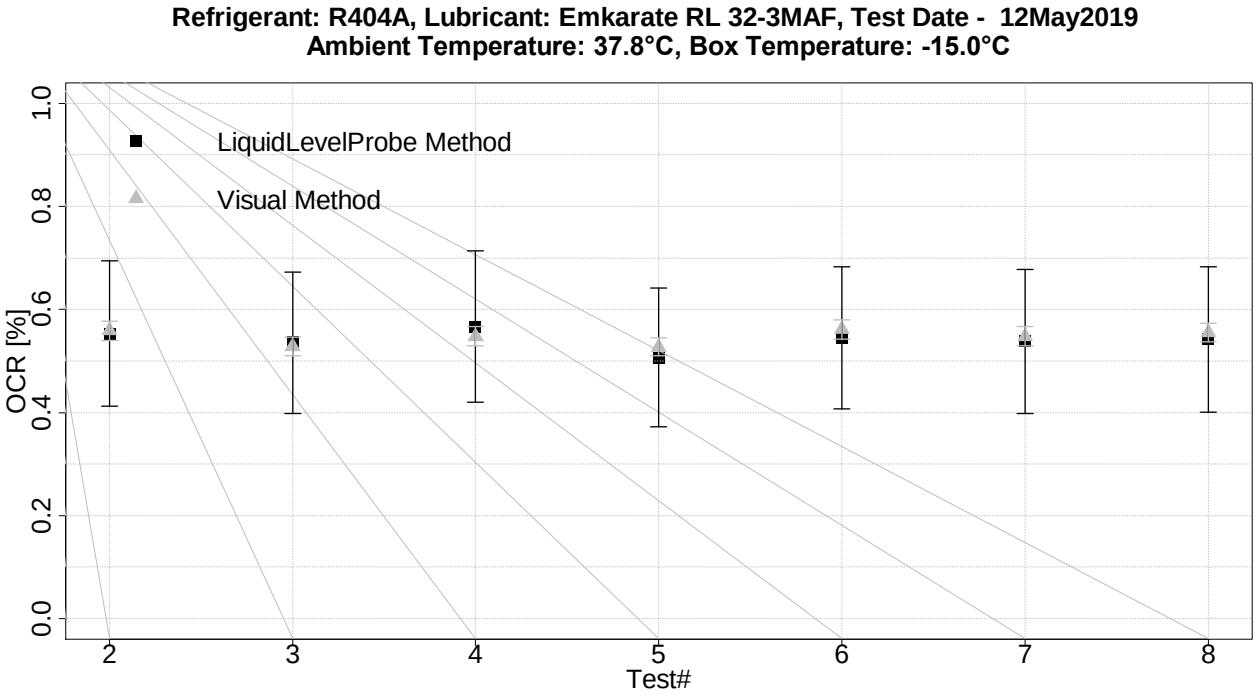

Figure 2.13: In-situ OCR measured simultaneously using liquid level probe method and visual method.

Uncertainty in OCR measurement using liquid level probe and visual method

The uncertainty in OCR measurement comes from the sources listed in Table 2.5. The measurement uncertainties of the liquid level probe and Coriolis-effect mass flow meter were obtained from the technical specifications of the manufacturer. The least count of the tape measure used to measure the level of oil in the collector was 0.1 cm and the uncertainty was considered as half of this least count. The uncertainty in time measurement using a stopwatch was considered to be 1 s and the uncertainty in solubility of refrigerant in oil was considered as 1 %.

Table 2.5: Sources of uncertainty in measurement

Sr.	Description	Uncertainty	Unit	Type of Uncertainty
1	Liquid level probe	0.1	V	Absolute
2	Refrigerant + Oil mass flow rate	0.01	kg/h	Relative
3	Level of sight tube	0.05	cm	Absolute
4	Stopwatch	1	s	Absolute
5	Solubility	0.01	-	Absolute

The uncertainty propagations in the OCR were evaluated using Engineering Equation Solver (EES) software (Klein, 2018).

Table 2.6 and Table 2.7 show the uncertainty propagation in the OCR measurement evaluated for Test Condition #4 using the liquid level probe and visual methods, respectively. The error bars representing these uncertainties are shown in Figure 2.13. The percentage uncertainty for the liquid level probe method was approximately 26 %, whereas the percentage uncertainty for the visual method was approximately 3.4 %. It would be ideal to have the uncertainty of the liquid level probe method within 3% ~ 4%. The voltage measurement from the level probe contributes to the majority of the error and therefore a probe with better accuracy should be used. Alternatively, the diameter of the oil collector can be reduced, so that for the same difference in mass there is higher difference in level which would give better resolution of the voltage measurement and improve its precision.

Table 2.6: Uncertainty propagation in OCR measurement using liquid level probe method

Test ID	Refrigerant + Oil Mass Flow Rate	Duration of Oil Collection	Voltage at the beginning of collection	Voltage at the end of collection	Mass flow rate of oil	Solubility	OCR (LLP Method)	Percentage Error
	[kg/h]	[s]	[V]	[V]	[g/s]			
2	354.8±3.548	118	3.952±0.1	4.505±0.1	0.5621±0.1436	0.03±0.01	0.5533±0.1416	25.59%
3	354.2±3.542	122	3.962±0.1	4.516±0.1	0.5434±0.1389	0.03±0.01	0.5357±0.1372	25.60%
4	354.4±3.544	114	3.956±0.1	4.504±0.1	0.5756±0.1487	0.03±0.01	0.5672±0.1467	25.87%
5	353.8±3.538	124	3.975±0.1	4.506±0.1	0.5135±0.1367	0.03±0.01	0.5069±0.1351	26.65%
6	353.2±3.532	122	3.958±0.1	4.519±0.1	0.5511±0.1389	0.03±0.01	0.5448±0.1376	25.25%
7	353.7±3.537	120	3.961±0.1	4.507±0.1	0.5452±0.1412	0.03±0.01	0.5382±0.1396	25.95%
8	353.6±3.536	119	3.959±0.1	4.504±0.1	0.5489±0.1424	0.03±0.01	0.542±0.1409	25.99%

Table 2.7: Uncertainty propagation in OCR measurement using visual method.

Test ID	Refrigerant + Oil Mass Flow Rate	Duration of Oil Collection	Level at the beginning of collection	Level at the end of collection	Mass flow rate of oil	Solubility	OCR (Visual Method)	Percentage Error
	[kg/h]	[s]	[cm]	[cm]	[g/s]			
2	354.8±3.548	129±1	269.4±0.05	268.4±0.05	0.5678±0.01731	0.03±0.01	0.5589±0.01884	3.37%
3	354.2±3.542	131±1	269.3±0.05	268.5±0.05	0.5358±0.01699	0.03±0.01	0.5282±0.01839	3.48%
4	354.4±3.544	129±1	269.3±0.05	268.4±0.05	0.556±0.01729	0.03±0.01	0.5478±0.01877	3.43%
5	353.8±3.538	140±1	269.4±0.05	268.4±0.05	0.5341±0.01589	0.03±0.01	0.5272±0.01742	3.30%
6	353.2±3.532	129±1	269.3±0.05	268.4±0.05	0.5678±0.01731	0.03±0.01	0.5614±0.01892	3.37%
7	353.7±3.537	132±1	269.3±0.05	268.4±0.05	0.5549±0.0169	0.03±0.01	0.5478±0.01844	3.37%
8	353.6±3.536	133±1	269.3±0.05	268.3±0.05	0.5622±0.01678	0.03±0.01	0.5552±0.01839	3.31%

2.3.3 Oil Circulation Ratio Measurement Using ASHRAE Standard 41.4

To validate in-situ OCR measurement results, a standard gravimetric method of measuring OCR was also used. ASHRAE (2015) was followed for this measurement. An evacuated sample cylinder of 50 ml was installed with manual ball valves in the liquid line of the TRU as shown in Figure 2.14. The mass of the empty sample cylinder was 159 g, while the mass of the combination of the empty cylinder and ball valve assembly was 603 g. For a particular condition, once the OCR measurements using the liquid level probe and visual method were recorded, the TRU was allowed to run at the same condition and then the valve of the sample cylinder was opened to collect a sample of oil and liquid refrigerant. The filled sample cylinder was removed from the TRU and weighed on a scale with an accuracy of 0.01 g. The refrigerant in the cylinder was then slowly released to avoid expelling any oil with the refrigerant. Acetone, a solvent, was then poured into the cylinder and the acetone-oil mixture was removed from the cylinder into a clean dry glass beaker. This process of acetone mixing and removing oil was repeated twice to ensure all the oil was extracted out of the cylinder. The oil-acetone mixture was then boiled off on a hot plate to vaporize the acetone. The remaining oil was then measured with the beaker on a scale with an accuracy of 0.1 mg. The empty mass of the sample cylinder as well as the beaker was pre-measured at the beginning of each test to then calculate the proportion of oil and refrigerant inside the sample cylinder, which gives the oil concentration in the refrigerant. Assuming that the oil and refrigerant were miscible, the values of oil concentration and OCR are equal. These readings were taken for all the four test conditions and the results are presented in the following Section.

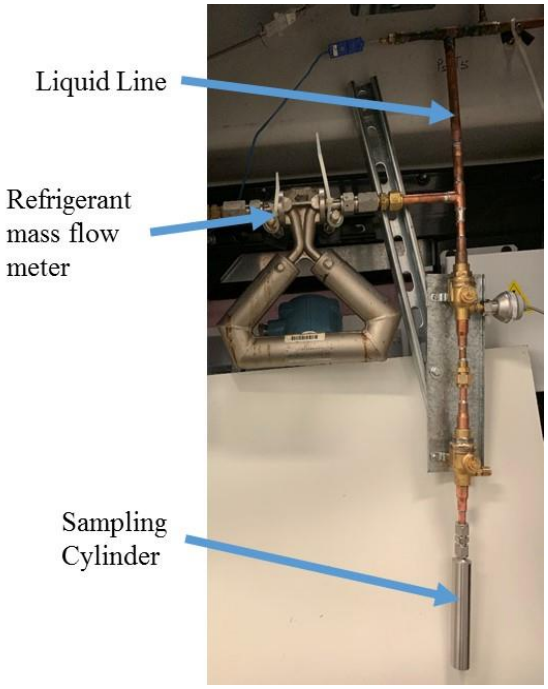

Figure 2.14: Sample cylinder connected to the liquid line

2.4 Experimental Results

Table 2.8 shows comparison of all three methods for the four different conditions that are at different refrigerant mass flow rates. In this table, the OCR results from the liquid level probe and visual methods were averages, whereas only one sample reading was taken using the ASHRAE Standard method for each condition, which is also presented. Compressor discharge and suction conditions are also shown in the table to get an idea of the state points. The relative differences in the OCR measurement between the liquid level probe and visual methods are less than 5 %, whereas differences between the liquid level probe and ASHRAE standard methods are less than 12 %. If only test conditions 1, 2 and 4 are considered, then the relative difference between all three methods are less 6 %. Even though the weight measurements for the sampling method are carried out on a scale with high accuracy, the method has several processes with human intervention from taking the sample until the collected oil is weighed, which can introduce several measurement uncertainties. This may explain the difference in OCR measurement result between the liquid level probe and sampling methods carried out for test condition 3. An observation from data is that the OCR stays relatively constant across different operating conditions and a wide range of refrigerant mass flow rates. As suggested by the manufacturer, OCR values between 0.52 %

and 0.65 % are typical for a fixed speed scroll compressor running in a steady-state condition. All of the measured OCR values were within this range.

Table 2.8: Data of OCR measured with three different methods for all four conditions with different mass flow rate

Test	Ref. Mass Flow Rate	OCR Method			Compressor Discharge				Compressor Suction			
		Level Probe	Visual Scale	ASHRAE Standard	Pressure	Discharge Sat Temp	Discharge Temp	Super -heat	Pressure	Suction Sat Temp	Suction Temp	Super -heat
	kg/h				kPa	°C	°C	ΔK	kPa	°C	°C	ΔK
1	453.7	0.635	0.633	0.608	2245	49.02	95.38	46.36	374.1	-14.01	3.09	17.1
2	427.3	0.517	0.537	0.548	2173	47.61	91.46	43.85	347.1	-16.08	-2.39	13.69
3	400.2	0.621	0.653	0.555	2158	47.31	88.90	41.59	319.8	-18.31	-8.61	9.699
4	354.0	0.541	0.547	0.542	2131	46.77	91.26	44.49	282.5	-21.6	-12.35	9.248

2.5 Future Work in OCR Measurement Using Separation Method

2.5.1 OCR Measurement in Discharge Line

An attempt was made to measure OCR by engaging the oil measurement loop in the discharge line. However, a few technical challenges need to be overcome to measure OCR accurately in the discharge line. The oil separator, oil collector and the lines connecting them were all in the psychrometric chamber maintaining ambient temperature. While measuring OCR in the discharge line, the saturation temperature in the components of the oil loop was that of the discharge line, which is higher than the ambient temperature. This condition led the refrigerant to condense into the oil collector. The oil collector itself was insulated and the temperature was controlled; however, the oil separator and the lines connecting them were not insulated, which led the refrigerant to condense and flow along with the oil. The liquid level sensor ended up measuring the level of liquid refrigerant along with the oil, which led to inaccuracy in measuring OCR. While running discharge line tests, two liquid menisci were observed at certain test conditions in the transparent tube connected in parallel to the oil collector. In addition, this observation also confirmed that the liquid refrigerant with maybe different concentrations of oil was present. This observation also confirmed that the refrigerant and oil were not miscible or partially miscible at this condition. Therefore, if this method is implemented in the discharge line, it is important to overcome the challenge of refrigerant being condensed in the collector. During the suction line tests, the saturation temperature in the oil loop remained lower than the ambient temperature, which kept the refrigerant in a vapor state. Therefore, OCR measurement results carried out using only the suction line are reported.

2.5.2 Temperature Correction in the Liquid Level Probe Measurement

The liquid level probe installed in the oil collector is a critical sensor for the OCR measurement system that has been developed. During one of the tests, it was observed that OCR measurement was sensitive to the oil collector temperature as shown in Figure 2.15. Even though the actual OCR may not have changed as the system was running at steady-state, the calculated OCR was affected. On detailed investigation, it was found that the oil level sensor used for measurement was sensitive to the oil collector temperature and it does not correct for the effects of temperature. Therefore, to account for the temperature variation, the oil level sensor was re-calibrated.

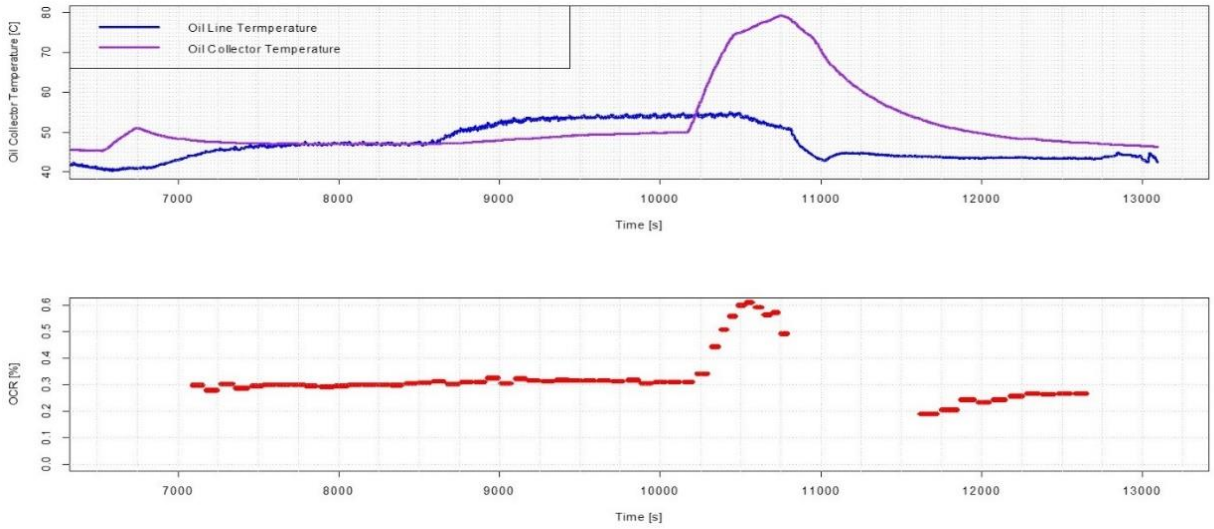

Figure 2.15: (Above) Time series plot of average oil temperature on the surface wall of the collector as well as inline oil temperature. (Below) OCR calculated for suction line testing

Calibration Setup

Refrigerant from the TRU was evacuated and the oil collector was emptied and opened up to air. Then, the oil discharge valve at the bottom of the oil collector was shut. A known amount of oil was then injected from an access port at the top of the collector. A port at the top (see schematic in Figure 2.9) was opened to atmosphere to vent out the air. The oil that was injected into the oil collector was measured on a weighing scale (see Figure 2.16), which has an accuracy of 0.01 g and the weight measurements were manually recorded.

A scale was attached next to the sight tube (see Figure 2.17), which is in parallel to the oil collector. Therefore, as the level inside the oil collector changes, the level in the sight tube also varies. The level of oil in the collector was also marked on the sight tube at certain intervals and the level measurements were recorded manually. Five thermocouples were attached on the surface of the oil collector on the top half of the oil collector at two different levels as shown in Figure 2.9. Heat tape was installed on the bottom half of the oil collector. The heat input rate was controlled using a PI feedback controller to maintain a particular set-point temperature. The reference temperature was fed to the controller from one of the five thermocouples attached on the surface of the oil collector. The calibration was carried out inside a psychrometric chamber and the chamber

temperature was maintained at 37.8 °C, which was the ambient room temperature in all four conditions mentioned in Table 2.2.

Figure 2.16: Mass measurement of oil before injection in the oil collector

Figure 2.17: Scale attached to the sight tube for a reference of the level and the green marks on the sight tube.

Calibration Procedure

Step 1: Inject measured amount of oil (~20 gram) in the oil collector until the level in the sight tube increases. Keep a record of mass measurements as oil is injected.

Step 2: Change the temperature of oil collector from 30 °C to 70 °C with intervals of 10 °C.

Step 3: Repeat Step 1 and Step 2 three more times for a total of 4 different oil levels at 4 different temperatures.

During this entire process, the voltage from the liquid level probe was continuously recorded at 1 second intervals. Temperatures from all the five thermocouples and the ambient air temperature were also recorded.

Calibration Data

With four different levels and four different temperatures, steady-state data was collected for 16 different combinations of oil level and temperature as shown in Table 2.9.

Table 2.9: Calibration data of oil in terms of mass, voltage from probe and temperature of the oil collector

Sr.	Mass (g)	Level (cm)	Liquid Level Probe (V)	T_17 (°C)	T_18 (°C)	T_19 (°C)	T_20 (°C)	T_21 (°C)	T_avg (°C)	T_amb (°C)
1	101.84	0	0.2363	39.68	39.99	39.92	39.81	39.18	39.72	36.95
2	101.84	0	0.7908	48.45	49.95	49.78	49.49	47.14	48.96	37.70
3	101.84	0	1.5325	57.13	59.92	59.62	59.13	54.98	58.16	37.78
4	101.84	0	2.5150	65.84	69.88	69.47	68.73	62.78	67.34	37.78
5	179.51	2.6	0.9640	39.64	39.99	39.94	39.82	39.22	39.72	37.79
6	179.51	2.6	1.4960	48.42	49.95	49.78	49.46	47.11	48.94	37.78
7	179.51	2.6	2.2631	57.13	59.92	59.65	59.13	54.98	58.16	37.79
8	179.51	2.6	3.2443	65.82	69.88	69.49	68.74	62.84	67.35	37.78
9	256.67	5.2	1.6873	39.65	39.99	39.92	39.75	39.12	39.68	37.81
10	256.67	5.2	2.2217	48.41	49.95	49.78	49.49	47.14	48.95	37.77
11	256.67	5.2	2.9729	57.11	59.92	59.62	59.09	54.98	58.14	37.77
12	256.67	5.2	3.9372	65.78	69.88	69.47	68.72	62.84	67.34	37.80
13	334.57	7.7	2.4050	39.58	39.99	39.95	39.83	39.21	39.71	37.78
14	334.57	7.7	2.9344	48.37	49.95	49.79	49.48	47.14	48.95	37.79
15	334.57	7.7	3.6861	57.09	59.92	59.64	59.12	55.01	58.16	37.78
16	334.57	7.7	4.6609	65.75	69.88	69.46	68.73	62.86	67.34	37.76

Calibration Results

Figure 2.18 shows the voltage signal from the liquid level probe with respect to the amount of oil in the collector at different temperature levels. The relationship between voltage and oil mass is linear. Figure 2.19 shows the voltage signal from the liquid level probe with respect to the oil collector temperature. Different colored plots represent different oil amounts. It can be observed that the relation between voltage and temperature is nonlinear. A 2^{nd} order polynomial fit captured all the data points with an $R^2 = 0.99$. Based on this data, a 2^{nd} order polynomial fit with two input variables was developed as a revised calibration curve for the liquid level probe. The inputs to the equation are voltage from the probe and the temperature of the oil collector and the output is the mass of oil in the collector. The blue surface in the 3d plot shown in Figure 2.20 is the revised

curve, with the red spherical markers showing the data points from Table 2.9. The equation of the curve is also shown below the plot in Figure 2.20.

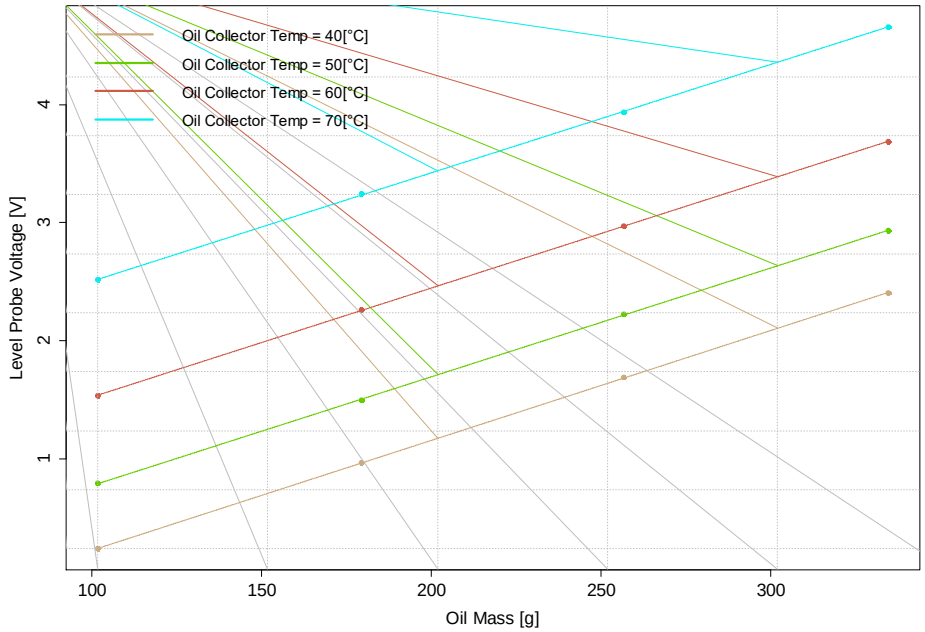

Figure 2.18: Change in level probe voltage with respect to the amount of oil added in the collector

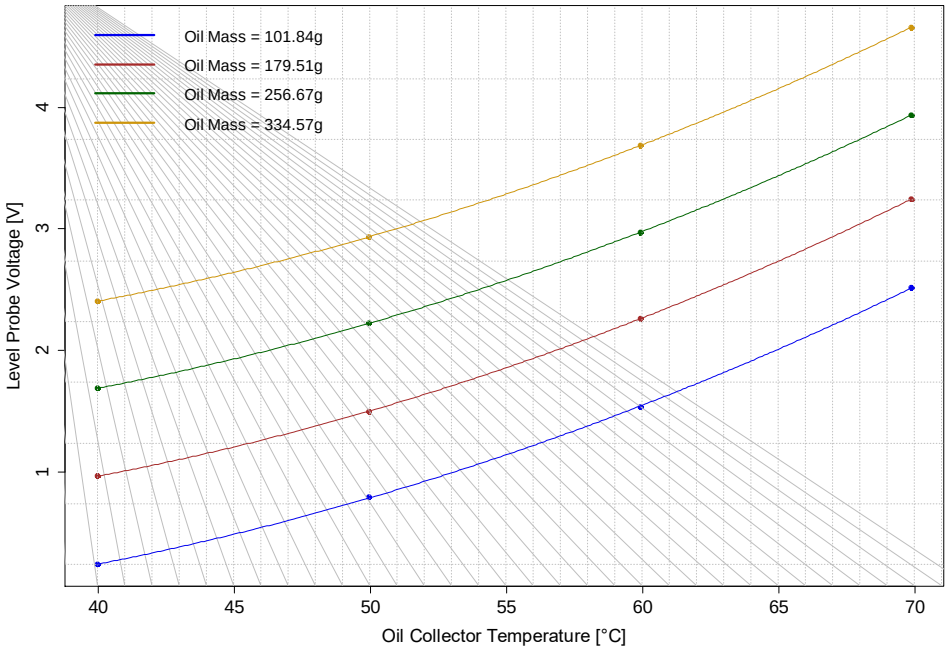

Figure 2.19: Change in level probe voltage due to the change in temperature of oil collector

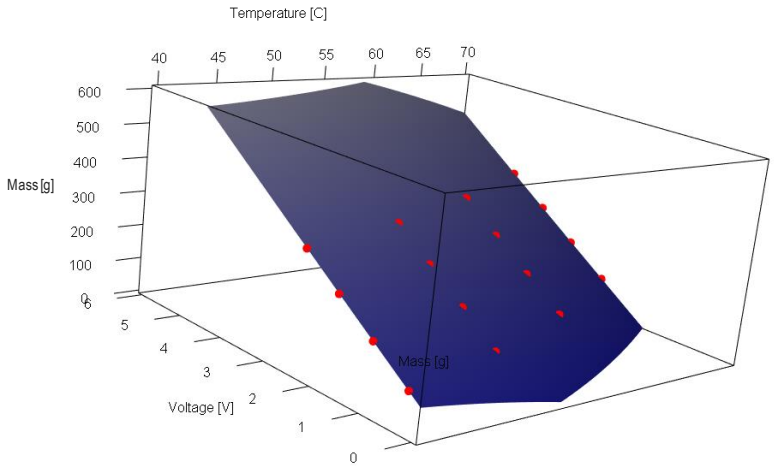

Equation: M = 66.09+107.05*V+0.34*V^2+5.073*T-0.121*T^2-0.01*T*V

Multiple R-squared: 1, Adjusted R-squared: 0.9999

Figure 2.20: Re-calibrated curve for measuring mass with respect to temperature and voltage

Issue with Liquid Level Probe to be Resolved as Future Work

While calibrating the probe, it was discovered that the location of the probe affects the voltage signal due to non-uniform and transient temperatures in the collector. Figure 2.21 shows a time series plot of the voltage signal of the liquid level probe (top) and the surface temperature of the oil collector (bottom) for the same timeline. During this plot duration, 256 g of oil was charged and the oil collector was exposed to air. The temperature was varied between 40 °C to 70 °C using the surface heater on the oil collector, while the ambient temperature of the room was maintained at 37 °C. It can be observed that the surface temperature of the collector reaches a steady-state value relatively quickly, compared to the voltage signal of the liquid level probe. This means that the location, which affects the voltage signal, is somewhere away from the collector surface and it takes time for that location to reach the steady temperature. For one of the conditions, as shown in Figure 2.21, the voltage signal takes approximately 3800 seconds (1.05 hours) to reach steady state, even though the temperature on the surface reaches steady state in a few minutes. So, controlling just the surface temperature of the oil collector, while collecting OCR measurement, may not accurately compensate for temperature.

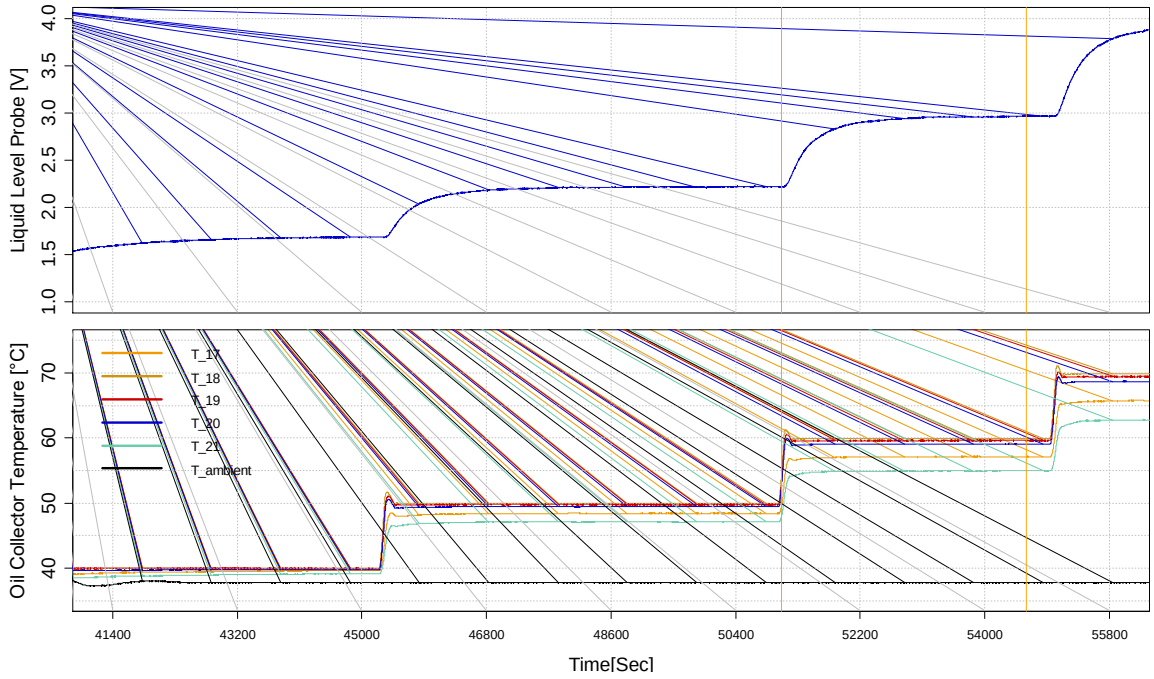

Figure 2.21: Raw signal of voltage from liquid level probe and the oil collector temperature varied for an oil mass of 256 g.

During the discharge line OCR measurement tests, there are instabilities in temperature inside the collector, due to liquid refrigerant being condensed in the oil collector and then evaporating due to the active heat control on the collector. These temperature differences affect the voltage reading of the liquid level probe when the superheated gas or liquid refrigerant comes in through the oil separator or from the pressure equalization line, even though the collector wall temperature is maintained at constant temperature. Therefore, even after giving a temperature correction to the liquid level probe calibration, it is challenging to accurately measure OCR in the discharge line, as the temperature at the actual location that affects the voltage reading of the sensor may be different from the wall temperature. As future work, it may be better to explore use of a level sensor, which compensates for temperature variations, and replace the current level sensor.

The suction line tests do not have much variation in the temperature. By comparing the plots in Figure 2.22 and Figure 2.23, it can be observed that the oil collector temperature remains stable in the suction line test. Therefore, OCR measurements for suction line testing were carried out using the calibration curve for the liquid level sensor with the temperature correction. During the suction line tests, the temperature of the oil collector was set at 60 °C.

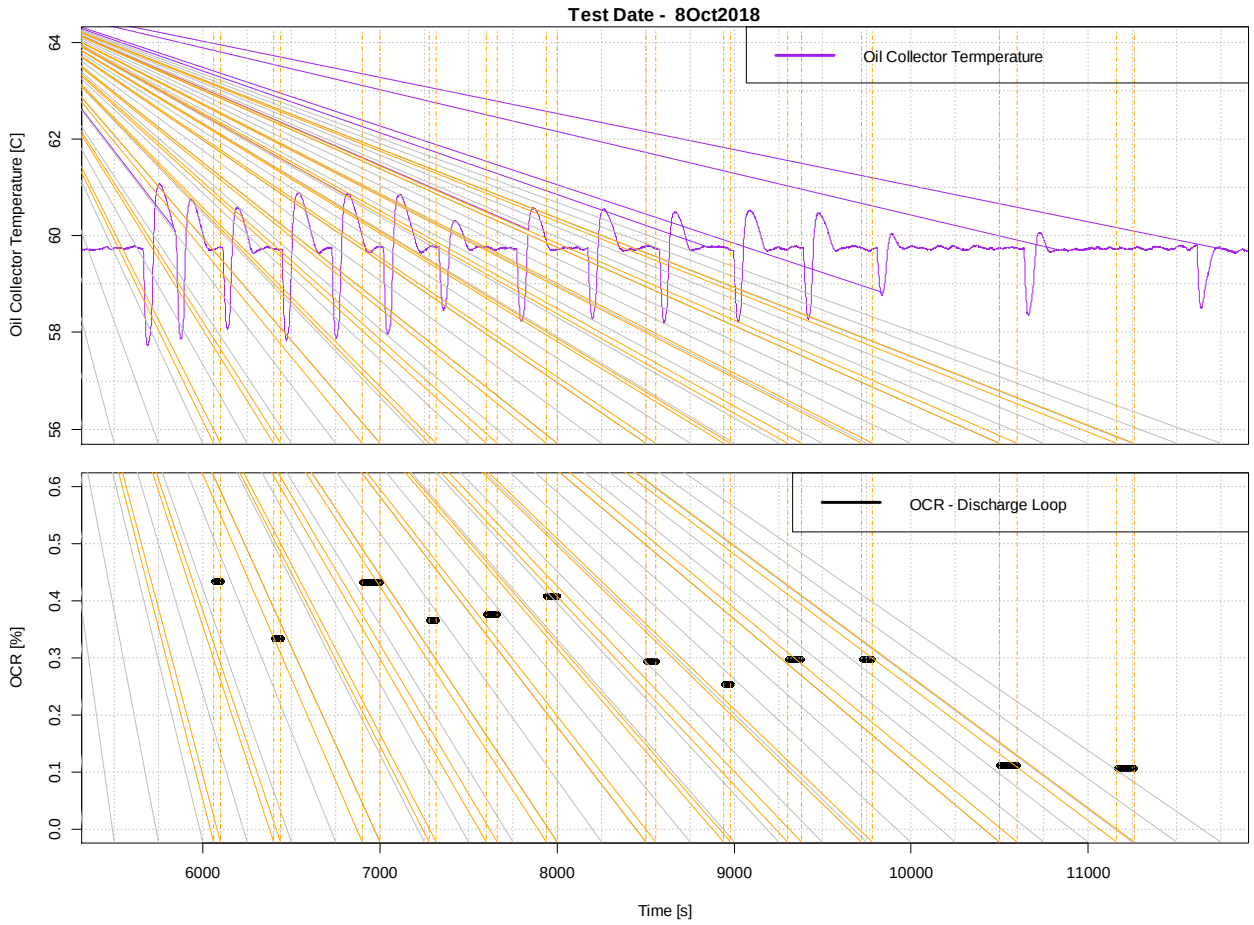

Figure 2.22: Time series plot of oil collector temperature (above) and OCR (below) for discharge line test.

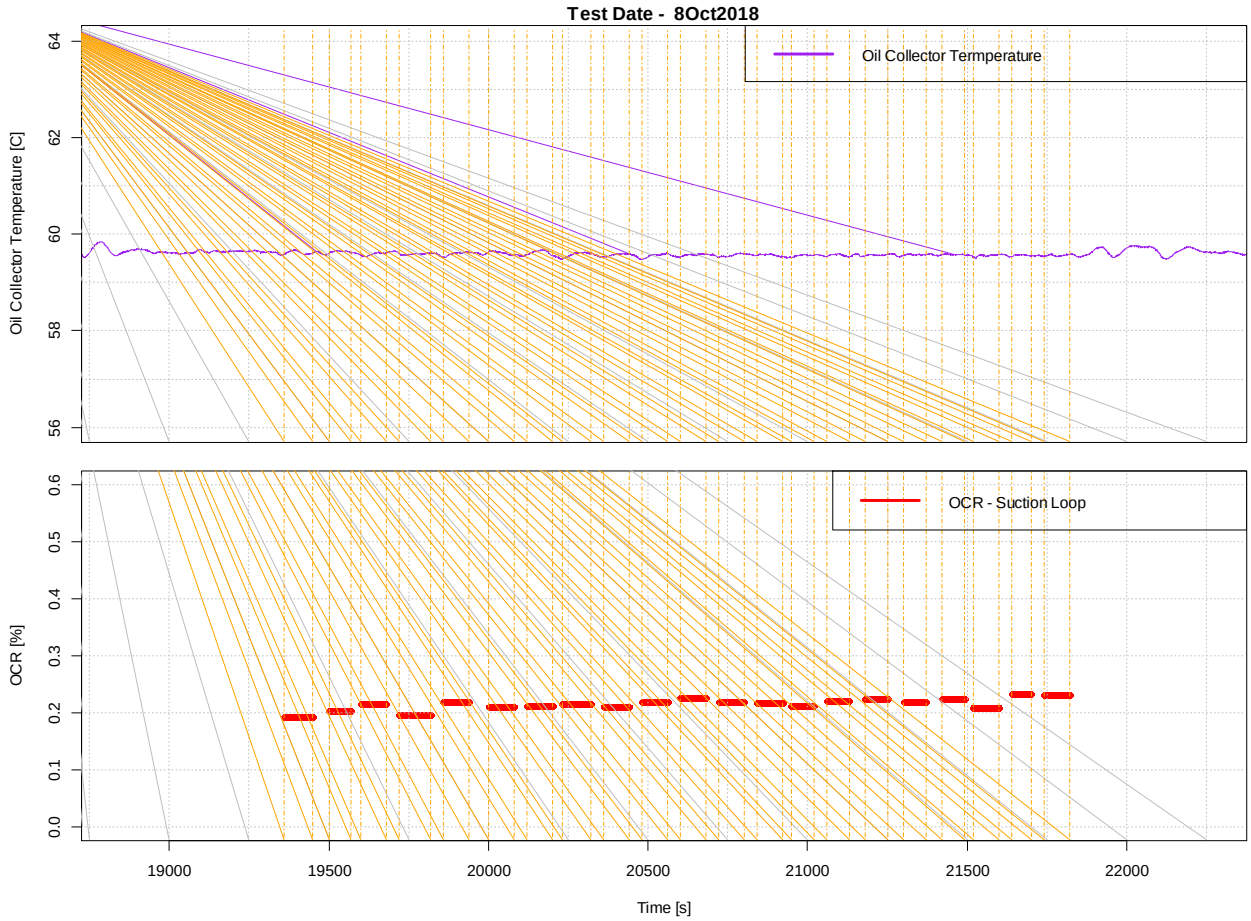

Figure 2.23: Time series plot of oil temperature (above) and OCR (below) for suction line test.

2.6 Summary of OCR Measurement Method

An in-situ method for measuring OCR was developed based on separating the oil from the refrigerant and measuring the oil flow rate using a liquid level probe. A major benefit of using this method is that multiple samples of oil can be taken, which will capture the low frequency dynamic behavior of OCR in the system. As the measurement system is automated, it minimizes human error. Measuring OCR with the current ASHRAE standard involves processes such as transferring solvent and oil from the cylinder to a beaker, measuring the mass of substances at a milligram level, and evaporating the solvent from the mixture, which are tedious and prone to human errors. Practically it is not possible to measure more than 3 or 4 samples using such a method at a particular condition. In addition, while taking the sample from the liquid line, if at any condition the oil and refrigerant are not miscible, then it is possible that the sample collected in the cylinder would be non-homogenous. In contrast, using the method proposed in this paper, the oil is separated out

when the refrigerant is in the vapor phase. The experimental setup in its current form uses post-processing of data to determine OCR. However, if it is desired to measure OCR in real time, a micro-controller can be easily developed that would process the data with the same logic that has been currently used for post-processing to output an OCR measurement value in real time. The controller would also contain information about the refrigerant and lubricant properties, so that the solubility can be calculated in real time and the OCR can be corrected. One of the disadvantages of this method is that due to the presence of an additional oil separator in the suction line, there is an impact on cycle performance; however, if the pressure drop across the oil separator is low, then this impact is not significant.

For a technical feedback, the OCR measurement method was presented to various companies involved in the HVAC&R business. This method was presented to engineers at Johnson Controls, Daikin, Emerson and Northpark Innovation Group. The engineers provided positive feedback on the ability of the method to measure OCR in the suction line as compared to other sensors, which were limited to using in the liquid line. Another vital feedback was that the apparatus in its current form is bulky and it involves too many components, which restricts its use to a laboratory environment. The market for developing a sensor that can cater only to lab equipment is limited and does not have a high commercial potential. However, these companies mentioned that if the technology for measuring OCR could be developed in a small form factor and simplified to reduce the cost, then it could have great market potential. This compact product could then be installed as an OCR sensor in air-conditioning, heat pumping, and refrigeration equipment, which would then open up many possibilities of actively managing oil using advanced control systems.

2.7 Smart Accumulator with OCR Sensing

2.7.1 Design Concept

Based on the technical feedback received from industry, a modified version of the OCR sensor was designed that is based on integration with a suction line accumulator. The accumulator protects the compressor in a typical HVAC&R system from liquid slugging and is often utilized in heat pumps, air conditioners, and commercial refrigeration. Integration of the OCR sensor within an accumulator addresses the issue of small form factor and significantly improves the overall

economics. An accumulator protects the compressor by separating out the liquid refrigerant and allows only vapor refrigerant to flow into the compressor. The idea is to modify an accumulator to implement the OCR measurement method that has already been developed. All the expensive components used in the currently built apparatus, such as mass flow meter, liquid level probe and oil separator are eliminated. However, the functionalities of all those components are maintained in the re-design. For example, as shown in Figure 2.24, the re-design utilizes two level switches positioned at pre-calibrated levels thereby eliminating the need of a continuous level reading for determining oil flow rate. The oil separation is done by designing the inlet line to face the wall of the vessel, so that the oil is separated from the refrigerant vapor as it hits the wall. If the separation is not adequate, then a filter as shown in Figure 2.24 can be added. The traditional orifice in the refrigerant vapor return line is replaced with a solenoid valve for controlling the oil flow returning to the compressor, which then helps to implement the developed OCR measurement method in the re-design.

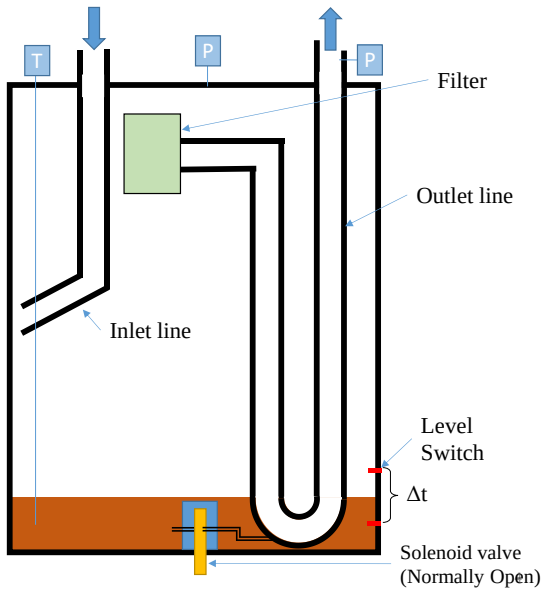

Figure 2.24: Schematic of re-designed version of Smart Accumulator with OCR Sensing

2.7.2 Working Principle of a Smart Accumulator

A computer aided design model is shown in Figure 2.25 that will be used to explain the operation of a smart accumulator while referring to the numbers marked next to each component. The refrigerant and oil mixture enter an inlet tube (1) and is deflected to hit a vertical baffle plate (2)

on one side and the inner wall of the shell (8) on the other side. This helps in separating liquid oil from the refrigerant vapor. Splitting the flow through the tee at the end of the inlet tube reduces the refrigerant vapor velocity, which helps in better oil separation. The liquid oil droplets coalesce and drip down to the bottom section of the accumulator.

The bottom section of the accumulator is pre-charged with compressor oil up to the level of a lower liquid level switch (4). A solenoid valve (5) controls the flow of oil from the bottom of the accumulator to a S-tube (7). Control logic will be developed such that when the oil liquid level is below an upper liquid level switch (3), the solenoid valve remains closed. As more oil gets separated from the upper section, it will accumulate at the bottom of the accumulator. The level of the oil will rise until it reaches the level of upper liquid level switch (3), which will trigger the controller to open the solenoid valve. When the solenoid valve opens, the oil from the bottom of the accumulator will flow into the S-tube and be drained out of the accumulator by flowing along with the refrigerant vapor through the outlet line (6). The oil return line (9), connecting the solenoid valve and the outlet line, is kept small to avoid large slugs of oil returning to the compressor, which may impact the performance of the system in which OCR is measured. The solenoid valve will remain open until the level of oil hits the lower liquid level switch (4). The solenoid valve will then closed to start accumulating the oil again. This cycle of draining and filling oil in the bottom section of the accumulator will be repeated to get continuous OCR measurements with discontinuity while the oil is draining in each cycle.

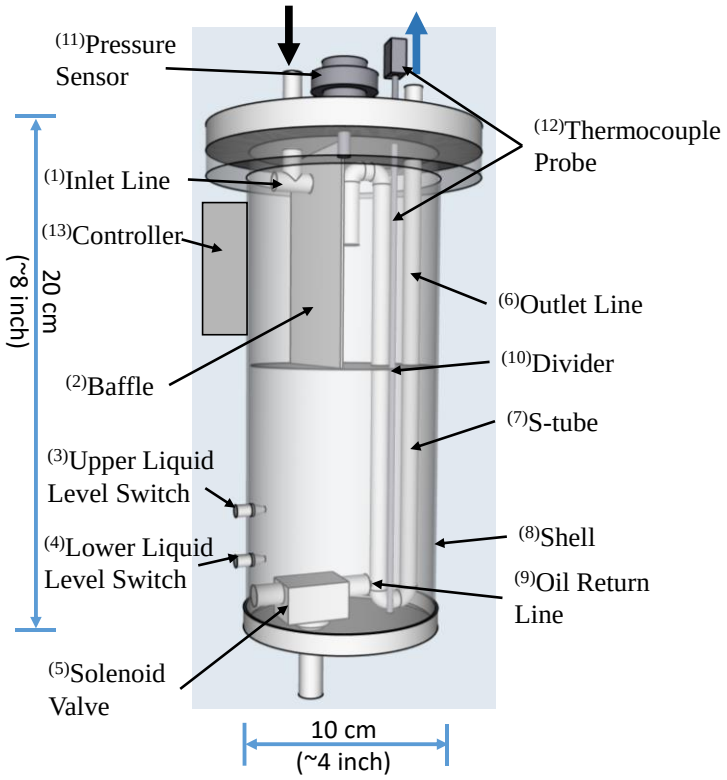

Figure 2.25: Computer aided design model of the Smart Accumulator

2.7.3 OCR Measurement in a Smart Accumulator

The difference in height between the upper and the lower liquid level switch is fixed. Therefore, the amount of oil between the switches can be assumed constant and can be pre-determined by filling up the volume by known amount (mass) of oil. A micro-processor can continuously measure the time taken to fill the oil between the two level switches. The mass flow rate of oil can then be simply calculated by dividing the mass of oil by the time taken to fill the known amount of oil. With the known mass flow rate of oil, the OCR can be determined by dividing the mass flow rate of oil with the mass flow rate of refrigerant and oil mixture, which can be obtained from a mass flow meter in the liquid line of the refrigeration cycle. In the absence of a mass flow meter, the compressor map may be used to obtain refrigerant mass flow rate.

The liquid oil accumulating at the bottom of the sensor will have some amount of liquid refrigerant dissolved in it. The solubility of this liquid refrigerant in oil is a function of temperature and pressure inside the vessel. Based on the solubility curves that are programmed in the micro-

processor, the oil flow rate can be corrected in real-time to account for the amount of liquid refrigerant dissolved in the oil. These solubility curves are experimentally determined and can be provided by an oil supplier.

2.7.4 Smart Accumulator Implemented in a System Running Vapor Compression Cycle

The smart accumulator will be designed such that it can be implemented in the suction line of a typical vapor compression cycle as shown in Figure 2.26. A sensor located in the suction line could provide information on oil flow returning to the compressor from the system. An onboard controller on the smart accumulator could then interact with the compressor controller to control the speed of the compressors or turn one or more of them on or off to ensure that the compressors do not starve of oil. In a situation, where liquid refrigerant comes through the inlet line of the smart accumulator, the design still functions as a traditional accumulator. The liquid refrigerant accumulates in the bottom section until the upper level switch is triggered and the liquid refrigerant is flashed through the solenoid valve into the S-tube. The smart accumulator will therefore provide protection to the compressor from liquid flooding as well as from oil starvation. The idea is to make the smart accumulator at a low cost, to enable the use of multiple sensors for systems with multi-staged and parallel compressors. It is important to note that the OCR sensing concept would not function during situations where liquid refrigerant is accumulating and the sensor would be smart to identify when the conditions are OK for OCR sensing. The onboard controller on the smart accumulator will receive signals from a pressure sensor, thermocouple probe and level switches. Based on the control logic, the controller will send a signal to open/close the solenoid valve.

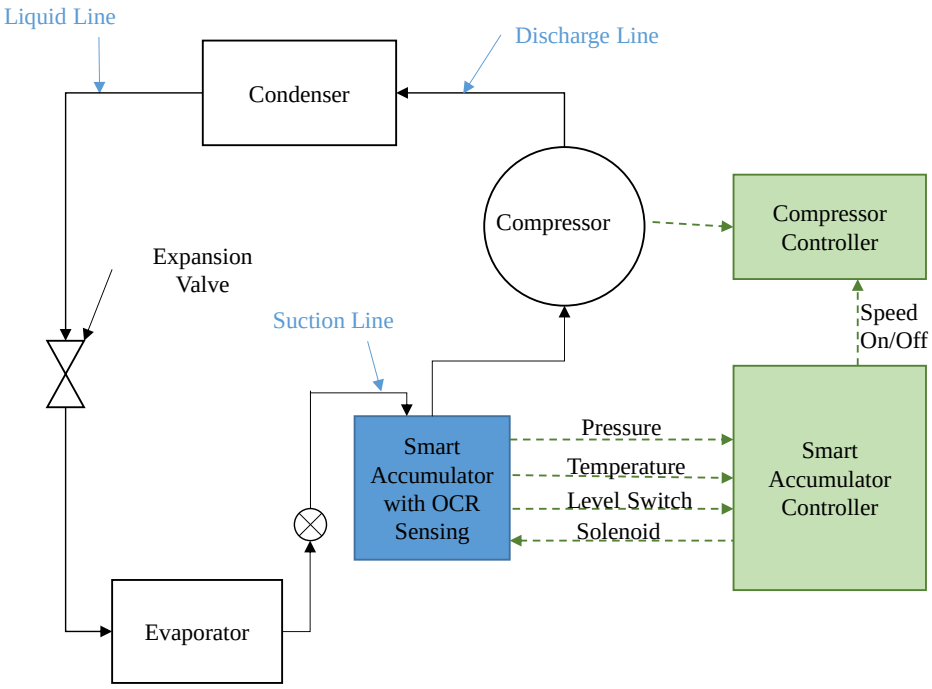

Figure 2.26: Smart Accumulator in a system running a typical vapor compression cycle

As future work, a prototype should be built and OCR measurement from the sensor should be validated in an existing setup. The prototype should then be tested in a system having multiple compressors for capacity control. This sensor will hopefully provide useful information to develop active oil management solutions which will greatly improve the system reliability and avoid compressor failures from oil starvation.

2.8 Conclusion

The growing use of variable-speed and tandem compressors coupled with emerging refrigerant/oil combinations has elevated the importance of measuring OCR. Researchers have looked into various measurement methods, however most of them rely on measuring oil concentration in the liquid line to determine OCR. These methods can be highly accurate, but they work only for miscible oil and refrigerant pairs and they require calibration. Some of these methods require expensive instrumentation, which prevents their use in field applications. An in-situ method for measuring OCR was developed based on separating the oil from the refrigerant and measuring the oil flow rate using a liquid level probe. A major benefit of using this method is that multiple samples of oil can be taken, which will capture the low frequency dynamic behavior of OCR in

the system. As the measurement system is automated, it minimizes human error. The oil separation technique used in this method overcomes the shortcoming of measuring OCR for immiscible refrigerant/lubricant pairs, while retaining features such as measuring in real-time, not needing to remove charge and not requiring calibration. Measuring OCR with the current ASHRAE standard involves processes such as transferring solvent and oil from the cylinder to a beaker, measuring the mass of substances at a milligram level, and evaporating the solvent from the mixture, which are tedious and prone to human errors. Practically it is not possible to measure more than 3 or 4 samples using such a method at a particular condition. In addition, while taking the sample from the liquid line, if at any condition the oil and refrigerant are not miscible, then it is possible that the sample collected in the cylinder would be non-homogenous. In contrast, using the method proposed in this chapter, the oil is separated out when the refrigerant is in the vapor phase. The experimental setup in its current form uses post-processing of data to determine OCR. However, a micro-controller can be easily developed that would process the data with the same logic that has been currently used for post-processing to output an OCR measurement value in real time.

OCR is important parameter along with refrigerant mass flux in characterizing oil retention in suction gas lines within HVAC&R systems, which is addressed in subsequent chapters.

3. EXPERIMENTAL SETUP TO COLLECT DATA OF OIL RETENTION IN GAS LINES

ASHRAE Handbook – Refrigeration (ASHRAE, 2014), Chapter 1, provides the basic principles of refrigerant piping as follows.

1) Ensure proper refrigerant feed to evaporators,
2) Provide practical refrigerant line sizes without excessive pressure drop,
3) Prevent excessive amounts of lubricating oil from being trapped in any part of the system,
4) Protect the compressor at all times from loss of lubricating oil,
5) Prevent liquid refrigerant or oil slugs from entering the compressor during operating and idle time, and
6) Maintain a clean and dry system.

It is important that these principles are fulfilled when designing piping for gas lines in unitary split systems. Points (3) to (5) are related to ensuring proper oil management. Current tables in Chapter 1 of 2014 ASHRAE Refrigeration Handbook provide design direction to avoid the problem of oil return. Based on the Jacobs limit, these design criteria mainly ensure that there exists enough mass flux in the vertical suction lines for oil to return to the compressor at minimum operating conditions, thereby keeping oil from accumulating in the system at an unacceptable rate when traditional, fixed capacity systems are employed. These tables address point number (3), however the tables consider only R-22 and R134a with mineral oil and POE oils. In addition to adding design criteria for emerging refrigerant-oil combinations, it is increasingly important to predict oil retention for rising applications of variable-speed and tandem compressors in order to develop robust oil management strategies. Quantifying oil retention for various conditions can help to address points (4) and (5), allowing a designer to account for effects of oil retention and pressure drop in piping. Various researchers have studied factors affecting oil retention and have quantified the amount of oil retention with various lubricant-refrigerant combinations under different conditions. However, there are many combinations yet to be explored and studied. In addition, the studies of oil retention mainly include suction lines and therefore more tests need to be performed to collect data for discharge lines.

3.1 Literature Review

Due to various factors such as miscibility between oil and refrigerant, different flow regimes, and varying viscosity, measuring oil retention and identifying the locations of oil retention within the system has been difficult. However, various measurement methods have been studied and developed by researchers. Jacobs et al. (1976), Scheideman et al. (1977), Alofs et al. (1990) and Biancardi et al. (1997) are some of the earlier researchers who studied oil holdup / oil transportation and their impact on pressure drop in vapor compression cycles.

Jacobs et al. (1976) studied oil retention in vertical suction risers by injecting oil at the bottom of a vertical pipe and observing the flow through sight glasses. They decreased the refrigerant mass flow rate until the oil started to accumulate in the bottom sight glass. Based on this visualization data, they developed a correlation for predicting the lower limit of refrigerant mass flux for oil return of R-12 and R-22 with mineral oil as shown in Equation (3.1). The tables presented in ASHRAE Refrigeration Handbook Ch. 1 for sizing refrigerant lines use this Jacobs limit, which mainly ensures oil return through vertical risers. It does not address oil retention.

$$G = j_g^{*\frac{1}{2}}\left[\rho_g g D\left(\rho_f - \rho_g\right)\right]^{0.5} \tag{3.1}$$

where,

$j_g^{*\frac{1}{2}} = 0.85$	Empirical coefficient developed for R12 and 150 SUS Oil
ρ_g	Vapor Density
ρ_f	Liquid Density
g	Acceleration due to gravity
D	Pipe diameter

In addition, the study by Jacobs et al. (1976) did not consider the effects of viscosity and miscibility of oil, which can be quite different for new low GWP refrigerants and synthetic oils developed to work with the new refrigerants. Fung and Sundaresan (1994) investigated oil return characteristics of R404A with a naphthenic mineral oil and POE in a low temperature display case refrigeration system. Sundaresan and Radermacher (1996) experimentally studied the oil return characteristics of R407C with mineral oil in a 10.6 kW heat pump system.

Two groups have primarily carried out experimental studies on oil retention in suction lines. One group uses an injection-extraction method and the other uses a weight measurement of the test section of the suction line. A summary of the results obtained by both groups has is presented in the following two sub-sections.

3.1.1 Oil Injection-Extraction Method to Determine Oil Retention

Mehendale and Radermacher (2000) were the first researchers to use the idea of an oil injection-extraction method to study the film flow reversal in a vertical pipe as an application to understand oil return in refrigeration systems. Hwang et al. (2000) explored the idea of the oil injection and extraction method and developed an experimental setup for studying oil retention in a vertical pipe. R134a with three different types of lubricants (mineral oil (MO) and two types of alkyl-benzenes (AB)) were used in the experiments. The experimental method was developed with an objective to study the issue of miscibility of oil in newly introduced HFC refrigerants in the market at that time. An oil loop was connected in parallel with the refrigerant loop, which injected oil in a vertical test section. The mean oil film thickness was calculated by integrating the oil flow rate difference between injected and returned quantities over time. The authors concluded that at a high refrigerant mass flow rate (0.57 g/s), the influence of oil type and viscosity was not dominant. However, at a low refrigerant mass flow rate (0.1 g/s), oil retention of the oils with poor miscibility and high viscosity increased. The authors also observed that for the lowest refrigerant mass flow rate, the flow pattern was churn flow. Even with churn flow, there was still a net forward oil flow.

Lee et al. (2002) further developed the oil injection-extraction method and built a test setup to investigate oil retention characteristics in a CO_2 air-conditioning system with Polyalkylene Glycol (PAG) lubricant. The objective of the study was to quantify the amount of oil retention and the distribution of the retained oil in the evaporator, gas cooler and suction line. The authors observed a similar phenomenon as observed by Hwang et al. (2000) regarding the effect of viscosity and refrigerant mass flow rate on oil retention. Comparing both heat exchangers, evaporator and gas cooler, the authors observed that for a refrigerant mass flow rate of 14 g/s with an oil circulation rate of 5 wt.%, the amount of oil retained in the gas cooler was 12 ml compared to 28 ml in the evaporator. The authors mentioned that the oil retention in the gas cooler is lower than in the

evaporator due to lower oil viscosity and higher refrigerant mass flux, which coincides with the conclusion made by Hwang et al. (2000)

Lee and his co-authors also studied the distribution of oil retention in different components of the air conditioning system using the injection-extraction method. To compare results, the authors used the oil retention volume ratio, which is defined as the ratio of the oil retention volume outside the compressor to the oil volume charged initially, expressed as a percentage. At a refrigerant mass flow rate of 14 g/s, the total oil retention volume ratio increased from 18% to 32% by increasing the oil circulation ratio from 1 wt.% to 5 wt.%. This means that more than 32% of the oil charged in the compressor sump was outside the compressor at this particular operating condition. The majority of the oil retention was in the suction line. With the higher refrigerant mass flow rate, the oil retention decreased with both 1 wt.% and 5 wt.% oil circulation ratios. Therefore, it was concluded that refrigerant mass flow rate and oil circulation ratio both have an effect on the oil retention in different components of the air-conditioning system. Based on this study, the authors recommended reducing the length of the suction piping where the majority of the oil was retained.

Using the same concept of oil injection-extraction, Cremaschi et al. (2004) investigated oil retention in residential heat pumps using R22 and R410A with miscible lubricants. Along with the heat exchangers and suction line, the authors also studied oil retention in the liquid line. The authors found that the oil retention in the R22 and R410A systems strongly depended on the oil circulation ratio. When the oil circulation ratio increased from 1 to 5 wt.%, the cumulative oil retention in the R22 system components increased from 10% up to 50% of the initial oil charged inside the compressor. It was also concluded that an increase of the refrigerant mass flow rate from 42 g/s to 59 g/s in the suction line produced an average decrease of oil retention volume of 26% for the R22/MO system. For the R410A/POE system, an increase of the refrigerant mass flow rate from 46 g/s to 77 g/s caused the oil retention to decrease by 15% on average. The authors also studied the effects of pressure drop caused by oil retention. To understand the effect of pressure drop across a component caused by oil retention, a pressure drop penalty factor (PDPF) was defined as the pressure drop across the component with oil circulation ratio of x wt.% divided by the pressure drop across the component with no oil, i.e. an oil circulation ratio of 0 (zero) wt.%.

A PDPF of 1.4 in the suction line and 1.15 in the evaporator were reported for an oil circulation ratio of 8 wt.%.

Cremaschi et al. (2005) published further results of oil retention in different components of an air-conditioning system. The authors mentioned that gravity effects are important and the oil retention can increase by up to 50% in vertical upward suction lines compared to horizontal suction lines at the same refrigerant mass flux and liquid film viscosity. The authors also confirmed the phenomenon described by previous authors that oil retention volume is proportional to the ratio of the liquid film over refrigerant vapor viscosity, which means that at constant mass flux and oil circulation rate, an increase in liquid film viscosity leads to increased oil retention.

Yatim et al. (2014) used the oil injection-extraction method to study oil retention in a microchannel type condenser and its effects on heat transfer and pressure drop characteristics. Using the refrigerant R410A and POE oil mixture in a microchannel condenser, the presence of oil with an OCR of 3 wt.% in the condenser caused pressure to increase by1.19 times compared to an oil-free condition. The authors mentioned that at a low oil concentration ratio of 0.5 wt.%, the heat transfer capacity of the coil was the same as that of oil-free conditions. However, at a high saturation temperature of 130 °F (54 °C) and high mass flux, the heat transfer capacity of the coil decreased as the oil concentration ratio increased and was apparent even at 1 wt.%. When the oil concentration ratio increased to 5 wt.%, the heat transfer capacity of the heat exchanger was penalized by up to 6%.

3.1.2 Direct Gravimetric Measurement Method to Determine Oil Retention

The second group of researchers used the method of direct gravimetric measurements to obtain oil retention. Crompton et al. (2004) studied oil hold up in horizontal copper pipes with various internal geometries, such as smooth and finned surfaces. The oil retention was calculated by collecting samples of refrigerant and oil in a test section. This was done by closing valves at both ends of the test section and isolating the refrigerant-oil mixture when the system reached steady-state. The test section was removed and weighed. Then, refrigerant was evaporated and the test section was weighed again to calculate the mass of oil retained in the test section. Zoellick (2010) developed a test set-up to study oil retention in horizontal and vertical suction lines using the

technique of removing the test section and directly measuring the net weight, similar to the method used by Crompton et al. The oil retention measurements were done for the refrigerant R410A with the lubricant POE32. The tests were carried out for two different pipe sizes of 7.2 mm and 18.5 mm and oil circulation ratios of 1 %, 3 % and 5 %. The mass fluxes were varied from the Jacobs limit of 42.9 kg/m^2-s to 250 kg/m^2-s. Zoellick also concluded that the oil circulation ratio had a significant effect on oil retention in the suction lines. A 2 % increase in the oil circulation ratio led to a 20 % increase in oil retention. He further mentioned that vertical suction lines tend to retain 10 % more oil than horizontal lines for high mass fluxes where the flow is annular. However, when the flow transitioned to stratified flow, the difference in oil retention between the vertical and the horizontal lines became more apparent. At flow rates near the Jacobs limit, the vertical suction line retained twice as much oil as the horizontal line. Zoellick endorsed the observation made by Hwang et al., Lee et al., and Cremaschi et al. that more refrigerant evaporates from the liquid in suction lines at higher superheats, which increases the mass fraction of oil in the liquid, and thus its viscosity. The higher viscosity liquids formed a thicker film on the tube wall, and retained more oil. They observed that a 5 °C increase in apparent superheat caused a 15 % increase in oil retention and suggested that if the superheat is lowered, a small amount of liquid refrigerant would exit the evaporator and the oil retained in the suction line could be washed out by the low viscosity liquid refrigerant. This could be an effective solution to return oil back to the compressor.

Sethi and Hrnjak (2011) employed the same basic setup as Zoellick, but with some modifications. They studied oil retention and pressure drop in 10.2 mm diameter horizontal, vertical and inclined suction lines for refrigerant/oil combinations of R134a/POE32 and R1234yf/POE 32. They observed that the oil retention sharply increased in vertical lines as the mass flux decreased below the point of liquid film reversal and as the flow regime transitioned to churn flow. They mentioned that even when the system runs above the Jacobs limit, the oil retention amount in the vertical suction line can be very large if the refrigerant mass flux is below the point where liquid film reversal begins. Based on this observation, they suggested that the criterion for design of suction lines in the ASHRAE Handbooks that is based only on the Jacobs limit should be modified. They also determined that inclined pipes retained more oil than horizontal or vertical pipes and that the oil retention reached a maximum value at an angle of inclination between 45° and 90°.

Ramakrishnan and Hrnjak (2012) studied oil retention in vertical and suction lines for a refrigerant-lubricant combination of R1234yf/POE 100 using the same setup as Zoellick and Sethi and Hrnjak with certain modifications of the pressure transducers. The motivation of the study was to understand the issue of using the low-GWP refrigerant R1234yf in automotive air-conditioning systems as a replacement for R134a. Comparative tests were carried out between R1234yf/POE 100, R134a/POE100, R410A/POE32 and R410A/POE100, along with the experimental data of R1234yf/POE32 from Sethi and Hrnjak (2011). It was found that R410A had lesser oil retention compared to R134a and R1234yf in both POE32 and POE100. Using POE32, it was noted that R1234yf had a 20-30 % increase in pressure drop compared to the other refrigerants at the same vapor velocity. Therefore, replacing R410A with R1234yf would have an impact on pressure drop and oil retention in suction lines.

3.1.3 Conclusions from Literature Review

Based on the literature review, the following conclusions can be drawn:

- The oil retention under certain conditions can be as high as 40 % of the oil charged into the system. Under such situations, the compressor can become starved of oil, which can cause permanent damage to the moving parts of the compressor. It is also shown that oil retention can increase pressure drops as much as 40 % and can also cause loss of heat transfer capacity, which can reduce the system efficiency. Point number (2) of the basic piping principles asks designers to prevent excessive pressure drops, which aligns with the issues of oil retention.
- Oil retention in vapor compression cycles is influenced by various factors, such as the oil circulation ratio, refrigerant vapor mass flow rate, orientation of the piping, pipe diameter, pipe surface roughness, miscibility of the oil, and the viscosity of the oil-refrigerant mixture.
- Broadly, two methods have been extensively used and researchers have been able to obtain significant results based on measurements of oil retention.

3.2 Test Matrix

Keeping in mind the factors that affect oil retention, a test matrix was developed that would capture a wide variety of test conditions. As the ultimate goal is to develop and validate a model that can predict oil retention, the richness in terms of variety of data is important. A preliminary test matrix

was provided by the ASHRAE project monitoring subcommittee (PMS) members for the research project RP1721. The matrix was further modified based on the limitations of the test setup. The test matrix includes combinations of the following parameters.

- Refrigerant: R134a, R410A, R32, R1234ze(E)
- Lubricant: POE32, POE68, POE100, POE170, PAG, PVE, AB
- Test Section Inner Diameter: 10.9 mm, 16.9 mm and 19.9 mm
- Test Section Orientation: Horizontal and Vertical
- Refrigerant Mass Flux: 0.3, 1, 2 and 3 times the Jacobs Limit
- Oil Circulation Ratio: 0.5 wt.%, 3 wt.% and 5 wt.%
- Saturation Temperature: 10 °C (Typical AC suction line) and 40 °C (Typical AC discharge line)

As there are multiple parameters for which testing needs to be performed, the test matrix can get complex and the number of tests increase greatly. To decrease experimental uncertainty, it was important to design a test matrix in such a manner that the testing procedure involved a minimum number of modifications between different test conditions. The test matrix was designed such that once a specific refrigerant/oil combination is charged, all the required data is collected for various refrigerant flow and oil circulation rates at the required temperatures. Then keeping the same oil, the refrigerant is changed as it is easier to change the refrigerant by evacuating the system. An oil change would require a complete system flushing to remove all the oil.

The experimental procedure (described in Section 3.4) to collect oil retention data was based on a gravimetric method which provided accurate oil retention measurement in a test section, however the time duration required for each test was too long. Therefore, to avoid the need of experimentally measuring oil retention for every combination of conditions, physics based semi-empirical models were developed to predict oil retention. These models were trained using a subset of experimental data points and were then validated using the remaining experimental data points. More information on the experimental data that was used for training the models versus the testing the models is described in Chapter 4.

Experimental data was collected for all combinations of parameters shown in Table 3.1. A detailed list of test conditions for different refrigerant/oil combinations is provided in APPENDIX D. It can be observed in Table 3.1 that only 10.9 mm and 16.9 mm lines were used to collect data. For the 19.9 mm line, spot tests were done as shown in Table 3.2. These spot tests were mainly used to validate the prediction models. As future work, spot tests with different oil viscosity will be carried out to validate the developed model.

Table 3.1: Combinations of parameters for which experimental data was collected

Oil-Viscosity	Refrigerant	Line Inner Diameter [mm]	Oil Circulation Ratio [wt.%]	Mass Flux [kg/m^2-s]	Sat. Temp [C]
POE32	R134a	16.92	0.5, 3, 5	1/3, 1, 2 and 3x of Jacobs Limit	10
					40
	R410A	16.92,10.92	0.5, 3, 5	1/3, 1, 2 and 3x of Jacobs Limit	10
					40
	R32	16.92,10.92	0.5, 3, 5	1/3, 1, 2 and 3x of Jacobs Limit	10
					40
	R1234ze(E)	16.92,10.92	0.5, 3, 5	1/3, 1, 2 and 3x of Jacobs Limit	10
					40

Table 3.2: Experimental data collected with 19.9 mm line

Sr. No.	Refrigerant - Lubricant	Inner Line Diameter [mm]	Jacobs Limit	Ref. Mass Flow Rate [kg/h]	OCR [%]	Oil Mass Flow Rate [kg/h]	Mode	Sat Temp [°C]	Test Section Inlet Temp [°C]
1	R410A/POE32	19.9	2 x	142	0.5	0.71	Suction	10	20
2	R410A/POE32	19.9	2.4 x	170	0.5	0.85	Suction	10	20
3	R410A/POE32	19.9	0.3 x	33	5	1.65	Discharge	40	70
4	R410A/POE32	19.9	1 x	98	3	2.94	Discharge	40	70
5	R32/POE32	19.9	2 x	121	0.5	0.605	Suction	10	20
6	R32/POE32	19.9	3 x	182	0.5	0.91	Suction	10	20
7	R32/POE32	19.9	0.3 x	27	5	1.35	Discharge	40	75
8	R32/POE32	19.9	1 x	82	3	2.46	Discharge	40	75

3.3 Experimental Setup

Based on the test matrix, the requirements of the experimental setup were defined and both the methods of determining oil retention that were studied in the literature were compared. At first look, the injection-extraction method seemed more automated compared to the tedious work of weighing involved in the direct gravimetric method. However, after taking a closer look and in particular considering the fact that different lubricants were to be tested, it was better to use a liquid refrigerant pump, which does not require any lubrication, unlike a compressor. Zoellick (2010) discussed another downside of the injection-extraction method that the flow does not mix very well after the oil is injected at the injection port and it does not simulate the flow of a real system, especially in the vertical lines unless a proper mixing method is applied. The injection-extraction method is surely more suitable for studying oil distribution in different components of the system, such as the condenser and evaporator, where it may be difficult to remove and weigh these components. However, as the focus of this study was on the gas lines, the direct gravimetric method was considered more beneficial.

3.3.1 Concept

The experimental setup was designed based on the concept used by Zoellick, (2010) for measuring oil retention. A schematic of the test setup is shown in Figure 3.1 (for a larger image of Figure 3.1, refer to APPENDIX C), where liquid refrigerant and oil flow in two parallel separate loops. Prior to entering the evaporator, the liquid refrigerant and oil are mixed. In the evaporator, the refrigerant vaporizes and exits at a desired superheat. Then, the refrigerant vapor and liquid oil mixture enters the horizontal test section and subsequently the vertical test section so that the testing for both orientations is done simultaneously. Three required pipe diameters are installed in parallel to reduce the effort of changing the pipes. The flow can be diverted to these sections as per the required conditions. After flowing through the horizontal and vertical test sections, the oil is separated from the refrigerant as it passes through a series of three oil separators. Pure refrigerant then flows through the condenser to the liquid receiver and the separated oil gets collected in an oil collector. Hot water and chilled water loops provide desired superheat through the evaporator and sub-cooling through the condenser. Pressure sensors, thermocouples, and mass flow meters are installed to measure the conditions at different state points through the system. The data from

all the sensors is sampled and stored at one-second intervals. Details of each of the sub-sections of the test-setup are described in the following sections. Brand name and model number of some of the key components used in the test setup are listed in APPENDIX E.

3.3.2 Refrigerant Loop

A magnetically driven gear pump is used to pump liquid refrigerant through the system. A variable frequency drive is installed to control the speed of the electric motor that drives the pump. As the pump has a magnetic drive, it does not require any additional lubrication. This ensures that the oil used for testing retention is not contaminated with any other lubricant. Initially, a diaphragm pump was used for pumping liquid refrigerant. One of the issues with the diaphragm pump was that, due to pulsations, the fluctuations in the mass flow rate were too high. Installing a pulsation dampener to get a smoother flow was one of the possible solutions. However, the range of backpressure at which the pulsation dampener works is too narrow and it depends on the operation pressure in the liquid line. As the testing involves a very wide range of pressures depending on the refrigerant as well as suction/discharge conditions, it would be tedious to adjust the backpressure of the pulsation dampener for each test condition. There would be a risk of damaging the dampener if the pressure was not set correctly and if accidentally the refrigerant pump was run at higher pressure. So, instead of installing a pulsation dampener, the pump was replaced with a gear pump. Using a gear pump, the fluctuations in the flow rate and pump discharge pressure were minimal. The impact of pump pulsation on the mass flow rate and pump discharge pressure for both the diaphragm and gear pumps is presented in Figure 3.3 and Figure 3.4.

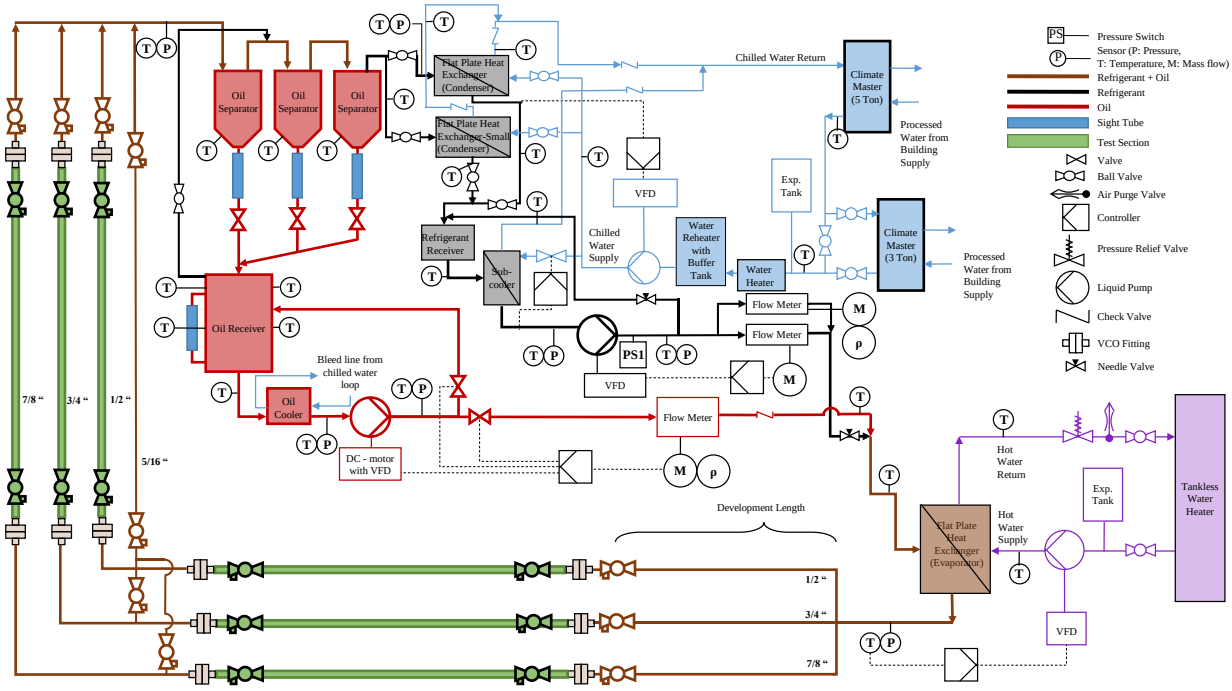

Figure 3.1: Schematic of the test setup for measuring oil retention in vertical and horizontal gas lines. (For a larger image, refer to APPENDIX C)

There are certain test conditions where the required mass flow rate in the test section is less than the minimum flow rate that the gear pump can deliver. For such conditions, some amount of refrigerant is bypassed back into the receiver, which then helps to reduce the flow rate through the system, keeping high enough flow through the pump. With the pressure sensor at the suction port along with an inline thermocouple probe, liquid sub-cooling is continuously monitored so that liquid is always fed into the suction port of the pump. A sight glass is also installed right before the suction port of the pump to get a visual check. Two Coriolis-effect mass flow meters, with nominal flow rate of 110 kg/h and 2100 kg/h are connected in parallel in the refrigerant liquid line before the mixing port. The accuracy of these flow meters stays within 0.05 % up to the turndown ratio of 20:1. Therefore, for a majority of the test conditions that are lower than 110 kg/h, the smaller flow meter is used. For flow rates higher than 110 kg/h, the larger flow meter is used, keeping the turndown ratio within 20:1 and thereby maintaining the accuracy. A picture of the test setup with all the components of the refrigerant loop is shown in Figure 3.2.

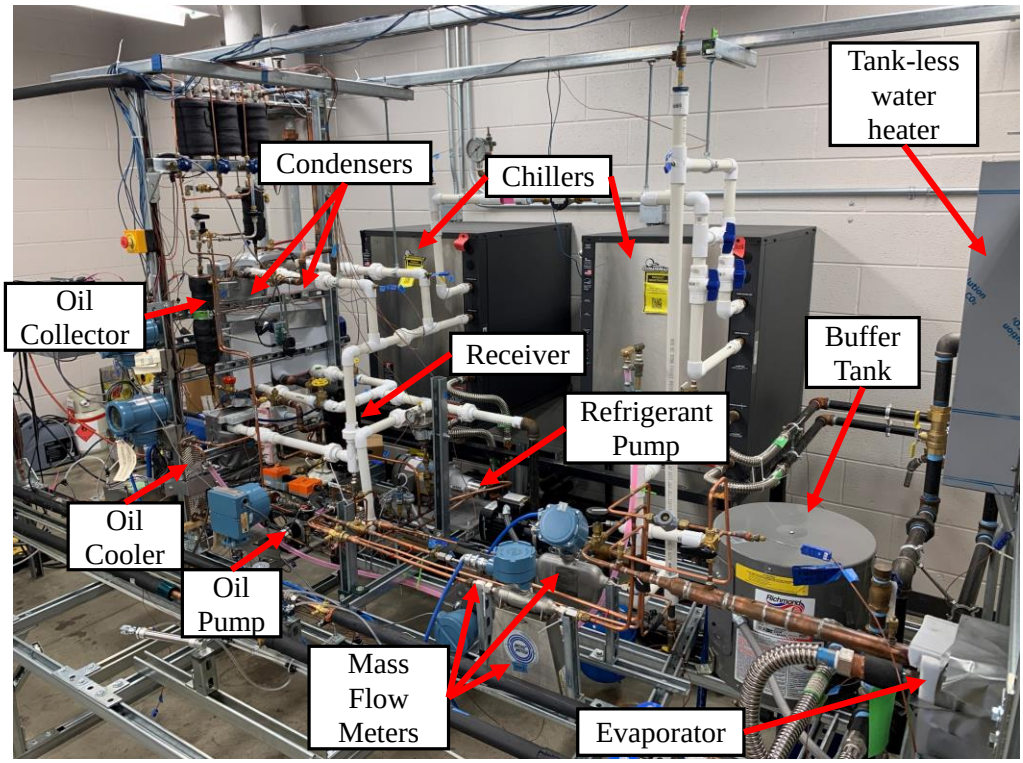

Figure 3.2 Picture showing chilled water loop and the refrigerant loop

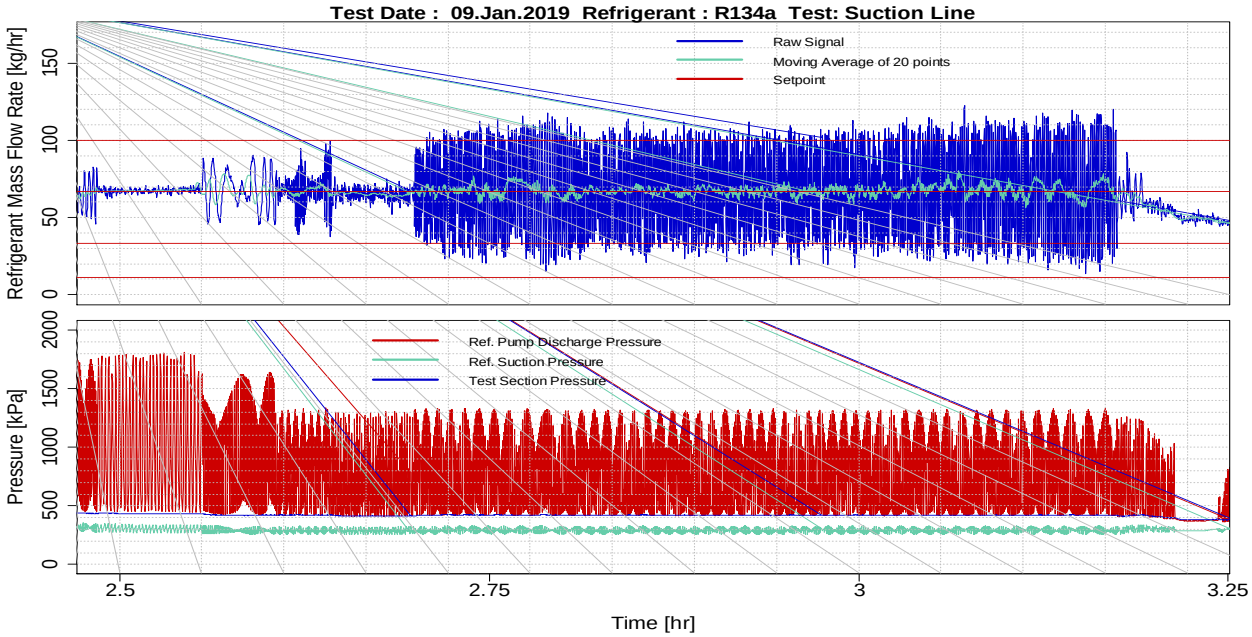

Figure 3.3: Time series plot of raw signal data showing fluctuation of refrigerant mass flow rate (top) and pump discharge pressure (bottom) due to the pulsations created while using diaphragm pump at an average flow rate of 66 kg/h using R134a

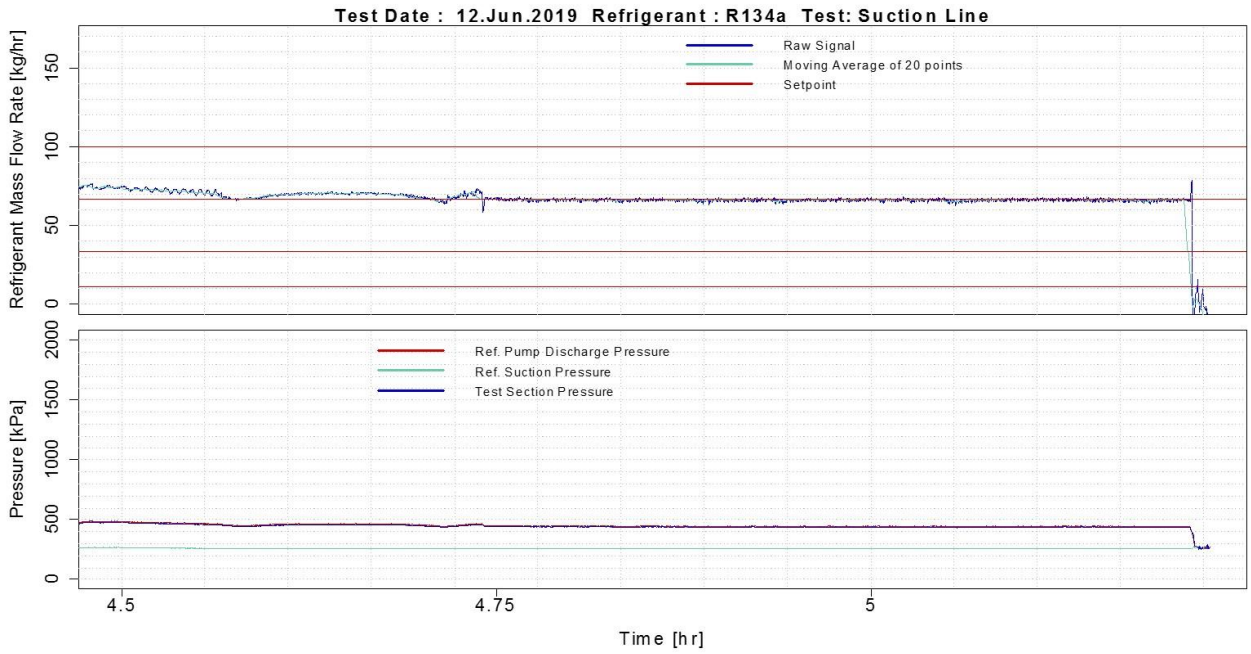

Figure 3.4: Time series plot of raw signal data of refrigerant mass flow rate (top) and pump discharge pressure (bottom) while using gear pump at a flow rate of 66 kg/h using R134a

3.3.3 Oil Loop

A mixture of refrigerant vapor and liquid oil from the test section passes through a series of oil separators, before the pure refrigerant flows back to the condenser. Three oil separators are installed in series to avoid any oil bypass as shown in Figure 3.5. It is important that all the oil is separated from the refrigerant before it flows to the condenser. This way, it can be assumed that the oil flow rate measured in the oil injection line is the oil that is going into the test section.

The oil separator selected for this setup has oil outlet on the top. A float valve sitting at the bottom of the oil separator is connected to the oil outlet with a tube and in a typical application, the valve opens and closes to keep the oil level relatively constant in the separator. Typically, the separator is installed in the high-pressure discharge line when employed in a vapor compression system and the oil outlet is connected in the low-pressure suction line. Therefore, when the float valve opens, the oil can flow because of the pressure difference. However, our test setup has a relatively small pressure difference between high and low sides of the refrigerant loop and this pressure difference may not be enough to drive the oil from the bottom of the separator to the oil outlet port on the top

of the oil separator. Therefore, a hole was drilled at the bottom of the oil separator to allow exit oil flow by gravity and thereby the oil discharge tube and internal float valve were bypassed.

To collect the majority of the oil that is separated in the oil receiver, the oil discharge valve of the first separator is kept open. The oil discharge valves for the second and the third separators are kept closed so that the operator can visually observe if there is any oil in the sight tubes installed downstream of the separators. The pressure in the oil receiver and the shell of the oil separator has to be the same for the oil to flow under gravity. In addition, when the oil is being filled in the collector, the refrigerant vapor needs to flow back to the refrigerant line to equalize the pressure. To achieve this, pressure equalization lines are installed from the oil receiver to the refrigerant line as shown in Figure 3.5. There is a pressure drop across each oil separator due to the coalescent filter that helps to separate the oil. Therefore, if the second oil separator is filled with oil and if there is a need to drain the oil from the separator to the collector, the drain valve and the pressure equalization valve in the first separator need to be shut and the corresponding drain and pressure equalization valves in the second oil separator need to be opened. Currently, all these valves are manually operated whenever there is a need to drain the oil.

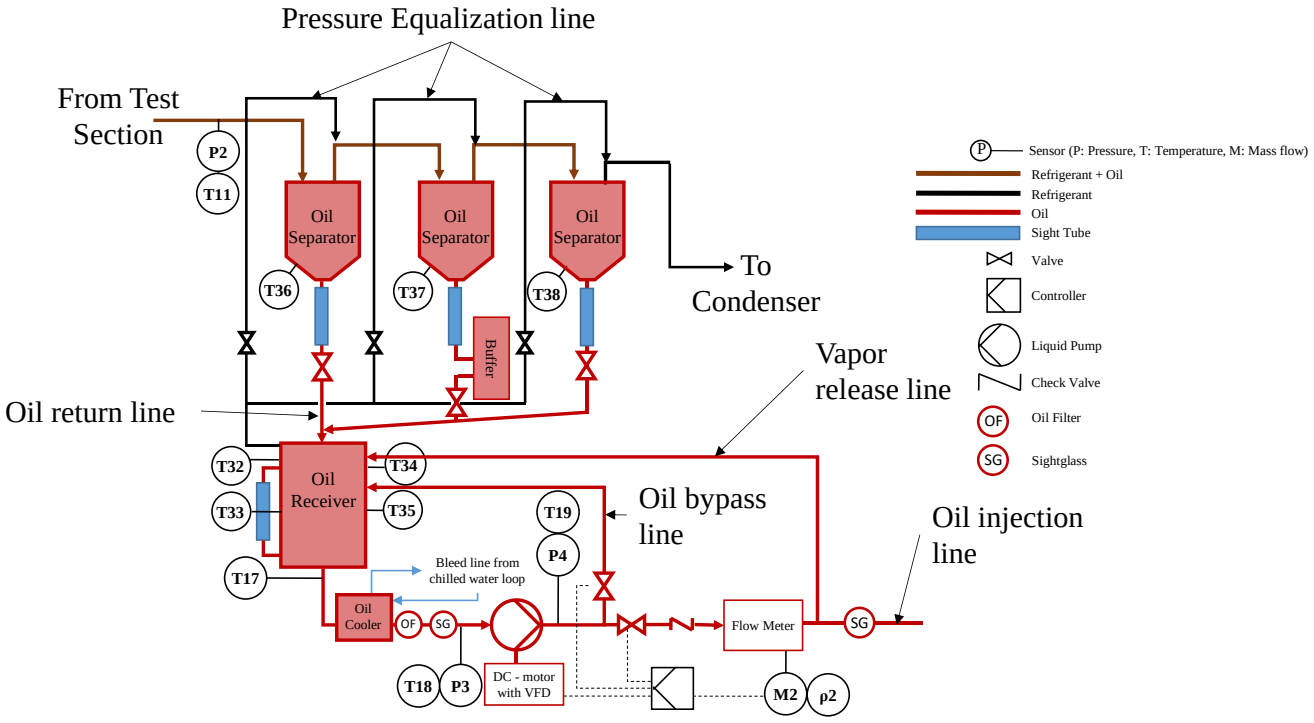

Figure 3.5: Schematic of oil loop of the test setup

Except for the high flow rate test, for all the other suction line and discharge line tests, there is not much oil bypass. However, for refrigerant mass flow rate conditions of higher than 150 kg/h, the oil bypass rate from the first separator is very high, especially at OCR values higher than 3 %. The rate is so high, that the sight tube below the second separator fills up in less than a minute. If the oil level gets too high in the second separator, the resistance for the refrigerant to flow increases, which creates higher pressure drop and disturbs the steady state of refrigerant mass flow rate. In addition, the oil in the receiver starts to exhaust to continue oil injection. If the drain valve of the second oil separator is opened to empty the oil, the suction pressure of the oil pump changes, which disturbs the steady oil injection rate. To resolve this issue, a buffer tank was added after the sight tube of the second oil separator. With this modification, the bypassed oil from the first separator gets collected in the buffer tank instead of the second oil separator, thereby not disturbing the refrigerant mass flow rate. The buffer tank is made large enough that it gives 15 minutes of steady-state operation. After the test, the oil from the buffer tank can be emptied into the oil collector by equalizing the pressure. A sight tube was added in parallel to the buffer tank to visualize the level inside the buffer tank.

A magnetically driven gear pump was selected to drive the oil in the loop. This variable-speed pump can deliver flow rates from 8.5 ml/min to 506 ml/min and can handle head pressures of up to 345 bar. For the flow rates below the minimum flow (8.5 ml/min), a bypass loop is engaged with manual metering valves on the bypass line as well as the oil injection line. Originally, two expansion valves were installed as automatic control valves to control the flow. However, the valves leaked even when they were completely closed. In addition, it was difficult to control them precisely for the required flow rate. Therefore, manual needle valves were added to the loop, which were much easier to operate in terms of achieving the flow rate. A Coriolis-effect mass flow meter with the nominal flow rate of 35 kg/h is installed in the oil injection line to measure the oil mass flow rate. Density of the mixture is also measured along with mass flow rate with this meter. A temperature probe right before the mixing port measures the oil temperature in the flow. After the oil injection port, a twisted tape is inserted inside the refrigerant line that ensures good mixing before the flow enters the evaporator. A picture taken before installation of the section with twisted tape is shown in Figure 3.6. A check valve is installed in the oil injection line to prevent refrigerant flow back into the oil loop. However, since the check valve is installed before the mass flow meter,

some refrigerant vapor flows into the remaining section of the oil injection line when the test is shut down. A vapor release line is installed along with a three-way valve near the oil injection port that helps to clear out refrigerant vapor in the entire oil injection line before starting oil injection, thereby releasing any trapped vapor.

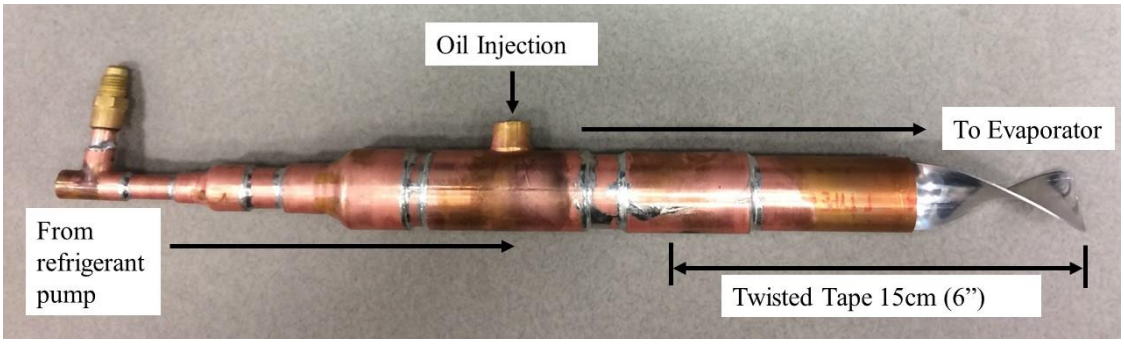

Figure 3.6: Picture taken before installing the section with mixing port and twisted tape.

Temperature controlled electric heat tapes are installed on the surface of all three oil separators and the oil receiver. Surface temperature of each of them is measured and a proportional-integral (PI) controller was developed to control the heater capacity to a particular set point temperature. The set point temperature is maintained 20 K higher than the saturation temperature at the system pressure while running suction line test conditions. While running discharge line tests, the set point temperature is increased to a higher temperature to match the superheat that is maintained in the test sections. This ensures that refrigerant does not condense into the oil separator or the oil collector, especially while running discharge line tests where the saturation temperature (~40 °C) is much higher than the ambient temperature (~20 °C). The refrigerant lines from the test section until the oil separators are insulated to minimize heat loss and possible condensation. The buffer tank is also insulated and has a temperature-controlled heat tape.

While injecting oil in the refrigerant line during certain conditions, disturbances in oil mass flow rate were observed as seen in the top plot of Figure 3.8. By monitoring the density measurement of oil and visually inspecting the sight glass in the oil injection line (before the mixing port), we realized there was vapor being trapped in the injection line which created the disturbances. The timing of the onset of the disturbances in the raw signal of oil density measurement matched the

timing for the oil mass flow rate disturbances as shown in the bottom plot of Figure 3.8. A visual check of the sight glass as shown in the picture of Figure 3.7 confirmed the vapor trap.

The vapor bubbles were generated mainly due to the low suction pressure of the oil pump. The pressure at the suction port of the oil pump tends to be lower than the refrigerant suction port. At certain test conditions, the corresponding saturation temperature reaches almost 0°C. With the ambient temperature at 20°C, the refrigerant that is dissolved in the oil started to vaporize at the pump suction port and generated vapor bubbles that eventually created disturbance in the oil injection line. These bubbles could cause damage to the oil pump in a long run. To resolve this problem, a flat plate heat exchanger as an oil cooler was added as shown in Figure 3.9. The heat exchanger is installed between the oil collector and the oil pump. A bleed line from the chilled water-glycol loop is connected to the flat plate heat exchanger in the counter flow direction. A manual flow control valve is installed in the bleed line to control the oil outlet temperature. A sight glass is also installed before the pump suction port to visually monitor for any bubbles.

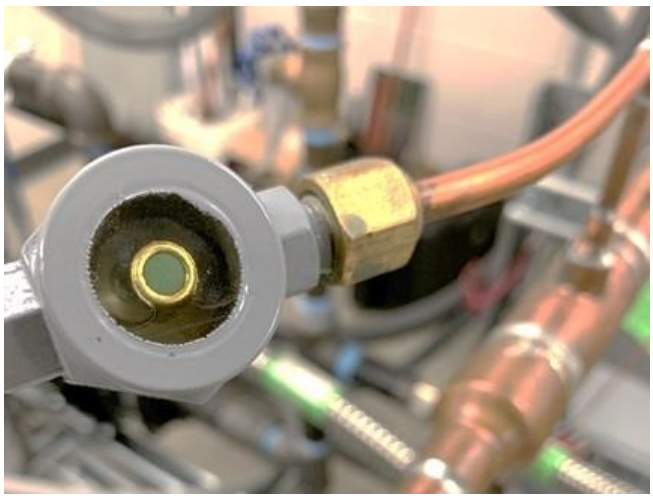

Figure 3.7: Picture of sight glass in oil injection line before mixing port

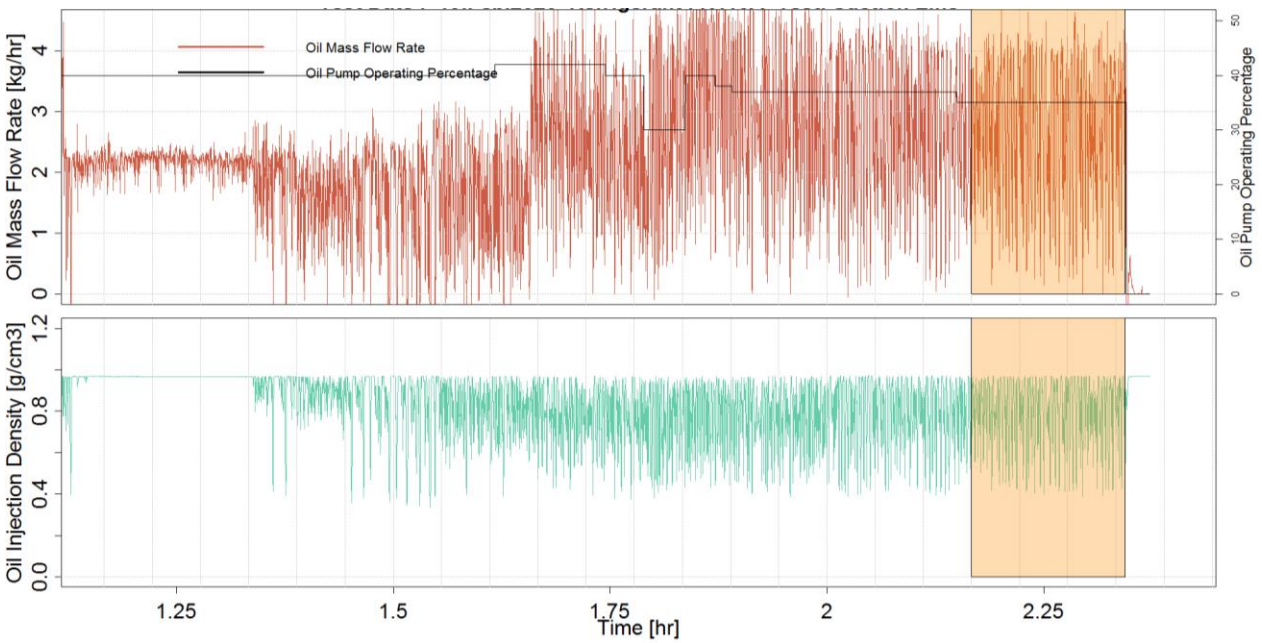

Figure 3.8: Time series plot of raw signal of oil mass flow rate (top) and density (bottom).

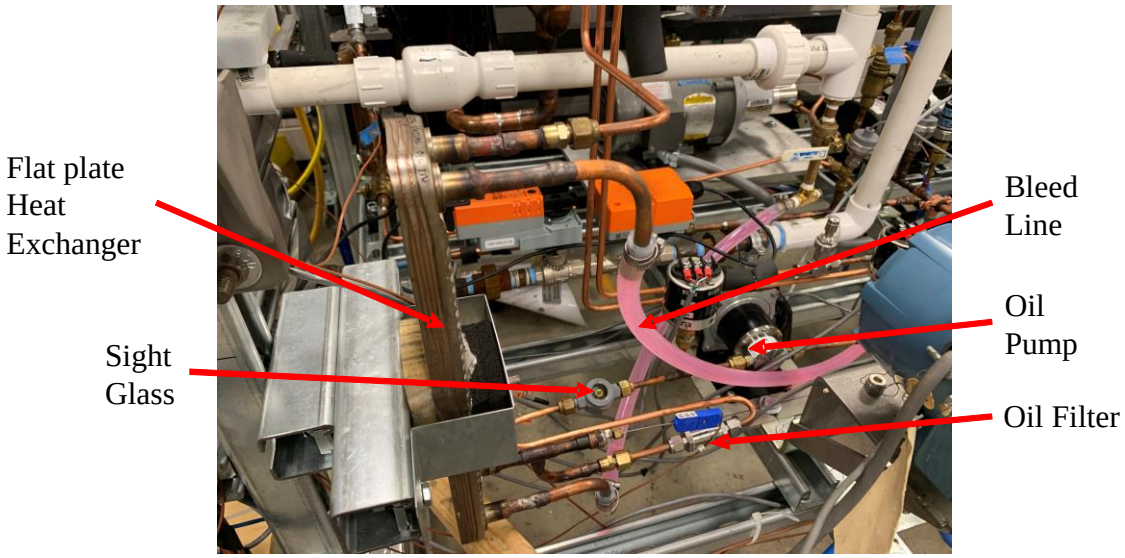

Figure 3.9: Picture of oil cooler installed before the oil suction port to avoid vapor bubble formation

3.3.4 Test Sections

Horizontal and vertical test sections ~2 m long, built using copper pipes each of three different diameters (ID:10.922 mm, ID:16.9164 mm, and ID:19.939) are shown in Figure 3.10. Before each of the horizontal test sections, another horizontal section of 1.0 m is installed which helps to develop the flow. The development length was calculated as fifty times the hydraulic diameter of the largest test section (20 mm x 50 = 1000 mm).

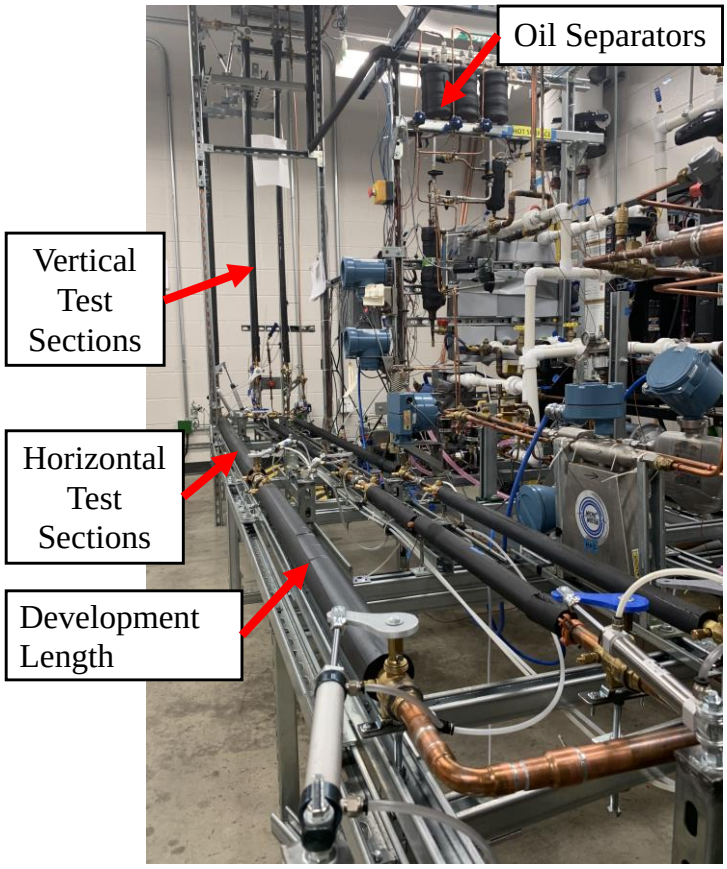

Figure 3.10: Picture of horizontal and vertical test section of 16.9 mm and 10.9 mm

To measure oil retention in the test section, the idea is to capture the refrigerant and oil at steady-state conditions. An initial thought was to use solenoid valves to stop the flow and capture the fluids in the test section. However, a solenoid valve would disturb the already developed flow in the horizontal line, because of the way the valve is constructed. In addition, there is a chance of leakage through solenoid valves. So manual ball valves, which do not have any flow restriction when they are open, are installed to capture the flow. To accurately measure oil retention, it is

essential that all four ball valves (two valves on both the ends of each horizontal and vertical test sections) are simultaneously shut. A pneumatic system consisting of an air cylinder attached to a custom designed and 3D printed lever arm was developed and implemented as shown in Figure 3.11. Through the pneumatic pressure in the cylinder, the valve can then be opened/closed. All the pneumatic lines to the cylinder are connected to a main air supply line that is fed from an air compressor. An air-solenoid valve that can be triggered via a digital signal from the controller is installed in the air supply line to control the valves. The control logic in the software is designed such that when the user clicks to shut the ball valves in the test sections, the refrigerant pump and oil pump are automatically shut down to protect them from over pressure.

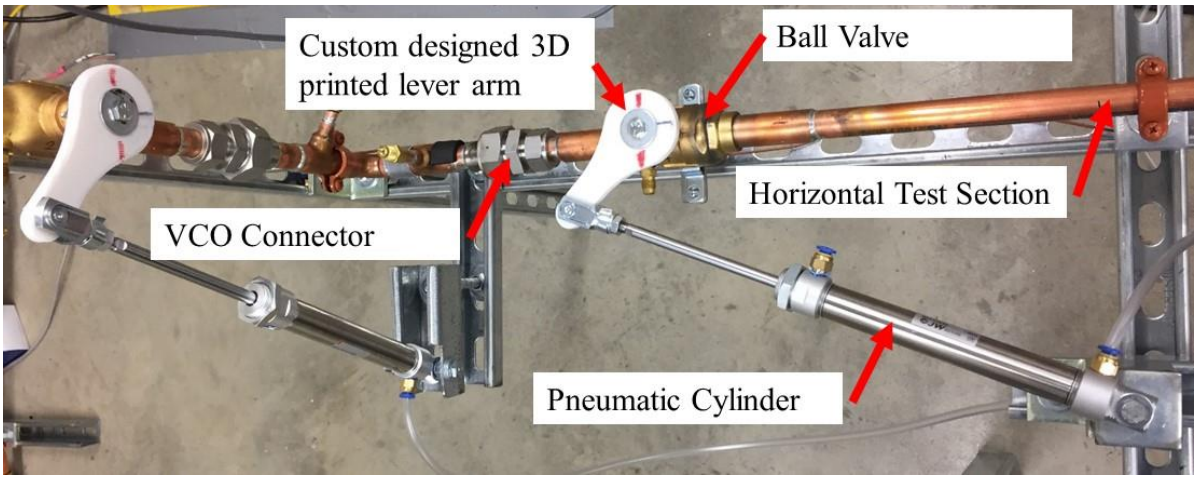

Figure 3.11: Pneumatic system to operate the ball valves installed in the test sections.

For easily removing the test sections for weight measurements, VCO fittings from Swagelok were selected as connectors (shown in Figure 3.11). These VCO fittings have an O-ring in the male part of the connector and flange with a flat surface in the female part of the connector that ensures tight sealing. After a few uses, only the O-ring wears off, and it can be easily replaced with a new one. In addition, the connector is designed such that when the nut on the female end is opened, it slides back and the test section can be easily removed without the need for additional clearance. The inner diameter of the fitting is 15.75 mm and inner diameter of the copper pipe is 16.92 mm. Therefore, there is a minor obstruction of 0.58 mm, which should not significantly disturb the already developed flow.

3.3.5 Chilled Water-Glycol Loop

A chilled water-glycol loop is a cooling source for the condenser and is shown with blue lines in the schematic in Figure 3.1. An actual picture of the chilled water loop is shown in Figure 3.2. Two water-to-water chillers with cooling capacities of 5 tons and 3 tons are connected in series. Depending on the capacity needs, either one or both can be switched on. The chilled water-glycol from the chiller(s) is supplied into a buffer tank, which is integrated with a 6 kW temperature controlled electric heater. The discharge temperature of water-glycol from the buffer tank is provided as a feedback to the temperature controller. The idea is to keep the chillers at a full load to prevent them from cycling on/off. Based on the temperature that is required at the condenser, the temperature set point for the controller of the buffer tank heater is adjusted. The minimum allowable temperature on the controller is set to -10 °C to protect the chiller from low suction pressure cutout. Below a water-glycol temperature of -10 °C, a low-pressure alarm triggers the chiller to shut down. The building utilities have a process water loop, which supplies water at ~18 °C (65 °F). Heat from the chillers is rejected to this process water loop. The reheated water-glycol from the buffer tank is then pumped to two condensers and a sub-cooler (flat plate heat exchangers). Depending on the required heat transfer capacity, either one or both of the condensers can be engaged through appropriate valves being opened and closed on the refrigerant and water-glycol lines. The pump in the water-glycol line is equipped with a variable frequency drive, which can control the mass flow rate of water-glycol flow. A maximum flow rate of 80 l/min (21 gpm) can be provided by the pump. By adjusting the water-glycol flowrate, the heat transfer capacity through the heat exchanger can be adjusted, which in turn adjusts the system pressure on the refrigerant side. Depending on the test condition, the required saturation temperature of the refrigerant for a typical suction line or discharge line can be accordingly adjusted. Water-glycol flow from the pump is split between the condensers and sub-cooler. An electronically controlled valve is installed in the sub-cooler inlet water-glycol line that can control the flowrate depending on the sub-cooling required on the refrigerant side. The water-glycol leaving the condensers and sub-cooler is fed back to the chiller to complete the loop.

For the discharge line tests, the system pressure has to be raised to reach the saturation temperature of 40 °C in the test sections. To increase the pressure, the supply temperature of water flowing to the condenser in the chilled water loop needs to be increased. At a lower refrigerant mass flow rate

of 7.5 kg/h (1/3 x Jacobs limit), the pressure induced by the pump is not high. In addition, the heat load from the condenser is greatly reduced compared to higher refrigerant mass flow rates. At such conditions, the majority of the heat load on the 3-ton chiller in the chilled water loop is provided by a 6 kW water heater in the buffer tank. As the cooling capacity of the chiller is higher than 6 kW, it leads to a situation where the chiller cools down the water-glycol to less than -10 °C and triggers a low pressure trip. Therefore, an additional inline water heater (4kW) was installed in the chilled water loop as shown in Figure 3.12. As the heater in the buffer tank already has a temperature controller, only on/off control is implemented on the additional 4kW heater. Temperature and pressure conditions at different points of the system before and after the 4 kW heater are shown in Figure 3.12. After installing the heater, a steady-state condition with 39.6 °C saturation temperature in the test section was achieved.

Before

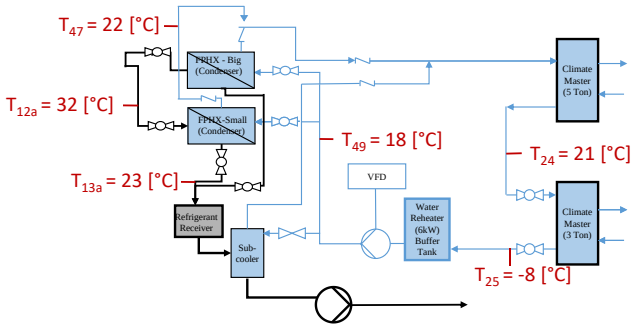

$\dot{m}_{ref} = 7.5 \left[\frac{kg}{h}\right]$

$\dot{V}_{water} = 3 \left[\frac{l}{min}\right]$ *(27 Hz)*

P_{sat} = 490 [kPa]
T_{sat} = 24.3 [°C]

After

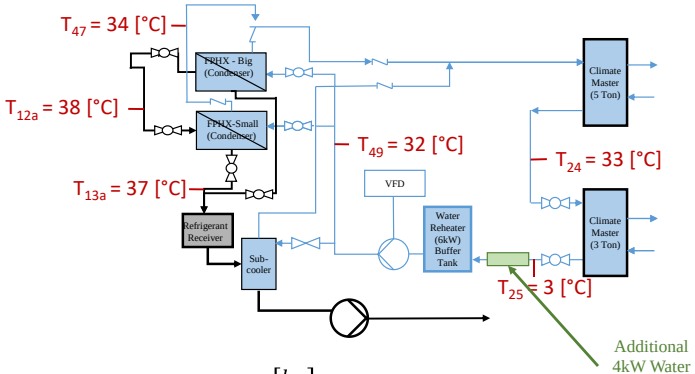

$\dot{m}_{ref} = 7.5 \left[\frac{kg}{h}\right]$

$\dot{V}_{water} = 3.6 \left[\frac{l}{min}\right]$ *(27 Hz)*

P_{sat} = 754 [kPa]
T_{sat} = 39.6 [°C]

Figure 3.12: 4 kW water heater in the chilled water loop to increase the system pressure to a desired target saturation temperature for discharge line tests with low refrigerant mass flow rate.

3.3.6 Hot Water Loop

For the evaporator, a heat source is provided using the hot water loop as shown in Figure 2.13. An electric tankless water heater with maximum capacity of 54 kW supplies hot water to the evaporator. The heater has its own independent temperature controller. The controller measures the temperature at the inlet and the outlet of the heater as well as the water flow rate. Based on these inputs, the controller adjusts the capacity of heating elements to precisely control the water outlet temperature as per the set point. A pump, equipped with a variable frequency drive supplies the hot water from the tankless water heater to the evaporator (flat plate heat exchanger). The flow rate of water can be adjusted to achieve the desired superheat on the refrigerant line. Usually, in the flat plate heat exchanger that serves as an evaporator, the liquid refrigerant is fed from the bottom of the evaporator and the super-heated vapor rises up and comes out of the evaporator from the top. However, in this setup, the liquid refrigerant is fed from the top and the vapor is forced to the bottom. This configuration may not be efficient from a heat exchanger perspective; however, it ensures that oil is not accumulated at the bottom of the heat exchanger. Other required components such as an expansion tank and other accessories such as the air purge valve, pressure relief valve for safety and service valves are also installed in the water loop.

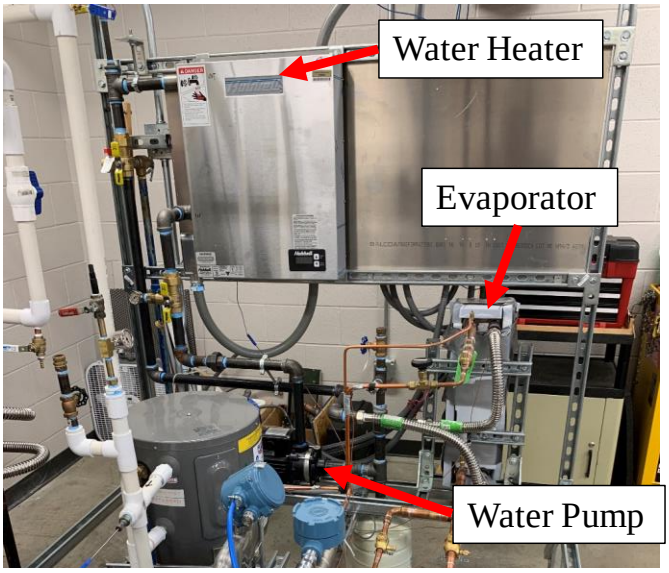

Figure 3.13: Picture showing hot water loop

3.3.7 Sensors

Pressure sensors with an accuracy of ±0.25 % are installed in the refrigerant loop. All the pressure sensors were calibrated using a higher accuracy (±0.06 %) handheld pressure calibrator (Brand: Omega, Model: PCL-1B). Temperatures are measured at several locations using Type T thermocouples. At most locations, the thermocouples are surface mounted and insulated. However,

at key locations where more accuracy is required, inline probes are inserted for temperature measurement. (For the location of the sensors, refer to the schematic of the test stand**)**

3.3.8 Controller

Control and DAQ software have been implemented in LabVIEW 2019. The signals from all the sensors are sampled at a frequency of 1 Hz and then stored in a database file. The speed of the liquid refrigerant pump, oil pump and the water pumps on the chilled water-glycol loop and the hot water loop are all controlled using analog signals from the software. PI controllers were developed and implemented for heaters to control the heating capacity to maintain the temperature on the oil separators and oil collector. The heat pumps, tank-less water heater and electric motors of pumps operate on high voltage circuits (480 VAC and 208 VAC). To protect this equipment, solid state relays are installed on the power lines and these relays are controlled through the digital signal from the software through the controller. This ensures all the components are safely shut off at the end of the testing period. In addition, shutdown criteria have been implemented to trigger shut down in an event where high pressures or temperatures occur in the system. In addition, two emergency stop switches, one inside the room on the test section and one outside the room are installed to cut the power of control signals to all the solid state relays, which then cut high voltage power from mains to the equipment.

3.3.9 Flammable Refrigerants

In the assigned test matrix, two of the four refrigerants are mildly flammable (R32 and R1234ze(E)). An approval was required from the department of Physical Facilities at Purdue University to safely test these refrigerants at the Herrick Laboratories. The amount of refrigerant required in the test setup was estimated based on the hold-up volume of different components of the test setup and their corresponding densities. With an additional 20 % contingency, approximately 14 kg of R1234ze(E) and 11 kg of R32 are required in the test setup.

The volume of the room where the test setup is installed is 197 m^3. Physical Facilities allowed 25 % of the lower flammability limit (LFL) value as a safe limit of refrigerant in the room. Based on the densities of both the refrigerants at room temperature of 20 °C and pressure of 1 atm and the

LFL values (obtained from the SDS), the allowable limit for R1234ze€ is 14.7 kg and the allowable limit for R32 is 15.1 kg. Therefore, the amount of refrigerant that is required for testing is below this allowable limit. Also, if there were a leak and all the refrigerant were to leak out from the test stand in the room, the concentration of R1234ze(E) in the room would not exceed 1.48 % (v/v) and the concentration of R32 would not exceed 2.58 % (v/v), which were acceptable.

Physical Facilities approved the testing with the following additional safety requirements.

- Refrigerant monitors that trigger room ventilation, a buzzer and a light alarm if a refrigerant leak is detected are installed. Along with these flammable refrigerants, the installed monitor also detects R134a and R410A.
- As the refrigerant is heavier than air at standard room temperature and pressure, the refrigerant would get collected at the floor level in case of leakage. To avoid any potential damage due to fire, all electronic components are installed 0.45 m (18 inch) above the floor level.
- The room is not allowed to be occupied when the test is running with flammable refrigerants. The test stand is operated remotely from the outside of the room.

3.3.10 Testing Capability

In general, some of the capabilities for testing oil retention with the current setup are as follows

- All components are designed to be able to handle a maximum pressure of 40 bar.
- Refrigerant flow rates can vary from 5 kg/h to 180 kg/h.
- Oil flow rate can vary from 0.05 kg/h to 7 kg/h.
- Heat transfer capacity can range from approximately 0.5 kW to 25 kW.
- The test facility can handle testing of mildly flammable refrigerants.
- Oil retention tests are being conducted with inner pipe diameters of 19.9 mm, 16.9 mm and 10.9 mm; however, the setup can easily be modified to test any other pipe size up to 26 mm.

Even though the basic concept of this test facility is the same as Zoellick's setup, several features are different. For example, copper pipes are used as test sections instead of clear PVC pipes, which

are more representative of actual air-conditioning and refrigeration systems. Having three oil separators in series ensures there is no oil bypass. The pneumatic system is used to ensure simultaneous closure of all the relevant valves.

3.4 Experimental Procedures

3.4.1 Test Setup Operation Procedure

The system was charged with 6.8 kg (15lbs) of R134a and 600 ml of POE 32 in the oil collector. The stagnation pressure of the system was 590 kPa at the ambient temperature of 21 °C, which matched the saturation pressure of R134a at 21 °C, confirming there were no other significant amounts of incondensable gases present in the system.

The system was run for several hours to understand its behavior and an operating procedure was developed. Key steps of operating the system are as follows.

- Step 1: Initially operate the chilled water-glycol pump (CWP) and hot water pump (HWP) at their maximum flow rates.
- Step 2: Start the 3-ton heat pump (CM3) and set the temperature of the water re-heater (CRH) to 20 °C in the cooling loop and temperature of the tank-less water heater (TWH) to 40 °C.
- Step 3: Once the chilled water supply temperature is 5 °C ~ 10 °C below the saturation temperature targeted for the suction line test (i.e. 10 °C), turn on the liquid refrigerant pump (LRP) and run at 45 % (27 Hz) speed. A sight glass is installed in the suction line of the LRP. Once liquid starts to show up in the sight glass, reduce/increase the frequency associated with the refrigerant flow rate to the target flow rate for a particular test condition and wait until it reaches steady-state.
- Step 4: Check pressure at the inlet and outlet of the test section. Adjust the chilled water temperature by changing the CRH temperature, such that the system pressure matches the desired pressure. Switch on the 5-ton heat pump (CM5) if additional cooling capacity is required. Alternatively, to reduce the capacity through the condenser, lower the flow rate of water-glycol from 100 % and thereby increase the system pressure. The desired

pressures associated with the saturation temperatures for each test for a particular refrigerant are shown in Table 3.3.

- Step 6: Adjust superheat at the test section inlet by changing the TWH temperature or the water flow rate of the HWP.
- Step 8: Start the oil pump (OP) and adjust the oil mass flow rate to meet the target OCR value. Wait until the oil return begins. The system pressure may need to be re-adjusted as it may have changed because of oil injection.
- Step 9: Let the system run at steady state for 10 minutes and then proceed to the oil retention measurement procedure.

Table 3.3: Saturation pressures and temperatures corresponding to discharge and suction line tests for different refrigerants

Sr.	**Refrigerant**	**Suction Line Test**		**Discharge Line Test**	
		Sat. Temp [°C]	**Sat. Pressure [kPa]**	**Sat. Temp [°C]**	**Sat. Pressure [kPa]**
1.	R134a	10	415	40	1017
2.	R410A	10	1085	40	2420
3.	R32	10	1107	40	2478
4.	R1234ze(E)	10	310	40	767

3.4.2 Steady-State Condition

Steady-state conditions for each test are determined by monitoring the refrigerant mass flow rate, system temperatures and pressures, and oil mass flow rate. However, the oil flow takes longer to reach steady-state. When the oil injection is started, the refrigerant and oil mixture go through the evaporator and the horizontal and vertical test sections and along the way, some oil starts to be retained and slowly, an oil film builds up in the test sections. During this initial period, there is no oil return. After a few minutes, the oil starts to return and can be visually seen in the sight tube connected in the drain port of the first oil separator. Eventually, when the mass flow rate of oil return becomes equal to the mass flow rate of injection, the condition of the oil flow in the system is considered to be at steady-state. At steady state, the level in the oil collector remains at a constant level. This level can be visually monitored by looking at the oil meniscus in the sight tube that is connected in parallel to the oil collector as shown in Figure 3.14. A tape measure is also attached next to the sight tube to observe the relative change of meniscus and a camera is installed to monitor this level on the operator's computer screen. The system is run at a steady-state condition for ten minutes before the valves of the test sections are shut for gravimetric oil retention measurement.

Figure 3.14: Picture of sight tube connected in parallel to the oil collector for monitoring level

3.4.3 Gravimetric Test Measurement Procedure

The gravimetric method is tedious, but is one of the most accurate methods to measure oil retention. ASHRAE Standard 41.4 recommends using the gravimetric method as a primary method to measure the proportion of lubricant in liquid refrigerant. If any alternate method is used, the standard recommends calibrating the method against this primary gravimetric method. So, for

measuring oil retention data for the initial tests, the gravimetric method is being used. As this method is being considered as a primary method, a detailed stepwise procedure of the method is described in this section.

- **Step 1- Isolating test sections to capture oil retention:**

Once the system reaches a steady state at the desired test condition in terms of OCR, refrigerant mass flow rate, system pressure and superheat; oil and refrigerant in the test sections are captured by pneumatically closing the ball valves before and after the test sections.

- **Step 2- Test section disassembly from the setup:**

After isolating the test sections, the ball valves on the system side are also closed manually to ensure the refrigerant in the system stays inside when the test sections are removed. VCO connectors between the system and the test sections are unscrewed to easily remove the test sections. The O-rings from the VCO connections are removed so that they do not come in contact with acetone and wear out. The thermocouples measuring the test section temperatures are also disconnected from the quick disconnects and the pneumatic cylinders are detached from the lever arms. The disassembled test section is then secured vertically on a collection stand as shown in Figure 3.15**.**

Figure 3.15: Test section held vertically on a stand.

- **Step 3- Empty beaker weight measurement:**

Two 50 ml (~34 g) beakers along with a magnetic stirrer in each are washed thoroughly with soap water and then dried. Using an electronic weighing scale (accuracy 0.1 mg) as shown in Figure 3.17, the mass of each empty beaker along with its stirrer is measured in grams. One beaker is used to collect oil from the horizontal test section and another beaker used for the vertical test section. The beakers are labeled to avoid any confusion.

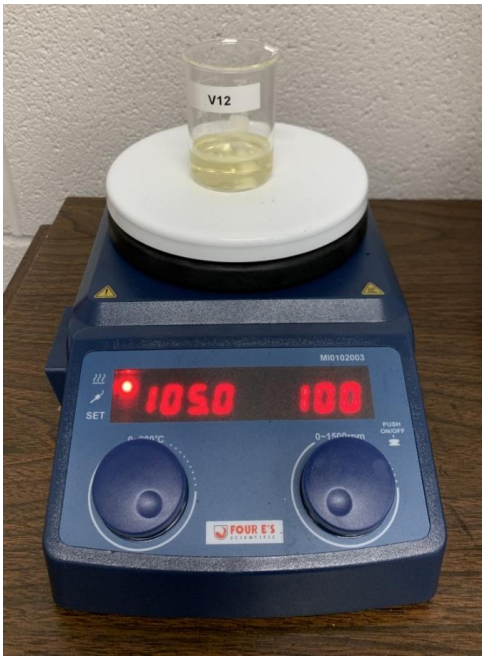

Figure 3.16: Temperature and rotational speed controlled heater with magnetic stirrer

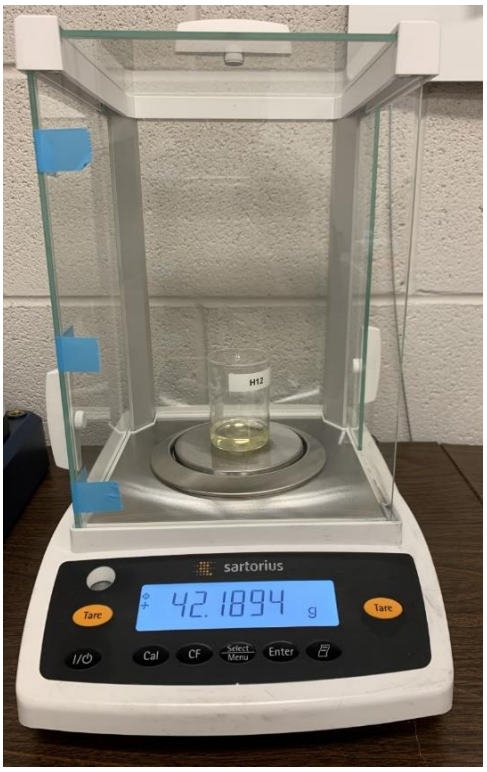

Figure 3.17: Electronic weighing scale to measure net oil mass

- **Step 4- Releasing refrigerant and recovering oil into the beaker using acetone:**

As the refrigerant in the test section is less than 20 g (0.7 oz), it is difficult to recover this small amount of refrigerant. Therefore, the refrigerant is released to the ambient by slowly opening the valve on the top ensuring no oil escapes along with the refrigerant. Keeping the bottom valve closed, 20 ml acetone is poured in from the top valve using a graduated glass dropper. The test section is manually shaken to ensure oil is dissolved in the acetone and is not stuck to the walls of the test section. The test section is then mounted back on the stand and pressure built up due to shaking is relieved by opening the top valve. By opening the bottom valve slowly, the oil-acetone mixture is carefully collected in the beaker. The bottom valve is then closed and 10 ml of acetone is poured from the top to rinse and collect any residual oil.

- **Step 5- Evaporating acetone from the mixture using a heater and magnetic stirrer:**

The collected oil-refrigerant mixture in the beaker is placed on a hot plate, which has the capability of rotating the magnetic stirrer as shown in Figure 3.16. The device has control of temperature and rotational speed. The temperature of the hot plate is set to 105 °C to evaporate acetone which has a boiling point of 56 °C and any water, if present. The boiling point of POE 32 being >200 °C, the oil does not evaporate at the set temperature. For uniform heating, the stirrer speed is set to the lowest speed of 100 rpm, which is fast enough for a small beaker. The mixture is heated until no vapor bubbles are seen on the free surface of the oil. The time for evaporation varies depending on the amount of mixture, however it is about 25 to 30 minutes.

- **Step 6- Test section assembly and evacuation using vacuum pump:**

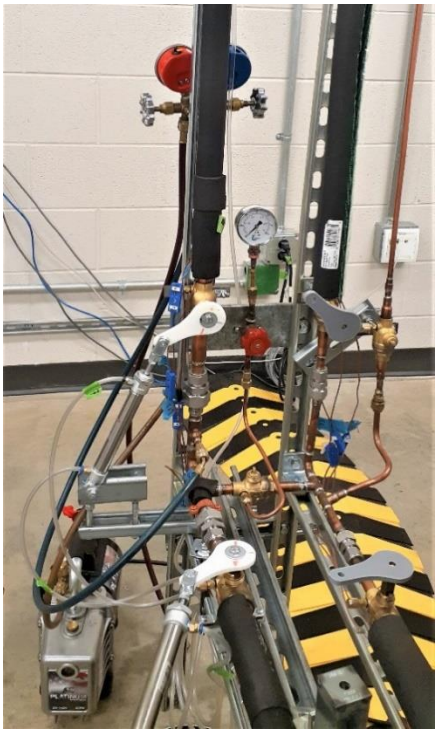

Figure 3.18: Evacuating the test sections before charging back with refrigerant

While the acetone is evaporating, the test section is put back in place. The O-rings are checked visually for any wear and replaced with new ones if needed. They are placed back into the slots in the VCO connectors and the test sections are mounted on the test stand. Connectors are tightened, thermocouples are connected back, and the pneumatic cylinders are attached back to the levers. A vacuum pump is connected through a service port on the test section as shown in Figure 3.18. The test section is then evacuated by running the vacuum pump for 20 minutes. The pump is switched off and the valve on the gauge set is shut to monitor the vacuum pressure of the test section using an analog dial for 30 minutes. If the pressure does not rise in 30 minutes, the test sections are considered leak proof. The vacuum pump is again run for 30 minutes and then the ball valves isolating the test sections from the stand are opened and the refrigerant is charged in to be ready for the next test. A digital vacuum gauge is connected to monitor the vacuum pressure. A vacuum pressure of 1000 microns is achieved to ensure all the non-condensable gases are evacuated.

- **Step 7- Oil weight measurement:**

Once all the acetone is evaporated and no more bubbles are seen, the beaker is left to cool down. The mass of the beaker along with stirrer and oil is measured in grams. The empty weight beaker and the oil-filled beaker for both the test sections (horizontal and vertical) are recorded in a test data register in an electronic form of an MS Excel spreadsheet. The difference in the recorded masses gives the actual oil retention in the horizontal and vertical test sections at a particular operating condition.

3.4.4 Uncertainty in Measurement

To determine the uncertainty of this gravimetric measurement method, multiple tests were carried out by adding a known amount of oil in the test sections and then following the measurement procedure to recover the oil. The process that was used is shown pictorially in Figure 3.19. The differences in the amount of oil added and recovered were compared to estimate the measurement uncertainty.

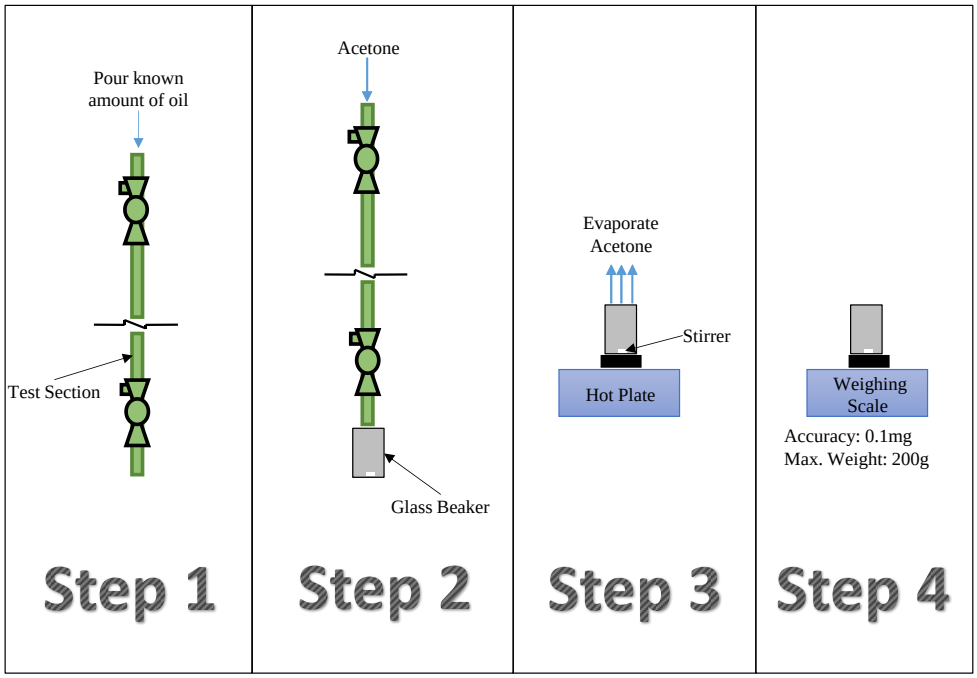

Figure 3.19: Procedure followed for evaluating uncertainty in oil retention measurement method

- The mass of oil charged in the test section was calculated by measuring a glass beaker before and after filling oil into the test section from the beaker.

- The test sections were cleaned two times between each measurement to ensure that the there was no residual oil left over from any previous measurements.
- For cleaning, 20 ml of acetone was poured in the test section and it was then thoroughly shaken to dissolve any oil and then rinsed off.

Ten measurements were carried out as per the mentioned procedure. Table 3.4 shows the test data of these ten measurements. It can be seen that the maximum relative difference between the amount of oil charged and amount of oil recovered is less than 6 %. A parity plot of the same data is shown in Figure 3.20. The average relative difference is 3.3 %, therefore we assumed a relative uncertainty in measurement of oil retention of 3.3 %.

Table 3.4: Data showing the relative difference in oil retention measurement using gravimetric method

Sr.	Test Section		Oil Mass Charged [g]			Oil Mass Recovered [g]			Difference [g]	Relative Diff
	Name	Inner Diameter [mm]	Before	After	Net	Empty Beaker	Oil + Beaker	Retained		
1	H34	16.9	12.1246	8.6098	3.5148	37.659	41.172	3.5130	-0.0018	-0.1 %
2	V34	16.9	15.7881	8.3964	7.3917	34.0609	40.9104	6.8495	-0.5422	-7.3 %
3	H12	10.9	10.5405	8.4828	2.0577	34.5679	36.6307	2.0628	0.0051	0.2 %
4	V12	10.9	11.9261	8.3997	3.5264	34.9813	38.4084	3.4271	-0.0993	-2.8 %
5	H34	16.9	32.5875	24.676	7.9112	37.6553	45.0919	7.4366	-0.4746	-6.0 %
6	V34	16.9	39.1771	24.728	14.449	34.0592	48.0275	13.9683	-0.4807	-3.3 %
7	H12	10.9	14.0206	8.4472	5.5734	34.5669	39.9741	5.4072	-0.1662	-3.0 %
8	V12	10.9	16.2328	8.4541	7.7787	34.9807	42.6979	7.7172	-0.0615	-0.8 %
9	H34	16.9	49.5058	30.1535	19.3523	37.6559	55.9771	18.3212	-1.0311	-5.3 %
10	H12	10.9	36.1306	24.6763	11.4543	34.5722	45.5411	10.9689	-0.4854	-4.2 %

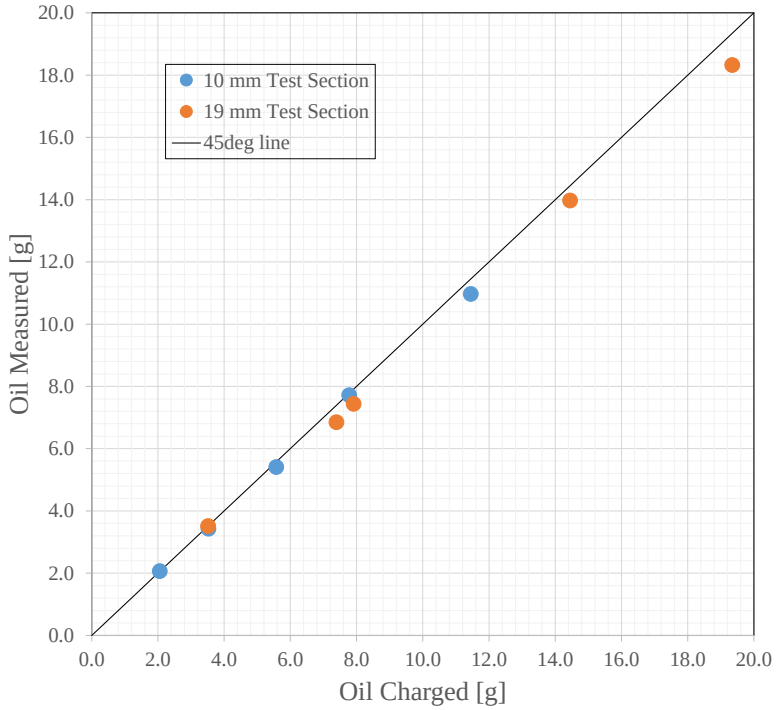

Figure 3.20: Recovered oil measured in test section compared with amount of oil charged

The desired length of each test section was 2 m. However, due to practical limitations there is a variance in the actual length of the test section. The test section length was measured with a tape that had a minimum scale of 1 mm. Therefore, the absolute uncertainty in the length measurement was considered to be 1 mm.

3.4.5 Solubility of Acetone in Oil

In step 3 of Figure 3.19, the acetone-oil mixture is heated to evaporate the acetone. At the end of evaporation, some amount of acetone stays dissolved in the oil based on its solubility. In order to understand the solubility of acetone in oil, a known amount of oil was taken in a clean and dry glass beaker with a magnetic stirrer in it. Approximately, 20 ml of acetone was added in the beaker with oil. The mixture was then weighed for a reference. The mixture was boiled at a temperature of 105 °C until there were no bubbles seen in the beaker and it was assumed that the acetone was evaporated. The beaker was set aside to cool off for one hour. The oil in the beaker with the stirrer was measured again and compared with the amount of oil that was added in the beaker. As shown in Table 3.5, the relative difference in the mass measurement was less than 0.45 % for three of the four cases. In one case, the relative difference was 1.75 %. As these differences are not significant,

the solubility of acetone in the oil is assumed to be negligible and is not corrected in the experimental data points collected.

Table 3.5: Solubility of acetone in oil during oil retention measurement

Sr.	Beaker Name	Beaker + Stirrer [g]	Beaker + Stirrer + Oil [g]	Beaker + Stirrer + Oil + Acetone [g]	Beaker + Stirrer + Oil after boiling [g]	Difference [g]	Relative Difference
1	H34	37.657	52.173	74.582	52.407	0.234	0.45 %
2	V34	34.057	42.694	65.615	42.835	0.141	0.33 %
3	H12	34.906	39.525	62.945	39.577	0.052	0.13 %
4	V12	34.977	57.091	80.258	58.093	1.001	1.75 %

3.5 Experimental Data

3.5.1 Discussion of Experimental Data

Test conditions associated with the refrigerant/oil combination, R134a/POE32 with 16.9 mm pipe for discharge and suction line conditions are listed in Table 3.6 and Table 3.7. The plots in Figure 3.21 and Figure 3.22 show the amount of oil retained per unit length in the test section with respect to the refrigerant mass flux for suction line and discharge line conditions respectively. Similar tables and plots for the other refrigerant/oil combinations are listed in APPENDIX D . Refer to APPENDIX F for the steady-state data for a particular test condition. The following inferences derived from these results are consistent with the literature:

- As the refrigerant mass flux drops below the Jacobs limit, the oil retention drastically increases for the horizontal line test section. Oil retention for the vertical line is not measured below the Jacobs limit, as the oil flow will not reach steady operating conditions because of oil accumulation.
- Oil retention increases for the entire range of refrigerant mass flux as the OCR increases, which is intuitive.
- The vertical lines retain more oil compared to the horizontal lines because of the gravity effects. However, the difference in oil retention between vertical lines and horizontal lines decreases as the refrigerant mass flux increases, because the gravity effects become less dominant at higher refrigerant flow rates.

- Figure 3.22 and Figure 3.23 provide plots of oil retention versus mass flux for discharge and suction conditions for the horizontal and vertical lines. In comparing these results, the discharge line conditions retain more oil than the suction line conditions.

These trends of oil retention are consistent with other refrigerant/oil combinations. For ease of plotting, the OCR values were discretized to 0.5 % (blue), 3 % (orange) and 5 % (green), whereas the actual steady-state OCR values were different and are labeled in a text box next to each data point for easy reference. It is also important to note that the oil flow rate in these plots was not corrected for the amount of liquid refrigerant dissolved in the oil. Therefore, the OCR reported is simply based on the measured mass flow rate of refrigerant and the measured mass flow rate of oil injection, which includes liquid refrigerant based on its solubility. However, this solubility is corrected in the modeling work, so the prediction results from the model includes the corrected OCR. Also, the saturation temperature and superheat of all the points on the suction line test (Figure 3.21) are not the same. For example, the saturation temperature for 11 kg/h and 33 kg/h was 10 °C, however for 66 kg/h, it was 15 °C. It is important to be aware of these differences, while making any inferences from these plots. The steady-state saturation temperature and superheat are also part of the label.

Due to the practical limitations of the test stand, a few conditions were modified or eliminated (stroked out in red) in Table 3.6 and Table 3.7:

- Oil flow rates below 0.08 kg/h and above 5 kg/h were eliminated due to a practical limitation of the oil pump.
- During the suction line tests, especially for higher flow rates of 66 kg/h and 100 kg/h, the test section pressure reaches almost 800 kPa (Saturation Temperature @ 800 kPa = 31°C). This pressure increases substantially with oil injection, especially at 3% and 5% OCR. To get the test section saturation temperature down to 10°C, the water supply temperature that is fed to the condenser is reduced. But the water temperature cannot be lowered below -10°C, because the chiller trips due to low suction pressure. So, for the refrigerant flow rates of 66 kg/h and 100 kg/h, the test section saturation temperature for suction line testing was changed to 20°C instead of 10°C in the test matrix as shown in Table 3.6.

- Similarly, for other refrigerant/oil combination there were certain conditions where the refrigerant mass flow rates at 3 x Jacobs limit were reduced down to 2.5 x Jacobs limit to stay under the refrigerant pump operation limit.
- All such modifications have been marked in red. However, the ultimate goal was to build a model using the experimental data. Having a rich variation in the data at steady-state conditions, helped to build a good model. Therefore, it is not absolutely necessary to accurately match the target as long as we had steady-state values with some variance.

Table 3.6: Test matrix for R134a/POE32 suction line conditions

Sr. No.	Refrigerant/ Lubricant	Test Section ID [mm]	Ref. Mass Flow Rate [kg/hr]	Oil Mass Flow Rate [kg/hr]	Test Section Saturation Temperature [C]	Test Section Inlet Temperature [C]	Test ID
1 (Baseline)	R134a/POE 32	16.9	11±3	~~0.055~~	~~10~~	~~20~~	-
				0.33±0.05	10±2	20±2	37
				0.55±0.11	10±2	20±2	34
			33±5	0.165±0.13	10±2	20±2	35
				0.99±0.17	10±2	20±2	36
				1.65±0.33	10±2	20±2	33,39
			66±5	0.33+0.26	~~10~~ 15±4	~~20~~ 25±2	41,42
				1.98±0.33	~~10~~ 15±4	~~20~~ 25±2	58
				3.3±0.66	~~10~~ 15±4	~~20~~ 25±2	59
			100±5	0.5±0.4	~~10~~ 20±4	~~20~~ 30±2	43
				3±0.5	~~10~~ 20±4	~~20~~ 30±2	60
				~~5±1~~	~~10±2~~	~~20±2~~	-

Table 3.7: Test matrix for R134a/POE32 discharge line conditions

Sr. No.	Refrigerant/ Lubricant	Test Section ID [mm]	Ref. Mass Flow Rate [kg/hr]	Oil Mass Flow Rate [kg/hr]	Test Section Saturation Temperature [C]	Test Section Inlet Temperature [C]	Test ID
1 (Baseline)	R134a/POE32	16.9	17±3	~~0.085±0.068~~	~~40±4~~	~~64±4~~	-
				0.51±0.085	40±4	64±4	50,51
				0.85±0.17	40±4	64±4	52
			51±5	0.255±0.20	40±4	64±4	49
				1.53±0.26	40±4	64±4	47
				2.55±0.51	40±4	64±4	48
			103±5	0.515±0.41	40±2	64±4	55
				3.09±0.52	40±2	64±4	53
				5.15±1.03	40±2	64±4	54
			155±5	0.775±0.62	40±2	64±4	57
				4.65±0.775	40±2	64±4	56
				~~7.75±1.55~~	~~40±2~~	~~64±4~~	-

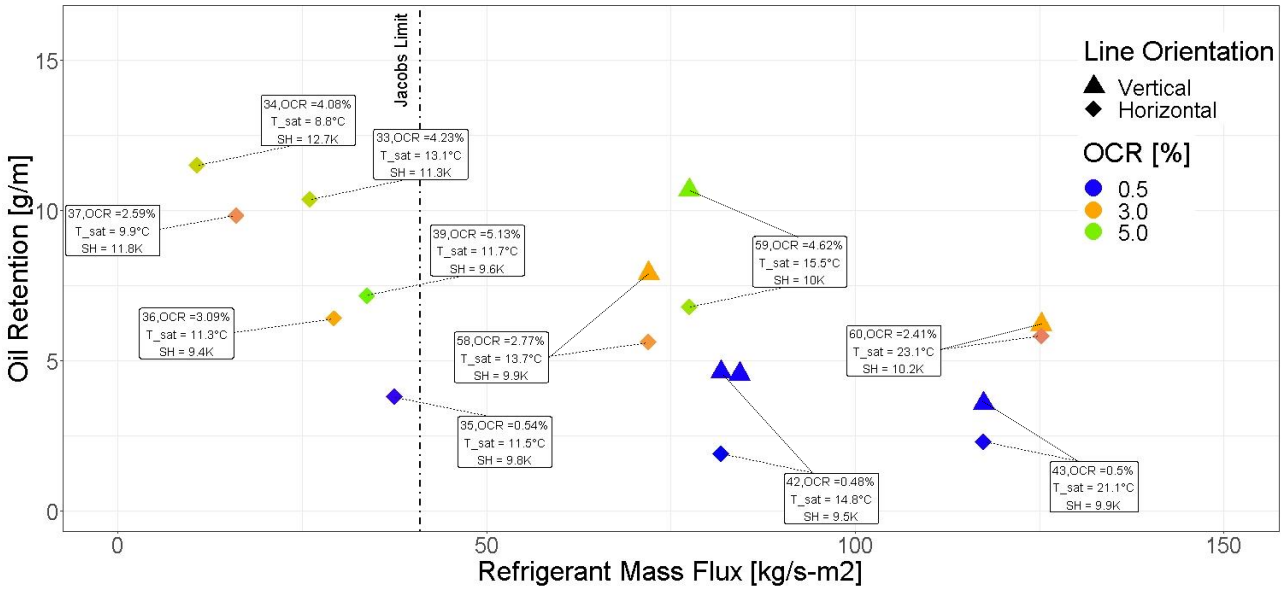

Figure 3.21: Oil retention in16.9 mm vertical and horizontal suction gas lines with R134a/POE32

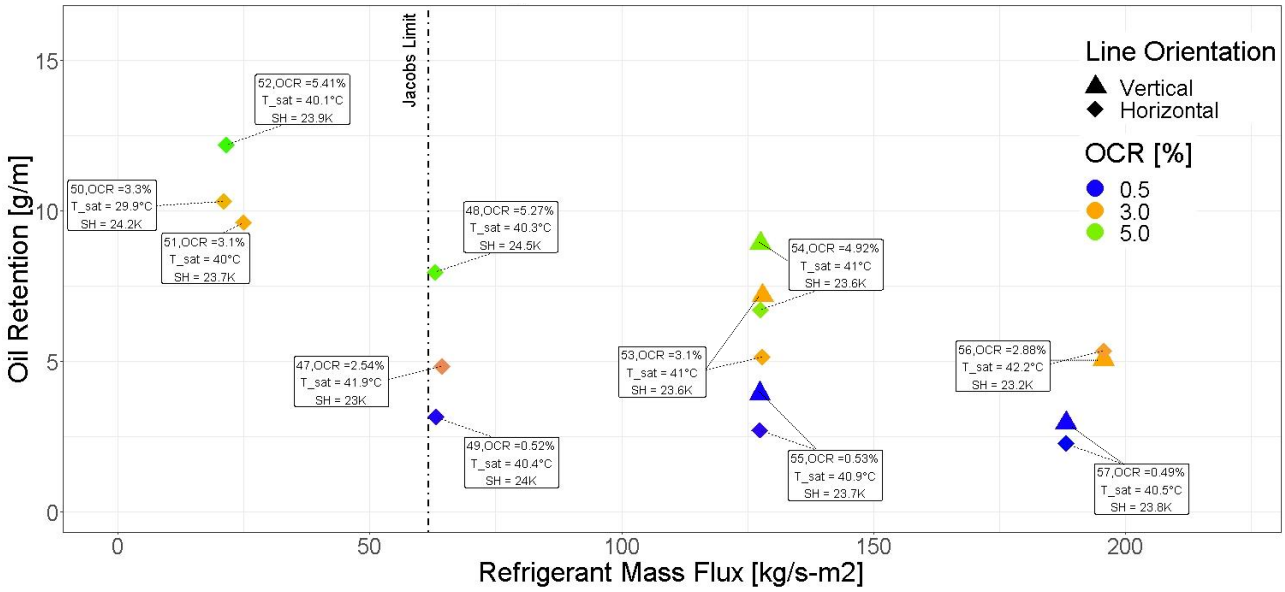

Figure 3.22: Oil retention in 16.9 mm vertical and horizontal discharge gas lines with R134a/POE32

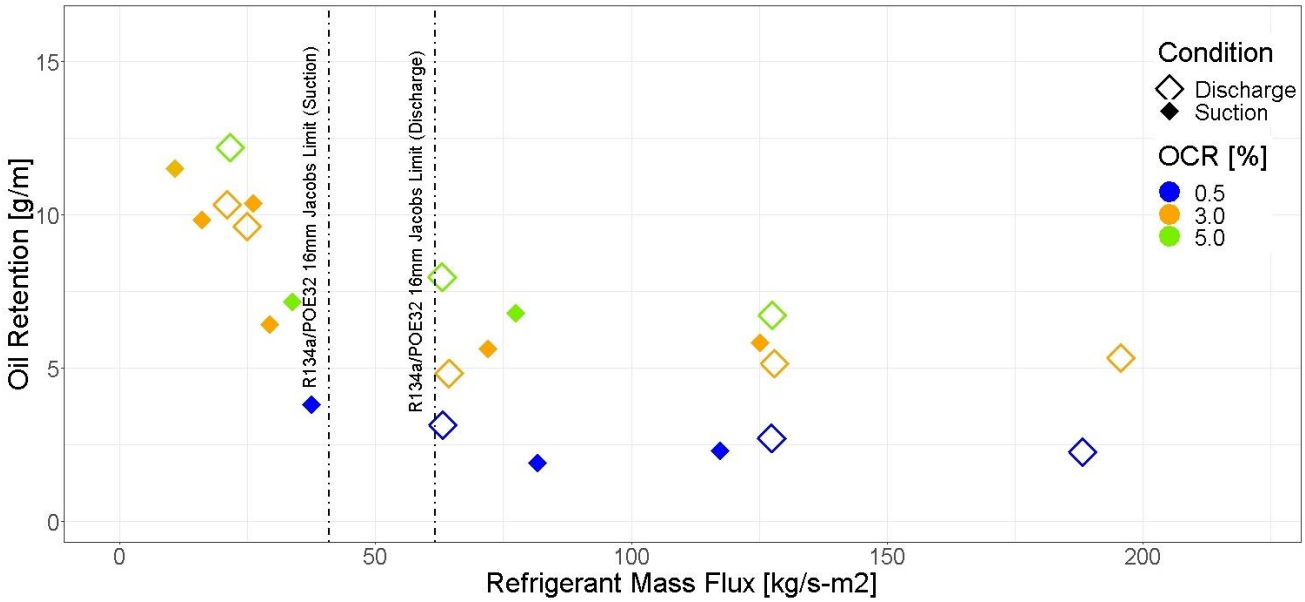

Figure 3.23: Oil retention in16.9 mm horizontal suction and discharge lines with R134a/POE32

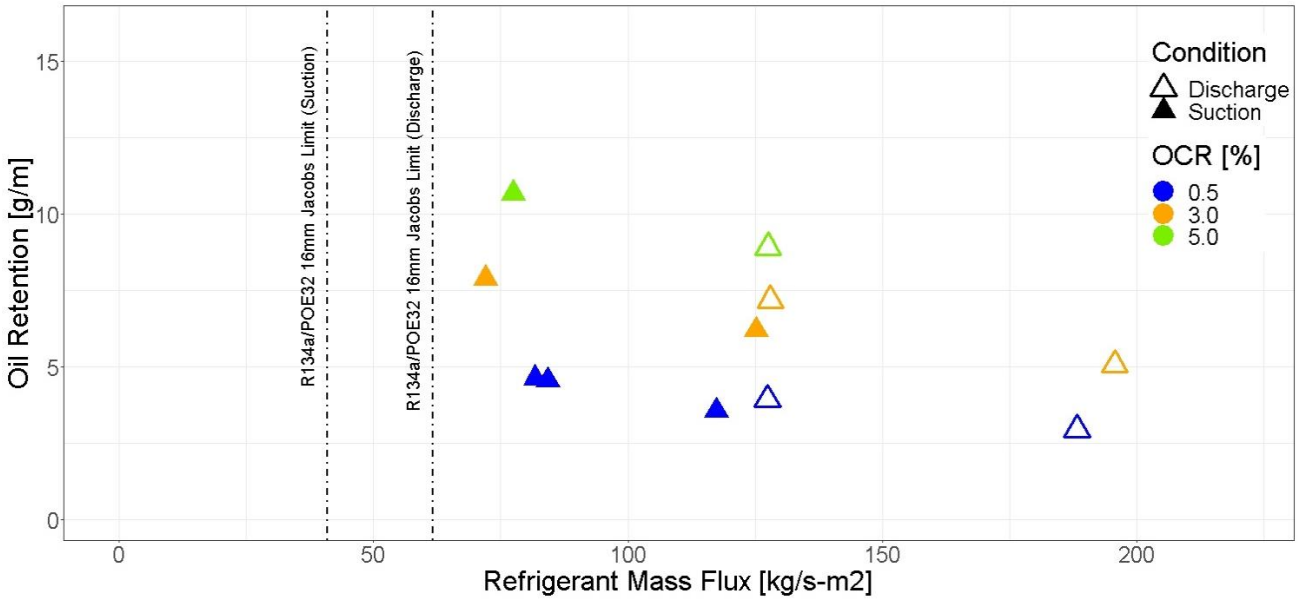

Figure 3.24: Oil retention in 16.9 mm vertical suction and discharge lines with R134a/POE 32

3.5.2 Oil Return in Vertical Lines at Mass Flux Lower than Jacobs Limit

As we inject oil in the system, some amount of oil starts to reverse in the vertical line and starts to accumulate, especially at refrigerant flow rates near or lower than the Jacobs limit. This oil accumulation increases the pressure in the test section, which creates fluctuations in the oil injection because of the change in pressure difference at the injection port. Also, the refrigerant mass flow rate starts to decline, because at the same refrigerant pump frequency, the pressure increases and the pump cannot maintain the mass flow rate. After a few minutes, the accumulated oil flows out of the test section as a slug and a high amount of oil flow is observed to return in the sight tube connected at the discharge of oil separator. As all the oil clears out from the test section, the test section pressure starts to reduce and eventually, the oil injection starts again. With this cyclic behavior, it is practically impossible to achieve a steady state of oil flow.

This cyclic behavior is mainly observed at low refrigerant mass flow rates, which are at 1x Jacobs limit and 1/3x Jacobs limit, respectively. At these low refrigerant mass flow rates, it is meaningless to measure oil retention in the vertical line; however, it is crucial to understand the oil retention in horizontal lines. To be able to measure oil retention in a horizontal line, a bypass line with a valve was added between the 16.9 mm and 10.9 mm lines near the 90° elbow that connects the horizontal and vertical test sections. A similar bypass line was added for the 19.9 mm line. For the test

conditions with the low refrigerant mass flow rate, the flow after the horizontal test section is diverted to the smaller diameter line in the vertical section, which increases the mass flux and helps to easily return the oil back to the oil collector and eventually steady oil flow is achieved. Comparing serial numbers 1 and 2 of Table 3.8, it can be observed that at the same refrigerant mass flow rate of 33 kg/h, the mass flux can be increased to 2.4x Jacobs limit in the vertical line by reducing the pipe size. This helps in oil return in the vertical section while keeping a constant oil flow rate in the horizontal section. For a mass flow rate of 11 kg/h, an additional line with an inside diameter of 6.3 mm was installed for increasing the mass flux. In conclusion, for refrigerant flow rates near or lower than the Jacobs limit, oil retention is measured only for horizontal lines.

Table 3.8: Jacobs limit at lower refrigerant mass flux and different pipe size

Sr. No.	Test Section	Refrigerant Mass Flow Rate [kg/h]	Test Section Inside Diameter [mm]	Mass Flux [kg/s-m^2]	Jacobs Limit	Nominal Pipe Size [inch]
1.	Horizontal	33	16.9	40.79	1.00	3/4
2.	Vertical	33	10.9	97.84	2.40	1/2
3.	Horizontal	11	16.9	13.56	0.33	3/4
4.	Vertical	11	6.3	98.04	2.40	5/16

3.5.3 Oil Retention Comparison of R1234ze(E)/POE32 and R410A/POE32

POE oils are commonly used with conventional refrigerants such as R134a and R410A due to their chemical stability and lubricity. It would be beneficial if the newer systems with HFO refrigerants could use the same POE oils. Therefore, it is essential to investigate if the newer refrigerants have good enough transport properties to carry the oil and keep the oil retention to minimum levels. The compatibility of R1234ze(E) in terms of miscibility and solubility with POE oils has been studied (Jia, Wang et.al, 2020). However, it is important to evaluate how oil retention with HFO refrigerants compares with conventional refrigerants in gas lines of typical air-conditioning systems.

Test results for R1234ze(E)/POE32 for 16.9 mm and 10.9 mm inner diameter piping simulating suction line conditions are presented in Figure 3.25 and Figure 3.26, respectively. The plots show

the amount of oil retained per unit length in the test sections with respect to the refrigerant mass flux for suction lines at steady-state conditions. Oil retention measurements for R410A/POE32 are overlaid on the plots for comparison. Interestingly, oil retention with R1234ze(E) in general was lower than for R410A over the entire range of refrigerant mass fluxes in both the line sizes. Therefore, from the experimental results it seems that the transport properties of R1234ze(E) are better than R410A.

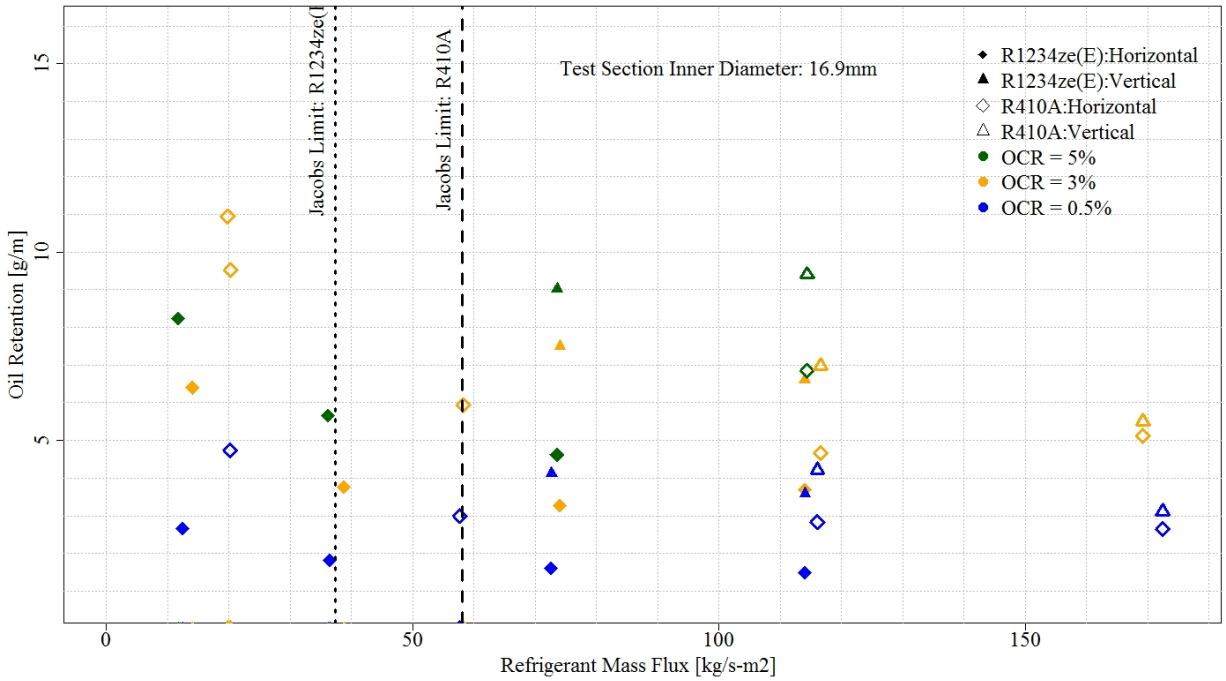

Figure 3.25: Oil retention in vertical and horizontal suction gas lines (ID: 16.9 mm) with R1234ze(E)/POE32 and R410A/POE32

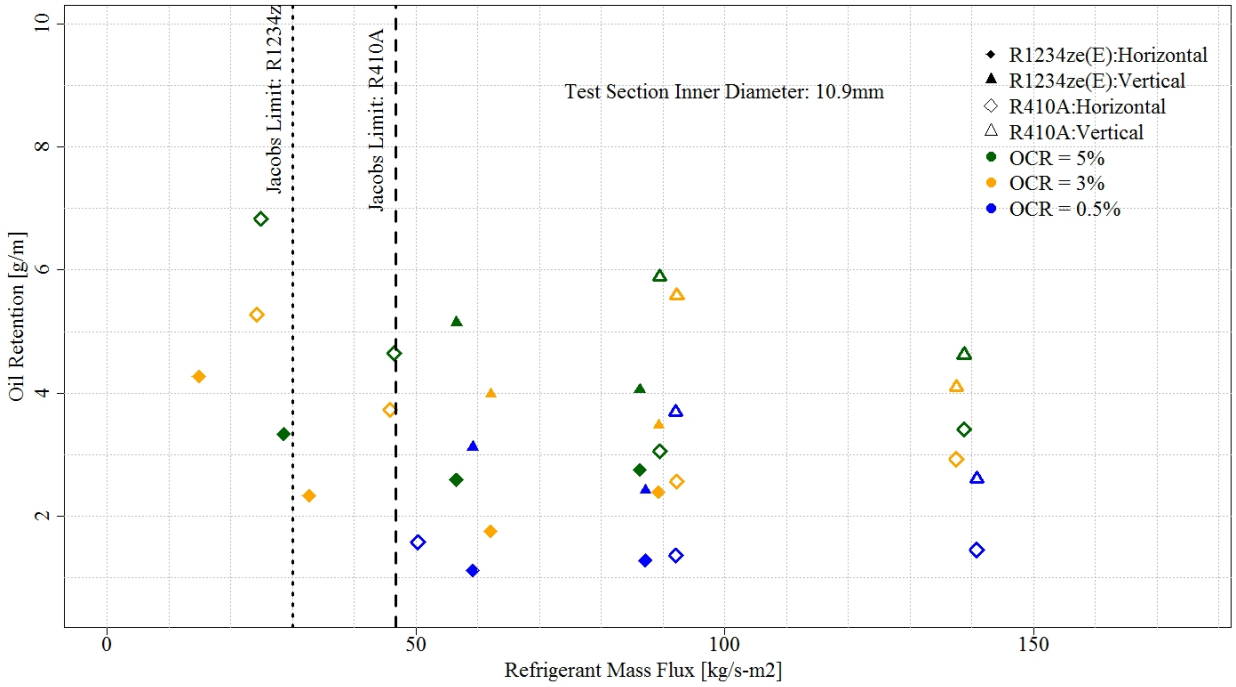

Figure 3.26: Oil retention in vertical and horizontal suction gas lines (ID: 10.9 mm) with R1234ze(E)/POE32 and R410A/POE32

3.5.4 Repeatability in Oil Retention Measurement

To understand the repeatability in the measurement method, a test must be repeated at the exact same condition for multiple times. However, due to the complexity of the setup and the experimental procedure, it is difficult to achieve identical test conditions. There were two instances where a particular test was repeated. These repeated tests were not at the exact same condition, but were similar. These experimental data points were compared to get some level of confidence in the repeatability of experimental measurements.

For example, while testing R134a/POE32 for the 16.9 mm suction line, the lever arm that connects the pneumatic cylinder to close the ball valve of the horizontal test section got stuck because of mis-alignment. Therefore, the test was repeated and two oil retention measurements for the vertical line were obtained at a similar condition. As shown in Figure 3.21, the oil retention in the vertical line at refrigerant mass flux of 2 x Jacobs limit and OCR of 0.5 % for the two measurements was similar.

Similarly, while testing R32/POE32 for a 10.9 mm line at 5% OCR, a test at 2 x Jacobs limit was repeated as the oil got spilled from the test section while doing the weight measurements. Consequently, two readings at a similar condition for the horizontal line were obtained and compared. As shown in Figure 3.27, the oil retention in the horizontal for both points (ID123 and ID128) was similar showing a good repeatability of testing.

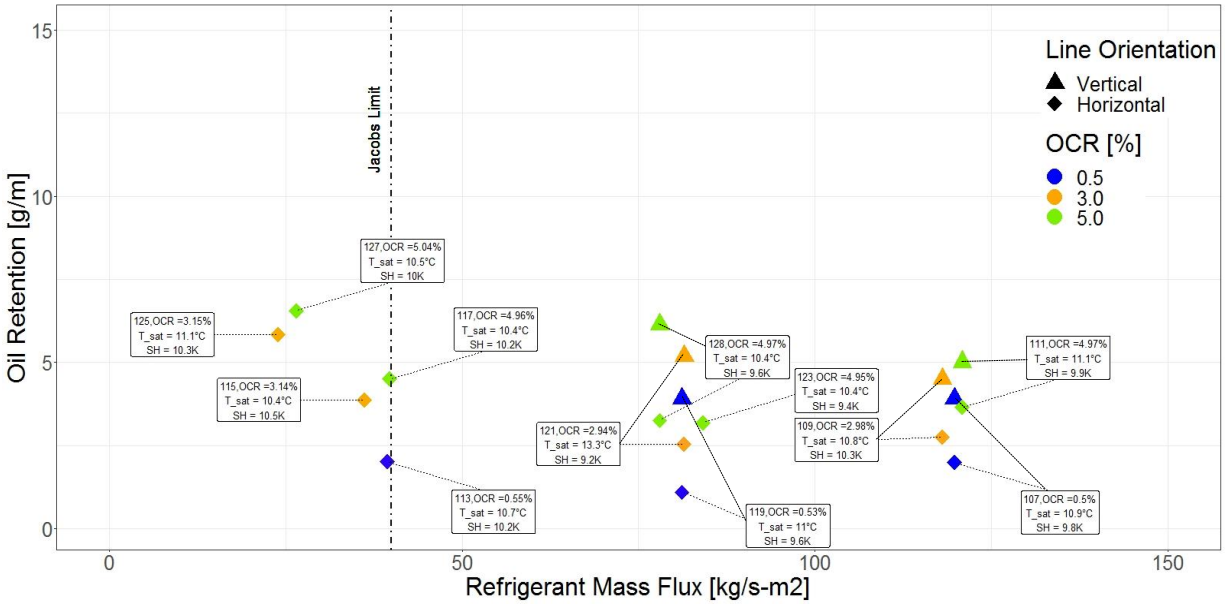

Figure 3.27: Repeatability in oil retention measurement observed while testing 10.9 mm suction gas line with R32/POE32

3.5.5 R1234ze(E) Aerosol and Foam Grade Working Fluid

It is important to note that the R1234ze(E) supplier mistakenly sent aerosol and foam (AF) grade and not refrigerant grade working fluid that was used for testing. The R1234ze(E) was procured from Honeywell in September 2020, but it was not until the end of March 2021 that the supplier realized that they had provided a different grade and then informed us. As the oil retention measurement was almost completed by then, the oil retention measurements with the AF grade are reported. Honeywell mentioned that the only difference between the refrigerant grade and the AF grade is a slightly higher percentage of non-condensable in the AF grade compared to the refrigerant grade. According to their reports and their email conversation shown in APPENDIX G, the moisture specification in refrigerant grade is 10 ppm whereas that in the AF grade is 50 ppm. They do not suspect any difference in the compatibility or transport properties of refrigerant

with the POE32 lubricant. However, a higher percentage of non-condensable gases was a concern for the committee members of the ASHRAE Research Project. Therefore, a further analysis was done to quantify the level of non-condensable gases in the working fluid and its possible impact on oil retention.

While running the experiments, two-phase refrigerant exists only in the evaporator and condenser and temperature measurements were not available inside the heat exchangers. However, data of temperature and pressure readings at the equilibrium condition before system startup were available for tests run with R1234ze(E)/POE32. From the experiments that were run on different days, data was selected for runs where the system would have reached a thermal equilibrium due to no operation over the night. The initial few seconds of steady-state pressure and temperature data in the suction port of the refrigerant pump were reviewed before, operations (pumps, heater, chillers) were started.

Table 3.9 shows the average measured temperature and pressure at the pump suction port. The saturation pressure corresponding to the measured temperature is calculated using properties from CoolProp. The maximum absolute difference between the measured pressure and the saturation pressure was 10.15 [kPa] (1.47 psi). This differences was within the measurement uncertainty of the pressure sensor. The accuracy of the sensor was 17 kPa (2.5 psi) (Setra Model: 209, Range: 0-1000 psi, Accuracy: 0.25% FS). The maximum relative difference in the pressure was 2.35%. These average pressure readings are plotted as a function of temperature as shown in Figure 3.28. The differences were not considered to be significant and it was concluded that there was not a large impact on the pressure temperature relationship because of using a different grade.

To understand the impact of pressure difference due to possible non-condensable gases, on the prediction of oil retention, a sensitivity analysis was carried out using the model that was developed to predict oil retention in horizontal lines with refrigerant R410A/POE32.

Table H.1 to Table H.4 in APPENDIX H shows the deviation in oil retention prediction due to a 3% uncertainty in the test section pressure for suction and discharge conditions of both 10.9 mm and 16.9 mm lines. For the suction line, the maximum deviation in oil retention prediction is 3.5 %,

whereas in the discharge line the maximum deviation is 0.82 %. It is to be noted that this analysis was done with R410A to get an idea of the impact of pressure on oil retention. However, R1234ze(E) should also have a similar impact. It was concluded from this analysis that the impact on oil retention measurement due to AF grade R1234ze(E) should not be significant because of the possible non-condensable impurities.

Table 3.9: Saturation temperature and pressure data at refrigerant pump suction port

Sr	Date/Time of Experiment	Duration of Data Considered [sec]	Refrigerant Pump Suction			Pressure Difference	
			Measured Average Temp [°C]	Saturation Pressure calculated from CoolProp [kPa]	Measured Average Pressure [kPa]	Absolute [kPa]	Relative Difference [%]
1	2/11/2021 10:36	236	20.29	431.1	423.5	7.65	1.77
2	2/25/2021 08:58	145	19.78	424.7	420.8	3.82	0.90
3	3/04/2021 10:52	125	20.40	432.7	425.5	7.22	1.67
4	3/11/2021 11:53	426	21.24	444.6	435.9	8.72	1.96
5	3/16/2021 09:45	32	23.04	470.9	461.0	9.94	2.11
6	3/17/2021 09:15	23	23.31	475.1	466.8	8.29	1.74
7	3/19/2021 10:25	36	20.26	431.5	421.4	10.15	2.35
8	4/02/2021 13:02	81	21.11	442.7	438.1	4.60	1.04

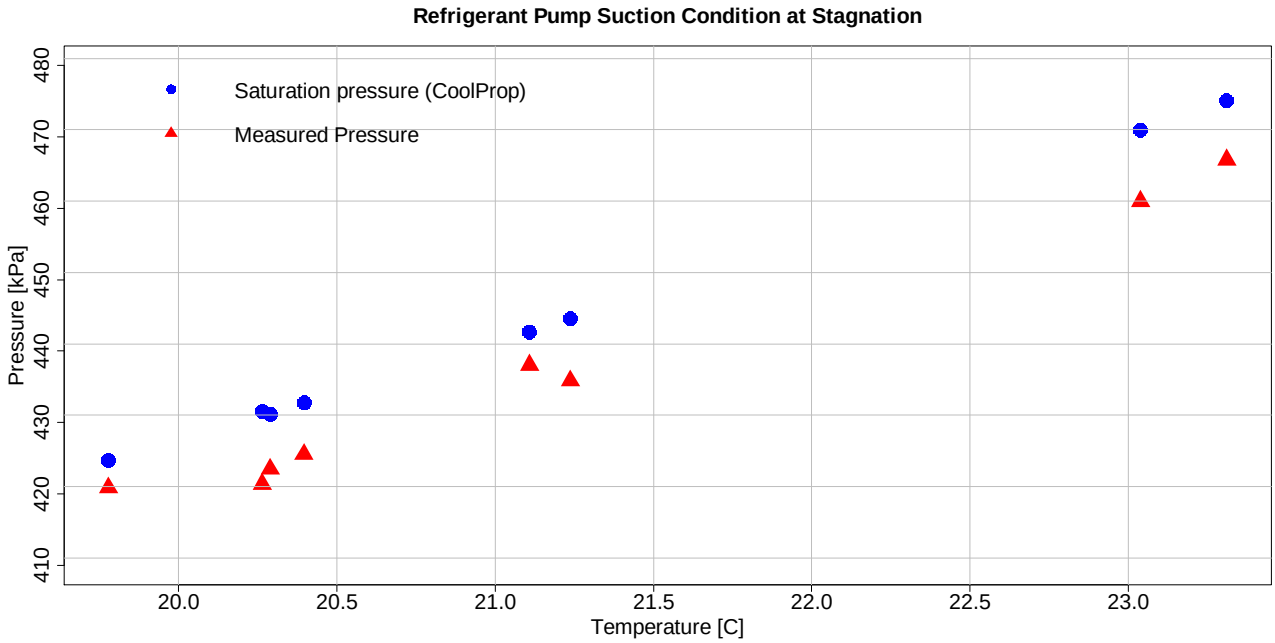

Figure 3.28: Measured and saturation pressure at pump suction port as a function of temperature to understand the impact of non-condensable gases in Aerosol and Foam grade R1234ze(E).

4. MODELING WORK

4.1 Model to Predict Oil Retention in Gas Lines

The goal of the work described in this chapter was to develop a physics-based, semi-empirical model that can capture the effects on oil retention on different parameters that characterize the refrigerant vapor and liquid oil flowing in circular pipes oriented in horizontal and vertical directions. This model would then be a backbone of a tool that would help design engineers to select refrigerant line sizes based on maintaining proper oil return. For this semi-empirical physics-based model, experimental data was utilized to determine the coefficients of the correlations. The correlations were developed with a subset of experimental data points while the remaining experimental data was used for model validation.

Two desired model outputs are as follows.

- Oil retention in both horizontal and vertical orientation refrigerant lines
- Minimum refrigerant mass flow rate required for the oil to return in upward flow in a vertical line.

Model inputs are as follows.

- Refrigerant/Oil along with their mixture properties
- Pipe inner diameter
- Temperature and pressure in the pipe
- Refrigerant mass flow rate
- Oil circulation ratio (OCR) or Oil mass flow rate

4.2 Modeling Structure Based on Flow Regime

Depending on the flow regimes, different models for predicting the amount of oil in the pipe (oil retention) are implemented. A high-level structure of the overall model is shown in Figure 4.1.

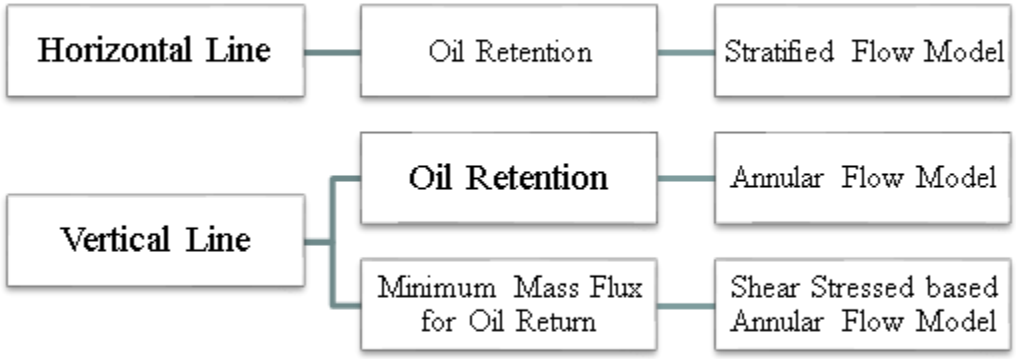

Figure 4.1: Model structure based on orientation and flow regime.

4.2.1 Stratified Flow Model for Predicting Oil Retention in Horizontal Lines

Flow Regime – Modified Bakers Map

In order to get insight into the flow regime for the horizontal orientation, the measured experimental data points were overlaid on a Modified Baker's Map (1987), which is a widely used standard flow regime map for adiabatic horizontal flow.

The parameters λ and ψ, were calculated using Equations (4.1) and (4.2). The required properties of air and water were evaluated at room temperature (20°C) and atmospheric pressure (1 atm). Mass flux of the liquid (G_L) and gas (G_G) were known. Properties of refrigerant and lubricant were evaluated at the test section condition. For these estimates the surface tension of oil was assumed to be constant, σ_L= 0.046 [N/m].

$$\lambda = \left[\frac{\rho_G \rho_L}{\rho_{air}\rho_{water}}\right]^{\frac{1}{2}} \quad (4.1)$$

$$\psi = \left(\frac{\sigma_{water}}{\sigma_L}\right)\left[\frac{\mu_L}{\mu_{water}}\left(\frac{\rho_{water}}{\rho_L}\right)^2\right]^{\frac{1}{3}} \quad (4.2)$$

Experimental data points for R410A/POE32 flowing in the horizontal lines are plotted in Figure 4.2. It can be observed that most of the data points were in the stratified flow and wavy flow regimes. Therefore, for predicting oil retention in horizontal line, a stratified flow model was

implemented to predict the oil retention. The wavy flow models have the same basic structure as the stratified flow model with additional complexities that capture the effects of waves. However, to keep the model simple, a stratified flow model was implemented. In the literature, no model was found for predicting void fraction or pressure drop specifically for refrigerant/oil flow in the stratified flow regime. However, a few models were found for stratified flow of air-water, air-oil and other similar combinations, which were mainly applied in the oil and gas industry and in the operation of nuclear and chemical reactors. Stratified flow with a smooth interface is rather simple to model compared to more complex flow patterns, such as annular or slug flow, because the two phases are completely separated. However, the complexity increases when the gas flow is much faster than the liquid flow, which creates waves at the gas-liquid interface that requires different techniques and empirical correlations for accurate predictions.

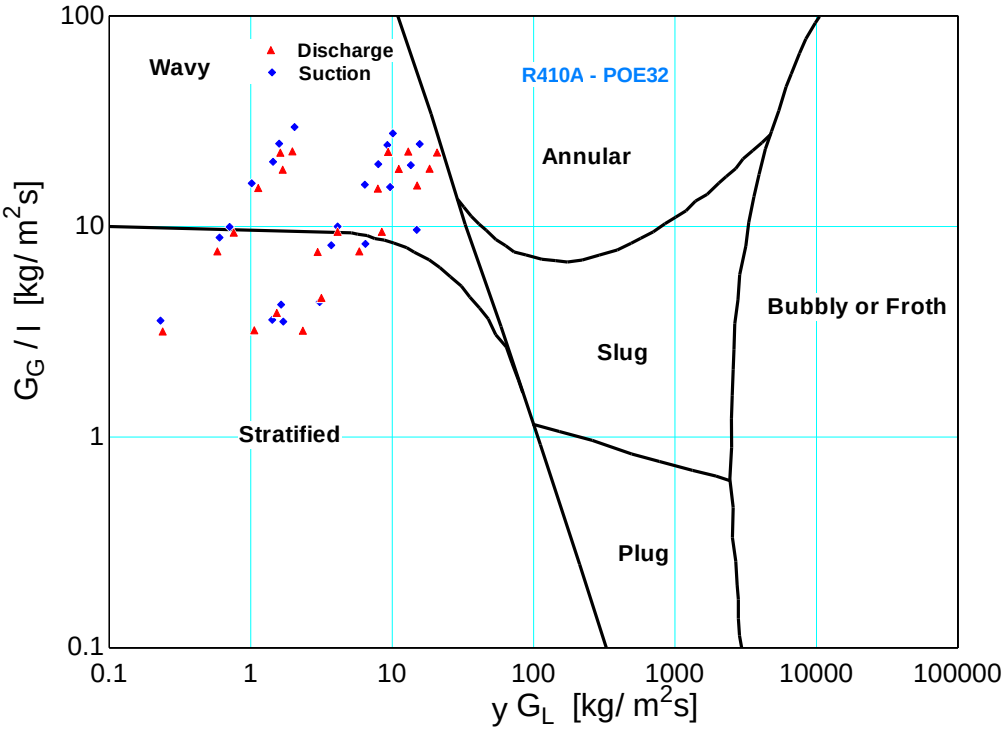

Figure 4.2: Experimental points in horizontal line overlaid on flow regime map.

Stratified Flow Model along with Empirical Correlation for Interfacial Friction Factor

Govier and Aziz, (1972) presented a simplified physics-based model to determine the frictional pressure gradient and in-situ volume fractions that accounts for shear stress at the gas-liquid interface. Their model is mainly for a smooth interface and does not capture any effects of waves

at the interface. However, their work provided a basic structure, based on which researchers developed more advanced models. For example, Agrawal et. al, (1973) proposed a model with a modified procedure for the evaluation of liquid phase friction factor that considers the velocity profile of the liquid phase. Taitel and Dukler (1976) developed a model that has been widely used for predicting transitions in flow regimes in horizontal and near horizontal gas-liquid flow. Recent models published by Tzotzi and Andritsos (2013) account for the interfacial waves using different techniques.

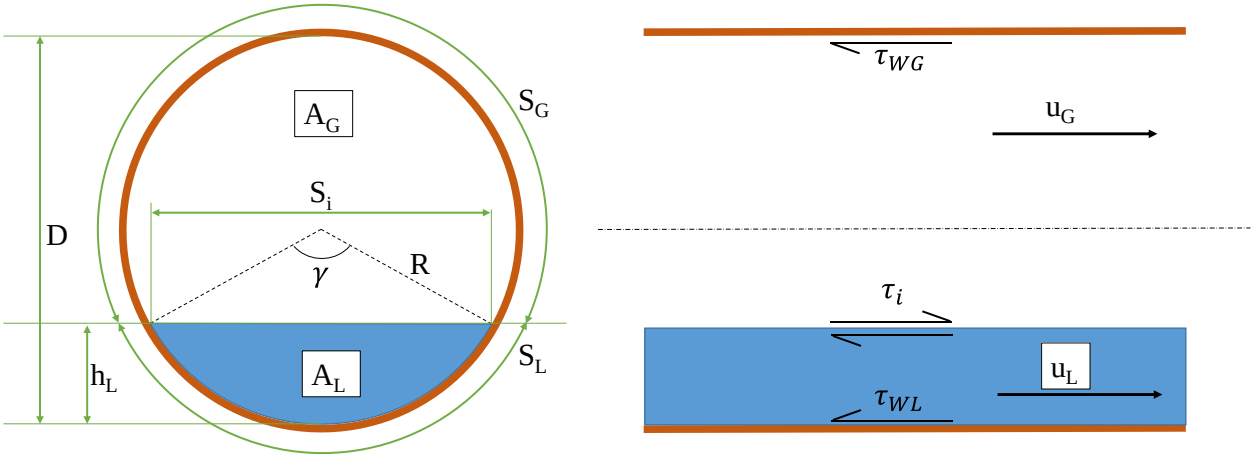

D: Hydraulic Diameter h_L: Interface height S_L: Liquid Perimeter S_G: Gas Perimeter S_i: Interface width
τ_{WG}: Wall Shear stress – Gas τ_{WL}: Wall Shear stress – Liquid τ_i: Interfacial Shear stress

Figure 4.3: Schematic of cross section and longitudinal section of a pipe showing the geometric parameters defining the stratified flow.

The same basic structure provided by Govier and Aziz, (1972) has been used to develop the model presented here. The important geometric parameters and shear stresses are shown in Figure 4.3. The inner pipe diameter D is known. This inner pipe diameter is used to calculate the cross sectional area A and perimeter S. h_L is defined as the vertical height of the liquid-gas interface. A_L and A_G are defined as the areas occupied by the liquid (oil) and gas (refrigerant vapor) within the cross section of the pipe. $S_L$and S_G are the perimeters covered by liquid and gas and S_i is the width of the liquid-gas interface. γ is the inner angle of the sector created by the liquid interface. The ratio $\frac{h_L}{D}$ is defined in terms of γ and S in Equation (4.3). The ratio $\frac{S_i}{D}$ is then defined using the ratio $\frac{h_L}{D}$ in Equation (4.4).

$$\frac{h_L}{D} = \frac{1}{2}\left(1 - \cos\left(\frac{\gamma}{S}\right)\right) \quad (4.3)$$

$$\frac{S_i}{D} = 2\sqrt{\frac{h_L}{D} - \left(\frac{h_L}{D}\right)^2} \quad (4.4)$$

Area fraction is defined as area occupied by the particular phase divided by the total area of the pipe. Accordingly, area fractions for liquid and gas, α_L and α_G are defined as shown in (4.5) and (4.6) respectively. Similarly, perimeter ratios $\frac{S_L}{S}$ and $\frac{S_G}{S}$ are also defined using γ as shown in (4.7)

$$\alpha_L = \frac{A_L}{A} = \frac{1}{2\pi}(\gamma - \sin(\gamma)) \quad (4.5)$$

$$\alpha_G = \frac{A_G}{A} = 1 - \alpha_L \quad (4.6)$$

$$\frac{S_L}{S} = \frac{\gamma}{2\pi} = 1 - \frac{S_G}{S} \quad (4.7)$$

A key component of the model for oil retention is the determination of liquid (oil) area fraction (α_L) in terms of flow conditions and fluid properties. First of all, the velocities of both the fluids, u_L and u_G, are estimated with Equations (4.8) and (4.9) using the mass flow rates of refrigerant and oil, cross-sectional area of each phase defined by the geometric parameters, and densities of each fluid, $\rho_L$and ρ_G, at a particular operating condition. The mass flow rates are corrected by accounting for the solubility of liquid refrigerant in the oil. Refer to Section 4.3 for information on the solubility correction. In addition, the superficial velocities of both the fluids, j_L and j_G, are calculated using Equations (4.10) and (4.11). The Reynolds numbers for both the phases, Re_L and Re_G, are then determined using the superficial velocities, diameter of the pipe, and kinematic viscosities of each phase (ν_L) and (ν_G) as shown in Equations (4.14) and (4.15). The Reynolds numbers calculated using the experimental data obtained in this study indicated that the liquid flow was laminar for all operating conditions while gas flow was turbulent. For R410A/POE32, Reynolds numbers of the gas phase for all the data points were higher than 21500, whereas, the Reynolds numbers of the liquid phase for all the data points were lower than 48.

$$u_L = \frac{\dot{m}_{oil}}{\rho_L A_L} \quad (4.8) \qquad u_G = \frac{\dot{m}_{ref}}{\rho_G A_G} \quad (4.9)$$

$$j_L = u_L \alpha_L \quad (4.10) \qquad j_G = u_G \alpha_G \quad (4.11)$$

$$Re_L = \frac{j_L D}{\nu_L} \quad (4.12) \qquad Re_G = \frac{j_G D}{\nu_G} \quad (4.13)$$

The wall shear stresses for individual fluids, τ_{WG} and τ_{WL} are calculated using single-phase friction factors f_G and f_L, superficial velocities and the densities of each fluid as shown in (4.14) and (4.15). Friction factor correlations in terms of Reynolds number for the turbulent refrigerant (gas) flow and laminar oil (liquid) flow are given in (4.16) and (4.17).

$$\tau_{WG} = \frac{f_G \rho_G j_G^2}{2} \quad (4.14)$$

$$\tau_{WL} = \frac{f_L \rho_L j_L^2}{2} \quad (4.15)$$

$$f_G = C_G Re_G^{-m} \quad (4.16)$$

$$f_L = C_L Re_L^{-n} \quad (4.17)$$

where,

$C_G = 0.046 \; and \; m = 0.2 \; for \; turbulent \; refrigerant \; flow$

$C_L = 16 \; and \; n = 1.0 \; for \; laminar \; oil \; flow$

$Re < 1000 \Rightarrow Laminar \; Flow$

$Re > 2000 \Rightarrow Turbulent \; Flow$

The interfacial shear stress, τ_i, cannot be determined analytically, and various researchers have proposed different empirical correlations. However, no correlations were found in the literature for refrigerant and compressor oil. With the known value of oil retention from the experimental data, the model was used to back calculate the interfacial friction factor. For this purpose, the

experimental data of only 16.9 mm with R410A/POE32 was used. Then, to develop an empirical correlation for the proposed model, the interfacial friction factor, f_i, was plotted as a function of refrigerant Reynolds number as shown in Figure 4.4. This friction factor follows a trend, which is similar to the friction factor in the gas phase, f_g, as shown in Figure 4.5. In addition, it can be observed that the interfacial friction factor, f_i, is a function of OCR. Therefore, a form of interfacial shear stress and friction factor is proposed that is shown in Equations (4.18) and (4.19). The values of *h1*, *h2* and *h3* were determined using a curve fit of experimental data for R410/POE32 for only the16 mm line. The predicted friction factors, f_i, are overlaid as solid lines on the plot in Figure 4.4. The R^2 value of this fit was 96.34%

$$\tau_i = \frac{f_i \rho_g \left(j_g - j_l\right)^2}{2} \tag{4.18}$$

$$f_i = \left(h1\ Re_G^{-h2}\right) + h3 * OCR \tag{4.19}$$

where,

$h1 = 0.1446$
$h2 = 0.5049$
$h3 = 0.0111$

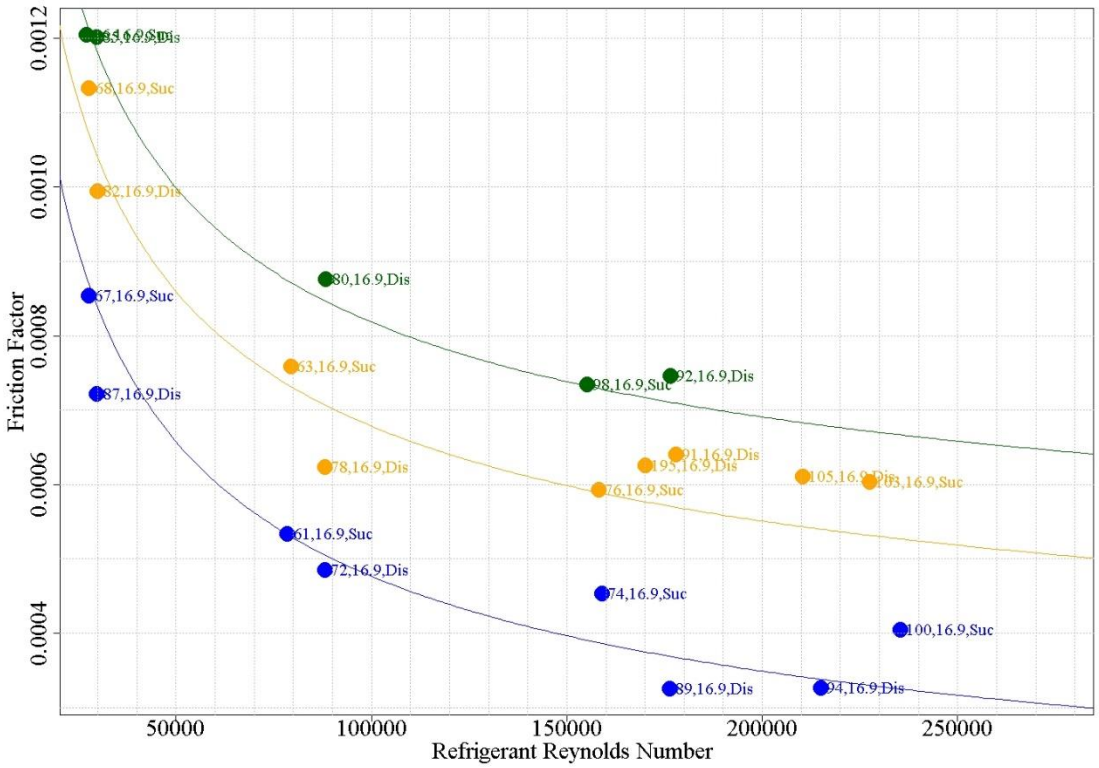

Figure 4.4: Friction factor of the interface with respect to refrigerant Reynolds number obtained from experimental data of R410A/POE32 for different OCR.

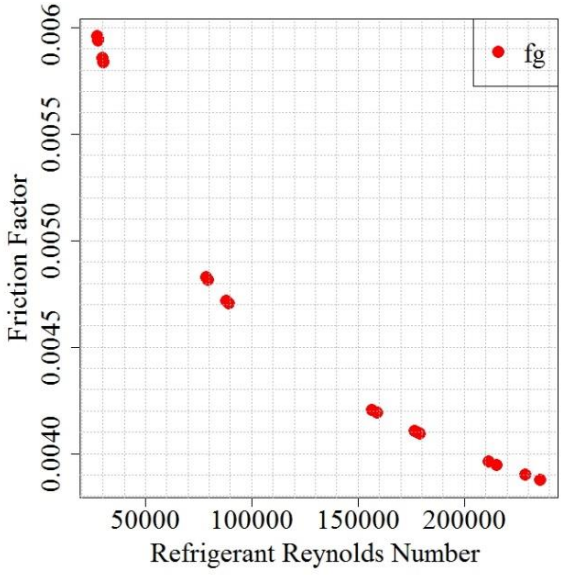

Figure 4.5: Friction factor of the refrigerant gas phase with respect to refrigerant Reynolds number.

For fully developed flow in a pipe, the one-dimensional momentum equations for the two phases can be written as shown in Equations (4.20) and (4.21), which relate the pressure gradients across the pipe flow, $\left(\frac{\Delta P}{L}\right)_{TP,G}$ and $\left(\frac{\Delta P}{L}\right)_{TP,L}$, with the shear stresses of the fluids at the wall and the shear stress at the liquid gas interface. By eliminating the pressure gradient under the assumption that the pressure drops in both the phases are equal, Equations (4.20) and (4.21) reduce to Equation (4.22).

The prediction of the area fraction, based on the proposed model requires an iterative solution. A value for α_L is guessed, based on which all the geometric parameters are defined. Using the known mass flow rates, the velocities are determined for individual phases, which then allows determination of the Reynolds numbers and friction factors. With the known friction factors, all the shear stresses can be evaluated for both phases. By evaluating all the parameters, if Equation (4.22) does not converge to zero, the guess value of α_L is updated (e.g., using a Newton's method or other numerical updating scheme) and the procedure is repeated. At convergence, the value of liquid area fraction (α_L) becomes the prediction of the model. With the known value of α_L, the mass of oil retention, m_{oil} is calculated using Equation (4.23). The solubility correction for the refrigerant dissolved in the oil is applied to predict the true oil retained in the test section as described in Section 4.3.

$$A_G\left(\frac{\Delta P}{L}\right)_{TP,G} = \tau_{WG}S_G - \tau_i S_i \tag{4.20}$$

$$A_L\left(\frac{\Delta P}{L}\right)_{TP,L} = \tau_{WL}S_L + \tau_i S_i \tag{4.21}$$

$$\frac{\tau_{WG}S_G}{A_g} - \frac{\tau_{WL}S_L}{A_L} - \tau_i S_i\left(\frac{1}{A_L} + \frac{1}{A_G}\right) = 0 \tag{4.22}$$

$$m_{oil} = \alpha_L AL\rho_l(1 - \omega_{ref}) \tag{4.23}$$

Model Prediction Results and Discussion

This stratified flow model was implemented in the Engineering Equation Solver (EES) software (Klein 2018). The software is designed to simultanously solve equations and uses default guess values for variables as a starting point for converging to a solution.

The plots in Figure 4.6 and Figure 4.7 show oil retention with respect to refrigerant mass flux for suction conditions with R410/POE32 for the 16.9 mm and 10.9 mm lines, respectively. Similarly, Figure 4.8 and Figure 4.9 show oil retention in discharge conditions for the 16.9 mm and 10.9 mm lines, respectively. Figure 4.10 and Figure 4.11 show the oil retention prediction in 19.9 mm suction and discharge lines, respectively. The solid lines are the predictions from the model, whereas the markers are the experimental data points. The transparent color bands are ±1 g/m wide to get an idea of the deviation of predictions compared to the actual experimental data points.

Following are some comments related to the model predictions and comparisons with the experimental data.

- The oil retention predictions in Figure 4.6 to Figure 4.11 were calculated for specific values of OCR corresponding to average experimental values for the different target OCRs in the tests. The values of OCR for experimental data points varied from the average values and are noted on the plot. For example, in Figure 4.7, the orange solid line represents the prediction at an average value of OCR at 2.08%. However, the four experimental data points had different OCR. This difference explains some of the deviation in predictions from the experimental data points.
- There are also some variations in the experimental saturation temperatures and the test section temperatures from the original targets that were used in the model. The actual saturation temperatures along with the superheat values for the experimental data points are also marked in the labels for a quick reference.
- A parity plot eliminates all such variations as the prediction is made for the actual experimental conditions for the particular experimental data point to get a true comparison. Figure 4.12 shows the parity plot and it can be observed that the R^2 value of prediction vs experimental value is 0.9036 and all the data points fall within a relative error of ±38.3% relative error.

- The coefficients for the friction factor correlation were obtained using the experimental data for only the 16.9 mm line. However, the model predicted oil retention within ±37.4% relative error for all the points which includes the 10.9 mm line and 19.9 mm line data points for R410A/POE32. This indicates that the model does a reasonable job of capturing the effect of pipe size on oil retention.

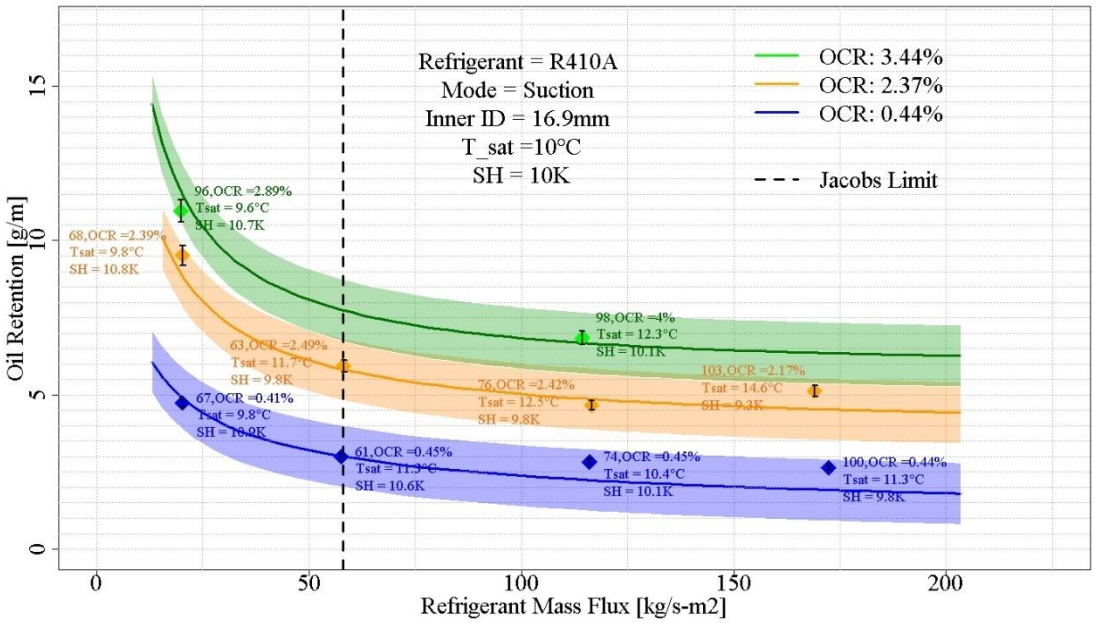

Figure 4.6: Oil retention vs refrigerant mass flux model prediction (lines) compared with experimental data (markers) for stratified flow for R410A/POE32 in 16.9 mm suction line

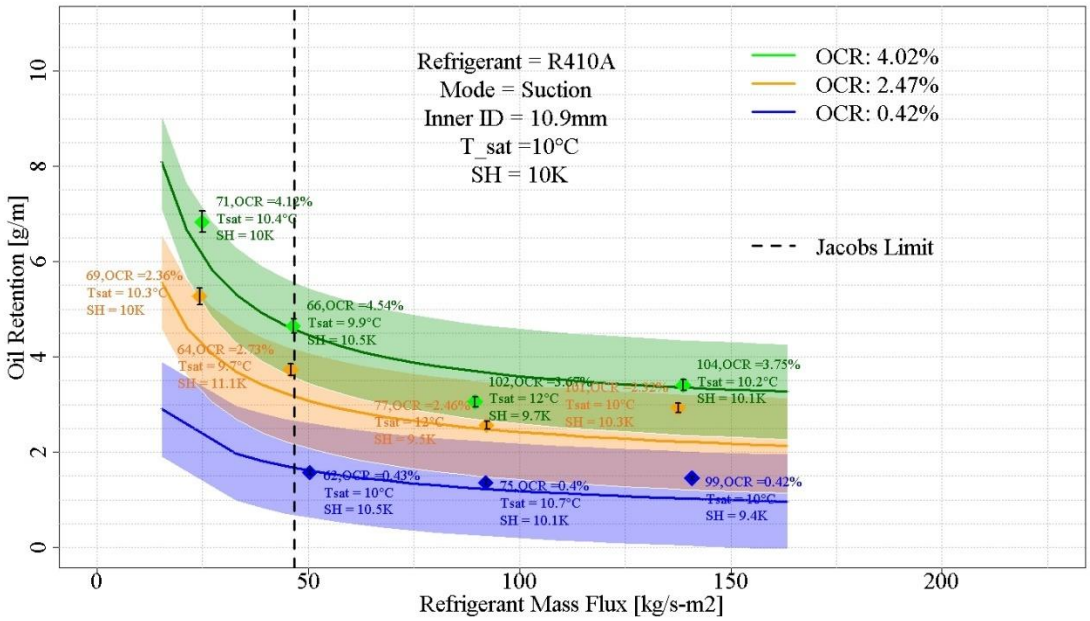

Figure 4.7: Oil retention vs refrigerant mass flux model prediction (lines) compared with experimental data (markers) for stratified flow for R410A/POE32 in 10.9 mm suction line

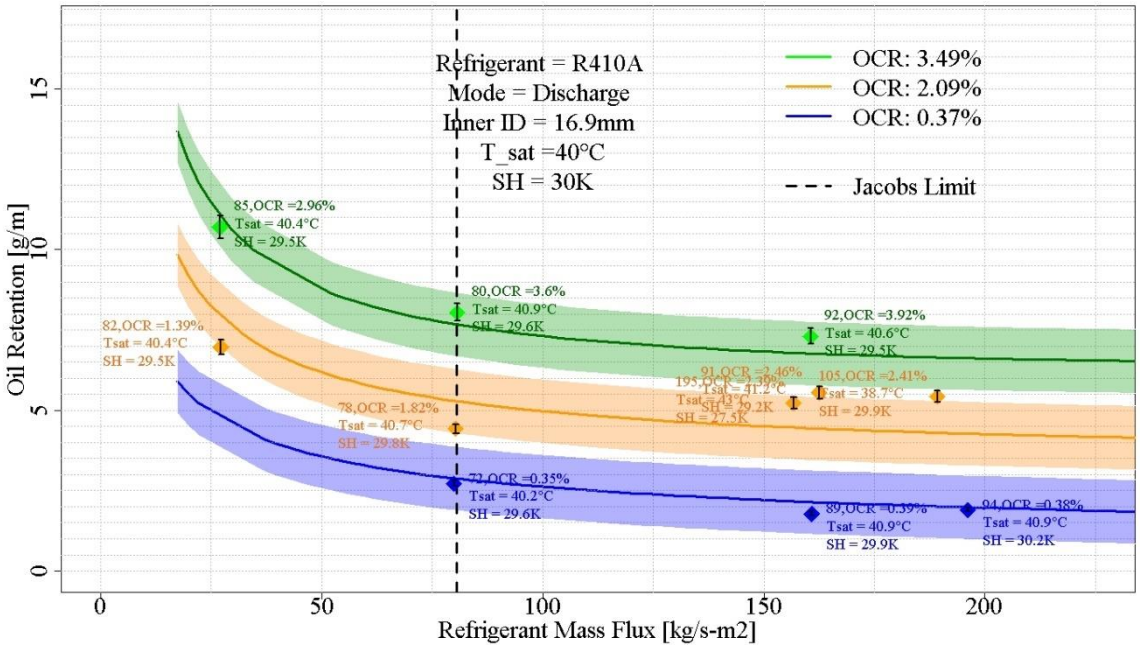

Figure 4.8: Oil retention vs refrigerant mass flux model prediction (lines) compared with experimental data (markers) for stratified flow for R410A/POE32 in 16.9 mm discharge line

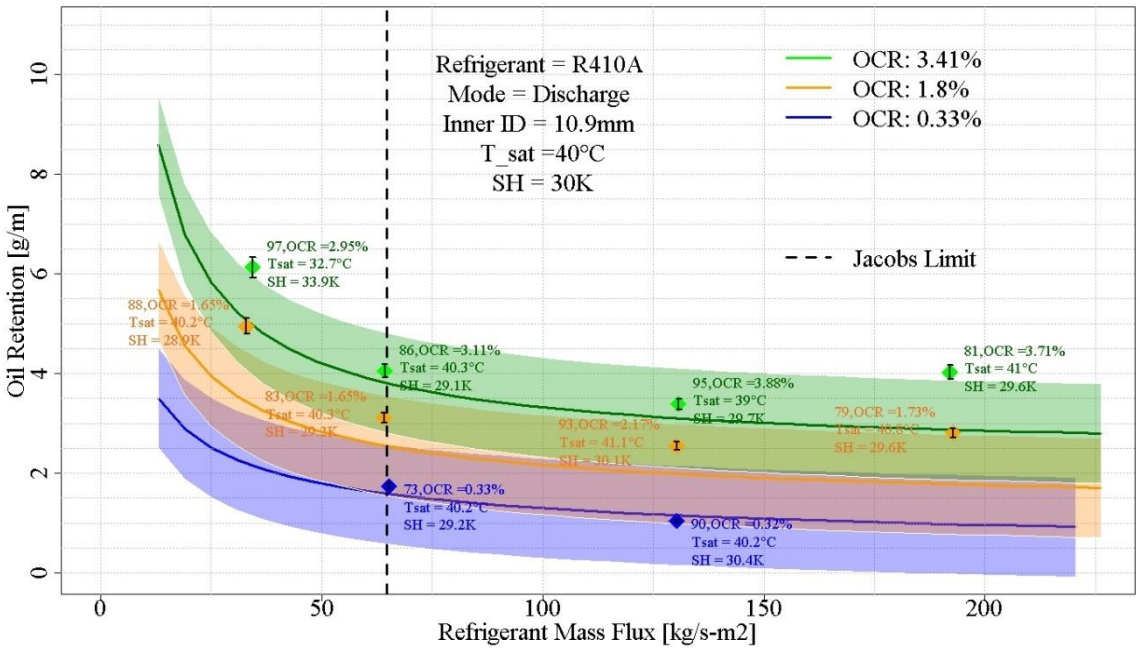

Figure 4.9: Oil retention vs refrigerant mass flux model prediction (lines) compared with experimental data (markers) for stratified flow for R410A/POE32 in 10.9 mm discharge line

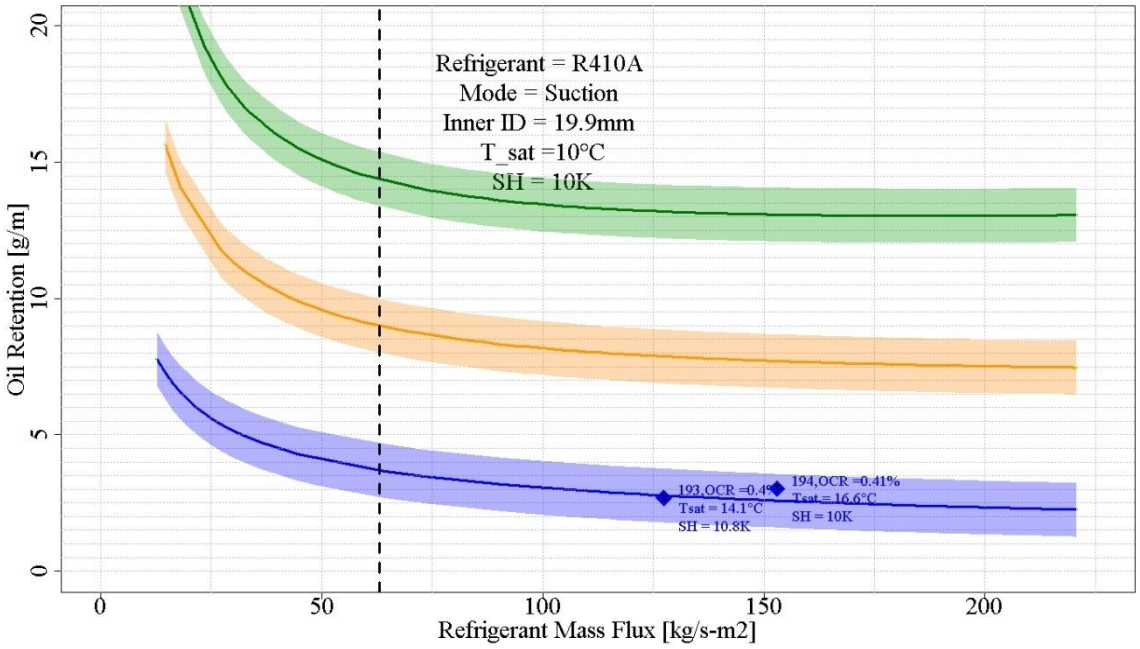

Figure 4.10: Oil retention vs refrigerant mass flux model prediction (lines) compared with experimental data (markers) for stratified flow for R410A/POE32 in 19.9 mm suction line

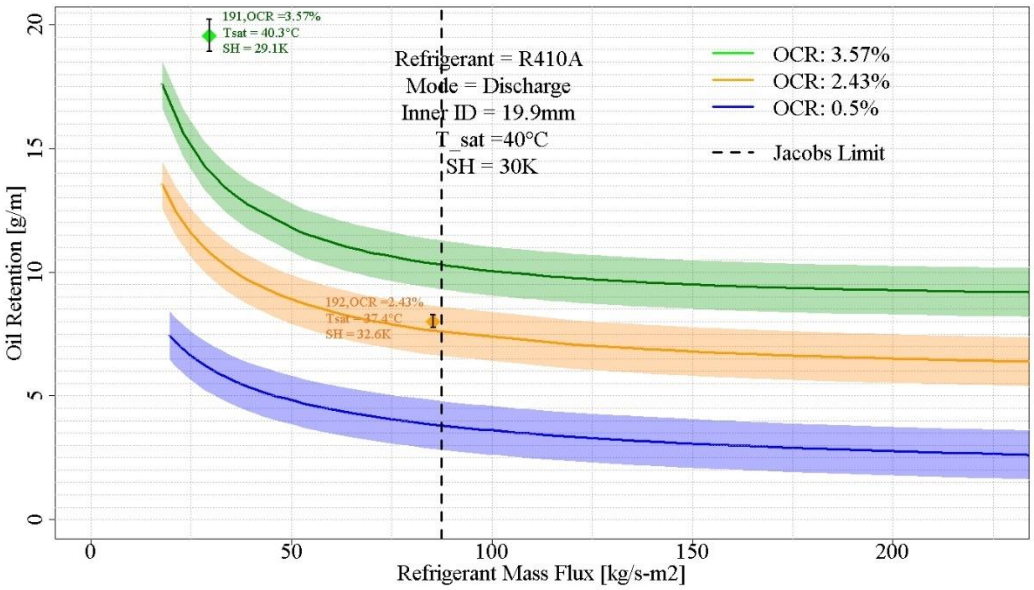

Figure 4.11: Oil retention vs refrigerant mass flux model prediction (lines) compared with experimental data (markers) for stratified flow for R410A/POE32 in 19.9 mm discharge line

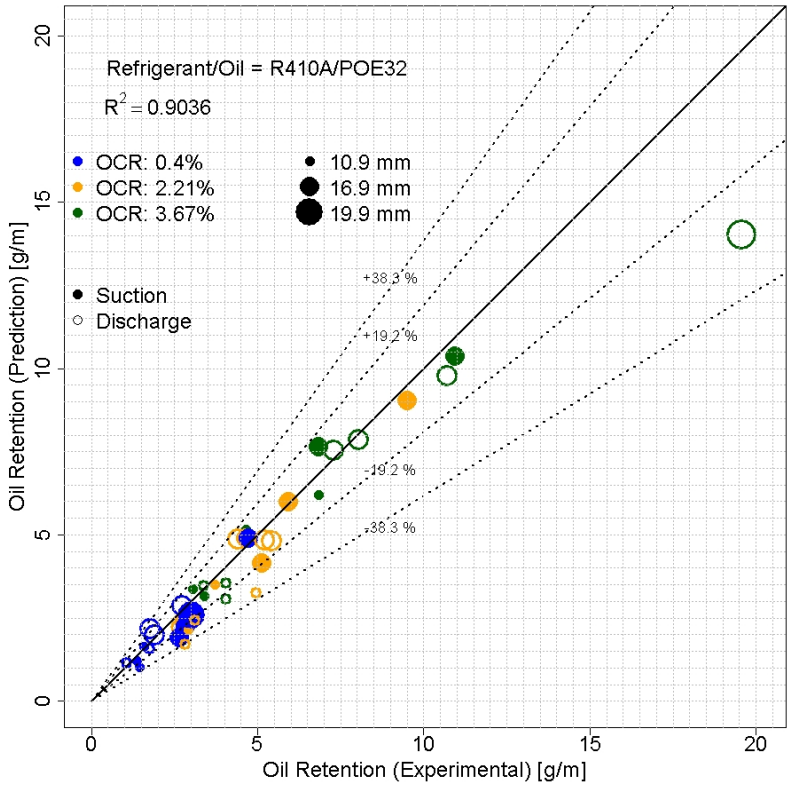

Figure 4.12: Parity plot showing the accuracy of the model for all the data points of R410A/POE32

The stratified flow model was run for different refrigerant/oil combinations and the coefficients of the empirical correlation for interfacial friction factor were determined and are presented in Table 4.1. The model prediction results for R1234ze(E)/POE32, R134a/POE32 and R32/POE32 using the determined coefficients are shown as parity plots in Figure 4.13, Figure 4.14 and Figure 4.15 respectively. The experimental and predicted oil retention values used in the parity plots are tabulated in APPENDIX L to APPENDIX O. The values of pressure drop per unit length and void fraction are also provided in the tables.

The model prediction for R134a/POE32 is not as good as R410A/POE32 and R1234ze(E)/POE32. A probable cause for this inaccuracy may be due to the inaccurate OCR correction for the oil that was injected in the refrigerant loop. The density and temperature of oil and liquid refrigerant mixture that is injected in the refrigerant loop was not measured while running tests with R134a/POE32. As this data was not available, these values were assumed to be constant, which may not be true for actual experimental data points. A detailed explanation regarding solubility of refrigerant in oil is provided in Section 4.3

Table 4.1: Coefficients of empirical correlation for interfacial friction factor

Sr.	**Refrigerant/Oil Combination**	h_1	h_2	h_3
1.	R410A/POE32	0.1447	0.5049	0.0111
2.	R32/POE32	0.0592	0.4367	0.0079
3.	R1234ze(E)/POE32	0.0950	0.4934	0.0095
4.	R134a/POE32	0.0417	0.3874	0.0068

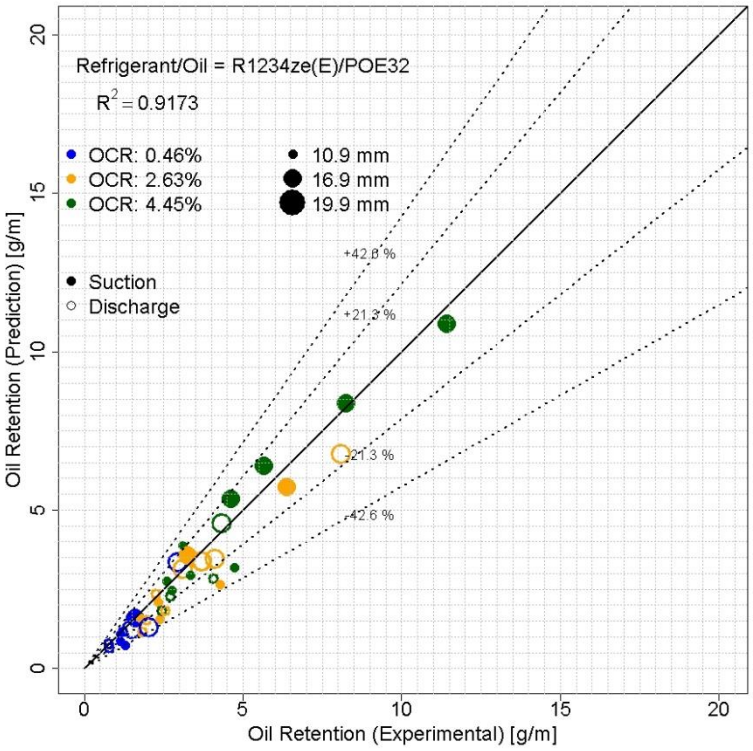

Figure 4.13: Parity plot for R1234ze(E)/POE32 in horizontal line

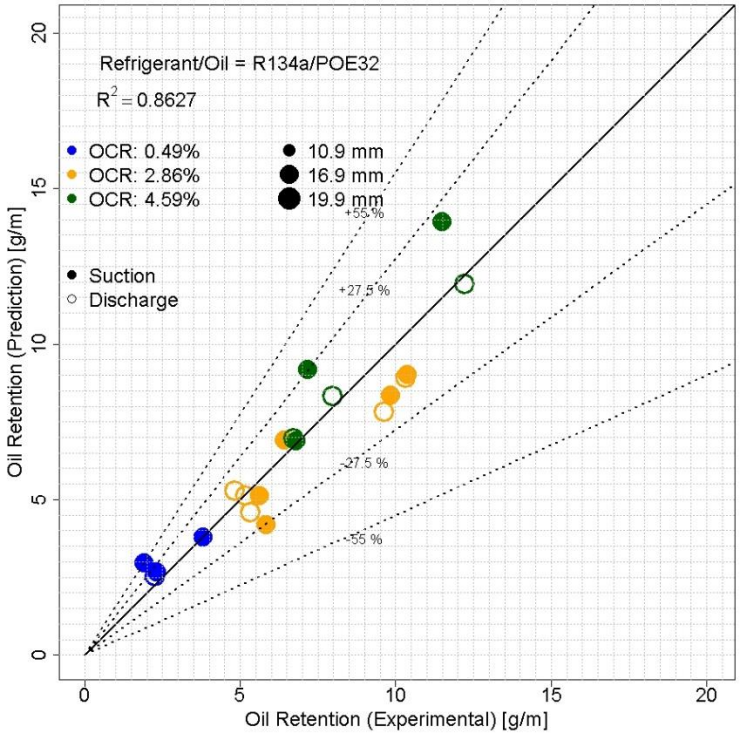

Figure 4.14: Parity plot for R134a/POE32 in horizontal line

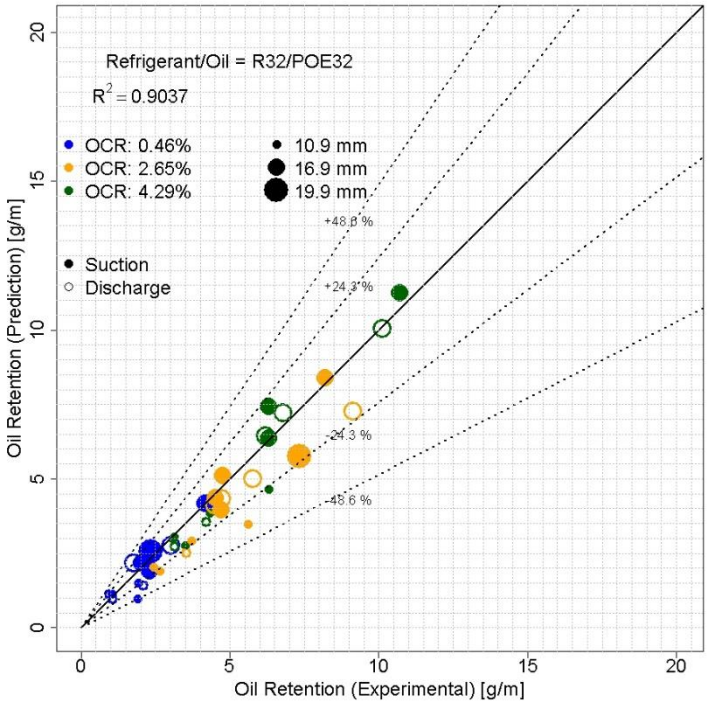

Figure 4.15: Parity plot for R32/POE32 in horizontal line

4.2.2 Annular Flow Model for Predicting Oil Retention in Vertical Lines

Researchers have developed annular flow models to predict oil return and retention in vertical upward flow by applying the Navier-Stokes equation to both fluid phases and using empirical correlations. Mehendale and Radermacher (2000) investigated film flow reversal in vertical pipes to understand oil return for refrigeration systems. They developed an analytical model with minimal empirical input that could predict the critical refrigerant mass flow mass flow rate for five different refrigerant-lubricant combinations (R22/Mineral Oil, R407C/Mineral Oil, R407C/POE, R410A/Mineral Oil, R410A/POE). They validated the model with experimental data and compared it with the Jacobs et al. (1976) correlation.

Using a similar idea, Radermacher et al. (2006) and Cremaschi (2004) developed semi-empirical models for estimating oil retention in suction lines and evaporators for R22, R410A and R134a air-conditioning systems. They developed correlations for predicting interfacial friction factors in horizontal and vertical suction lines. The correlations showed the interfacial friction factor is inversely proportional to the dimensionless liquid film thickness, refrigerant vapor Reynolds number and mixture Weber number. They published a correlation for interfacial friction factor for

R22/MO in horizontal and vertical suction lines and another generic correlation for all refrigerant and oil mixtures in horizontal suction lines.

Similarly, Sethi (2011) and Ramakrishnan (2012) developed correlations for interfacial friction factor. Sethi (2011) published an interfacial friction factor correlation for R134a/POE32, which is valid for annular flow in a vertical suction pipe. Ramakrishnan (2012) published a revised correlation which was developed from more experimental data that included R134a/POE32, R134/POE100, R1234yf/POE100 and R410A/POE32. The correlation is valid for upward flow in vertical suction lines with annular flow. Sethi (2011) and Ramakrishnan (2012) have also presented a model to predict critical mass flux limits for oil return in vertical upward flow and have compared it to the limits proposed by Kesim et al. (2000) and Jacobs et al. (1976).

Using the model developed by Sethi (2011), oil retention was predicted and compared with the experimental data collected for R410A/POE 32. A section of vertical pipe is shown as a schematic in Figure 4.16 with the defined geometric parameters and a force balance. The refrigerant vapor flows in the central core and the liquid flows in the annulus. The liquid consists of oil with liquid refrigerant dissolved in it. The amount of dissolved liquid refrigerant depends on the solubility of the refrigerant/oil pair. This solubility curve as a function of temperature and pressure is usually provided by a lubricant supplier (Refer Section 4.3). The analysis of the model is carried out in polar coordinates where, *z* represents vertical direction and *r* represents radial direction. The inner radius of the pipe is defined as R, which remains constant for a particular pipe size. The oil film thickness is defined by δ. Densities of liquid (oil) and gas (refrigerant vapor) are denoted by ρ_L and ρ_G, respectively. Dynamic viscosities of liquid and gas are defined by μ_L and μ_G, respectively. Acceleration due to gravity is represented by g and the pressure gradient in the *z* direction is given by $\frac{dP}{dz}$.

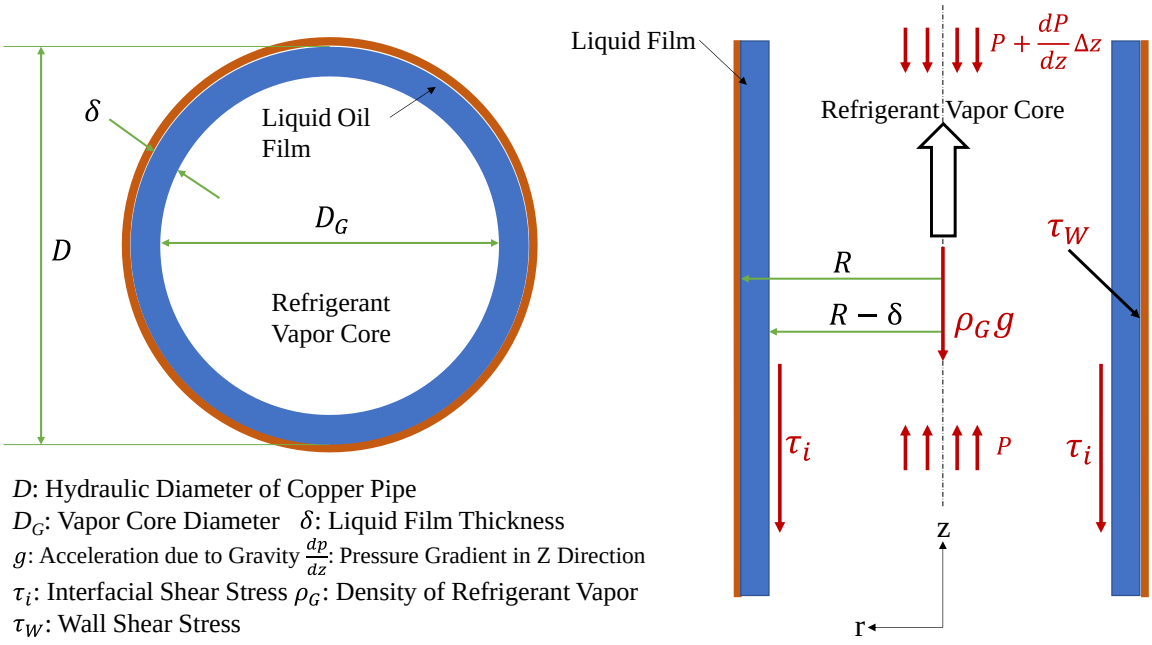

D: Hydraulic Diameter of Copper Pipe
D_G: Vapor Core Diameter δ: Liquid Film Thickness
g: Acceleration due to Gravity $\frac{dp}{dz}$: Pressure Gradient in Z Direction
τ_i: Interfacial Shear Stress ρ_G: Density of Refrigerant Vapor
τ_W: Wall Shear Stress

Figure 4.16: Schematic of upward annular flow of refrigerant core and liquid oil film in vertical copper pipe showing geometric parameters.

The Navier-stokes and continuity equations were applied on the liquid film in the annulus. The following assumptions were made for simplifying the Navier-stokes equations.

Assumptions

1. The flow is axi-symmetric and there is no 'swirl' velocity.

$$\frac{\partial}{\partial \theta}(\ldots) = 0 \text{ and } u_\theta = 0$$

2. The flow is steady

$$\frac{\partial}{\partial t}(\ldots) = 0$$

3. The flow is fully developed in the z-direction

$$\frac{\partial u_r}{\partial z} = \frac{\partial u_z}{\partial z} = 0$$

4. The flow is adiabatic (no heat loss through pipes)
5. There is no oil entrained in the vapor core
6. The liquid film thickness is uniform across the pipe
7. The fluid in liquid film is incompressible

The continuity equation in the radial direction for the liquid film is shown in (4.24). Using assumptions #1 and #3, the continuity equation simplifies to (4.25)

$$\frac{1}{r}\frac{\partial(ru_r)}{\partial r}+\frac{1}{r}\frac{\partial u_\theta}{\partial \theta}+\frac{\partial u_z}{\partial z}=0 \tag{4.24}$$

$$\frac{1}{r}\frac{d(ru_r)}{dr}=0 \tag{4.25}$$

Integrating Equation (4.25) with respect to *r* gives (4.26).

$$r\cdot u_r = constant \tag{4.26}$$

As there is no flow going out of the pipe, the radial velocity at the wall is zero, which means $u_r(r=R)=0$, which leads to Equation (4.27)

$$u_r = 0\ (\forall\ R-\ \delta \le r \le R) \tag{4.27}$$

The Navier-Stokes momentum equation in the *z*-direction is shown in Equation (4.28) along with an indication of the terms that are canceled based on the list of assumptions leading to a simplified form given in Equation (4.29).

$$\rho\left(\underbrace{\frac{\partial u_z}{\partial t}}_{=0(\#2)}+\underbrace{u_r}_{=0}\frac{\partial u_z}{\partial r}+\underbrace{\frac{u_\theta}{r}\frac{\partial u_z}{\partial \theta}}_{=0(\#1)}+u_z\underbrace{\frac{\partial u_z}{\partial z}}_{=0(\#3)}\right)=-\frac{\partial P}{\partial z}+\mu_L\left[\frac{1}{r}\frac{\partial}{\partial r}\left(r\frac{\partial u_z}{\partial r}\right)+\frac{1}{r^2}\underbrace{\frac{\partial^2 u_z}{\partial \theta^2}}_{=0(\#1)}+\underbrace{\frac{\partial^2 u_z}{\partial z^2}}_{=0(\#3)}\right]-\rho_L g \tag{4.28}$$

$$\frac{\mu_L}{r}\frac{d}{dr}\left(r\frac{du_z}{dr}\right)=\frac{dP}{dz}+\ \rho_L g \tag{4.29}$$

Integrating Equation (4.29) gives Equation (4.30), where C_1 is the constant of integration.

$$\mu_L r \frac{du_z}{dr} = \left(\frac{dP}{dz} + \rho_L g\right)\frac{r^2}{2} + C_1 \tag{4.30}$$

Equation (4.31) gives the shear stress for a Newtonian fluid

$$\tau = -\mu_L \frac{du_z}{dr} \tag{4.31}$$

Substituting Equation (4.31) into Equation (4.30) gives Equation (4.32)

$$-\tau \cdot r = \left(\frac{dP}{dz} + \rho_L g\right)\frac{r^2}{2} + C_1 \tag{4.32}$$

The shear stress at the interface $(r = R - \delta)$ is denoted by τ_i. The interfacial shear stress is a boundary condition and can be represented as shown in Equation (4.33). τ_i is used to eliminate the constant C_1

$$-\tau_i(R - \delta) = \left(\frac{dP}{dz} + \rho_L g\right) \cdot \frac{(R-\delta)^2}{2} + C_1 \tag{4.33}$$

Substituting, C_1 into Equation (4.32) leads to Equation (4.34)

$$\tau = \tau_i \frac{(R-\delta)}{r} - \frac{1}{2}\left(\frac{dP}{dz} + \rho_L g\right)\left(\frac{r^2 - (R-\delta)^2}{r}\right) \tag{4.34}$$

From Equation (4.31), the shear stress can be written in terms of velocity gradient and is substituted into Equation (4.34), which leads to Equation (4.35)

$$-\mu_L \frac{du_z}{dr} = \tau_i \frac{(R-\delta)}{r} - \frac{1}{2}\left(\frac{dP}{dz} + \rho_L g\right)\left(\frac{r^2 - (R-\delta)^2}{r}\right) \tag{4.35}$$

Integrating Equation (4.35) with respect to *r*, leads to Equation (4.36)

$$-\mu_L u_z = \tau_i(R-\delta)\, ln\, r - \frac{1}{2}\left(\frac{dP}{dz} + \rho_L g\right)\left(\frac{r^2}{2} - (R-\delta)^2\, In\, r\right) + C_2 \qquad (4.36)$$

At, $r = R$, the velocity is zero ($u_z = 0$) as there is no slip at the pipe wall. This is the second boundary condition, which eliminates the constant C_2 and leads to an expression of liquid film velocity as shown in Equation (4.37).

$$u_z = \frac{1}{\mu_L}\left[\left(\tau_i(R-\delta) + \left(\frac{(R-\delta)^2}{2}\left(\frac{dP}{dz} + \rho_L g\right)\right)\right) In\frac{R}{r} - \frac{1}{4}\left(\frac{dP}{dz} + \rho_L g\right)(R^2 - r^2)\right] \qquad (4.37)$$

The mass flow rate of the liquid film, $\dot{m}_L$, can be expressed as shown in Equation (4.38)

$$\dot{m}_L = \int_{R-\delta}^{R} \rho_L 2\pi u_z r dr \qquad (4.38)$$

Substituting the expression for u_z from Equation (4.37) in Equation (4.38) and integrating it with respect to *r* over the thickness of the liquid film leads to the expression of mass flow rate of liquid film as shown in Equation (4.39)

$$\dot{m}_L = \frac{2\pi\rho_L}{\mu_L}\left[\left(\tau_i(R-\delta) + \left(\frac{(R-\delta)^2}{2}\left(\frac{dP}{dz} + \rho_L g\right)\right)\right)\left(\frac{R^2-(R-\delta)^2}{4} - \frac{(R-\delta)^2}{2}\ln\left(\frac{R}{R-\delta}\right)\right)\right] - \frac{\pi\rho_L}{8\mu_L}\left(\frac{dP}{dz} + \rho_L g\right)(R^2 - (R-\delta)^2)^2 \qquad (4.39)$$

In Equation (4.39), the radius is constant for a particular pipe size and acceleration due to gravity is assumed to be constant. The density and viscosity of the liquid oil-refrigerant mixture is determined from properties at the test section pressure and temperature. Therefore, the film thickness, pressure gradient and interfacial shear stress are the only unknowns. To solve for these three parameters, two more equations relating these parameters are needed.

The interfacial shear stress is defined as shown in Equation (4.40) in terms of superficial velocity instead of actual velocity, which is different from the model proposed by Sethi (2011). The

interfacial friction factor (f_i) in this equation can be obtained using an empirical correlation. The friction factor correlation of the form shown in Equation (4.41) was attempted, where f_s is the friction factor of a smooth pipe which is a function of Reynolds number of the vapor as shown in Equation (4.42) and $\delta^+$is a non-dimensional film thickness which is given in Equation (4.43). This form of friction factor was proposed by Sethi, (2011).

$$\tau_i = \frac{1}{2} f_i \rho_G {j_G}^2 \tag{4.40}$$

$$\frac{f_i}{f_s} = 1 + (v_1 Re_l^{v_2})(Re_g^{v_3})(\delta^{+v_4}) \tag{4.41}$$

$$f_s = 0.046 Re_g^{-0.2} \tag{4.42}$$

$$\delta^+ = \frac{\delta}{\nu_g}\sqrt{\frac{\tau_i}{\rho_g}} \tag{4.43}$$

Superficial velocity of the vapor core (j_G) can be calculated using the known mass flow rate of vapor $(\dot{m}_G)$, cross sectional area of pipe (A) and the density of vapor (ρ_G) as shown in Equation (4.44). Similarly, the superficial velocity for the liquid film (j_L) can be calculated as shown in Equation (4.45). Equations for Reynolds number of both the vapor core (Re_G) and liquid film (Re_L) in terms of superficial velocities are presented in Equations (4.46) and (4.47), respectively.

$$j_G = \frac{\dot{m}_G}{\rho_G A} \tag{4.44}$$

$$j_L = \frac{\dot{m}_L}{\rho_L A} \tag{4.45}$$

$$Re_G = \frac{j_G \rho_G D}{\mu_G} \tag{4.46}$$

$$Re_L = \frac{j_L \rho_L D}{\mu_L} \tag{4.47}$$

From a force balance on the refrigerant core, Equation (4.48) relates pressure gradient to film thickness and interfacial shear stress. In Equation (4.48), D_g is the diameter and A_g is the cross-sectional area that is occupied with the refrigerant vapor core.

(4.48)

$$\frac{dP}{dz} + \rho_G g + \frac{\tau_i \pi D_G}{A_G} = 0$$

The coefficients of Equation (4.41) were determined using a curve fit of the experimental data for R410A/POE32 for only the 16 mm line. A plot of interfacial friction factor (f_i) as a function of refrigerant Reynolds number is shown in Figure 4.17. With the coefficients obtained from the first attempt, the predictions of oil retention were not good. On further investigation, an outlier (data point #91) was identified in the experimental data. As the refrigerant mass flux increases, the influence of gravity decreases and the oil retention difference between the vertical line and horizontal line becomes smaller. Therefore, the usual trend has been that the difference in the oil retention between the horizontal and vertical line is higher at mass flux of 2 x Jacobs limit compared to a mass flux of 3 x Jacobs limit. However, in the plot shown in Figure 4.18, it is observed that the difference in the oil retention between the vertical line and horizontal line for data point #91 is smaller compared to the difference for data point #105. A re-test (data point #195) was done at the same condition as point #91. Comparing to the usual trend, the oil retention in the vertical line for data point #195 seems more reasonable as shown in Figure 4.18. Therefore, the coefficients of Equation (4.41) were re-derived by using the replaced experimental data point and the updated results are shown in Figure 4.19. Oil retention predictions were made using these coefficients for the interfacial friction factor.

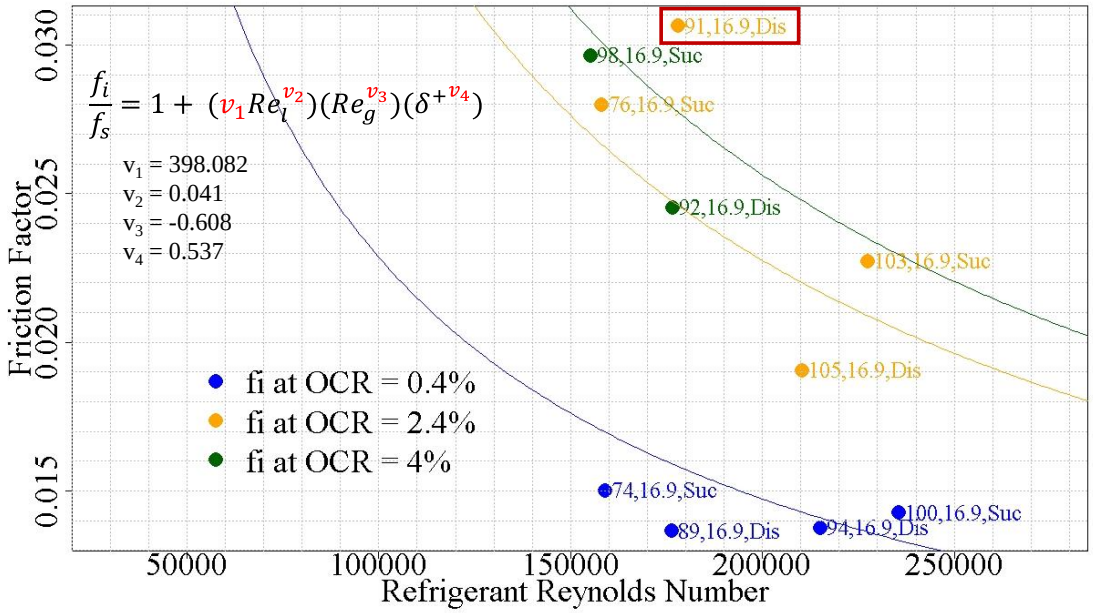

Figure 4.17: First attempt of obtaining coefficients for friction factor of the interface

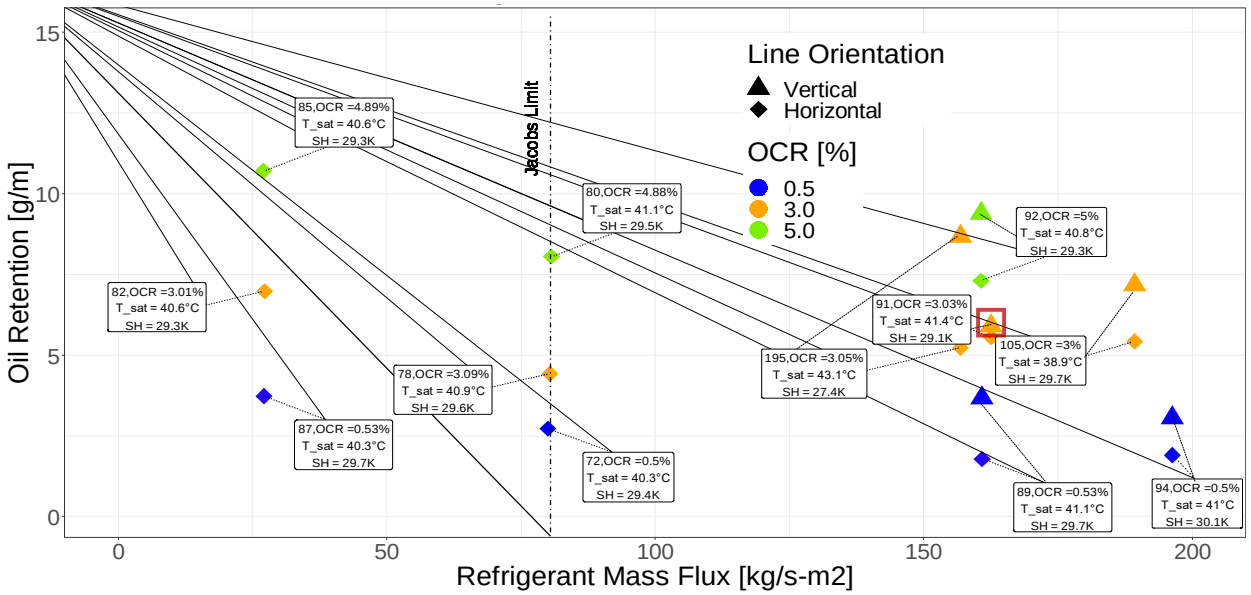

Figure 4.18: Oil retention in discharge line for R410A/POE32 for line size 16.9 mm

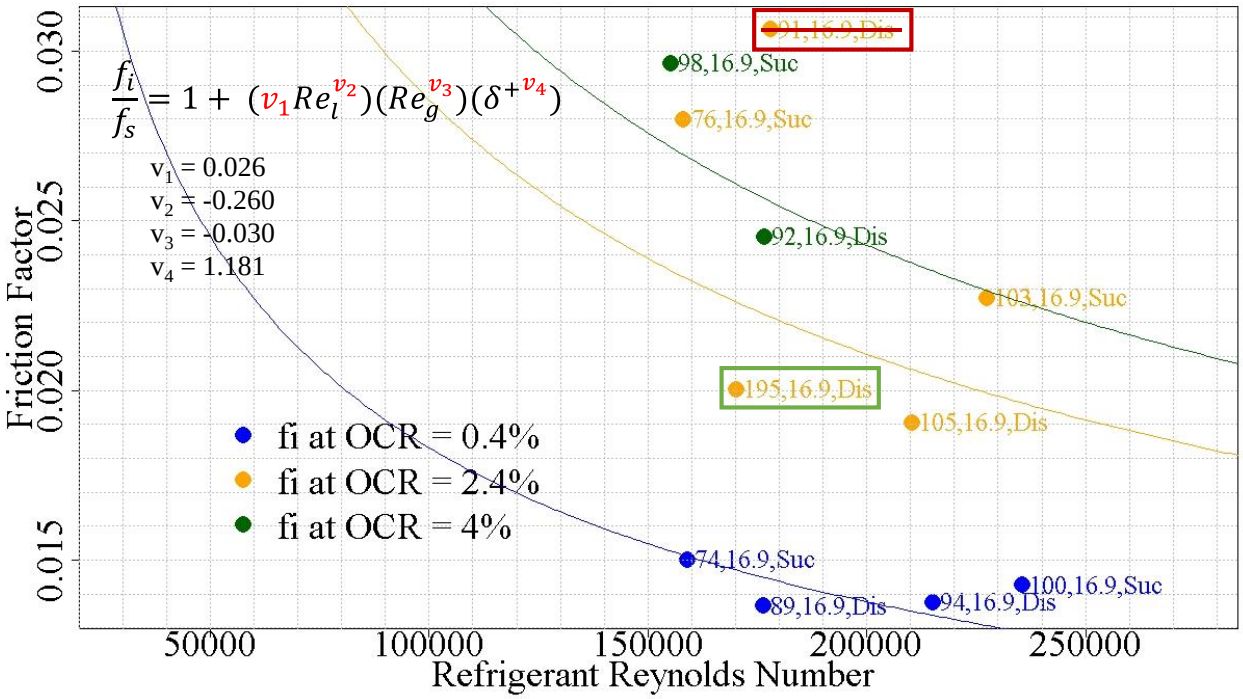

Figure 4.19: Second attempt of obtaining coefficients for friction factor of the interface with a replaced data point. Data point #91 was eliminated and data point #195 was added.

With the known coefficients for the interfacial friction factor, Equations (4.39) to (4.48) can be iteratively solved simultaneously by guessing an initial value of the film thickness. With the known value of film thickness at convergence, the mass of oil retained per unit length can be predicted using Equation (4.49). The term $(1 - \omega_{ref})$ corrects for the refrigerant dissolved in the liquid film based on the solubility of the oil-refrigerant pair as described in Section 4.3.

$$m_{oil} = 2\pi R \rho_l \delta (1 - \omega_{ref}) \tag{4.49}$$

Predicting Minimum Refrigerant Mass Flux for Oil Return

The minimum refrigerant mass flux that is required for the oil to return in a vertical riser can be determined from the developed annular flow model. Physically, the oil does not get transported through a vertical riser when the film reversal begins. At this instance, the shear stress at the wall goes to zero. The shear stress at the wall, τ_w, is determined using Equation (4.50), which was derived by substituting $r = R$ in Equation (4.34).

$$\tau_w = \tau_i \frac{(R-\delta)}{R} - \frac{1}{2}\left(\frac{dP}{dz} + \rho_l g\right)\left(\frac{R^2-(R-\delta)^2}{R}\right) \quad (4.50)$$

A relationship between τ_i, δ and $\frac{dP}{dZ}$ is then determined by setting $\tau_w = 0$ leading to Equation (4.51)

$$\tau_i \frac{(R-\delta)}{\delta} = \frac{1}{2}\left(\frac{dP}{dz} + \rho_l g\right)(2R-\delta) \quad (4.51)$$

By solving Equations (4.39) to (4.48) along with Equation (4.51), the refrigerant mass flux at the instance where shear stress is zero can be calculated. This refrigerant mass flux is then identified as the limit beyond which oil would not return in a vertical riser. This limit is equivalent to that proposed by Jacobs et al. (1976). Refrigerant mass flux limits calculated with this approach have also been published by Mehendale and Radermacher (2000), Sethi (2011) and Ramakrishnan (2012)

Model Prediction Results and Discussion

Both the models for predicting oil retention and minumum refrigerant mass flow required for oil return in vertical lines were implemented in Engineering Equation Solver (EES, Klein 2018). Oil retention predictions compared with the experimental data, whereas the minimum refrigerant mass flux predictions are compared with the Jacobs limit.

The plots in Figure 4.20 and Figure 4.21 show vertical line oil retention predictions and experimental results with respect to refrigerant mass flux for suction conditions with R410A/POE32 for the 16.9 mm and 10.9 mm lines, respectively. The solid lines are predictions from the model, whereas the markers are the experimental data points. The transparent color bands are ±1 g/m wide to get an idea of the deviation of predictions compared to the actual experimental data points. The error bars show measurement uncertainty of 3%. The dotted colored lines show the proposed critical limits of minimum refrigerant mass flux for the oil to return at the OCR mentioned in the legend. Figure 4.22 and Figure 4.23 show results for oil retention in discharge conditions for the 16.9 mm and 10.9 mm lines, respectively. Similarly, the plot in Figure 4.24

shows the two spot tests and oil retention predictions for suction conditions in the 19.9 mm line. For the, 19.9 mm line, there was no experimental data collected for the discharge condition, and therefore Figure 4.25 shows only the prediction results.

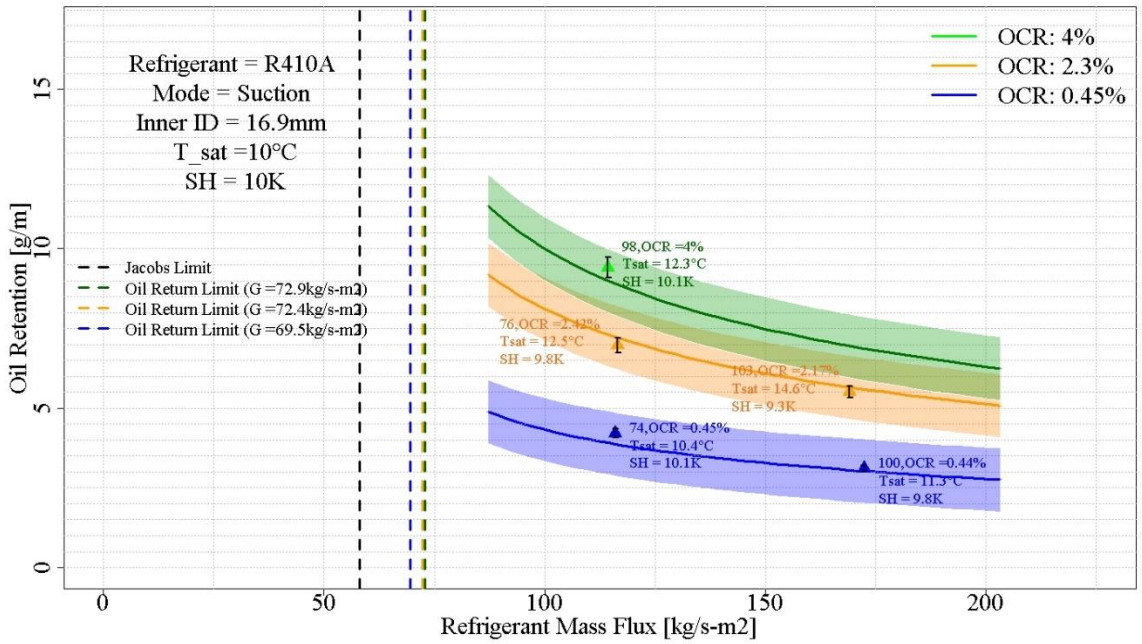

Figure 4.20: Oil retention vs refrigerant mass flux model prediction (lines) compared with experimental data (markers) for annular flow for R410A/POE32 in 16.9 mm vertical suction line

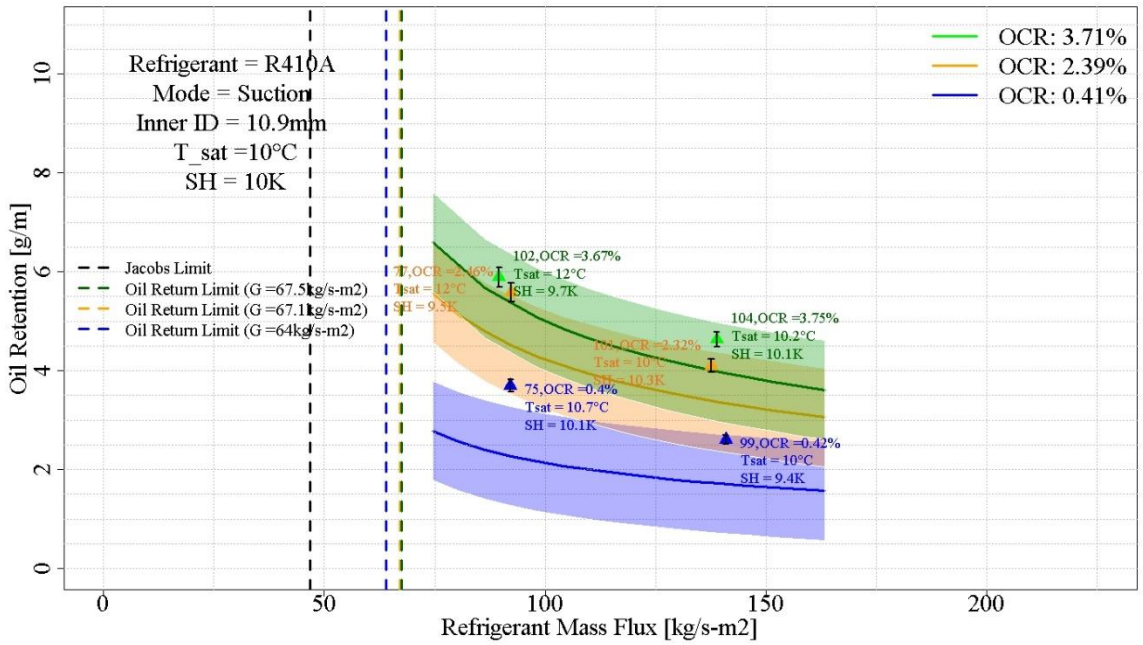

Figure 4.21: Oil retention vs refrigerant mass flux model prediction (lines) compared with experimental data (markers) for annular flow for R410A/POE32 in 10.9 mm vertical suction line

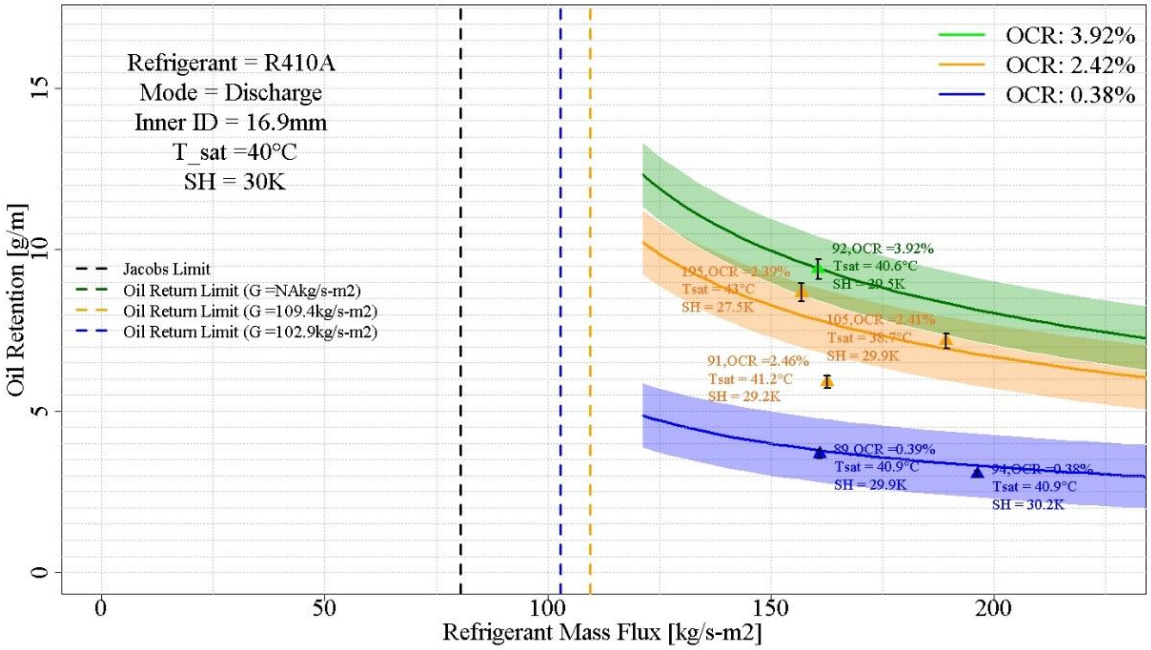

Figure 4.22: Oil retention vs refrigerant mass flux model prediction (lines) compared with experimental data (markers) for annular flow for R410A/POE32 in 16.9 mm vertical discharge line

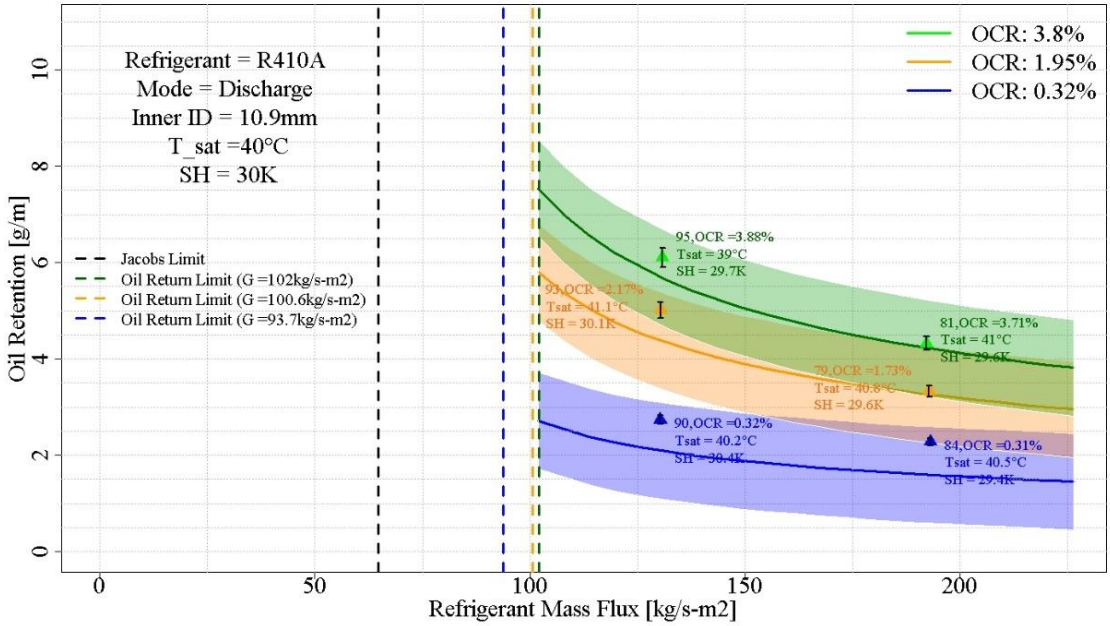

Figure 4.23: Oil retention vs refrigerant mass flux model prediction (lines) compared with experimental data (markers) for annular flow for R410A/POE32 in 10.9 mm vertical discharge line

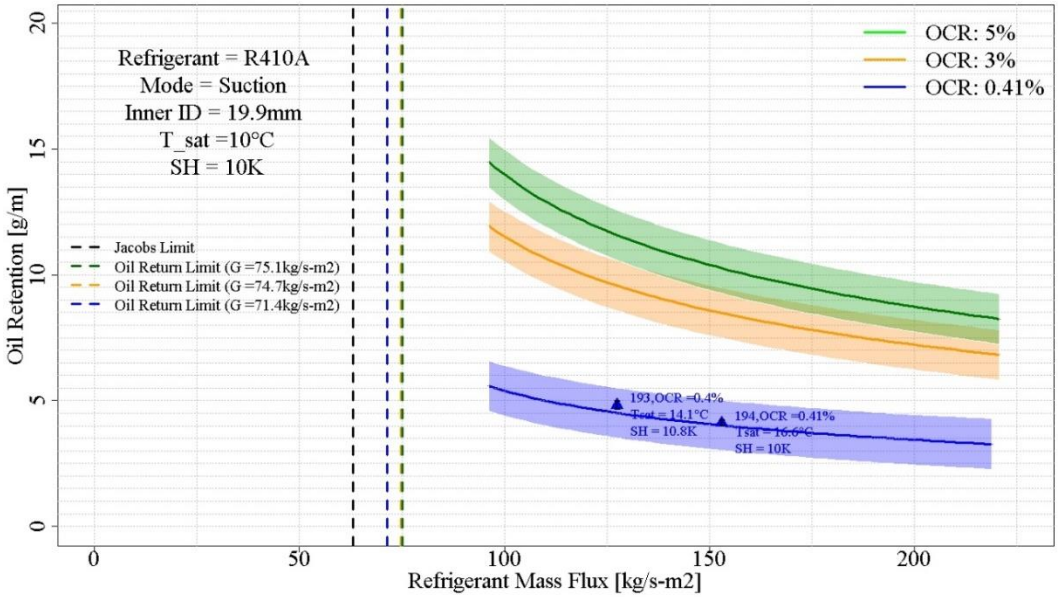

Figure 4.24: Oil retention vs refrigerant mass flux model prediction (lines) compared with experimental data (markers) for annular flow for R410A/POE32 in 19.9 mm vertical suction line

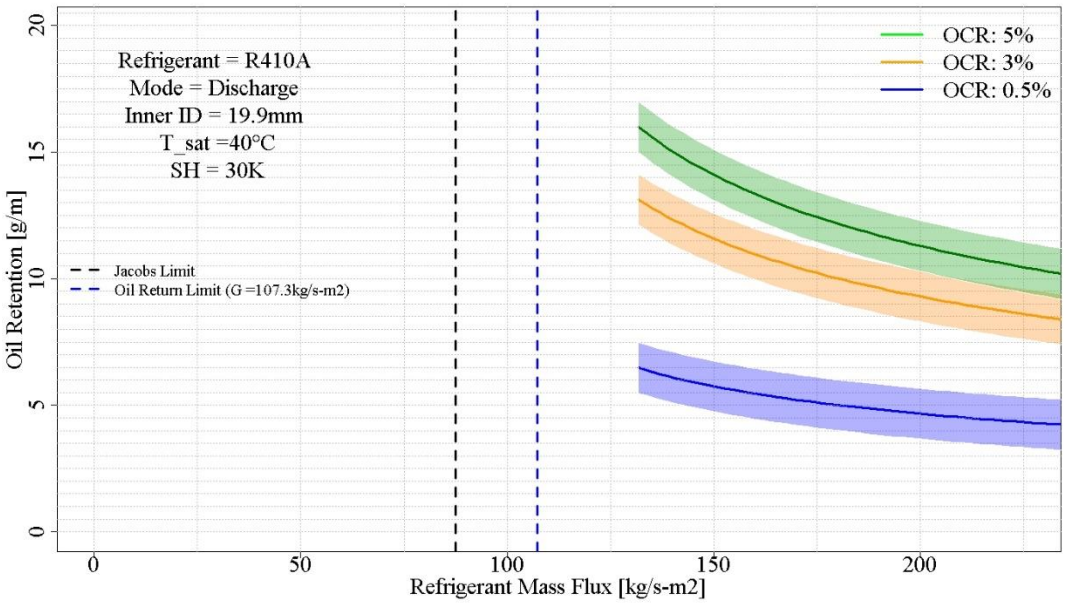

Figure 4.25: Oil retention vs refrigerant mass flux model prediction (lines) for annular flow for R410A/POE32 in 19.9 mm vertical discharge line

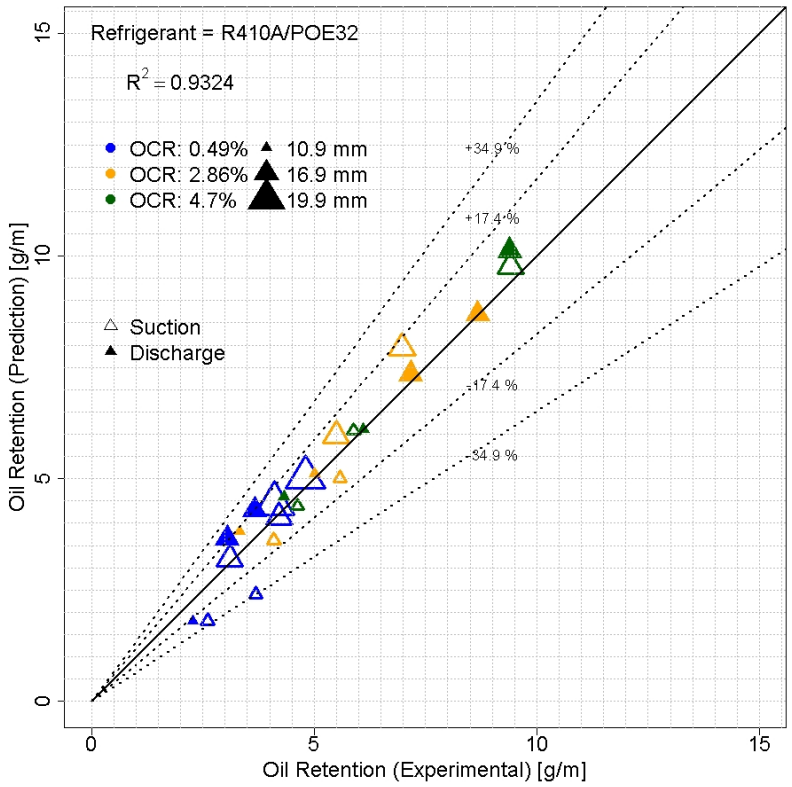

Figure 4.26: Parity plot showing the accuracy of the vertical pipe annular flow model for all the data points of R410A/POE32

Following are comments related to the model predictions and comparisons with experimental data.

- The oil retention predictions in Figure 4.20 to Figure 4.24 were calculated for specific values of OCR corresponding to average experimental values for the different target OCRs in the tests. The values of OCR for experimental data points varied from the average values and are noted on the plot.
- There are also some variations in the experimental saturation temperatures and the test section temperatures from the original targets that were used in the model. The actual saturation temperatures along with the superheat values for the experimental data points are also marked in the labels for a quick reference.
- A parity plot eliminates all such variations as the prediction is made for the actual experimental conditions for the particular experimental data point to get a true comparison. Figure 4.26 shows the parity plot and it can be observed that the R^2 value of prediction vs experimental value is 0.9315 and all the data points fall within a relative error of ±38.3 % relative error. It should be noted that the outlier data point #91 was eliminated from the parity plot. Including data point #91 reduced the R^2 value to 0.9324, but with the same maximum relative error of ±38.3 %.
- The coefficients for the friction factor correlation were obtained using the experimental data for only the 16.9 mm line. However, the model predicted oil retention within ±38.3 % relative error for all the points which includes the 10.9 mm line data points for R410A/ POE32 and two data points from 19.9 mm. This shows that that model is capable of reasonable predictions for different pipe sizes.

The annular flow model was run for different refrigerant/oil combination and the coefficients of the empirical correlation for interfacial friction factor were determined and are presented in Table 4.2. The parity plots in Figure 4.27, Figure 4.28 and Figure 4.29 show the model prediction results for R1234ze(E)/POE32, R134a/POE32 and R32/POE32. The experimental and predicted oil retention values used in the parity plots are tabulated in APPENDIX L to APPENDIX O. The values of pressure drop per unit length and void fraction are also provided in the tables.

Table 4.2: Coefficients of empirical correlation for interfacial friction factor

Sr.	Refrigerant/Oil Combination	v_1	v_2	v_3	v_4
1.	R410A/POE32	0.0255	-0.2597	-0.0301	1.1807
2.	R32/POE32	0.0696	-0.1625	-0.1086	1.1489
3.	R1234ze(E)/POE32	4.3941	-0.2673	-0.5645	1.4221
4.	R134a/POE32	0.4994	-0.0637	-1.669	0.8708

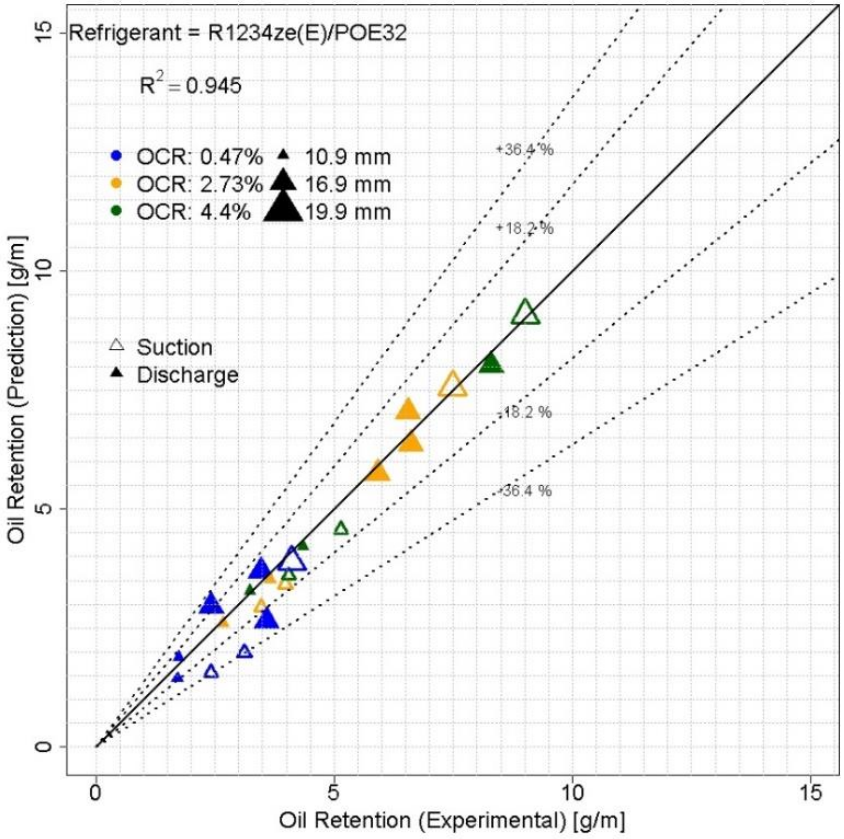

Figure 4.27: Parity plot for R1234ze(E)/POE32 in vertical line

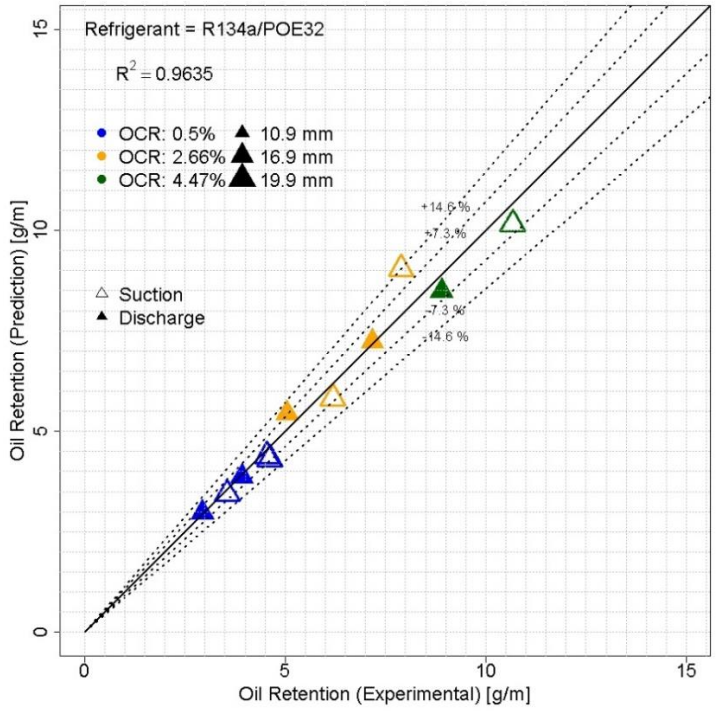

Figure 4.28: Parity plot for R134a/POE32 in vertical line

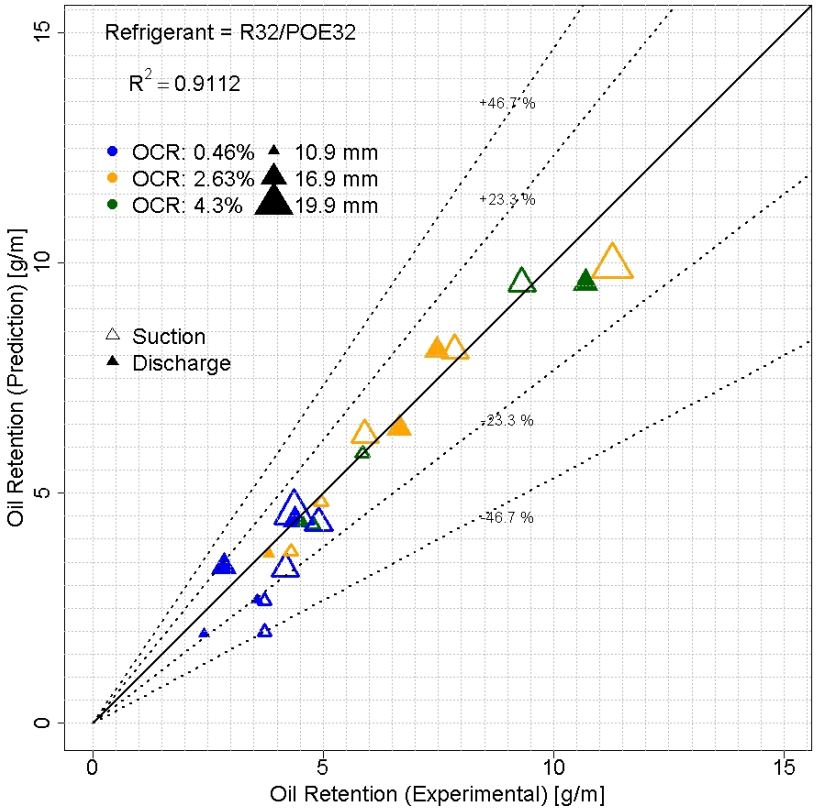

Figure 4.29: Parity plot for R32/POE32 in vertical line

4.3 Refrigerant-Oil Mixture Properties

Based on the refrigerant-oil chemistry, there is some amount of liquid refrigerant dissolved in the oil. The properties of this liquid refrigerant-oil mixture are different compared to pure oil or pure liquid refrigerant. To account for these differences in the model, properties such as liquid density, vapor pressure and viscosity at bulk concentrations of refrigerant over a range of temperature were provided by Shrieve (2020). This data is experimentally recorded and then presented in the form of mathematical models, which helped in implementing them in the models. The form of these correlations were same, and different coefficients were provided for different refrigerant/oil combinations.

The solubility data was used for two different purposes in this study. The first purpose was to correct the rate of mass flow rate of oil that was injected in the refrigerant. While running experiments, based on the solubility, the oil injected through the oil line had some amount of liquid refrigerant dissolved in it. When this liquid oil-refrigerant mixture passes through the Coriolis mass flow meter, the density of this mixture is also measured along with the mass flow rate. In addition, the temperature of this mixture is measured using an in-line thermocouple probe in the oil line before the oil is injected in the refrigerant line. With the temperature and the density of this mixture, the concentration of liquid refrigerant in oil (ω_{inj}) can be determined. With the known concentration, the measured mass flow rates of oil and refrigerant are corrected with this concentration. The experimental data points shown with the model prediction plots for both stratified and annular flow models are based on corrected refrigerant and oil mass flow rates. The density and temperature of oil and liquid refrigerant mixture was not measured while running tests with R134a/POE32. Therefore, the mixture density was assumed to be 0.98 g/cm^3 and the temperature was assumed to be 25°C. Based on these assumed values of density and temperature, the concentration of refrigerant R134a in POE32 was determined and the mass flow rates were corrected. For R32/POE32 the mixture density as a function of temperature and liquid refrigerant concentration were not available, therefore the concentration of liquid refrigerant in oil was assumed to be 10% based on the concentration observed in R410A/POE32 and R1234ze(E)/POE32.

The second purpose for the solubility was to calculate the mixture properties of the liquid phase in the test section. There is liquid refrigerant dissolved in the oil for both the liquid phase in the stratified flow for horizontal lines and the liquid film in the annular flow for vertical lines. Therefore, the density and viscosity of the liquid phase have to be calculated for the mixture and not for pure oil. At the test section pressure and temperature, the concentration of the liquid refrigerant (ω_{ref}) was determined using the solubility correlation. With the known concentration and the temperature of the test section, the mixture density (ρ_L) and kinematic viscosity (ν_L) were obtained. In addition, when the oil retention was calculated from the model, the amount of liquid refrigerant was subtracted from the oil retention based on the concentration of liquid refrigerant (ω_{ref}) calculated at the test section temperature and pressure at the steady-state condition. Table 4.3 presents properties for the different refrigerant/oil combinations at typical suction line and discharge line conditions for easy reference.

Table 4.3: Refrigerant-oil mixture properties for typical conditions in suction and discharge line.

Sr.	**Refrigerant/Oil**	T	T_{sat}	P	ω_{ref}	ρ_L	ν_L
		[°C]		**[kPa]**	**[-]**	**[kg/m^3]**	**[cSt]**
1.	R410A/POE32	20	10	1088	0.2709	1001.0	5.026
		70	40	2426	0.1930	939.9	2.697
2.	R32/POE32	20	10	1107	0.207	1000.7	5.902
		75	40	2487	0.1367	947.4	3.071
3.	R1234ze(E)/POE32	20	10	310	0.3812	1070	4.079
		55	40	767	0.3355	1022	2.160
4.	R134a/POE32	20	10	415	0.2706	1047	7.966
		60	40	1017	0.2308	997	3.604

4.4 Conclusions

Both the stratified flow model and the annular flow models work well in predicting oil retention in horizontal lines and vertical lines with upward flow. The empirical correlations required for the interfacial friction factor were developed using a 16.9 mm line. These correlations provided good predictions for 10.9 mm as well as 16.9 mm lines. Based on this initial experience, the correlations should also predict oil retention when employing the same type of oil with different viscosity grades. For example, the correlations developed with R410A/POE32 should work for

R410A/POE100. As future work, spot tests with different refrigerant/oil pair will be carried out to check the validity of the model.

Some physical aspects are not captured fully in the current model. For example, in the stratified flow model, the impact of waves at the interface is not captured. Some advanced models, such as proposed by Tzotzi and Andritsos (2013), that, use different correlations for friction factor based on the flow regime, may have better accuracy. At higher mass flow rates when the flow starts to transition from stratified flow towards the annular flow, the gas-liquid interface does not remain straight and it exhibits a concave downward curved configuration. Chen, et. al. (1997) proposed a "double-circle" model that can capture these effects and may improve the accuracy of the model at higher refrigerant mass flow rate.

In general, from the trends it is observed that oil retention decreases as the refrigerant mass flux increases. However, in many cases it was observed that the oil retention in horizontal lines at 3 x Jacobs limit was a bit higher compared to the oil retention at 2 x Jacobs limit, especially at OCR 3 % and 5 %. For example, in Figure D.1 the oil retention in the horizontal line for ID#103 is higher compared to ID#76. Similarly, in Figure D.2, ID#104 has higher oil retention compared to ID#102. Also, in Figure D.4 oil retention in ID#81 and ID#79 is higher compared to ID#95 and ID#93. This behavior is also observed in some cases of R32/POE32 and R1234ze(E)/POE32. The cause of this behavior is unknown and the stratified flow model does not capture this behavior, but it seems that there may be waves forming at the interface at 3 x Jacobs limit which may be increasing the oil retention compared to that at 2 x Jacobs limit. Although the difference in the oil retention is not significant, this phenomenon may be worth exploring in future work.

5. CONCLUSIONS

The motivation of this study was to provide design tools to engineers within the HVAC&R industry to address the problems of oil return and oil retention in systems utilizing the vapor compression cycle. These tools should help in designing oil management strategies that provide better reliability in advanced vapor compression cycles having continuous capacity control, needed to improve the system efficiency.

In particular, the focus of this study was to build a design tool that provides information of oil retention in long gas lines of air-conditioning systems, along with the minimum refrigerant mass flux required for the oil to return in vertical risers. Physics-based semi-empirical models were developed to predict oil retention and they were validated with a wide range of experimental data obtained in this study. The annular flow model developed to predict oil retention in vertical lines was found to be accurate within ±36 % with an $R^2 = 0.93$ or better. Similarly, the stratified flow model was able to predict oil retention in horizontal lines with an accuracy of ±42% with $R^2 = 0.90$ or better, except for prediction with R134a/POE32, which was within ±55% with $R^2 = 0.86$. Overall, the oil retention predictions are reasonable and consistent with those observed in the literature for other refrigerant/oil combinations. The annular flow model also provides the minimum refrigerant mass flux required for the oil to return in a vertical upward flow. These limits are equivalent to the traditionally used Jacobs limit.

The models developed in this work can be used in selecting an appropriate refrigerant line size for a particular application. As an example, say a design engineer wants to determine the required diameter for oil return and compressor oil retention within a suction line that is configured as a 60 m long horizontal line and a 20 m long vertical line for a unitary split system running with refrigerant R410A. At a design condition, assume the refrigerant mass flow rate is 40 g/s, the oil discharge from the compressor leads to an OCR of 0.5% and the suction line has a saturation temperature of 10 °C with a superheat of 10 K. In addition, assume that the compressor sump is charged with 1500 g of POE32 oil. If the designer selects a 7/8” nominal line (inner diameter of 19.9 mm), then using the model, the total oil retention in the horizontal and vertical suction line would be 270 g, which is 18% of the oil charged in the compressor sump. The refrigerant mass

flux would be 128 kg/s-m^2 and the total pressure drop predicted in the lines would be 68 kPa. However, if the designer selects a smaller, 3/4" nominal line (inner diameter of 16.9 mm), then the total oil retention would reduce down to 179 g, which is 12 % of the oil charged in the compressor. However, the pressure drop would increase to 120 kPa with the refrigerant mass flux of 178 kg/s-m^2. Therefore, selecting a smaller line would reduce the oil retention at the design condition but would increase the pressure drop and reduce the overall system performance. Alternatively, if the system has a variable-speed compressor, then the designer could select the 7/8" line to get a benefit of lower pressure drop and implement a control strategy of increasing the refrigerant mass flow rate to 90 g/s for short durations to return the oil back to the compressor sump. The oil retention in the 7/8" line with a refrigerant mass flow rate of 90 g/s would be 191 g (13 % of oil sump) with a pressure drop of 235 kPa and the refrigerant mass flux would be 288 kg/s-m^2. In any case, for the oil to successfully return through the vertical riser, the refrigerant mass flux should not be reduced to less than a limit of 72.87 kg/s-m^2 that is predicted by the annular flow model. This means for a refrigerant flow rate of 40 g/s, the line diameter should not be more than 1-1/8" (inner diameter of 26 mm). Such design simulations studies can be carried out with models developed in this study in order to have a good understanding of oil retention and oil return in the gas lines for a particular system design.

The test setup built to measure oil retention in gas lines was designed such that a wide range of parameters can be tested. Using a gravimetric method, oil retention was measured in horizontal and vertical test sections with four refrigerant/oil pairs (R134a/POE32, R410A/POE32, R32/POE32 and R1234ze(E)/POE32) in three line sizes having inner diameters of 19.9 mm, 16.9 mm and 10.9 mm. These tests were carried out at conditions simulating typical suction lines ($T_{sat} = 10$ ℃) as well as discharge line ($T_{sat} = 40$ ℃). The refrigerant mass flow rate was varied from 1/3rd x Jacobs limit to 3 x Jacobs limit with three oil circulation ratios (0.5 wt.%, 3 wt.% and 5 wt.%). With these combinations, 162 tests were carried out that provided experimental data of oil retention for a wide range of test parameters. The steady-state data of these tests are tabulated in APPENDIX F. A subset of this experimental data was used to develop the empirical correlations of interfacial friction factor for each refrigerant/oil pair and the remaining data was used to validate the models.

In addition to oil retention in the system, Oil Circulation Ratio (OCR) is an important parameter that quantifies the amount of oil circulating in the system. It also one of the inputs to the model that predicts oil retention. Although OCR is dependent on various factors such as the refrigerant mass flow rate, properties of refrigerant etc., it mainly accounts for oil that is discharged from the compressor, which varies for different types of compressors operating at different conditions. Therefore, a compressor level research is needed to develop a model to predict OCR. As this study was focused on system level oil management rather than the compressor level, the objective here was not to develop a model to predict OCR. Instead a non-invasive, in-situ method based on oil separation has been developed to measure OCR in real time, which involves minimal human intervention. Based on this method, a design of a low-cost small form factor Smart Accumulator was proposed that has a capability of measuring OCR in a suction line of a vapor compression cycle. This OCR measurement approach along with oil retention models can provide real-time monitoring and control of oil in the system. In conclusion, the developed tools will help in designing better oil management strategies and may support the development of high efficiency HVAC&R systems with multiple compressors for capacity control.

5.1 Unique Contributions from the Study

This study resulted in a few unique contributions to the literature. A stratified flow model was developed to predict oil retention in the horizontal flow of refrigerant in suction lines for new refrigerant/oil pairs. In addition, experimental data of oil retention in horizontal lines at mass flux less than 1 x Jacobs limit was obtained that was previously unavailable. The experimental data and models are useful in developing a better understanding of the amount of oil retention in horizontal lines especially at low mass flux, which may be helpful in analyzing oil retention when using variable-speed compressors running at partial load conditions. The experimental setup built to measure oil retention is highly flexible in measuring oil retention for a wide range of test parameters and includes the capability to run upcoming mildly flammable A2L refrigerants.

In addition, a separation-based method to measure OCR was developed. This represents a new and novel approach for non-invasive, in-situ measurement of OCR that can be applied in the suction line of a refrigeration system where oil and refrigerant are immiscible. Previous proposed approaches of measuring OCR have been limited to the liquid line with miscible refrigerant and

oil mixtures. Based on this separation-based method of measuring OCR, a design of a low-cost, small form factor smart accumulator was proposed that has capability of real-time sensing of OCR. A non-provisional patent has been filed for the measurement method as well as the smart accumulator.

5.2 Recommendations for Future Work

The accuracies of models predicting oil retention should be improved by capturing better physical aspects of the oil-refrigerant flow in circular pipes. For example, while predicting oil retention in horizontal lines for the flows in stratified/wavy flow regime, advanced models accounting for the waves at the interface may help in improving the accuracy of oil retention and pressure drop predictions.

Similar to an OCR sensor, a low-cost capacitance-based sensor to measure real-time oil retention in circular tubes may be developed. Due to the difference in the dielectric constants of refrigerant vapor and liquid oil, the void fraction of refrigerant vapor in the refrigerant-oil flow has a direct correlation with capacitance measured across the circular pipe. This phenomenon can be used to develop an oil retention sensor which can be used in conjunction with the OCR sensor to implement active oil management strategies.

The annular flow model predicts the minimum refrigerant mass flux required for the oil to return in a vertical riser. The limit is calculated based on an assumption that the wall shear stress goes to zero when the oil film reversal occurs. The current test setup may be modified to add transparent sections in the vertical line and the film reversal can be visually identified by varying the refrigerant mass flow rate. These experimental results can help to validate the proposed limits of the model. Similarly, differential pressure sensors may also be added across the test sections to validate the pressure drop predictions from the test setup. In addition, transparent sections may also be added in the horizontal test section, to verify the flow regime visually.

APPENDIX A. TEST DATA OF OCR MEASUREMENT USING THE LIQUID LEVEL PROBE METHOD AND VISUAL SCALE METHOD FOR FOUR TEST CONDITIONS MENTIONED IN TABLE 2.2

Table A.1: Test results of OCR for condition 1 from Table 2.2 with two different methods.

Test	Refrigerant Flow Rate	Solubility	Level Probe Measurement				Visual Scale Measurement			
			Oil Mass Collected	Duration	Rate	OCR	Oil Mass Collected	Duration	Rate	OCR
	kg/h	[%]	[g]	[s]	[kg/h]	%	[g]	[s]	[kg/h]	%
2	457.31±4.57	6±1%	70.61±15.95	97	2.621±0.592	0.573±0.130	76.03±2.19	99±1	2.765±0.084	0.605±0.019
3	456.36±4.56		68.59±15.95	92	2.684±0.624	0.588±0.137	76.03±2.19	95±1	2.881±0.088	0.631±0.020
4	456.35±4.56		72.52±15.95	92	2.838±0.624	0.622±0.137	70.29±2.16	96±1	2.636±0.086	0.578±0.020
5	454.94±4.55		67.88±15.95	78	3.133±0.736	0.689±0.162	71.72±2.17	86±1	3.002±0.097	0.660±0.022
6	453.46±4.53		72.62±15.95	87	3.005±0.660	0.663±0.146	71.72±2.17	88±1	2.934±0.095	0.647±0.022
7	452.08±4.52		75.15±15.95	92	2.941±0.624	0.650±0.138	76.03±2.19	95±1	2.881±0.088	0.637±0.021
8	451.21±4.51		71.68±15.95	88	2.932±0.652	0.650±0.145	76.03±2.19	91±1	3.008±0.093	0.667±0.022
9	448.07±4.48		68.72±15.95	85	2.910±0.675	0.650±0.151	70.29±2.16	89±1	2.843±0.093	0.635±0.022

Table A.2: Test results of OCR for condition 2 from Table 2.2 with two different methods

Test	Refrigerant Flow Rate	Solubility	Level Probe Measurement				Visual Scale Measurement			
			Oil Mass Collected	Duration	Rate	OCR	Oil Mass Collected	Duration	Rate	OCR
	kg/h	[%]	[g]	[s]	[kg/h]	%	[g]	[s]	[kg/h]	%
4	429.94±4.30	6±1%	63.75±15.95	97	2.366±0.592	0.550±0.138	73.16±2.17	102±1	2.582±0.081	0.601±0.020
5	429.96±4.30		64.65±15.95	103	2.259±0.557	0.526±0.130	70.29±2.16	106±1	2.387±0.077	0.555±0.019
7	428.25±4.28		64.65±15.95	107	2.175±0.536	0.508±0.125	70.29±2.16	112±1	2.259±0.072	0.528±0.018
8	425.78±4.26		63.09±15.95	105	2.163±0.547	0.508±0.128	70.29±2.16	112±1	2.259±0.072	0.531±0.018
9	426.59±4.27		66.92±15.95	105	2.294±0.547	0.538±0.128	70.29±2.16	110±1	2.300±0.074	0.539±0.018
10	426.68±4.27		66.68±15.95	108	2.223±0.532	0.521±0.125	73.16±2.17	116±1	2.270±0.070	0.532±0.017
11	425.96±4.26		65.93±15.95	116	2.046±0.495	0.480±0.116	73.16±2.17	122±1	2.159±0.067	0.507±0.016
12	425.30±4.25		63.15±15.95	106	2.145±0.542	0.504±0.127	67.42±2.15	113±1	2.148±0.071	0.505±0.017

Table A.3: Test results of OCR for condition 3 from Table 2.2 with two different methods

Test	Refrigerant Flow Rate	Solubility	Level Probe Measurement				Visual Scale Measurement			
			Oil Mass Collected	Duration	Rate	OCR	Oil Mass Collected	Duration	Rate	OCR
	kg/h	[%]	[g]	[s]	[kg/h]	%	[g]	[s]	[kg/h]	%
1	404.43±4.04	4±1%	64.07±16.28	89	2.592±0.659	0.641±0.163	71.78±2.20	96±1	2.692±0.087	0.666±0.023
2	403.31±4.03		62.26±16.28	87	2.576±0.674	0.639±0.167	70.32±2.20	91±1	2.782±0.092	0.690±0.024
3	402.05±4.02		64.86±16.28	96	2.432±0.611	0.605±0.152	74.72±2.21	101±1	2.663±0.083	0.662±0.022
4	400.62±4.01		63.67±16.28	93	2.465±0.630	0.615±0.157	74.72±2.21	104±1	2.586±0.081	0.646±0.021
5	399.01±3.99		68.42±16.29	100	2.463±0.586	0.617±0.147	76.18±2.22	104±1	2.637±0.081	0.661±0.021
6	399.63±4.00		65.32±16.28	85	2.766±0.690	0.692±0.173	74.72±2.21	92±1	2.924±0.092	0.732±0.024
7	399.74±4.00		64.13±16.28	104	2.220±0.564	0.555±0.141	71.78±2.20	110±1	2.349±0.075	0.588±0.020
9	400.55±4.01		71.06±16.29	107	2.391±0.548	0.597±0.137	71.78±2.20	110±1	2.349±0.075	0.587±0.020
10	399.14±3.99		65.16±16.28	94	2.496±0.624	0.625±0.156	71.78±2.20	98±1	2.637±0.085	0.661±0.022
11	399.76±4.00		65.64±16.28	101	2.340±0.580	0.585±0.145	71.78±2.20	106±1	2.438±0.078	0.610±0.021
12	398.74±3.99		68.44±16.29	93	2.649±0.630	0.664±0.158	71.78±2.20	96±1	2.692±0.087	0.675±0.023

Table A.4: Test results of OCR for condition 4 from Table 2.2 with two different methods

Test	Refrigerant Flow Rate	Solubility	Level Probe Measurement				Visual Scale Measurement			
			Oil Mass Collected	Duration	Rate	OCR	Oil Mass Collected	Duration	Rate	OCR
	kg/h	[%]	[g]	[s]	[kg/h]	%	[g]	[s]	[kg/h]	%
2	354.75±3.55	3±1%	64.33±16.45	118	1.963±0.502	0.553±0.142	71.05±2.22	129±1	1.983±0.064	0.559±0.019
3	354.23±3.54		64.31±16.45	122	1.898±0.485	0.536±0.137	68.09±2.21	131±1	1.871±0.062	0.528±0.018
4	354.38±3.54		63.65±16.45	114	2.010±0.520	0.567±0.147	69.57±2.21	129±1	1.941±0.064	0.548±0.019
5	353.78±3.54		61.76±16.45	124	1.793±0.478	0.507±0.135	72.53±2.22	140±1	1.865±0.059	0.527±0.017
6	353.21±3.53		65.21±16.45	122	1.924±0.486	0.545±0.138	71.05±2.22	129±1	1.983±0.064	0.561±0.019
7	353.71±3.54		63.46±16.45	120	1.904±0.494	0.538±0.140	71.05±2.22	132±1	1.938±0.062	0.548±0.018
8	353.60±3.54		63.36±16.45	119	1.917±0.498	0.542±0.141	72.53±2.22	133±1	1.963±0.062	0.555±0.018

APPENDIX B. VISCOSITY, SOLUBILITY AND GAS FRACTIONATION OF EMKARATE RL32S WITH R404A CAVESTRI, (1995)

Viscosity, Solubility, and Gas Fractionation
EMKARATE RL32S with R-404A at 60°C
Figure M.3

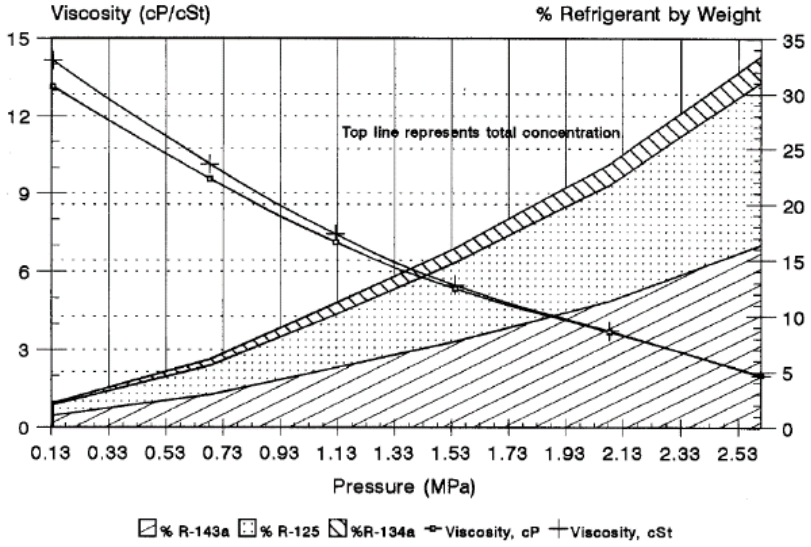

Viscosity via Gas Solubility Equilibrium
Oil degassed to 20 Millitorr

Viscosity, Solubility, and Gas Fractionation
EMKARATE RL32S with R-404A at 40°C
Figure M.4

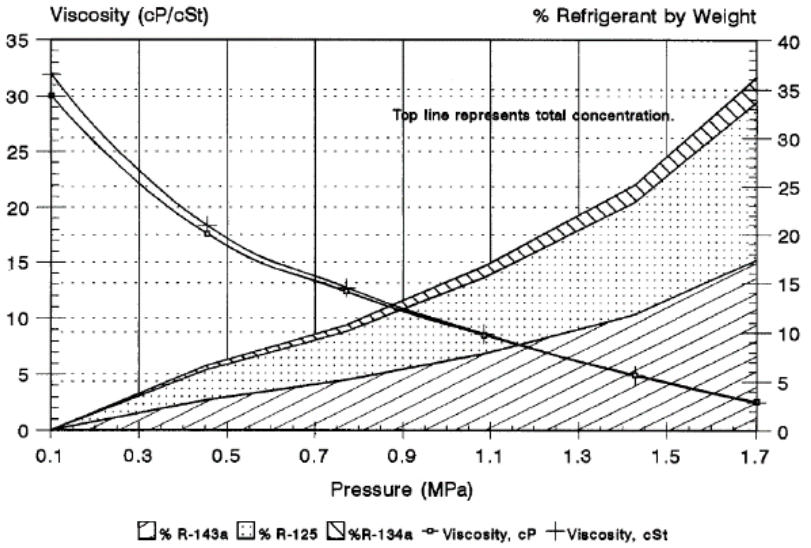

Viscosity via Gas Solubility Equilibrium
Oil degassed to 20 Millitorr

APPENDIX C. SCHEMATIC OF TEST STAND TO MEASURE OIL RETENTION

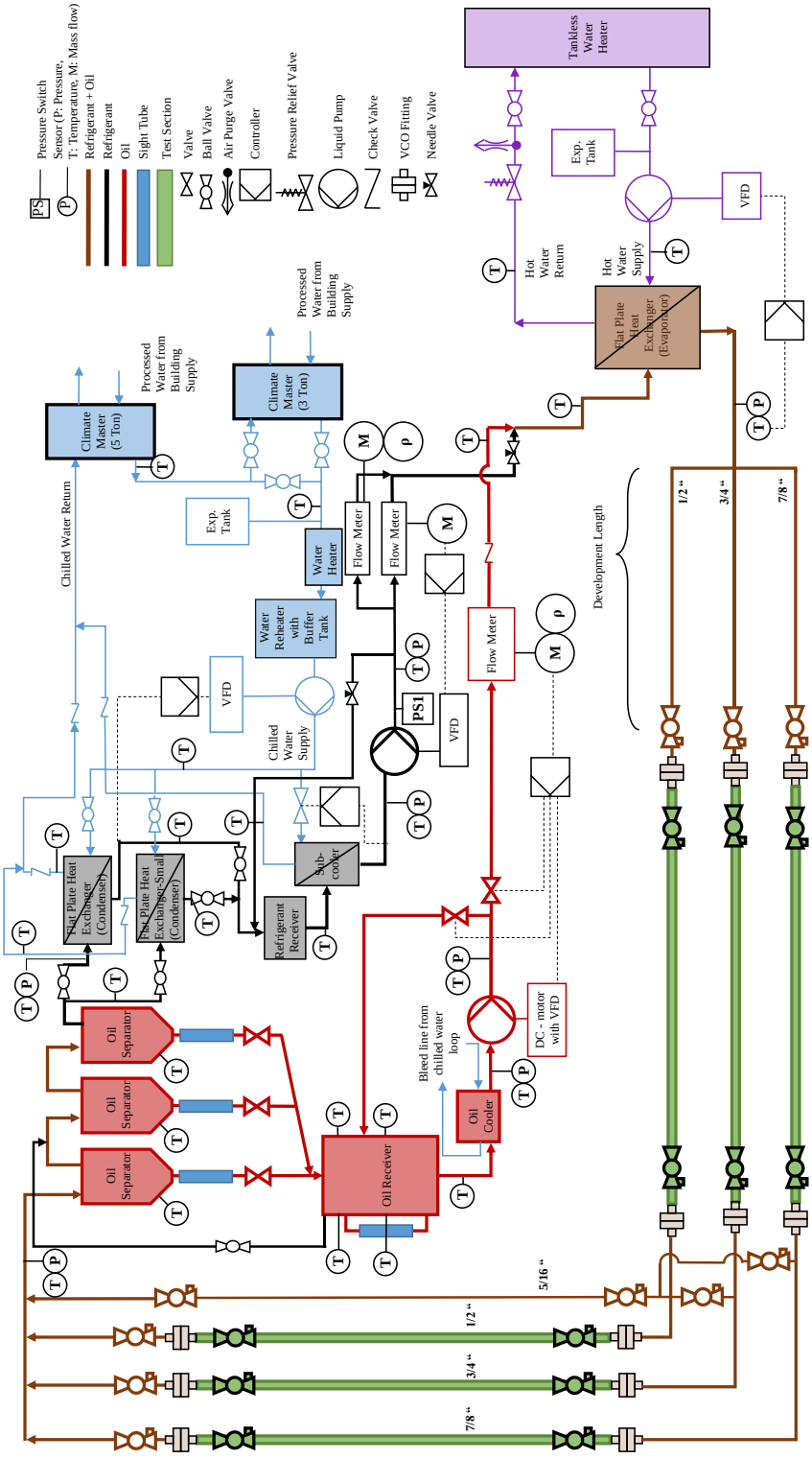

APPENDIX D. TEST CONDITIONS AND EXPERIMENTAL RESULTS OF OIL RETENTION MEASUREMENTS FOR DIFFERENT REFRIGERANT/OIL COMBINATIONS AT VARYING MASS FLOW RATES AND OCR IN HORIZONTAL AND VERTICAL LINES AT TYPICAL COMPRESSOR SUCTION AND DISCHARGE CONDITIONS OF AN AIR-CONDITION SYSTEM

Table D.1: Oil retention in 16.9 mm suction line with R410A/POE32

Sr. No.	Refrigerant/ Lubricant	Inner Line Diameter [mm]	Ref. Mass Flow Rate [kg/hr]	Oil Mass Flow Rate [kg/hr]	Test Section Saturation Temperature [C]	Test Section Inlet Temperature [C]	Test ID
2	R410A/POE 32	16.9	16±3	0.08±0.06	10±2	20±2	67
				0.48±0.1	10±2	20±2	68
				0.8±0.16	10±2	20±2	96
			47±5	0.235±0.19	10±2	20±2	61
				1.41±0.28	10±2	20±2	63
				~~2.35±0.47~~	~~10±2~~	~~20±2~~	~~65~~
			94±5	0.47+0.38	10±4	20±2	74
				2.82±0.56	10±4	20±2	76
				4.7±0.94	10±4	20±2	98
			141±5	0.71±0.56	10±4	20±2	100
				4.23±0.85	10±4	20±2	103
				~~7.05±1.41~~	~~10±4~~	~~20±2~~	-

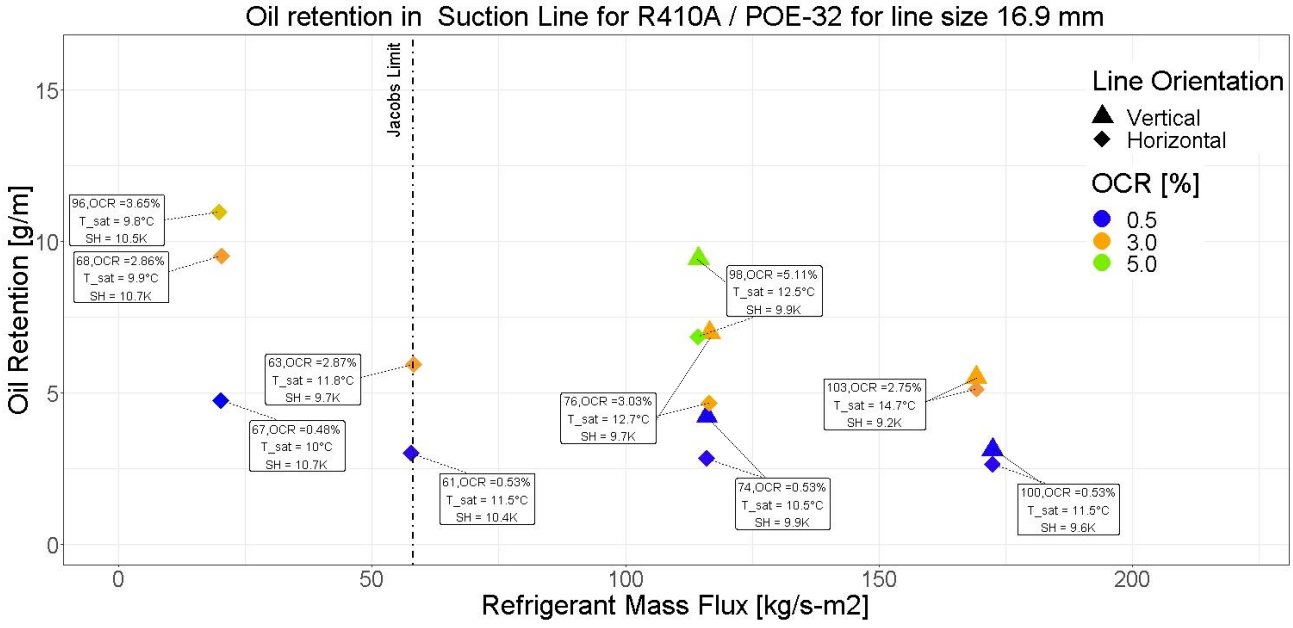

Figure D.1: Oil retention in 16.9 mm suction line with R410A/POE32

Table D.2: Oil retention in 10.9 mm suction line with R410A/POE32

Refrigerant /Lubricant	Inner Line Diameter [mm]	Ref. Mass Flow Rate [kg/hr]	Oil Mass Flow Rate [kg/hr]	Test Section Saturation Temperature [C]	Test Section Inlet Temperature [C]	Test ID
R410A/POE 32	10.9	~~5±3~~ 8±3	~~0.03~~	~~10~~	~~20~~	-
			~~0.15±0.1~~ 0.24±0.05	10±2	20±2	69
			~~0.25±0.2~~ 0.4±0.08	10±2	20±2	71
		16±5	0.08±0.07	10±2	20±2	62
			0.48±0.1	10±2	20±2	64
			0.8±0.16	10±2	20±2	66
		31±5	0.16+0.12	10±2	20±2	75
			0.93±0.19	10±2	20±2	77
			1.55±0.31	10±2	20±2	102
		47±5	0.24±0.19	10±2	20±2	99
			1.41±0.28	10±2	20±2	101
			2.35±0.47	10±2	20±2	104

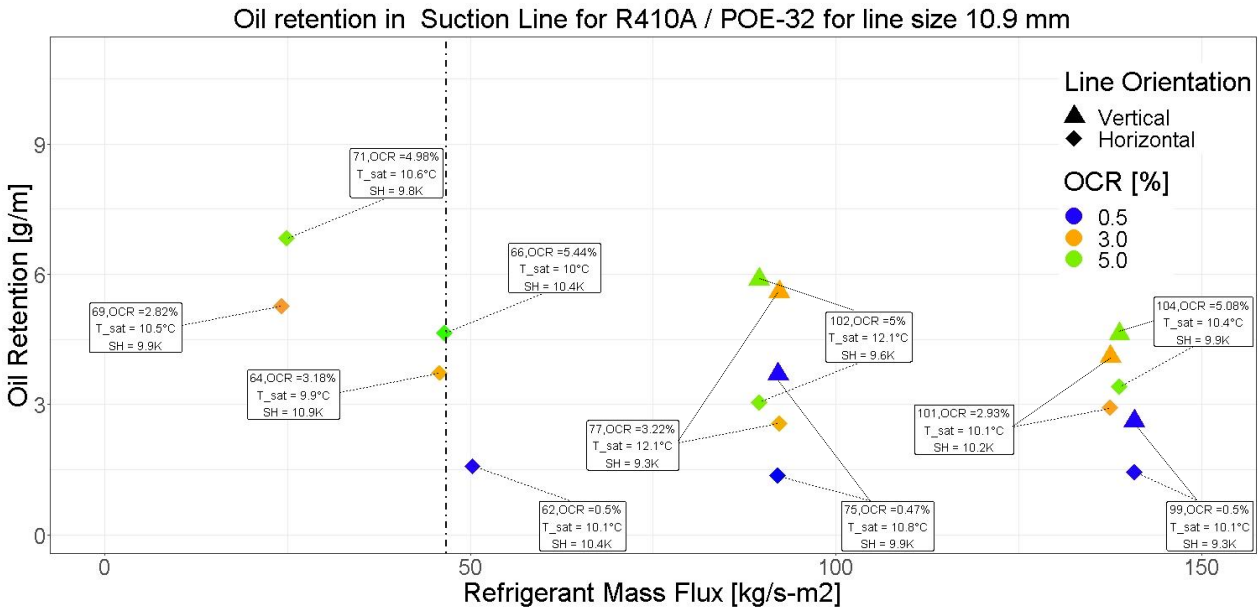

Figure D.2: Oil retention in 10.9 mm suction line with R410A/POE32

Table D.3: Oil retention in 16.9 mm discharge line with R410A/POE32

Refrigerant /Lubricant	Inner Line Diameter [mm]	Ref. Mass Flow Rate [kg/hr]	Oil Mass Flow Rate [kg/hr]	Test Section Saturation Temperature [C]	Test Section Inlet Temperature [C]	Test ID
R410A/POE 32	16.9	22±3	0.11±0.09	40±4	70±4	87
			0.66±0.13	40±4	70±4	82
			1.1±0.22	40±4	70±4	85
		65±5	0.325±0.26	40±4	70±4	72
			1.95±0.39	40±4	70±4	78
			3.25±0.65	40±4	70±4	80
		130±5	0.65±0.52	40±2	70±4	89
			3.9±0.78	40±2	70±4	91,195
			6.5±1.3	40±2	70±4	92
		~~195±5~~ 160±5	~~0.975±0.78~~ 0.8±0.64	40±2	70±4	94
			~~5.85±1.17~~ 4.8±0.96	40±2	70±4	105
			~~9.75±1.95~~	~~40±2~~	~~70±4~~	

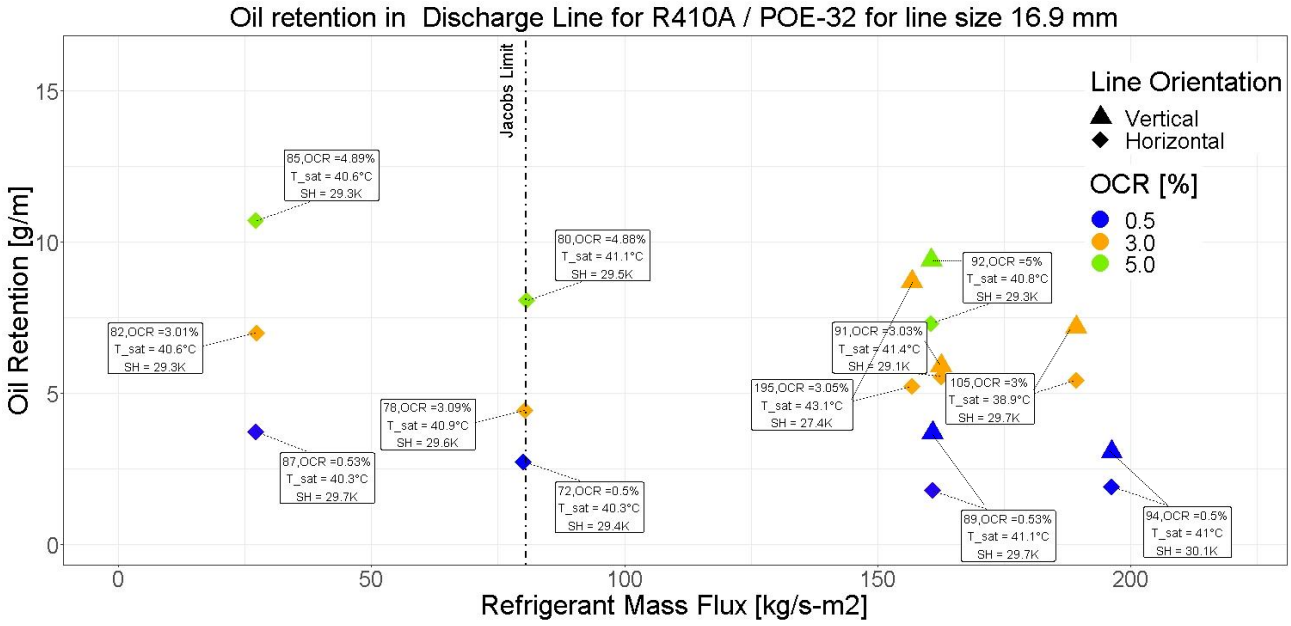

Figure D.3: Oil retention in 16.9 mm discharge line with R410A/POE32

Table D.4: Oil retention in 10.9 mm discharge line with R410A/POE32

Refrigerant /Lubricant	Inner Line Diameter [mm]	Ref. Mass Flow Rate [kg/hr]	Oil Mass Flow Rate [kg/hr]	Test Section Saturation Temperature [C]	Test Section Inlet Temperature [C]	Test ID
R410A/POE 32	10.9	~~7±3~~ 11±3	~~0.04±0.03~~	~~40±4~~	~~70±4~~	-
			~~0.21~~ 0.33±0.07	40±4	70±4	88
			~~0.35~~ 0.55±0.11	~~40±4~~ 33±4	~~70±4~~ 66±4	97
		22±5	0.11±0.09	40±4	70±4	73
			0.66±0.13	40±4	70±4	83
			1.10±0.22	40±4	70±4	86
		44±5	0.22±0.18	40±2	70±4	90
			1.32±0.26	40±2	70±4	93
			2.20±0.44	40±2	70±4	95
		65±5	0.33±0.26	40±2	70±4	84
			1.95±0.39	40±2	70±4	79
			3.25±0.65	40±2	70±4	81

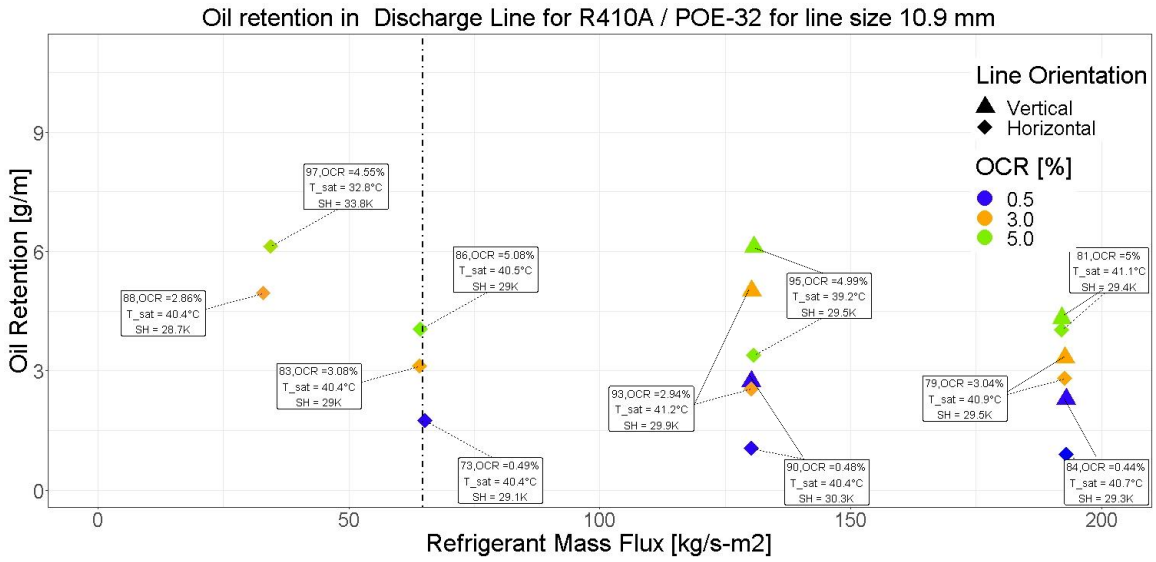

Figure D.4: Oil retention in 10.9 mm discharge line with R410A/POE32

Table D.5: Oil retention in 16.9 mm suction line with R32/POE32

Refrigerant/ Lubricant	Inner Line Diameter [mm]	Ref. Mass Flow Rate [kg/hr]	Oil Mass Flow Rate [kg/hr]	Test Section Saturation Temperature [C]	Test Section Inlet Temperature [C]	Test ID
R32/POE32	16.9	13±3	0.065±0.05	10±2	20±2	112
			0.39±0.08	10±2	20±2	114
			0.65±0.13	10±2	20±2	116
		40±5	0.2±0.16	10±2	20±2	106
			1.2±0.24	10±2	20±2	108
			2±0.4	10±2	20±2	110
		80±5	0.4±0.32	10±4	20±2	118
			2.4±0.48	10±4	20±2	120
			4±0.8	10±4	20±2	122
		120±5	0.6±0.48	~~10±4~~ 15±4	20±2	124
			3.6±0.72	~~10±4~~ 15±4	20±2	126
			~~6.0±1.2~~	~~10±4~~	~~20±2~~	-

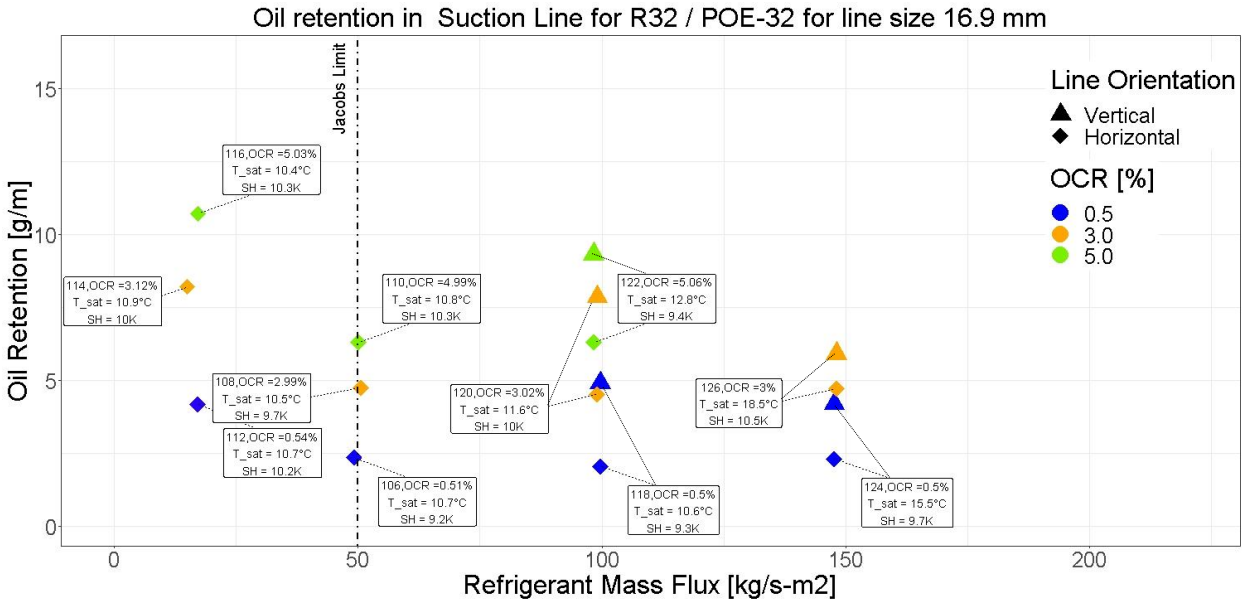

Figure D.5: Oil retention in 16.9 mm suction line with R32/POE32

Table D.6: Oil retention in 10.9 mm suction line with R32/POE32

Refrigerant/ Lubricant	Inner Line Diameter [mm]	Ref. Mass Flow Rate [kg/hr]	Oil Mass Flow Rate [kg/hr]	Test Section Saturation Temperature [C]	Test Section Inlet Temperature [C]	Test ID
R32/POE32	10.9	~~4.5±3~~ 9±3	~~0.0225±0.02~~	~~10±2~~	~~20±2~~	-
			~~0.135±0.03~~ 0.27±0.05	10±2	20±2	125
			~~0.225±0.05~~ 0.45±0.09	10±2	20±2	127
		13±5	0.065±0.05	10±2	20±2	113
			0.39±0.08	10±2	20±2	115
			0.65±0.13	10±2	20±2	117
		27±5	0.135±0.11	10±4	20±2	119
			0.81±0.16	10±4	20±2	121
			1.35±0.27	10±4	20±2	123,128
		40±5	0.2±0.16	10±4	20±2	107
			1.2±0.24	10±4	20±2	109
			2±0.4	10±4	20±2	111

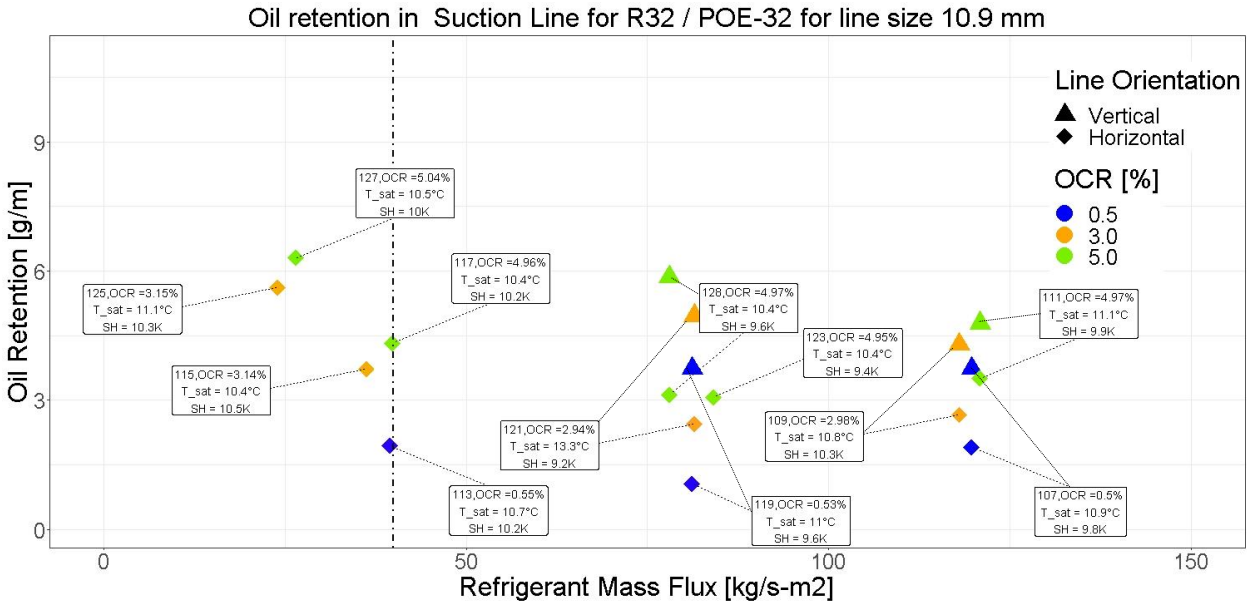

Figure D.6: Oil retention in 10.9 mm suction line with R32/POE32

Table D.7: Oil retention in 16.9 mm discharge line with R32/POE32

Refrigerant/ Lubricant	Inner Line Diameter [mm]	Ref. Mass Flow Rate [kg/hr]	Oil Mass Flow Rate [kg/hr]	Test Section Saturation Temperature [C]	Test Section Inlet Temperature [C]	Test ID
R32/POE32	16.9	18±3	0.09±0.07	40±2	75±2	135
			0.54±11	40±2	75±2	137
			0.9±18	40±2	75±2	139
		54±5	0.27±22	40±2	75±2	144
			1.62±32	40±2	75±2	131
			2.7±54	40±2	75±2	133
		108±5	0.54±43	40±4	75±2	141
			3.24±65	40±4	75±2	143
			5.4±1.08	40±4	75±2	197
		162±5	0.81±.65	40±4	75±2	199
			4.86±0.97	40±4	75±2	200
			~~8.1±1.62~~	~~40±4~~	~~75±2~~	-

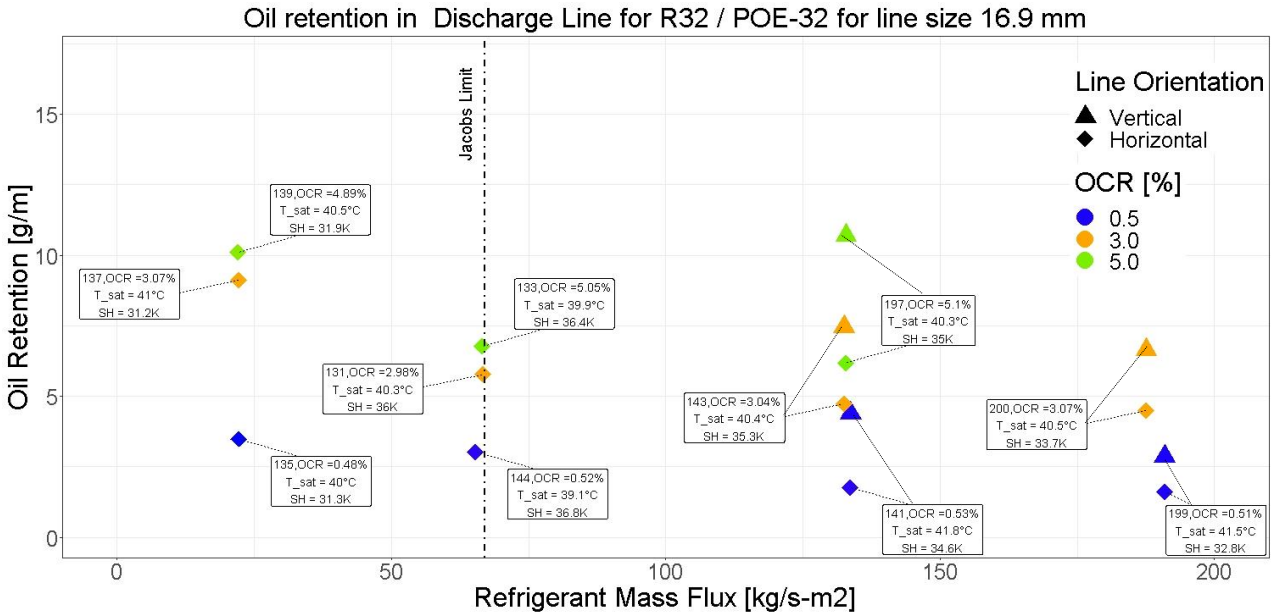

Figure D.7: Oil retention in 16.9 mm discharge line with R32/POE32

Table D.8: Oil retention in 10.9 mm discharge line with R32/POE32

Refrigerant/ Lubricant	Inner Line Diameter [mm]	Ref. Mass Flow Rate [kg/hr]	Oil Mass Flow Rate [kg/hr]	Test Section Saturation Temperature [C]	Test Section Inlet Temperature [C]	Test ID
R32/POE32	10.9	~~6±3~~ 9±3	~~0.03±0.02~~ 0.045±0.04	~~40±2~~	~~75±2~~	-
			~~0.18±0.04~~ 0.27±0.05	~~40±2~~	~~75±2~~	-
			~~0.3±0.06~~ 0.45±0.09	~~40±2~~	~~75±2~~	-
		18±5	0.09±0.07	40±2	75±2	136
			0.54±0.11	40±2	75±2	138
			0.9±0.18	40±2	75±2	140
		36±5	0.18±0.14	40±4	75±2	142
			1.08±0.22	40±4	75±2	203
			1.8±0.36	40±4	75±2	204
		54±5	0.27±0.22	40±4	75±2	130
			1.62±0.32	40±4	75±2	132
			2.7±0.54	40±4	75±2	134

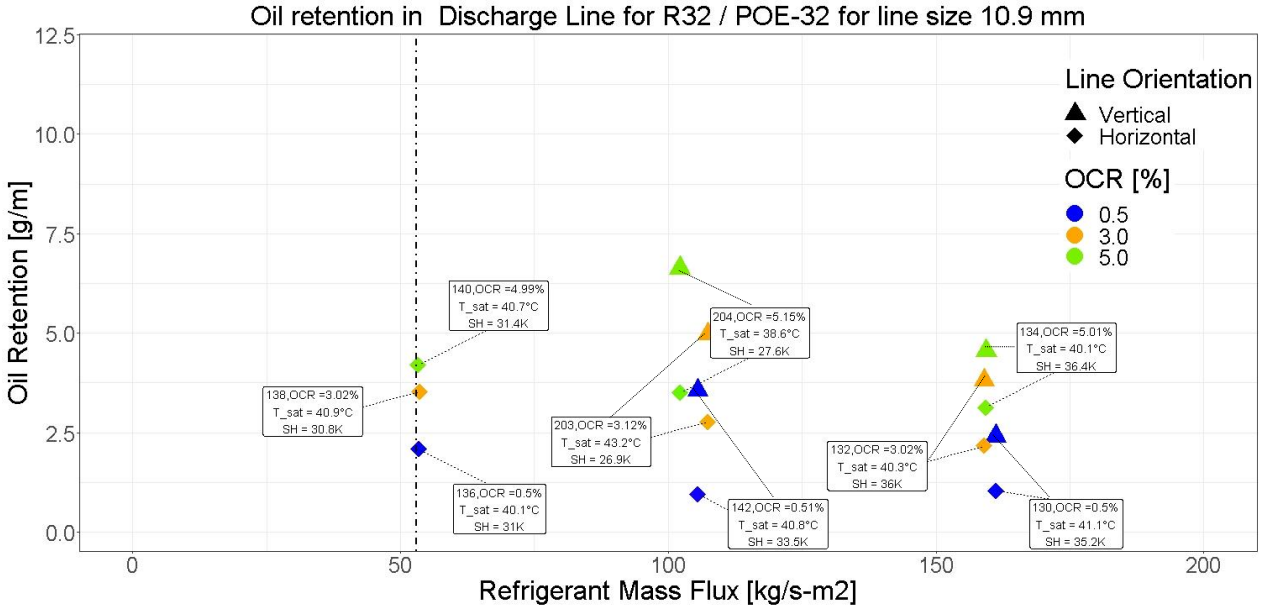

Figure D.8: Oil retention in 10.9 mm discharge line with R32/POE32

Table D.9: Oil retention in 16.9 mm suction line with R1234ze(E)/POE32

Refrigerant /Lubricant	Inner Line Diameter [mm]	Ref. Mass Flow Rate [kg/hr]	Oil Mass Flow Rate [kg/hr]	Test Section Saturation Temperature [C]	Test Section Inlet Temperature [C]	Test ID
R1234ze(E)/ POE32	16.9	10±3	0.05±0.04	10±2	20±2	166
			0.3±0.06	10±2	20±2	151
			0.5±0.1	10±2	20±2	153
		30±5	0.15±.12	10±2	20±2	149
			0.9±.18	~~10±4~~ 15±2	~~20±2~~ 25±2	165
			1.5±0.3	~~10±4~~ 15±2	~~20±2~~ 25±2	147
		60±5	0.3±0.24	~~10±4~~ 20±4	~~20±2~~ 30±2	155
			1.8±0.36	~~10±4~~ 20±4	~~20±2~~ 30±2	157
			3±0.6	~~10±4~~ 20±4	~~20±2~~ 30±2	159
		90±5	0.45±0.36	~~10±4~~ 30±4	~~20±2~~ 40±2	161
			2.7±0.54	~~10±4~~ 30±4	~~20±2~~ 40±2	163
			~~4.5±0.9~~	~~10±4~~	~~20±2~~	-

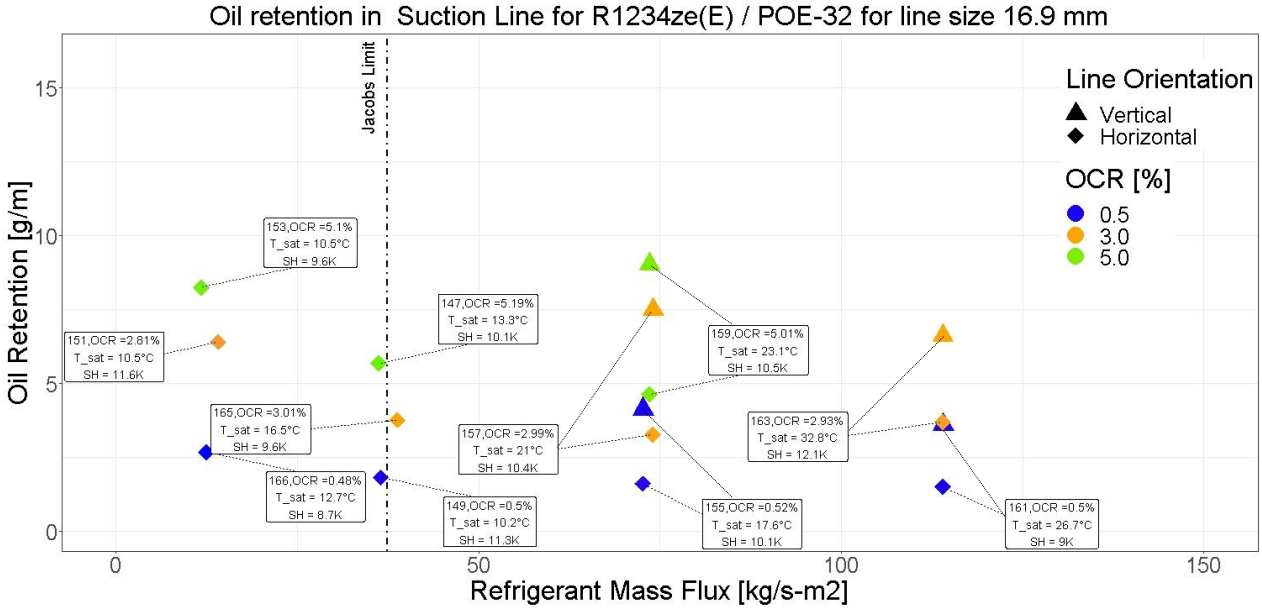

Figure D.9: Oil retention in 16.9 mm suction line with R1234ze(E)/POE32

Table D.10: Oil retention in 10.9 mm suction line with R1234ze(E)/POE32

Refrigerant /Lubricant	Inner Line Diameter [mm]	Ref. Mass Flow Rate [kg/hr]	Oil Mass Flow Rate [kg/hr]	Test Section Saturation Temperature [C]	Test Section Inlet Temperature [C]	Test ID
R1234ze(E) /POE32	10.9	~~3±3~~ 5±3	~~0.015±0.01~~ 0.025±0.02	~~10±2~~	~~20±2~~	-
			~~0.09±0.02~~ 0.15±0.03	10±2	20±2	164
			~~0.15±0.03~~ 0.25±0.05	10±2	20±2	187
		10±5	0.05±0.04	10±2	20±2	167
			0.3±0.06	10±2	20±2	152
			0.5±0.1	10±2	20±2	154
		20±5	0.1±0.08	10±2	20±2	156
			0.6±0.12	10±2	20±2	158
			1±0.2	10±2	20±2	160
		30±5	0.15±0.12	10±2	20±2	150
			0.9±0.18	10±2	20±2	146
			1.5±0.3	10±2	20±2	148

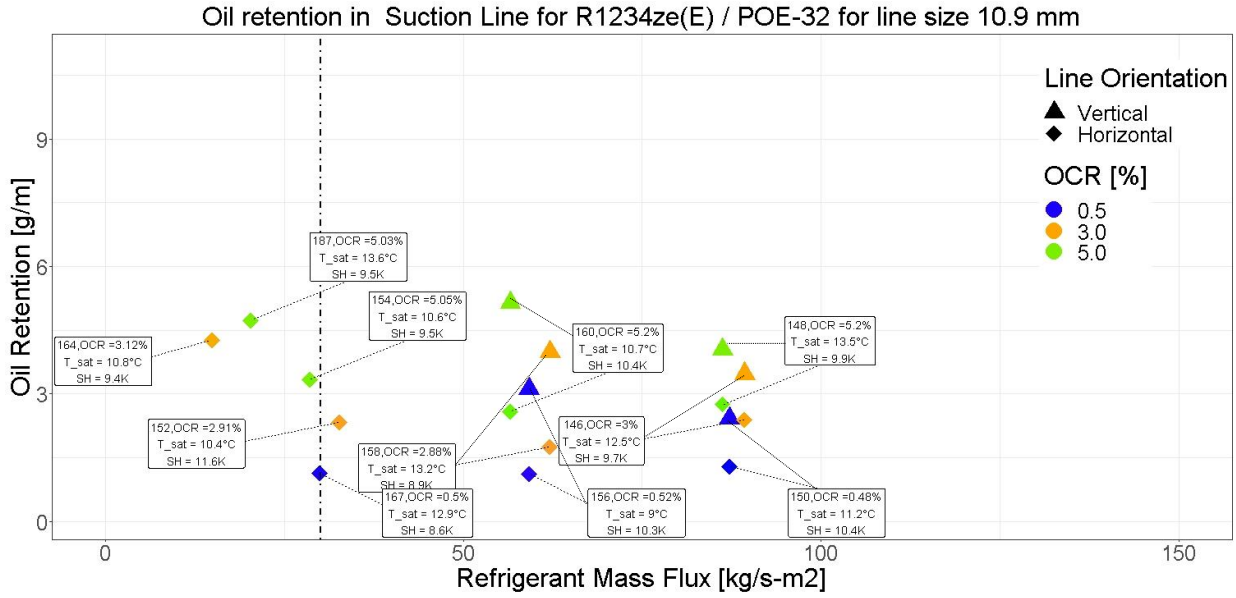

Figure D.10: Oil retention in 10.9 mm suction line with R1234ze(E)/POE32

Table D.11: Oil retention in 16.9 mm discharge line with R1234ze(E)/POE32

Refrigerant /Lubricant	Inner Line Diameter [mm]	Ref. Mass Flow Rate [kg/hr]	Oil Mass Flow Rate [kg/hr]	Test Section Saturation Temperature [C]	Test Section Inlet Temperature [C]	Test ID
R1234ze(E) /POE32	16.9	15±3	0.07±0.06	~~40±2~~ 25±5	~~55±2~~ 47±5	180
			0.45±0.09	~~40±2~~ 25±5	~~55±2~~ 47±5	182
			0.75±0.15	~~40±2~~ 25±5	~~55±2~~ 47±5	184
		46±5	0.23±.18	40±2	55±2	168
			1.38±.28	40±2	55±2	170
			2.3±0.46	40±2	55±2	172
		92±5	0.46±0.37	40±4	55±2	174
			2.76±0.55	40±4	55±2	176
			4.6±0.92	40±4	55±2	178
		138±5	0.69±0.55	40±4	55±2	186
			4.14±0.83	40±4	55±2	188
			6.9±1.38	40±4	55±2	-

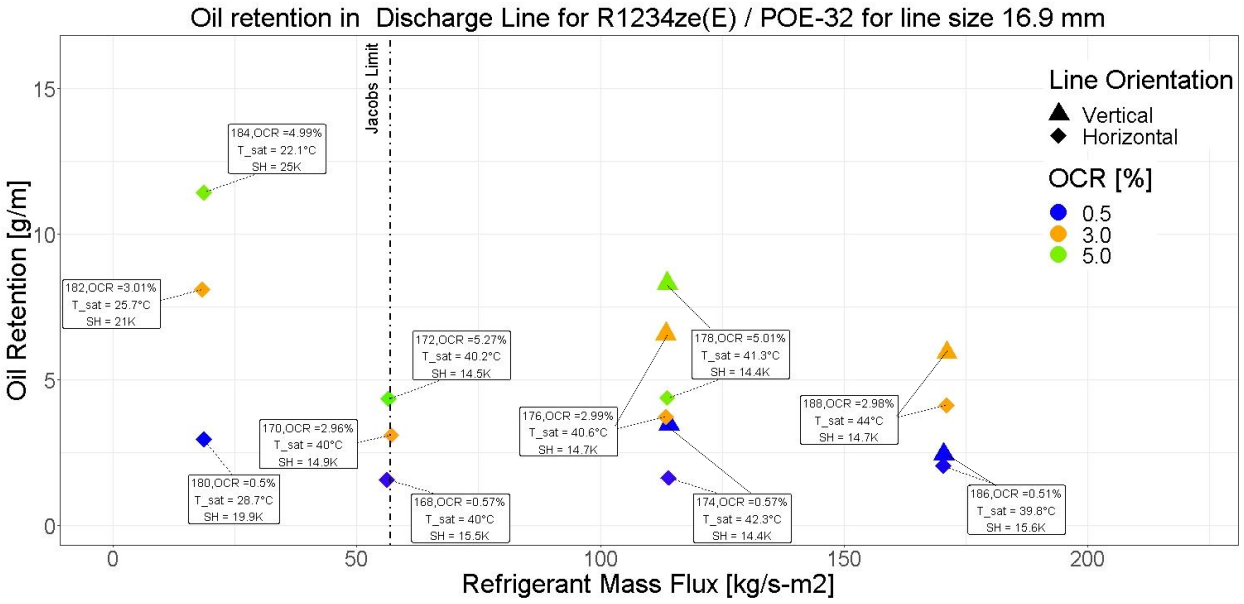

Figure D.11: Oil retention in 16.9 mm discharge line with R1234ze(E)/POE32

Table D.12: Oil retention in 10.9 mm discharge line with R1234ze(E)/POE32

Refrigerant /Lubricant	Inner Line Diameter [mm]	Ref. Mass Flow Rate [kg/hr]	Oil Mass Flow Rate [kg/hr]	Test Section Saturation Temperature [C]	Test Section Inlet Temperature [C]	Test ID
R1234ze(E) /POE32	10.9	~~5±3~~ 7.5±3	~~0.025±0.02~~	~~40±2~~	~~55±2~~	-
			~~0.15±0.03~~ 0.225±0.05	40±2	55±2	189
			~~0.25±0.05~~ 0.375±0.08	40±2	55±2	190
		15±5	0.075±0.06	~~40±2~~ 25±5	~~55±2~~ 47±2	181
			0.45±0.09	~~40±2~~ 25±5	~~55±2~~ 47±2	183
			0.75±0.15	~~40±2~~ 25±5	~~55±2~~ 47±2	185
		31±5	0.155±0.12	40±4	55±2	175
			0.93±0.19	40±4	55±2	177
			1.55±0.31	40±4	55±2	179
		46±5	0.23±0.18	40±4	55±2	169
			1.38±0.28	40±4	55±2	171
			2.3±0.46	40±4	55±2	173

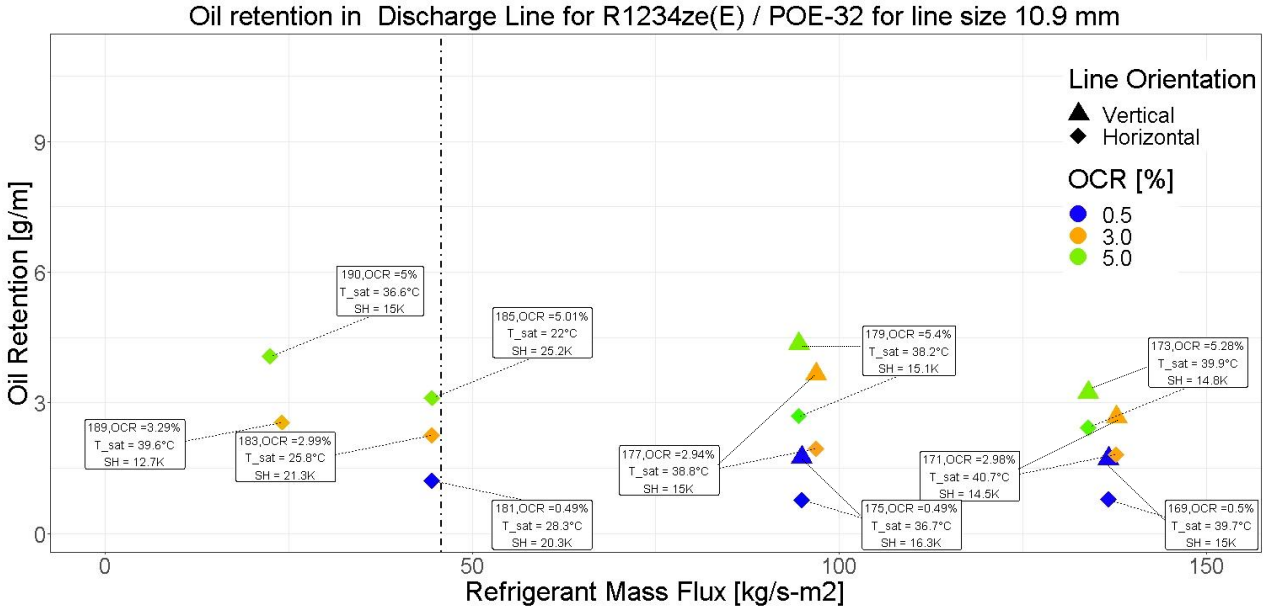

Figure D.12: Oil retention in 10.9 mm discharge line with R1234ze(E)/POE32

APPENDIX E. LIST OF KEY COMPONENTS FOR EXPERIMENTAL SETUPS BUILT TO MEASURE OCR AND OIL RETENTION

List of Key Components for the Experimental Setup Built for OCR Measurement

Sr. No.	Components	Manufacturer	Description
1.	Single Compressor	Copeland	Model No. ZF22-KVE-TFD Type: Hermetic Scroll; Displacement: 8.81 in^3/rev Refrigerant: R404A Oil: Uniqema Emkarate RL-32-3MAF 460V 3-Phase 60 Hz
2.	Mass Flow Meter (MF-1) (For Refrigerant)	Micro motion	Type: Coriolis-effect Mass Flow Meter Model: DH025 Maximum Mass Flow: 680 kg/h
3.	Mass Flow Meter (MF-2) (For Oil)	Micro motion	Type: Coriolis-effect Mass Flow Meter Model: CMF010 Maximum Mass Flow: 108 kg/hr
4.	Oil Separator	Temprite	Type: Coalescent Model: 924 -Accessible for changing filter
5.	Liquid Level Probe	Henry Technologies	Part Number: LLP-8R Output: 0 – 5 V Working pressure – 1000 psi Supply Voltage – 12-32 VDC
6.	Data Acquisition and Control System	National Instruments	-cRIO- Real Time Power PC Controller -Reconfigurable chasis for compactRIO -16-ch Thermocouple Modules – 3 Nos -32-ch Analog Input Module – 1 Nos (Output Modules shall be purchased later)
7.	Pressure Sensors	Omega/ Setra	Omega Model: PX309 Setra Model: 206
8.	Thermocouple	Omega	T Type along with probe for inline measurement

List of Key Components for Experimental Setup Built for Oil Retention Measurement

Sr. No.	Components	Manufacturer	Description
1.	Refrigerant Liquid Pump	Micropump	Type: Gear Pump
2.	Oil Liquid Pump	Micropump	Type: Gear Pump Model: GAH-T23 J9F5S.4 Flow Rate: 8.5 ml/min – 506 ml/min
3.	Chiller	Climate Master	Type: Water Sourced Model: TMW060BGC00C0CS Cooling Capacity: 60000 Btu/h (5Ton)
4.	Chiller	Climate Master	Type: Water Sourced Model: TMW036AGC00C0CS Cooling Capacity: 36000 Btu/h (3 Ton)
5.	Tank-less water Heater	Hubble Water Heaters	Type: Electric Model: HX054-6T4 Capacity: 54 kW
6.	Mass Flow Meter - Refrigerant	Micromotion	Type: Coriolis-effect Mass Flow Meter Model: CMF010
7.	Mass Flow Meter - Refrigerant	Micromotion	Type: Coriolis-effect Mass Flow Meter Model: DH025
8.	Mass Flow Meter - Oil	Micromotion	Type: Coriolis-effect Mass Flow Meter Model: CMF007S
9.	Condenser - Big	Swep	Type: Flat Plate Model: B120Tx50
10.	Condenser - Small	Swep	Type: Flat Plate Model: B80x20
11.	Evaporator	Swep	Type: Flat Plate Model:B80Hx20
12.	Water Pump for chilled water and hot water loop	Grundfos	Type: Circulator Pump Model: CM5-2 A-S-A-E

APPENDIX F. EXPERIMENTAL STEADY-STATE DATA SHOWING THE TEST SECTION CONDITION AND OIL RETENTION MEASUREMENT IN GAS LINES

Test ID	Ref/Oil	Horizontal Test Section ID	Vertical Test Section ID	Ref Mass Flow Rate	Oil Mass Flow Rate	Test Section Temp	Test Section Pressure	Test Section Sat Temp	Super Heat	Horizontal Line Oil Retention	Vertical Line Oil Retention
		mm	mm	kg/h	kg/h	°C	kPa	°C	°C	g/m	g/m
33	R134a/POE32	16.92	10.92	21.09	0.893	24.5	457.5	13.1	11.3	10.359	0.000
34	R134a/POE32	16.92	6.30	8.73	0.358	21.4	395.9	8.8	12.7	11.485	0.000
35	R134a/POE32	16.92	10.92	30.32	0.165	21.3	433.0	11.5	9.8	3.794	0.000
36	R134a/POE32	16.92	10.92	23.70	0.732	20.7	431.4	11.3	9.4	6.401	0.000
37	R134a/POE32	16.92	6.30	12.96	0.335	21.7	411.0	9.9	11.8	9.829	0.000
39	R134a/POE32	16.92	10.92	27.31	1.400	21.3	436.8	11.7	9.6	7.160	0.000
41	R134a/POE32	16.92	16.92	68.20	0.390	23.1	478.0	14.5	8.6	0.000	4.546
42	R134a/POE32	16.92	16.92	66.18	0.320	24.3	482.6	14.8	9.5	1.911	4.622
43	R134a/POE32	16.92	16.92	94.99	0.475	31.0	588.4	21.1	9.9	2.294	3.554
47	R134a/POE32	16.92	10.92	52.08	1.325	64.9	1063.8	41.9	23.0	4.822	0.000
48	R134a/POE32	16.92	10.92	50.99	2.685	64.8	1021.3	40.3	24.5	7.955	0.000
49	R134a/POE32	16.92	10.92	51.09	0.264	64.4	1023.4	40.4	24.0	3.138	0.000
50	R134a/POE32	16.92	6.30	16.97	0.561	54.1	764.1	29.9	24.2	10.308	0.000
51	R134a/POE32	16.92	6.30	20.16	0.625	63.7	1013.8	40.0	23.7	9.609	0.000
52	R134a/POE32	16.92	6.30	17.47	0.946	64.0	1014.7	40.1	23.9	12.190	0.000
53	R134a/POE32	16.92	16.92	103.59	3.208	64.6	1039.5	41.0	23.6	5.147	7.177
54	R134a/POE32	16.92	16.92	103.21	5.079	64.6	1040.3	41.0	23.6	6.703	8.903
55	R134a/POE32	16.92	16.92	103.14	0.547	64.5	1036.7	40.9	23.7	2.708	3.920
56	R134a/POE32	16.92	16.92	158.37	4.558	65.3	1072.4	42.2	23.2	5.331	5.054

Test ID	Ref/Oil	Horizontal Test Section ID	Vertical Test Section ID	Ref Mass Flow Rate	Oil Mass Flow Rate	Test Section Temp	Test Section Pressure	Test Section Sat Temp	Super Heat	Horizontal Line Oil Retention	Vertical Line Oil Retention
		mm	mm	kg/h	kg/h	°C	kPa	°C	°C	g/m	g/m
57	R134a/POE32	16.92	16.92	152.33	0.744	64.3	1026.4	40.5	23.8	2.259	2.938
58	R134a/POE32	16.92	16.92	58.25	1.613	23.6	465.7	13.7	9.9	5.607	7.892
59	R134a/POE32	16.92	16.92	62.70	2.900	25.6	494.1	15.5	10.0	6.786	10.673
60	R134a/POE32	16.92	16.92	101.34	2.443	33.3	626.5	23.1	10.2	5.826	6.191
61	R410A/POE32	16.92	10.92	46.69	0.249	21.9	1127.3	11.5	10.4	2.997	0.000
62	R410A/POE32	10.92	6.30	16.98	0.086	20.5	1084.4	10.1	10.4	1.577	0.000
63	R410A/POE32	16.92	10.92	47.16	1.355	21.5	1140.0	11.8	9.7	5.936	0.000
64	R410A/POE32	10.92	6.30	15.46	0.489	20.8	1075.3	9.9	10.9	3.730	0.000
66	R410A/POE32	10.92	6.30	15.69	0.855	20.4	1080.5	10.0	10.4	4.645	0.000
67	R410A/POE32	16.92	6.30	16.35	0.079	20.7	1080.0	10.0	10.7	4.737	0.000
68	R410A/POE32	16.92	6.30	16.41	0.469	20.6	1077.9	9.9	10.7	9.517	0.000
69	R410A/POE32	10.92	6.30	8.18	0.231	20.4	1096.2	10.5	9.9	5.271	0.000
71	R410A/POE32	10.92	6.30	8.40	0.419	20.4	1097.9	10.6	9.8	6.834	0.000
72	R410A/POE32	16.92	10.92	64.75	0.321	69.7	2428.3	40.3	29.4	2.721	0.000
73	R410A/POE32	10.92	6.30	22.00	0.108	69.4	2430.6	40.4	29.1	1.741	0.000
74	R410A/POE32	16.92	16.92	93.92	0.502	20.4	1097.0	10.5	9.9	2.830	4.214
75	R410A/POE32	10.92	10.92	31.06	0.147	20.8	1107.0	10.8	9.9	1.360	3.691
76	R410A/POE32	16.92	16.92	94.35	2.857	22.3	1168.3	12.7	9.7	4.658	6.976
77	R410A/POE32	10.92	10.92	31.11	1.002	21.5	1149.8	12.1	9.3	2.559	5.582
78	R410A/POE32	16.92	10.92	65.03	2.009	70.5	2460.2	40.9	29.6	4.424	0.000
79	R410A/POE32	10.92	10.92	65.01	1.979	70.4	2465.4	40.9	29.5	2.806	3.325
80	R410A/POE32	16.92	10.92	65.28	3.183	70.5	2472.6	41.1	29.5	8.049	0.000
81	R410A/POE32	10.92	10.92	64.79	3.243	70.5	2476.0	41.1	29.4	4.026	4.323
82	R410A/POE32	16.92	6.30	22.04	0.663	69.9	2443.0	40.6	29.3	6.978	0.000
83	R410A/POE32	10.92	6.30	21.61	0.666	69.4	2435.4	40.4	29.0	3.113	0.000

Test ID	Ref/Oil	Horizontal Test Section ID	Vertical Test Section ID	Ref Mass Flow Rate	Oil Mass Flow Rate	Test Section Temp	Test Section Pressure	Test Section Sat Temp	Super Heat	Horizontal Line Oil Retention	Vertical Line Oil Retention
		mm	mm	kg/h	kg/h	°C	kPa	°C	°C	g/m	g/m
84	R410A/POE32	10.92	10.92	65.09	0.287	70.0	2450.7	40.7	29.3	0.898	2.281
85	R410A/POE32	16.92	6.30	21.89	1.071	69.9	2443.4	40.6	29.3	10.700	0.000
86	R410A/POE32	10.92	6.30	21.67	1.102	69.4	2438.2	40.5	29.0	4.047	0.000
87	R410A/POE32	16.92	6.30	21.94	0.116	70.0	2430.0	40.3	29.7	3.726	0.000
88	R410A/POE32	10.92	6.30	11.12	0.318	69.1	2433.3	40.4	28.7	4.950	0.000
89	R410A/POE32	16.92	16.92	130.17	0.688	70.8	2472.8	41.1	29.7	1.781	3.668
90	R410A/POE32	10.92	10.92	43.93	0.212	70.7	2433.2	40.4	30.3	1.046	2.731
91	R410A/POE32	16.92	16.92	131.55	3.981	70.5	2490.3	41.4	29.1	5.547	5.895
92	R410A/POE32	16.92	16.92	130.01	6.498	70.1	2455.8	40.8	29.3	7.305	9.392
93	R410A/POE32	10.92	10.92	43.95	1.293	71.1	2481.6	41.2	29.9	2.545	5.015
94	R410A/POE32	16.92	16.92	158.84	0.795	71.1	2469.8	41.0	30.1	1.901	3.047
95	R410A/POE32	10.92	10.92	44.10	2.202	68.7	2362.1	39.2	29.5	3.384	6.105
96	R410A/POE32	16.92	6.30	16.05	0.585	20.3	1073.4	9.8	10.5	10.949	0.000
97	R410A/POE32	10.92	6.30	11.60	0.528	66.6	2016.9	32.8	33.8	6.128	0.000
98	R410A/POE32	16.92	16.92	92.56	4.731	22.4	1160.7	12.5	9.9	6.849	9.409
99	R410A/POE32	10.92	10.92	47.50	0.237	19.4	1084.8	10.1	9.3	1.449	2.608
100	R410A/POE32	16.92	16.92	139.51	0.745	21.1	1128.3	11.5	9.6	2.647	3.109
101	R410A/POE32	10.92	10.92	46.39	1.361	20.3	1084.5	10.1	10.2	2.924	4.096
102	R410A/POE32	10.92	10.92	30.19	1.507	21.7	1149.5	12.1	9.6	3.052	5.886
103	R410A/POE32	16.92	16.92	136.91	3.759	23.9	1239.5	14.7	9.2	5.121	5.501
104	R410A/POE32	10.92	10.92	46.81	2.378	20.3	1091.6	10.4	9.9	3.408	4.626
105	R410A/POE32	16.92	16.92	153.15	4.593	68.6	2344.0	38.9	29.7	5.421	7.169
106	R32/POE32	16.92	10.92	39.78	0.202	19.9	1124.4	10.7	9.2	2.345	0.000
107	R32/POE32	10.92	10.92	40.39	0.203	20.7	1131.2	10.9	9.8	1.913	3.727
108	R32/POE32	16.92	10.92	40.89	1.223	20.3	1119.7	10.5	9.7	4.747	0.000

Test ID	Ref/Oil	Horizontal Test Section ID	Vertical Test Section ID	Ref Mass Flow Rate	Oil Mass Flow Rate	Test Section Temp	Test Section Pressure	Test Section Sat Temp	Super Heat	Horizontal Line Oil Retention	Vertical Line Oil Retention
		mm	mm	kg/h	kg/h	°C	kPa	°C	°C	g/m	g/m
109	R32/POE32	10.92	10.92	39.82	1.186	21.1	1129.7	10.8	10.3	2.657	4.300
110	R32/POE32	16.92	10.92	40.54	2.024	21.1	1129.0	10.8	10.3	6.298	0.000
111	R32/POE32	10.92	10.92	40.78	2.030	21.0	1138.1	11.1	9.9	3.508	4.788
112	R32/POE32	16.92	6.30	13.86	0.075	20.9	1124.7	10.7	10.2	4.170	0.000
113	R32/POE32	10.92	6.30	13.31	0.073	20.9	1123.5	10.7	10.2	1.935	0.000
114	R32/POE32	16.92	6.30	12.12	0.376	21.0	1133.3	10.9	10.0	8.198	0.000
115	R32/POE32	10.92	6.30	12.22	0.379	20.9	1116.6	10.4	10.5	3.727	0.000
116	R32/POE32	16.92	6.30	13.91	0.699	20.7	1114.8	10.4	10.3	10.708	0.000
117	R32/POE32	10.92	6.30	13.42	0.666	20.6	1115.1	10.4	10.2	4.328	0.000
118	R32/POE32	16.92	16.92	80.68	0.407	19.9	1122.3	10.6	9.3	2.049	4.905
119	R32/POE32	10.92	10.92	27.38	0.145	20.6	1135.3	11.0	9.6	1.061	3.733
120	R32/POE32	16.92	16.92	80.15	2.420	21.7	1156.8	11.6	10.0	4.524	7.855
121	R32/POE32	10.92	10.92	27.49	0.809	22.6	1214.3	13.3	9.2	2.449	4.959
122	R32/POE32	16.92	16.92	79.56	4.028	22.3	1197.6	12.8	9.4	6.296	9.313
123	R32/POE32	10.92	10.92	28.38	1.403	19.8	1114.1	10.4	9.4	3.066	0.000
124	R32/POE32	16.92	16.92	119.49	0.598	25.3	1294.8	15.5	9.7	2.296	4.186
125	R32/POE32	10.92	6.30	8.08	0.255	21.4	1138.9	11.1	10.3	5.614	0.000
126	R32/POE32	16.92	16.92	119.85	3.600	29.0	1408.1	18.5	10.5	4.714	5.909
127	R32/POE32	10.92	6.30	8.96	0.451	20.5	1118.7	10.5	10.0	6.306	0.000
128	R32/POE32	10.92	10.92	26.32	1.309	19.9	1114.7	10.4	9.6	3.130	5.854
130	R32/POE32	10.92	10.92	54.37	0.273	76.3	2537.2	41.1	35.2	1.040	2.414
131	R32/POE32	16.92	10.92	53.93	1.607	76.3	2488.4	40.3	36.0	5.774	0.000
132	R32/POE32	10.92	10.92	53.63	1.619	76.3	2488.7	40.3	36.0	2.168	3.821
133	R32/POE32	16.92	10.92	53.81	2.716	76.3	2463.9	39.9	36.4	6.779	0.000
134	R32/POE32	10.92	10.92	53.75	2.690	76.5	2473.1	40.1	36.4	3.131	4.561

Test ID	Ref/Oil	Horizontal Test Section ID	Vertical Test Section ID	Ref Mass Flow Rate	Oil Mass Flow Rate	Test Section Temp	Test Section Pressure	Test Section Sat Temp	Super Heat	Horizontal Line Oil Retention	Vertical Line Oil Retention
		mm	mm	kg/h	kg/h	°C	kPa	°C	°C	g/m	g/m
135	R32/POE32	16.92	6.30	17.96	0.086	71.4	2471.5	40.0	31.3	3.489	0.000
136	R32/POE32	10.92	6.30	18.04	0.090	71.1	2475.8	40.1	31.0	2.083	0.000
137	R32/POE32	16.92	6.30	18.02	0.552	72.1	2527.2	41.0	31.2	9.122	0.000
138	R32/POE32	10.92	6.30	18.08	0.546	71.7	2524.1	40.9	30.8	3.535	0.000
139	R32/POE32	16.92	6.30	17.83	0.872	72.4	2498.8	40.5	31.9	10.116	0.000
140	R32/POE32	10.92	6.30	17.98	0.897	72.1	2510.7	40.7	31.4	4.197	0.000
141	R32/POE32	16.92	16.92	108.15	0.573	76.3	2577.1	41.8	34.6	1.773	4.389
142	R32/POE32	10.92	10.92	35.59	0.182	74.3	2518.0	40.8	33.5	0.953	3.562
143	R32/POE32	16.92	16.92	107.23	3.256	75.7	2491.5	40.4	35.3	4.736	7.466
144	R32/POE32	16.92	10.92	52.83	0.277	75.8	2412.9	39.1	36.8	3.033	0.000
146	R1234ze(E)/POE32	10.92	10.92	30.13	0.901	22.2	333.1	12.5	9.7	2.395	3.475
147	R1234ze(E)/POE32	16.92	10.92	29.35	1.526	23.5	343.1	13.3	10.1	5.667	0.000
148	R1234ze(E)/POE32	10.92	10.92	29.10	1.514	23.4	344.5	13.5	9.9	2.748	4.049
149	R1234ze(E)/POE32	16.92	10.92	29.56	0.148	21.5	309.0	10.2	11.3	1.815	0.000
150	R1234ze(E)/POE32	10.92	10.92	29.41	0.142	21.6	319.0	11.2	10.4	1.283	2.417
151	R1234ze(E)/POE32	16.92	6.30	11.37	0.319	22.1	311.7	10.5	11.6	6.399	0.000
152	R1234ze(E)/POE32	10.92	6.30	11.04	0.321	22.0	311.1	10.4	11.6	2.328	0.000
153	R1234ze(E)/POE32	16.92	6.30	9.54	0.488	20.1	312.3	10.5	9.6	8.242	0.000
154	R1234ze(E)/POE32	10.92	6.30	9.65	0.488	20.1	312.8	10.6	9.5	3.337	0.000
155	R1234ze(E)/POE32	16.92	16.92	58.80	0.304	27.7	394.0	17.6	10.1	1.601	4.118
156	R1234ze(E)/POE32	10.92	10.92	19.98	0.104	19.3	296.5	9.0	10.3	1.119	3.120
157	R1234ze(E)/POE32	16.92	16.92	59.94	1.794	31.4	438.2	21.0	10.4	3.260	7.490
158	R1234ze(E)/POE32	10.92	10.92	20.95	0.610	22.1	341.5	13.2	8.9	1.759	3.978
159	R1234ze(E)/POE32	16.92	16.92	59.53	2.984	33.6	467.9	23.1	10.5	4.618	9.014
160	R1234ze(E)/POE32	10.92	10.92	19.09	1.000	21.2	314.2	10.7	10.4	2.586	5.148

Test ID	Ref/Oil	Horizontal Test Section ID	Vertical Test Section ID	Ref Mass Flow Rate	Oil Mass Flow Rate	Test Section Temp	Test Section Pressure	Test Section Sat Temp	Super Heat	Horizontal Line Oil Retention	Vertical Line Oil Retention
		mm	mm	kg/h	kg/h	°C	kPa	°C	°C	g/m	g/m
161	R1234ze(E)/POE32	16.92	16.92	92.28	0.462	35.7	522.5	26.7	9.0	1.497	3.582
163	R1234ze(E)/POE32	16.92	16.92	92.26	2.705	44.8	623.5	32.8	12.1	3.692	6.613
164	R1234ze(E)/POE32	10.92	6.30	5.02	0.157	20.2	315.0	10.8	9.4	4.271	0.000
165	R1234ze(E)/POE32	16.92	6.30	31.38	0.946	26.1	380.5	16.5	9.6	3.759	0.000
166	R1234ze(E)/POE32	16.92	6.30	10.13	0.049	21.4	336.4	12.7	8.7	2.662	0.000
167	R1234ze(E)/POE32	10.92	6.30	10.11	0.050	21.5	337.7	12.9	8.6	1.131	0.000
168	R1234ze(E)/POE32	16.92	10.92	45.52	0.258	55.5	764.0	40.0	15.5	1.562	0.000
169	R1234ze(E)/POE32	10.92	10.92	46.10	0.231	54.8	757.9	39.7	15.0	0.781	1.714
170	R1234ze(E)/POE32	16.92	10.92	46.24	1.368	54.9	762.7	40.0	14.9	3.104	0.000
171	R1234ze(E)/POE32	10.92	10.92	46.48	1.383	55.2	777.6	40.7	14.5	1.815	2.666
172	R1234ze(E)/POE32	16.92	10.92	45.73	2.412	54.6	767.0	40.2	14.5	4.330	0.000
173	R1234ze(E)/POE32	10.92	10.92	45.17	2.385	54.8	761.8	39.9	14.8	2.432	3.235
174	R1234ze(E)/POE32	16.92	16.92	92.32	0.529	56.6	811.6	42.3	14.4	1.628	3.465
175	R1234ze(E)/POE32	10.92	10.92	32.01	0.156	53.0	696.5	36.7	16.3	0.770	1.738
176	R1234ze(E)/POE32	16.92	16.92	91.81	2.743	55.3	775.5	40.6	14.7	3.718	6.557
177	R1234ze(E)/POE32	10.92	10.92	32.67	0.961	53.8	737.8	38.8	15.0	1.948	3.658
178	R1234ze(E)/POE32	16.92	16.92	92.05	4.613	55.7	791.6	41.3	14.4	4.371	8.294
179	R1234ze(E)/POE32	10.92	10.92	31.88	1.722	53.3	725.8	38.2	15.1	2.697	4.351
180	R1234ze(E)/POE32	16.92	6.30	15.04	0.075	48.7	554.6	28.7	19.9	2.945	0.000
181	R1234ze(E)/POE32	10.92	6.30	15.02	0.074	48.6	547.1	28.3	20.3	1.215	0.000
182	R1234ze(E)/POE32	16.92	6.30	14.86	0.447	46.7	506.4	25.7	21.0	8.099	0.000
183	R1234ze(E)/POE32	10.92	6.30	15.04	0.450	47.1	508.4	25.8	21.3	2.258	0.000
184	R1234ze(E)/POE32	16.92	6.30	15.07	0.753	47.1	453.5	22.1	25.0	11.417	0.000
185	R1234ze(E)/POE32	10.92	6.30	15.04	0.753	47.3	453.3	22.0	25.2	3.112	0.000
186	R1234ze(E)/POE32	16.92	16.92	137.95	0.707	55.4	758.2	39.8	15.6	2.034	2.418

Test ID	Ref/Oil	Horizontal Test Section ID	Vertical Test Section ID	Ref Mass Flow Rate	Oil Mass Flow Rate	Test Section Temp	Test Section Pressure	Test Section Sat Temp	Super Heat	Horizontal Line Oil Retention	Vertical Line Oil Retention
		mm	mm	kg/h	kg/h	°C	kPa	°C	°C	g/m	g/m
187	R1234ze(E)/POE32	10.92	6.30	6.86	0.345	23.0	345.6	13.6	9.5	4.728	0.000
188	R1234ze(E)/POE32	16.92	16.92	138.47	4.126	58.8	850.4	44.0	14.7	4.124	5.920
189	R1234ze(E)/POE32	10.92	6.30	8.12	0.267	52.3	754.8	39.6	12.7	2.551	0.000
190	R1234ze(E)/POE32	10.92	6.30	7.57	0.379	51.6	695.2	36.6	15.0	4.069	0.000
191	R410A/POE32	19.94	6.30	33.17	1.641	69.3	2435.5	40.4	28.9	19.564	0.000
192	R410A/POE32	19.94	6.30	95.87	2.864	70.0	2267.8	37.5	32.5	8.010	0.000
193	R410A/POE32	19.94	19.94	143.30	0.739	24.9	1224.4	14.3	10.6	2.674	4.812
194	R410A/POE32	19.94	19.94	172.03	0.892	26.6	1314.0	16.8	9.8	3.030	4.106
195	R410A/POE32	16.92	16.92	126.90	3.868	70.5	2598.2	43.1	27.4	5.222	8.674
196	R32/POE32	19.94	19.94	121.59	3.721	27.1	1333.4	16.6	10.5	7.356	11.285
197	R32/POE32	16.92	16.92	107.51	5.485	75.3	2489.8	40.3	35.0	6.190	10.692
198	R32/POE32	19.94	19.94	155.34	0.814	28.3	1411.2	18.6	9.8	2.355	4.376
199	R32/POE32	16.92	16.92	154.49	0.783	74.3	2558.9	41.5	32.8	1.617	2.852
200	R32/POE32	16.92	16.92	151.78	4.658	74.2	2498.1	40.5	33.7	4.496	6.648
201	R32/POE32	19.94	6.30	79.38	3.979	69.1	2491.4	40.4	28.7	10.185	0.000
202	R32/POE32	19.94	6.30	25.12	0.773	66.2	2356.0	38.1	28.1	20.330	0.000
203	R32/POE32	10.92	10.92	36.24	1.132	70.1	2669.8	43.2	26.9	2.773	4.978
204	R32/POE32	10.92	10.92	34.46	1.775	66.2	2384.4	38.6	27.6	3.506	6.636

APPENDIX G. REPORTS AND EMAIL CONVERSATIONS RELATED HONEYWELL REFRIGERANT R1234ZE(E)

Honeywell
FLUORINE PRODUCTS

Customer Specification No. CS Solstice® ZE Refrigerant Rev. 3 T

Honeywell Solstice® ZE Refrigerant

Refrigeration Grade
Meets AHRI Standard 700 Specifications

Alternate Name(s):	R-1234ze(E); Trans-1,3,3,3-Tetrafluoroprop-1-ene; *trans*-HFO-1234ze
Chemical Formula:	$CHFCHCF_3$
CAS Number:	29118-24-9

Parameter	Limit[1]	Test Method
Trans-1,3,3,3-Tetrafluoroprop-1-ene	99.5% (w/w), min.	RDAM-618T
Moisture	10 ppm (w/w), max.	HFO-1234ze-52
Chlorides	3 ppm (w/w), max.	HFO-1234ze-4
Acidity		
as HCl	1 ppm (w/w) as HCl , max.	HFO-1234ze-2
As mg KOH/gm	0.0015 mg KOH/gm, max.	HFO-1234ze-2
Non-volatile residue	100 ppm (v/v), max.	HFO-1234ze-6
Particulates and Solids	Visually clean to pass	Visual Inspection
Non-condensable gases in vapor phase @25°C	1.5% (v/v), max.	HFO-1234ze-8
Impurities: Maximum Quantity in Liquid Phase Detected by This Method		
Total organic impurities	5,000 ppm (w/w), max.	RDAM-618T
(Z) 1,3,3,3-Tetrafluoroprop-1-ene,1234ze	1,000 ppm (w/w), max.	RDAM-618T

[1] All analyses shall be performed on the liquid phase of the sample, unless noted otherwise.

Approved by: Doris Weber Date: 06/26/17
Coordinator of Specifications
Fluorine Products

Specification History:
CS Solstice® ZE Refrigerant Rev. 3, Revised 06/26/17. Updated to correct CAS Number. Modified refrigerant name to match SDS.
CS Solstice® 1234ze-1 Rev. 2, revised 02/23/15. Revised Spec to be updated.
CS Solstice™ 1234ze-1 Rev. 1, revised 03/16/12. Revised Spec due to Name Change from HFO-1234ze to Solstice™ 1234ze.
New, issued 04/21/09

This is a *Controlled Document* when embossed as follows: **Honeywell - CONTROLLED DOCUMENT.**
Page 1 of 1

Honeywell

FLUORINE PRODUCTS

Customer Specification No. CS Solstice™ 1234ze-2 Rev. 1 T

Solstice™ 1234ze

(Blowing Agent and Propellant Grade)

Alternate Name(s): (E) 1,3,3,3-tetrafluoroprop-1-ene; *trans* HFO-1234ze
Chemical Formula: $CHF=CHCF_3$
CAS Number: 29118-24-9

Parameter	Limit[1]	Test Method
Assay as (E) 1,3,3,3-tetrafluoroprop-1-ene	99.5 % (w/w), min.	RDAM-623
Moisture	0.0050% (w/w), max.	HFO-1234ze-52
Acidity		
as HCl	0.0001% (w/w), max.	HFO-1234ze-2
as mg KOH/gm.	0.0015mg KOH/gm, max.	
Non-volatile residue	0.0050% (w/w), max.	HFO-1234ze-6

[1] All analyses shall be performed on the liquid phase of the sample, unless noted otherwise.

Approved by: Doris Weber Date: 12/13/11

Coordinator of Specifications
Fluorine Products

Specification History:
CS Solstice™ 1234ze Rev. 1, revised 12/13/11. Revised Spec due to Name Change from HFO-1234ze to Solstice™ 1234ze.
New, issued 10/13/10

PRINTED "CONTROLLED" COPY EXPIRES 24 HOURS AFTER
November 15, 2016 AT 9:39 AM

RE: [External] Re: Honeywell Refrigerants 1234ze

Funk, Jim (IL14) <Jim.Funk@Honeywell.com>
Thu 4/15/2021 4:30 PM
To: Vatsal M Shah <vshah@purdue.edu>
Cc: AndrewBrown@gwberkheimer.com <AndrewBrown@gwberkheimer.com>

2 attachments (158 KB)
CS Solstice 1234ze - Blowing Agent and Propellant Grade - T Spec.pdf; CS Solstice 1234ze - Refrigeration Grade - T Spec.pdf;

Vatsal,

Please see attached technical documents for product 1234ze both refrigerant grade and foam / aerosol grade.

Blowing agent is in % and refrigerant grade is ppm.
Here's guidance from tech team...

I see that the blowing agent spec is in % and refrigerant grade is in ppm. Multiply the foam blowing agent % values by 10,000 to convert to ppm. i.e. Divide by 100 to convert from % then multiply by 1,000,000 to convert to ppm. So for moisture on blowing agent spec, 0.0050% = 50 ppm. So the moisture spec is much higher.

Thanks,
Jim

From: Vatsal M Shah <vshah@purdue.edu>
Sent: Monday, April 12, 2021 4:08 PM
To: Funk, Jim (IL14) <Jim.Funk@Honeywell.com>
Cc: AndrewBrown@gwberkheimer.com
Subject: [External] Re: Honeywell Refrigerants 1234ze

Jim,

We were wondering if you can please provide us the percentage of impurities/non-condensable present in the AF grade vs. refrigerant grade of R1234ze(E). This information will help us to investigate further.

Thank You,
Vatsal

APPENDIX H. IMPACT OF OIL RETENTION DUE TO DEVIATION IN PRESSURE

Table H.1: Impact on oil retention due to deviation in pressure for 16.9 mm suction line with R410A/POE32

TestID	Refrigerant Mass Flow Rate	OCR	Test Section Temp	Test Section Pressure	Predicted Oil Retention	Deviation due to Pressure Uncertainty	Experimental Oil Retention
	[kg/h]	[%]	[°C]	[kPa]	[g/m]	[-]	[g/m]
100	139.5	0.53%	21.09	1128±33.84	2.021±0.02878	1.42%	2.647
74	93.92	0.53%	20.43	1097±32.91	2.355±0.03364	1.43%	2.83
61	46.69	0.53%	21.87	1127±33.81	3.150±0.04545	1.44%	2.997
76	94.35	3.03%	22.34	1168±35.04	5.878±0.1085	1.85%	4.658
67	16.35	0.48%	20.7	1080±32.4	5.028±0.07806	1.55%	4.737
103	136.9	2.75%	23.91	1240±37.2	5.036±0.08835	1.75%	5.121
63	47.16	2.87%	21.52	1140±34.2	6.633±0.1396	2.10%	5.936
98	92.56	5.11%	22.39	1161±34.83	9.863±0.1970	2.00%	6.849
68	16.41	2.86%	20.59	1078±32.34	10.18±0.2724	2.68%	9.517
96	16.05	3.65%	20.31	1073±32.19	12.36±0.3647	2.95%	10.95

Table H.2: Impact on oil retention due to deviation in pressure for 10.9 mm suction line with R410A/POE32

TestID	Refrigerant Mass Flow Rate	OCR	Test Section Temp	Test Section Pressure	Predicted Oil Retention	Deviation due to Pressure Uncertainty	Experimental Oil Retention
	[kg/h]	[-]	[°C]	[kPa]	[g/m]	[-]	[g/m]
75	31.06	0.47%	20.76	1107±33.21	1.257±0.0184	1.46%	1.36
99	47.5	0.50%	19.44	1085±32.55	1.055±0.01579	1.50%	1.449
62	16.98	0.50%	20.5	1084±32.52	1.679±0.02548	1.52%	1.577
77	31.11	3.22%	21.46	1150±34.5	2.981±0.06508	2.18%	2.559
101	46.39	2.93%	20.34	1085±32.55	2.558±0.04898	1.91%	2.924
102	30.19	5.00%	21.69	1150±34.5	4.483±0.1077	2.40%	3.052
104	46.81	5.08%	20.29	1092±32.76	4.251±0.0915	2.15%	3.408
64	15.46	3.18%	20.78	1075±32.25	3.900±0.09628	2.47%	3.73
66	15.69	5.45%	20.38	1081±32.43	6.14±0.1815	2.96%	4.645
69	8.181	2.82%	20.37	1096±32.88	4.691±0.1378	2.94%	5.271
71	8.399	4.98%	20.38	1098±32.94	7.372±0.2606	3.53%	6.834

Table H.3: Impact on oil retention due to deviation in pressure for 16.9 mm discharge line with R410A/POE32

TestID	Refrigerant Mass Flow Rate	OCR	Test Section Temp	Test Section Pressure	Predicted Oil Retention	Deviation due to Pressure Uncertainty	Experimental Oil Retention
	[kg/h]	[-]	[°C]	[kPa]	[g/m]	[-]	[g/m]
89	130.2	0.53%	70.81	2473±74.19	2.327±0.0124	0.53%	1.781
94	158.8	0.50%	71.11	2470±74.1	2.131±0.01126	0.53%	1.901
72	64.75	0.50%	69.74	2428±72.84	3.032±0.01574	0.52%	2.721
87	21.94	0.53%	70.05	2430±72.9	4.997±0.02495	0.50%	3.726
78	65.03	3.09%	70.48	2460±73.8	6.932±0.04806	0.69%	4.424
91	131.6	3.03%	70.45	2490±74.7	5.909±0.04408	0.75%	5.547
92	130	5.00%	70.09	2456±73.68	9.675±0.0789	0.82%	7.305
80	65.28	4.88%	70.53	2473±74.19	10.34±0.07952	0.77%	8.049
85	21.89	4.89%	69.87	2443±73.29	14.58±0.1057	0.72%	10.7

Table H.4: Impact on oil retention due to deviation in pressure for 10.9 mm discharge line with R410A/POE32

TestID	Refrigerant Mass Flow Rate	OCR	Test Section Temp	Test Section Pressure	Predicted Oil Retention	Deviation due to Pressure Uncertainty	Experimental Oil Retention
	[kg/h]	[-]	[°C]	[kPa]	[g/m]	[-]	[g/m]
84	65.09	0.44%	69.96	2451±73.53	1.0250±0.005383	0.53%	0.8983
90	43.93	0.48%	70.69	2433±72.99	1.2350±0.006188	0.50%	1.046
73	22	0.49%	69.42	2431±72.93	1.6700±0.008609	0.52%	1.741
93	43.95	2.94%	71.14	2482±74.46	2.751±0.01873	0.68%	2.545
79	65.01	3.04%	70.42	2465±73.95	2.593±0.01865	0.72%	2.806
83	21.61	3.08%	69.43	2435±73.05	3.534±0.02423	0.69%	3.113
95	44.1	4.99%	68.7	2362±70.86	4.399±0.03376	0.77%	3.384
81	64.79	5.01%	70.54	2476±74.28	4.135±0.03306	0.80%	4.026
86	21.67	5.08%	69.44	2438±73.14	5.347±0.04079	0.76%	4.047
97	11.6	4.55%	66.63	2017±60.51	6.442±0.03407	0.53%	6.128

APPENDIX I. EES CODE –STRATIFIED FLOW MODEL FOR PREDICTING OIL RETENTION IN HORIZONTAL LINES

```
$UnitSystem SI C kPa kJ mass rad

Subprogram stratified_horiz(TestID,R$, m_dot_ref,OCR_cor,D, T_1, P_sat,w_ref,rho_l,nu_l,h1,h2,h3,
- m_oil_ret_exp:m_oil_ret_pred,G_ref,Re_l,Re_g, rho_g, u_g, j_g, nu_g, u_l, j_l,f_g, f_l,f_i, Tau_i,alpha_l,
- dpdl)
 "Model to predict oil retention in horizontal line "
"Last modified on 1July 2021 by Vatsal Shah"

{
Inputs
R$: Refrigerant [-]
m_dot_ref: Corrected refrigerant mass flow rate [kg/s]
OCR_cor: OCR corrected for refrigerant dissolved in oil [-]
D: Pipe Hydraulic Diameter [m]
T_1: Pipe Temperature [C]
P_sat: Pipe Pressure [kPa]
w_ref: Concentration of refrigerant in oil at P_sat and T_1 [-]
rho_l: Density of oil+liquid refrigerant mixture at P_sat and T_1 [kg/m3]
nu_l: Kinematic viscosity of oil+liquid refrigerant mixture at P_sat and T_1 [m2/s]
h1,h2,h3: coefficients of interfacial friction factor [-]
TestID: Experimental test ID (not required) [-]
m_oil_ret_exp: Experimentally measured oil retention (not required) [g/m]

Outputs
m_oil_ret_exp: Model prediction of oil retention [g/m]
G_ref: Refrigerant mass flux [kg/m2-s]
Re_l: Reynolds number of liquid phase [-]
Re_g: Reynolds number of gas phase [-]
rho_g: density of vapor phase [kg/m3]
u_g: velocity of gas phase [m/s]
j_g: superficial velocity of gas phase [m/s]
nu_g: kinematic viscosity of gas phase [m2/s]
u_l: velocity of liquid phase [m/s]
j_l: superficial velocity of liquid phase [m/s]
f_g: friction factor of gas phase with wall [-]
f_l: friction factor of liquid phase with wall [-]
f_i: friction factor of gas phase at the interface [-]
Tau_i: Shear stress at gas-liquid interface [Pa]
alpha_l: Cross section area fraction of liquid phase [-]
dpdl: Pressure drop in pipe [Pa/m]
}

OCR_cor = m_dot_oil / (m_dot_oil + m_dot_ref)

"Oil properties"
T_K[1] = converttemp(C,K,T_1)                    "Pipe Temperature, K"
v_l = 1/rho_l                                    "Specific volume of oil with dissolved
- refrigerant"

"Refrigerant properties"
T_sat = temperature(R$, P = P_sat, x = 1)        "Pipe saturation temperature"
rho_g = density(R$, P = P_sat, T = T_1)          "Pipe vapor refrigerant density  "
v_g = 1/rho_g                                    "Pipe vapor refrigerant specific volume "
mu_g=viscosity(R$,T=T_1,P=P_sat)                 "Pipe vapor refrigerant viscosity"
T_sat = T_1 - DeltaT_SH                          "Pipe vapor refrigerant superheat"
```

```
R = D/2                                          "Inner radius of the Pipe"
mu_l = nu_l*rho_l                                "Viscocity of oil as a function of kinematic viscosity "
nu_g = mu_g/rho_g                                "Kinematic Viscosity of refrigerant as a function of viscosity"
Area = pi*D^2/4                                  "Pipe cross-section area"

"---------- Stratified Flow Model----------"

"Geometric Parameters"
alpha_g = 1- alpha_l
A_l = alpha_l*Area                               "alpha_l: Area Fraction of Liquid"
A_g = alpha_g*Area                               "alpha_g: Area Fraction of Gas"

alpha_l = (1/(2*pi)*(gamma - sin(gamma)))
h_l/D  = 0.5*(1 - cos(gamma/2))                  "h_l: Height of interface"
S = pi*D                                         "S: Perimeter"
S_l/S = gamma/(2*pi)                             "S_l: Wetted perimeter of liquid"
S_l/S = 1 - (S_g/S)                              "S_g: Wetted perimeter of gas"
(S_i/(2*D))^2 = (h_l/D) - (h_l/D)^2              "S_i: Width of interface"

D_l = 4*A_l/S_l
D_g =  4*A_g/(S_g + S_i)

m_dot_oil = rho_l*u_l*A_l
m_dot_ref = rho_g*u_g*A_g

j_l = u_l*alpha_l                                "Superficial Velocity of liquid"
j_g = u_g*alpha_g                                "Superficial Velocity of gas"

Re_l = j_l*D/nu_l                                "Liquid Oil Reynolds Number" "!Note: Using superficial velocity"
Re_g = j_g*D/nu_g                                "Vapor Refrigerant Reynolds Number" "!Note: Using superficial velocity"

C_L = 16
n = 1.0
C_G = 0.046
m = 0.2

f_l = C_L*Re_l^(-n)                              "friction factor of liquid oil (Laminar)"
f_g = C_G*Re_g^(-m)                              "friction factor of refrigerant vapor (Turbulent)"

Tau_wl = 0.5*f_l*rho_l*j_l^2                     "Wall shear stress on liquid oil""!Note: Using superficial velocity"
Tau_wg = 0.5*f_g*rho_g*j_g^2                     "Wall shear stress on refrigerant vapor""!Note: Using superficial velocity"

Tau_i = 0.5*f_i*rho_g*(j_g - j_l)^2              "Interfacial Shear Stress"

G_ref = m_dot_ref/(Area)                         "Refrigerant Mass Flux"

Tau_wg*S_g/A_g - Tau_wl*S_l/A_l - Tau_i*S_i*(1/A_l + 1/A_g) = 0 "Momentum balance after eliminating pressure gradient in each phase"

m_oil_ret_pred = rho_l*Area*alpha_l*1000[g/kg]*(1-w_ref)  {Oil retention in g/m including solubility correction}

 -A_g*dpdl - tau_wg*S_g - Tau_i*S_i = 0          "Equation for calculating pressure gradient"

//friction factor of form f_i = f(Re_g,OCR)
f_i = h1*Re_g^(-h2) + h3*OCR_cor                 "Interfacial friction factor"

End
```

APPENDIX J. EES CODE −ANNULAR FLOW MODEL FOR PREDICTING OIL RETENTION IN VERTICAL LINES

```
"Annular flow model to predict oil retention in vertical line"
"Last Modified by Vatsal Shah on 1Jul2021"

$TABSTOPS 0.5

Subprogram annular_verti(TestID,R$, m_dot_ref,OCR,D, T, P,w_ref,rho_l,nu_l,v1,v2,v3,v4,m_oil_ret_exp:m_oil_ret_pred,
G_ref,Re_l,Re_g,Tau_i,rho_g,u_g, j_g,nu_g,u_l, j_l, f_i,alpha_l,dpdz)
 {
Inputs
R$: Refrigerant [-]
m_dot_ref: Corrected refrigerant mass flow rate [kg/s]
OCR_cor: OCR corrected for refrigerant dissolved in oil [-]
D: Pipe Hydraulic Diameter [m]
T: Pipe Temperature [C]
P: Pipe Pressure [kPa]
w_ref: Concentration of refrigerant in oil at P_sat and T_1 [-]
rho_l: Density of oil+liquid refrigerant mixture at P_sat and T_1 [kg/m3]
nu_l: Kinematic viscosity of oil+liquid refrigerant mixture at P_sat and T_1 [m2/s]
v1,v2,v3,v4: coefficients of interfacial friction factor [-]
TestID: Experimental test ID (not required) [-]
m_oil_ret_exp: Experimentally measured oil retention (not required) [g/m]

Outputs
m_oil_ret_pred: Model prediction of oil retention [g/m]
G_ref: Refrigerant mass flux [kg/m2-s]
Re_l: Reynolds number of liquid phase [-]
Re_g: Reynolds number of gas phase [-]
Tau_i: Shear stress at gas-liquid interface [Pa]
rho_g: density of vapor phase [kg/m3]
u_g: velocity of gas phase [m/s]
j_g: superficial velocity of gas phase [m/s]
nu_g: kinematic viscosity of gas phase [m2/s]
u_l: velocity of liquid phase [m/s]
j_l: superficial velocity of liquid phase [m/s]
f_i: friction factor of gas phase at the interface [-]
alpha_l: Cross section area fraction of liquid phase [-]
dpdz: Pressure drop in pipe [Pa/m]
}

OCR = m_dot_oil / (m_dot_oil + m_dot_ref)          "Oil Mass flow rate from OCR"

R = D/2                                            "Radius of the pipe"
Area = pi*D^2/4                                    "Cross-section area of the pipe"
A_g = pi*(R-delta)^2                               "Cross-section area occupied by  vapor (refrigerant) in pipe"
A_l = Area - A_g                                   "Cross-section area occupied by liquid (oil) in the pipe"

alpha_g = A_g/Area                                 "Area fraction of vapor"
alpha_l = A_l/Area                                 "Area fraction of liquid"

{Properties of the refrigerant }
rho_g=density(R$,T=T,P=P)                          "Density of vapor"
mu_g=viscosity(R$,T=T,P=P)                         "Viscosity of vapor"
```

```
j_g = m_dot_ref/(rho_g*Area)                    "Superficial velocity of vapor"
j_l = m_dot_oil/(rho_l*Area)                    "Superficial velocity of liquid"

Re_g = j_g*rho_g*D/mu_g                         "Reynolds number of Vapor"
Re_l = j_l*rho_l*D/mu_l                         "Reynolds number of Liquid"

j_g = u_g*alpha_g                               "Actual velocity of vapor"
j_l = u_l*alpha_l                               "Acvtual velocity of liquid"

dpdz_kPa = dpdz*convert(Pa/m,kPa/m)
tau_i_kPa = tau_i*convert(Pa,kPa)

"Mass flow rate of oil as a function of R, delta, tau_i, dpdz and properties"
delta_by_R=delta/R
a=(2*pi*rho_l/mu_l)*((tau_i*(R-delta)+((R-delta)^(2)/2)*(dpdz+rho_l*g#))*(((R)^2-(R-delta)^2)/4-((R-delta)^(2)/2)*ln(1/(1-
- delta_by_R))))
b=(-1*pi*rho_l/(8*mu_l))*(dpdz+rho_l*g#)*(R^2-(R-delta)^2)^2
m_dot_oil = a+b

dpdz +rho_g*g# +Tau_i*pi*(D-2*delta)/A_g =0     "Momentum Balance"

Tau_i = 0.5*f_i*rho_g*(j_g)^2                   "Interfacial shear stress as a function of interfacial friction factor"

f_s = 0.046*Re_g^(-0.2)                         "Friction factor of smooth pipe (turbulant flow)"
delta_prime=(delta/(nu_g))*sqrt((tau_i/rho_g))  "Non-dimentional film thickness"

m_oil_ret_pred = rho_l*2*pi*R*delta*convert(kg/m,g/m)*(1-w_ref)     "Predicted oil retention"
Diff = m_oil_ret_pred - m_oil_ret_exp

//Diff = 0
f_i/f_s =1+ (v1*Re_l^v2)*(Re_g^v3)*(delta_prime^v4)          "Emperical Correlation for friction factor"

G_ref = m_dot_ref/Area                                      "Refrigerant Mass Flux"

End
```

APPENDIX K. EES CODE −ANNULAR FLOW MODEL FOR PREDICTING MINIMUM REFRIGERANT MASS FLUX FOR OIL RETURN IN VERTICAL LINES

```
"Annular flow model to predict oil return in vertical line"
"Last Modified by Vatsal Shah on 1July2021"

$TABSTOPS 0.5

Subprogram annular_returnlimit(R$, OCR,D, T, P,w_ref,rho_l,nu_l,v1,v2,v3,v4:G_ref_ll)
  {
Inputs
R$: Refrigerant [-]
OCR_cor: OCR corrected for refrigerant dissolved in oil [-]
D: Pipe Hydraulic Diameter [m]
T: Pipe Temperature [C]
P: Pipe Pressure [kPa]
w_ref: Concentration of refrigerant in oil at P_sat and T_1 [-]
rho_l: Density of oil+liquid refrigerant mixture at P_sat and T_1 [kg/m3]
nu_l: Kinematic viscosity of oil+liquid refrigerant mixture at P_sat and T_1 [m2/s]
v1,v2,v3,v4: coefficients of interfacial friction factor [-]

Outputs
G_ref_ll: Limit of refrigerant mass flux for oil to return in vertical riser [kg/m2-s]
}

OCR = m_dot_oil / (m_dot_oil + m_dot_ref)



R = D/2                                   "Radius of the pipe"
Area = pi*D^2/4                           "Cross-section area of the pipe"
A_g = pi*(R-delta)^2                      "Cross-section area occupied by  vapor (refrigerant) in pipe"
A_l = Area - A_g                          "Cross-section area occupied by liquid (oil) in the pipe"

alpha_g = A_g/Area                        "Area fraction of vapor"
alpha_l = A_l/Area                        "Area fraction of liquid"


 {Properties of the refrigerant }
rho_g=density(R$,T=T,P=P)                 "Density of vapor"
mu_g=viscosity(R$,T=T,P=P)                "Viscosity of vapor"

{Properties of the oil}
mu_l = rho_l * nu_l
mu_g = rho_g*nu_g

j_g = m_dot_ref/(rho_g*Area)              "Superficial velocity of vapor"
j_l = m_dot_oil/(rho_l*Area)              "Superficial velocity of liquid"

Re_g = j_g*rho_g*D/mu_g                   "Reynolds number of Vapor"
Re_l = j_l*rho_l*D/mu_l                   "Reynolds number of Liquid"

j_g = u_g*alpha_g                         "Actual velocity of vapor"
j_l = u_l*alpha_l                         "Acvtual velocity of liquid"
```

```
"Mass flow rate of oil as a function of R, delta, tau_i, dpdz and properties"
delta_by_R=delta/R
a=(2*pi*rho_l/mu_l)*((tau_i*(R-delta)+((R-delta)^(2)/2)*(dpdz+rho_l*g#))*(((R)^2-(R-delta)^2)/4-((R-delta)^(2)/2)*ln(1/(1-
delta_by_R))))
b=(-1*pi*rho_l/(8*mu_l))*(dpdz+rho_l*g#)*(R^2-(R-delta)^2)^2
m_dot_oil = a+b

dpdz +rho_g*g# +Tau_i*pi*(D-2*delta)/A_g =0    "Momentum Balance"

Tau_i = 0.5*f_i*rho_g*(j_g)^2                  "Interfacial shear stress as a function of interfacial friction factor"

f_s = 0.046*Re_g^(-0.2)
delta\nug = delta/nu_g                         "Friction factor of smooth pipe (turbulant flow)"
delta_prime=delta\nug*sqrt((tau_i/rho_g))      "Non-dimentional film thickness"


f_i/f_s =1+ (v1*Re_l^v2)*(Re_g^(v3))*(delta_prime^v4)      "Emperical Correlation for friction factor"


Tau_i*(R-delta)/delta = 0.5*(dpdz + rho_l*g#)*(2*R - delta)  "Special case when shear stress at wall is 0"
G_ref_ll = m_dot_ref/Area

End
```

APPENDIX L. MODEL PREDICTION RESULTS – R410A/POE32

Table L.1 Oil retention prediction results using stratified flow model for R410A/POE32 in horizontal line

Test ID	Ref Mass Flow Rate	Corrected OCR	Test Section			Oil Retention		Pressure Drop	Void Fraction
			Dia	Temp	Pres	Exp	Pred		
	[kg/h]	[%]	[mm]	[°C]	[kPa]	[g/m]	[g/m]	[Pa/m]	[-]
90	43.9	0.323	10.92	70.7	2433	1.046	1.153	165.0	0.984
75	31.1	0.404	10.92	20.8	1107	1.360	1.221	166.7	0.982
99	47.5	0.416	10.92	19.4	1085	1.449	1.015	365.0	0.985
62	17.0	0.432	10.92	20.5	1084	1.577	1.633	57.2	0.976
73	22.0	0.332	10.92	69.4	2431	1.741	1.577	46.9	0.978
89	130.2	0.391	16.92	70.8	2473	1.781	2.168	140.7	0.987
94	158.8	0.376	16.92	71.1	2470	1.901	1.989	202.5	0.988
93	44.0	2.172	10.92	71.1	2482	2.545	2.223	159.4	0.969
77	31.1	2.461	10.92	21.5	1150	2.559	2.440	158.3	0.964
100	139.5	0.438	16.92	21.1	1128	2.647	1.913	301.5	0.988
72	64.8	0.354	16.92	69.7	2428	2.721	2.856	40.4	0.983
79	65.0	1.729	10.92	70.4	2465	2.806	1.730	325.1	0.976
74	93.9	0.452	16.92	20.4	1097	2.830	2.259	151.8	0.986
101	46.4	2.316	10.92	20.3	1085	2.924	2.134	347.2	0.969
194	172.0	0.414	19.94	26.6	1314	3.030	2.572	172.0	0.989
102	30.2	3.673	10.92	21.7	1150	3.052	3.369	150.0	0.950
83	21.6	1.649	10.92	69.4	2435	3.113	2.439	44.9	0.966
95	44.1	3.881	10.92	68.7	2362	3.384	3.469	167.6	0.951
104	46.8	3.751	10.92	20.3	1092	3.408	3.147	348.9	0.954
64	15.5	2.734	10.92	20.8	1075	3.730	3.494	48.4	0.950
81	64.8	3.710	10.92	70.5	2476	4.026	3.083	319.6	0.956
86	21.7	3.108	10.92	69.4	2438	4.047	3.552	44.9	0.950
78	65.0	1.821	16.92	70.5	2460	4.424	4.859	39.8	0.971
66	15.7	4.540	10.92	20.4	1081	4.645	5.159	49.5	0.925
76	94.3	2.420	16.92	22.3	1168	4.658	4.895	141.3	0.970
67	16.4	0.408	16.92	20.7	1080	4.737	4.895	6.6	0.970
88	11.1	1.653	10.92	69.1	2433	4.950	3.276	13.5	0.954
103	136.9	2.171	16.92	23.9	1240	5.121	4.149	260.2	0.974
195	126.9	2.390	16.92	70.5	2598	5.222	4.850	123.7	0.971
69	8.2	2.362	10.92	20.4	1096	5.271	4.174	15.0	0.939
105	153.2	2.410	16.92	68.6	2344	5.421	4.811	195.6	0.972

63	47.2	2.489	16.92	21.5	1140	5.936	5.977	41.4	0.963
71	8.4	4.122	10.92	20.4	1098	6.834	6.207	15.8	0.909
98	92.6	3.996	16.92	22.4	1161	6.849	7.650	137.3	0.953
92	130.0	3.916	16.92	70.1	2456	7.305	7.527	138.2	0.956
80	65.3	3.604	16.92	70.5	2473	8.049	7.844	39.7	0.954
68	16.4	2.389	16.92	20.6	1078	9.517	9.034	6.6	0.945
85	21.9	2.956	16.92	69.9	2443	10.700	9.779	5.6	0.943
96	16.0	2.892	16.92	20.3	1073	10.950	10.350	6.3	0.937
191	33.2	3.571	19.94	69.3	2435	19.560	14.030	5.4	0.941

Table L.2: Oil retention prediction results using annular flow model for R410A/POE32 in vertical line

Test ID	Ref Mass Flow Rate	Corrected OCR	Test Section			Oil Retention		Pressure Drop	Void Fraction
			Dia	Temp	Pres	Exp	Pred		
	[kg/h]	[%]	[mm]	[°C]	[kPa]	[g/m]	[g/m]	[Pa/m]	[-]
84	65.1	0.431	10.92	70.0	2451	2.281	1.799	1860	0.975
99	47.5	0.488	10.92	19.4	1085	2.608	1.808	1865	0.974
94	158.8	0.489	16.92	71.1	2470	3.047	3.658	1529	0.979
100	139.5	0.522	16.92	21.1	1128	3.109	3.206	1785	0.980
79	65.0	2.901	10.92	70.4	2465	3.325	3.810	2540	0.947
89	130.2	0.517	16.92	70.8	2473	3.668	4.291	1320	0.975
75	31.1	0.464	10.92	20.8	1107	3.691	2.404	1080	0.965
101	46.4	2.799	10.92	20.3	1085	4.096	3.621	2734	0.948
194	172.0	0.507	19.94	26.6	1314	4.106	4.447	1232	0.980
74	93.9	0.522	16.92	20.4	1097	4.214	4.128	1091	0.975
81	64.8	4.681	10.92	70.5	2476	4.323	4.600	2786	0.936
104	46.8	4.750	10.92	20.3	1092	4.626	4.383	3148	0.937
193	143.3	0.504	19.94	24.9	1224	4.812	5.027	1051	0.978
93	44.0	2.807	10.92	71.1	2482	5.015	5.108	1723	0.929
103	136.9	2.624	16.92	23.9	1240	5.501	5.969	2253	0.963
77	31.1	3.063	10.92	21.5	1150	5.582	5.015	1553	0.927
102	30.2	4.673	10.92	21.7	1150	5.886	6.081	1682	0.912
95	44.1	4.670	10.92	68.7	2362	6.105	6.104	1911	0.916
76	94.3	2.886	16.92	22.3	1168	6.976	7.940	1483	0.952
105	153.2	2.859	16.92	68.6	2344	7.169	7.349	1951	0.958
195	126.9	2.905	16.92	70.5	2598	8.674	8.692	1626	0.949
92	130.0	4.675	16.92	70.1	2456	9.392	10.120	1797	0.941
98	92.6	4.775	16.92	22.4	1161	9.409	9.770	1647	0.941

APPENDIX M. MODEL PREDICTION RESULTS – R1234ZE(E)/POE32

Table M.1: Oil retention prediction results for R1234ze(E)/POE32 in horizontal line

Test ID	Ref Mass Flow Rate	Corrected OCR	Test Section			Oil Retention		Pressure Drop	Void Fraction
			Dia	Temp	Pres	Exp	Pred		
	[kg/h]	[%]	[mm]	[°C]	[kPa]	[g/m]	[g/m]	[Pa/m]	[-]
175	32.0	0.430	10.92	53.0	696.5	0.770	0.779	214.2	0.988
169	46.1	0.409	10.92	54.8	757.9	0.781	0.646	379.4	0.990
156	20.0	0.496	10.92	19.3	296.5	1.119	0.870	197.9	0.986
167	10.1	0.484	10.92	21.5	337.7	1.131	1.066	50.6	0.982
181	15.0	0.430	10.92	48.6	547.1	1.215	1.158	70.1	0.984
150	29.4	0.467	10.92	21.6	319.0	1.283	0.737	372.6	0.988
161	92.3	0.476	16.92	35.7	522.5	1.497	1.239	224.2	0.991
155	58.8	0.491	16.92	27.7	394.0	1.601	1.575	130.3	0.989
158	21.0	2.843	10.92	22.0	341.5	1.759	1.573	184.9	0.974
171	46.5	1.994	10.92	55.2	777.6	1.815	1.163	369.1	0.982
177	32.7	2.593	10.92	53.8	737.8	1.948	1.523	205.4	0.976
186	138.0	0.496	16.92	55.4	758.2	2.034	1.292	336.7	0.992
183	15.0	2.807	10.92	47.1	508.4	2.258	2.369	74.6	0.968
152	11.0	2.639	10.92	22.0	311.1	2.328	2.087	64.3	0.968
146	30.1	2.939	10.92	22.2	333.1	2.395	1.567	366.1	0.975
173	45.2	3.568	10.92	54.8	761.8	2.432	1.834	355.5	0.971
189	8.1	1.888	10.92	52.3	754.8	2.551	1.834	16.1	0.970
160	19.1	4.992	10.92	21.1	314.2	2.586	2.764	169.6	0.957
179	31.9	4.237	10.92	53.3	725.8	2.697	2.269	198.8	0.965
148	29.1	4.905	10.92	23.4	344.5	2.748	2.454	331.8	0.960
180	15.0	0.427	16.92	48.7	554.6	2.945	3.350	8.4	0.980
170	46.2	2.001	16.92	54.9	762.7	3.104	3.144	45.6	0.979
185	15.0	4.741	10.92	47.3	453.3	3.112	3.875	84.3	0.949
157	59.9	2.903	16.92	31.4	438.2	3.260	3.548	120.1	0.976
154	9.7	4.718	10.92	20.1	312.8	3.337	2.938	49.6	0.952
163	92.3	2.879	16.92	44.8	623.5	3.692	3.370	188.6	0.977
176	91.8	2.723	16.92	55.3	775.5	3.718	3.370	153.9	0.978
190	7.6	3.393	10.92	51.6	695.2	4.069	2.848	15.5	0.956
188	138.5	2.965	16.92	58.8	850.4	4.124	3.439	294.8	0.977
164	5.0	2.915	10.92	20.2	315.0	4.271	2.654	15.2	0.957
172	45.7	3.516	16.92	54.6	767.0	4.330	4.583	44.1	0.970
159	59.5	4.651	16.92	33.6	467.9	4.618	5.338	111.0	0.963

187	6.9	4.660	10.92	23.0	345.6	4.728	3.191	24.4	0.948
147	29.4	4.943	16.92	23.5	343.1	5.667	6.378	41.4	0.957
151	11.4	2.557	16.92	22.1	311.7	6.399	5.728	8.3	0.964
182	14.9	2.827	16.92	46.7	506.4	8.099	6.752	8.9	0.961
153	9.5	4.782	16.92	20.1	312.3	8.242	8.355	5.9	0.944
184	15.1	4.704	16.92	47.1	453.5	11.420	10.860	10.3	0.941

Table M.2: Oil retention prediction results for R1234ze(E)/POE32 in vertical line

Test ID	Ref Mass Flow Rate	Corrected OCR	Test Section			Oil Retention		Pressure Drop	Void Fraction
			Dia	Temp	Pres	Exp	Pred		
	[kg/h]	[%]	[mm]	[°C]	[kPa]	[g/m]	[g/m]	[Pa/m]	[-]
169	46.1	0.409	10.92	54.8	757.9	1.714	1.439	1177.0	0.978
175	32.0	0.430	10.92	53.0	696.5	1.738	1.882	880.8	0.972
150	29.4	0.467	10.92	21.6	319.0	2.417	1.573	1108.0	0.975
186	138.0	0.496	16.92	55.4	758.2	2.418	2.964	1090.0	0.981
171	46.5	1.994	10.92	55.2	777.6	2.666	2.600	1579.0	0.959
156	20.0	0.496	10.92	19.3	296.5	3.120	1.984	749.2	0.969
173	45.2	3.568	10.92	54.8	761.8	3.235	3.282	1817.0	0.949
174	92.3	0.501	16.92	56.6	811.6	3.465	3.703	756.7	0.975
146	30.1	2.939	10.92	22.2	333.1	3.475	2.941	1716.0	0.953
161	92.3	0.476	16.92	35.7	522.5	3.582	2.643	709.1	0.981
177	32.7	2.593	10.92	53.8	737.8	3.658	3.516	1250.0	0.946
158	21.0	2.843	10.92	22.0	341.5	3.978	3.422	1056.0	0.943
148	29.1	4.905	10.92	23.4	344.5	4.049	3.612	1894.0	0.942
155	58.8	0.491	16.92	27.7	394.0	4.118	3.895	557.5	0.974
179	31.9	4.237	10.92	53.3	725.8	4.351	4.213	1405.0	0.936
160	19.1	4.992	10.92	21.1	314.2	5.148	4.576	1356.0	0.929
188	138.5	2.965	16.92	58.8	850.4	5.920	5.751	1427.0	0.962
176	91.8	2.723	16.92	55.3	775.5	6.557	7.036	1028.0	0.954
163	92.3	2.879	16.92	44.8	623.5	6.613	6.373	1045.0	0.957
157	59.9	2.903	16.92	31.4	438.2	7.490	7.570	839.0	0.949
178	92.0	4.032	16.92	55.7	791.6	8.294	8.017	1113.0	0.947
159	59.5	4.651	16.92	33.6	467.9	9.014	9.084	936.9	0.939

APPENDIX N. MODEL PREDICTION RESULTS – R134A/POE32

Table N.1: Oil retention prediction results for R134a/POE32 in horizontal line

Test ID	Ref Mass Flow Rate	Corrected OCR	Test Section			Oil Retention		Pressure Drop	Void Fraction
			Dia	Temp	Pres	Exp	Pred		
	[kg/h]	[%]	[mm]	[°C]	[kPa]	[g/m]	[g/m]	[Pa/m]	[-]
42	66.2	0.473	16.92	24.3	482.6	1.911	2.962	140.9	0.982
57	152.3	0.477	16.92	64.3	1026.0	2.259	2.555	332.1	0.985
43	95.0	0.489	16.92	31.0	588.4	2.294	2.686	224.3	0.984
35	30.3	0.531	16.92	21.3	433.0	3.794	3.803	38.2	0.978
47	52.1	2.436	16.92	64.9	1064.0	4.822	5.295	45.5	0.970
53	103.6	2.950	16.92	64.6	1040.0	5.147	5.124	161.4	0.971
56	158.4	2.748	16.92	65.3	1072.0	5.331	4.588	335.9	0.974
58	58.2	2.645	16.92	23.6	465.7	5.607	5.134	114.9	0.970
60	101.3	2.312	16.92	33.3	626.5	5.826	4.202	235.3	0.975
36	23.7	2.940	16.92	20.7	431.4	6.401	6.929	24.3	0.959
54	103.2	4.606	16.92	64.6	1040.0	6.703	6.973	159.7	0.960
59	62.7	4.341	16.92	25.6	494.1	6.786	6.905	123.7	0.959
39	27.3	4.788	16.92	21.3	436.8	7.160	9.177	31.0	0.946
48	51.0	4.913	16.92	64.8	1021.0	7.955	8.332	45.8	0.953
51	20.2	2.952	16.92	63.7	1014.0	9.609	7.830	8.6	0.955
37	13.0	2.476	16.92	21.7	411.0	9.829	8.372	8.7	0.952
50	17.0	3.139	16.92	54.1	764.1	10.310	8.928	8.3	0.951
33	21.1	3.987	16.92	24.5	457.5	10.360	9.037	18.8	0.948
34	8.7	3.851	16.92	21.4	395.9	11.480	13.950	4.4	0.921
52	17.5	5.043	16.92	64.0	1015.0	12.190	11.930	6.7	0.932

Table N.2: Oil retention prediction results for R134a/POE32 in vertical line

Test ID	Ref Mass Flow Rate	Corrected OCR	Test Section			Oil Retention		Pressure Drop	Void Fraction
			Dia	Temp	Pres	Exp	Pred		
	[kg/h]	[%]	[mm]	[°C]	[kPa]	[g/m]	[g/m]	[Pa/m]	[-]
57	152.3	0.477	16.92	64.3	1026.0	2.938	2.977	1843	0.983
43	95.0	0.489	16.92	31.0	588.4	3.554	3.444	1224	0.980
55	103.1	0.518	16.92	64.5	1037.0	3.920	3.867	1134	0.978
41	68.2	0.558	16.92	23.1	478.0	4.546	4.386	894	0.974
42	66.2	0.473	16.92	24.3	482.6	4.622	4.306	835	0.975
56	158.4	2.748	16.92	65.3	1072.0	5.054	5.440	2915	0.969
60	101.3	2.312	16.92	33.3	626.5	6.191	5.822	1906	0.965
53	103.6	2.950	16.92	64.6	1040.0	7.177	7.230	1641	0.959
58	58.2	2.645	16.92	23.6	465.7	7.892	9.042	1120	0.948
54	103.2	4.606	16.92	64.6	1040.0	8.903	8.492	1829	0.952
59	62.7	4.341	16.92	25.6	494.1	10.670	10.160	1361	0.941

APPENDIX O. MODEL PREDICTION RESULTS – R32/POE32

Table O.1: Oil retention prediction results for R32/POE32 in horizontal line

Test ID	Ref Mass Flow Rate	Corrected OCR	Test Section			Oil Retention		Pressure Drop	Void Fraction
			Dia	Temp	Pres	Exp	Pred		
	[kg/h]	[%]	[mm]	[°C]	[kPa]	[g/m]	[g/m]	[Pa/m]	[-]
142	35.6	0.457	10.92	74.3	2518	0.953	1.118	155.8	0.985
130	54.4	0.45	10.92	76.3	2537	1.04	0.97	336.2	0.987
119	27.4	0.475	10.92	20.6	1135	1.061	1.132	182.8	0.985
141	108.2	0.474	16.92	76.3	2577	1.773	2.16	139.5	0.988
107	40.4	0.45	10.92	20.7	1131	1.913	0.984	371	0.987
113	13.3	0.489	10.92	20.9	1123	1.935	1.494	50.4	0.98
118	80.7	0.452	16.92	19.9	1122	2.049	2.159	158.8	0.988
136	18	0.448	10.92	71.1	2476	2.083	1.413	45.6	0.981
132	53.6	2.637	10.92	76.3	2489	2.168	1.893	331.2	0.975
124	119.5	0.448	16.92	25.3	1295	2.296	1.891	281.3	0.989
198	155.3	0.469	19.94	28.3	1411	2.355	2.556	188.2	0.989
121	27.5	2.571	10.92	22.6	1214	2.449	2.04	169.5	0.972
109	39.8	2.602	10.92	21.1	1130	2.657	1.915	357.9	0.974
144	52.8	0.47	16.92	75.8	2413	3.033	2.764	41.4	0.985
123	28.4	4.246	10.92	19.8	1114	3.066	2.968	194.6	0.96
128	26.3	4.258	10.92	19.9	1115	3.13	3.042	170	0.959
134	53.8	4.29	10.92	76.5	2473	3.131	2.743	333.6	0.964
111	40.8	4.264	10.92	21	1138	3.508	2.761	367.9	0.963
138	18.1	2.639	10.92	71.7	2524	3.535	2.529	44.3	0.967
115	12.2	2.743	10.92	20.9	1117	3.727	2.912	42.9	0.961
112	13.9	0.484	16.92	20.9	1125	4.17	4.179	6.6	0.977
140	18	4.276	10.92	72.1	2511	4.197	3.562	44.1	0.953
117	13.4	4.254	10.92	20.6	1115	4.328	3.857	50.6	0.948
200	151.8	2.68	16.92	74.2	2498	4.496	4.124	259.7	0.977
120	80.2	2.637	16.92	21.7	1157	4.524	4.349	150.7	0.976
126	119.8	2.624	16.92	29	1408	4.714	3.96	257.1	0.977
143	107.2	2.651	16.92	75.7	2491	4.736	4.334	140.5	0.976
108	40.9	2.616	16.92	20.3	1120	4.747	5.107	46.1	0.971
125	8.1	2.746	10.92	21.4	1139	5.614	3.476	19.9	0.953
131	53.9	2.605	16.92	76.3	2488	5.774	4.986	40.9	0.973
197	107.5	4.369	16.92	75.3	2490	6.19	6.435	140.2	0.965
122	79.6	4.337	16.92	22.3	1198	6.296	6.362	142.3	0.964

110	40.5	4.278	16.92	21.1	1129	6.298	7.414	45	0.959
127	9	4.317	10.92	20.5	1119	6.306	4.658	24.3	0.937
133	53.8	4.325	16.92	76.3	2464	6.779	7.21	41	0.961
196	121.6	2.672	19.94	27.1	1333	7.356	5.748	126.5	0.977
114	12.1	2.72	16.92	21	1133	8.198	8.378	5.1	0.953
137	18	2.677	16.92	72.1	2527	9.122	7.262	5.4	0.96
139	17.8	4.198	16.92	72.4	2499	10.12	10.05	5.3	0.945
116	13.9	4.309	16.92	20.7	1115	10.71	11.25	6.6	0.937

Table O.2: Oil retention prediction results for R32/POE32 in vertical line

Test ID	Ref Mass Flow Rate	Corrected OCR	Test Section			Oil Retention		Pressure Drop	Void Fraction
			Dia	Temp	Pres	Exp	Pred		
	[kg/h]	[%]	[mm]	[°C]	[kPa]	[g/m]	[g/m]	[Pa/m]	[-]
130	54.4	0.45	10.92	76.3	2537	2.414	1.94	1622	0.975
199	154.5	0.454	16.92	74.3	2559	2.852	3.402	1505	0.981
142	35.6	0.457	10.92	74.3	2518	3.562	2.676	1081	0.965
107	40.4	0.45	10.92	20.7	1131	3.727	1.987	1623	0.973
119	27.4	0.475	10.92	20.6	1135	3.733	2.661	973.4	0.964
132	53.6	2.637	10.92	76.3	2489	3.821	3.684	2393	0.953
124	119.5	0.448	16.92	25.3	1295	4.186	3.37	1410	0.981
109	39.8	2.602	10.92	21.1	1130	4.3	3.728	2620	0.951
198	155.3	0.469	19.94	28.3	1411	4.376	4.576	1098	0.981
141	108.2	0.474	16.92	76.3	2577	4.389	4.413	1068	0.976
134	53.8	4.29	10.92	76.5	2473	4.561	4.352	2764	0.944
111	40.8	4.264	10.92	21	1138	4.788	4.319	3153	0.943
118	80.7	0.452	16.92	19.9	1122	4.905	4.346	918.7	0.976
121	27.5	2.571	10.92	22.6	1214	4.959	4.803	1422	0.936
128	26.3	4.258	10.92	19.9	1115	5.854	5.857	1676	0.923
126	119.8	2.624	16.92	29	1408	5.909	6.26	2128	0.965
200	151.8	2.68	16.92	74.2	2498	6.648	6.404	2213	0.965
143	107.2	2.651	16.92	75.7	2491	7.466	8.1	1449	0.956
120	80.2	2.637	16.92	21.7	1157	7.855	8.107	1405	0.955
122	79.6	4.337	16.92	22.3	1198	9.313	9.56	1550	0.947
197	107.5	4.369	16.92	75.3	2490	10.69	9.562	1633	0.949
196	121.6	2.672	19.94	27.1	1333	11.28	9.942	1282	0.96

REFERENCES

Agrawal, S.S., Gregory, G.A., Govier, G.W., 1973. An analysis of horizontal stratified two phase flow in pipes. Can. J. Chem. Eng. 51, 280–286.

Alofs, D.J., Hasan, M.M., Sauer, H.J.J., 1990. Influence of oil on pressure drop in refrigerant compressor suction lines - RP-336. ASHRAE Trans. 961.

ASHRAE, 2015. Standard 41.4: Method for measurement of proportion of lubricant in liquid refrigerant, American Society for Heating, in: Refrigeration, and Air-Conditioning Engineers.

ASHRAE, 2014. ASHRAE Handbook--Refrigeration. SI Ed. Atlanta ASHRAE.

Baustian, J.J., Pate, M.B., Bergles, A.E., 1988a. Measuring the concentration of a flowing oil-refrigerant mixture with a bypass viscometer. ASHRAE Trans. 94, 588–601.

Baustian, J.J., Pate, M.B., Bergles, A.E., 1988b. Measuring the concentration of a flowing oil-refrigerant mixture with an acoustic velocity sensor. ASHRAE Trans. 94, 602–615.

Baustian, J.J., Pate, M.B., Bergles, A.E., 1988c. Measuring the concentration of a flowing oil-refrigerant mixture with a vibrating U-tube densimeter. ASHRAE Trans. 94, 571–587.

Baustian, J.J., Pate, M.B., Bergles, A.E., 1986a. Properties of oil refrigerant liquid mixtures with applications to oil concentration measurement: Part 2 - Electrical and optical properties. ASHRAE TRANS. 92, 74–92.

Baustian, J.J., Pate, M.B., Bergles, A.E., 1986b. Properties of oil refrigerant liquid mixtures with applications to oil concentration measurement: Part 1-thermophysical and transport properties. ASHRAE TRANS. 92, 55–73.

Bayani, A., Thome, J.R., Favrat, D., 1995. Online measurement of oil concentrations of R-134a/oil mixtures with a density flowmeter. HVAC&R Res. 1, 232–241. https://doi.org/10.1080/10789669.1995.10391321

Biancardi, F., Sienel, T., Pandy, D., Michels, H., 1997. Study of lubricant circulation in HVAC systems, Winter meeting of the American Society of Heating, Refrigerating and Air-Conditioning Engineers, Inc. and exposition, Philadelphia.

Cavestri, Richard (Imagination Resources, I.., 1995. MEASUREMENT OF VISCOSITY , DENSITY , AND GAS SOLUBILITY OF REFRIGERANT BLENDS IN SELECTED SYNTHETIC LUBRICANTS. https://doi.org/DOE/CE/23810-46

Chen, X.T., Cal, X.D., Brill, J.P., 1997. Gas-Liquid Stratified-Wavy Flow in Horizontal Pipelines. J. Energy Resour. Technol. 119, 209–216. https://doi.org/10.1115/1.2794992

Cremaschi, L., 2004. Experimental and Theoretical Investigation of Oil Retention in Vapor Compression Systems. Thesis. University of Maryland.

Cremaschi, L., Hwang, Y., Radermacher, R., 2005. Experimental investigation of oil retention in air conditioning systems. Int. J. Refrig. https://doi.org/10.1016/j.ijrefrig.2005.03.012

Cremaschi, L., Hwang, Y., Radermacher, R., 2004. Investigation of oil retention in residential heat pumps, in: Refrigeration And Air Conditioning. pp. 1–9.

Crompton, J.A., Newell, T.A., Chato, J.C., 2004. Experimental Measurement and Modeling of Oil Holdup.

Fukuta, M., Yanagisawa, T., Miyamura, S., Ogi, Y., 2004. Concentration measurement of refrigerant/refrigeration oil mixture by refractive index. Int. J. Refrig. 27, 346–352. https://doi.org/10.1016/J.IJREFRIG.2003.12.007

Fukuta, M., Yanagisawa, T., Ogi, Y., Tanaka, J., 1999. Measurement of concentration of refrigerant in refrigeration oil by capacitance sensor. Trans. Japan Soc. Refrig. Air Cond. Eng. 16, 239–248.

Fukuta, M., Yanagisawa, T., Shimasaki, M., Ogi, Y., 2006. Real-time measurement of mixing ratio of refrigerant/refrigeration oil mixture. Int. J. Refrig. 29, 1058–1065. https://doi.org/10.1016/J.IJREFRIG.2006.03.010

Fung, K.K., Sundaresan, S.G., 1994. Study of Oil Return Characteristics in a Display Case Refrigeration System. Purdue University.

Gao, L., Nakamura, A., Watanabe, Y., Honda, T., Takigawa, R., Shimizu, T., 2011. Measurement of oil circulation ratio in CO2 Heat Pump Systems. 10th IEA Heat Pump Conference 2011.

Henderson, D.R., 1994. Solubility, viscosity and density of refrigerant/lubricant mixtures. https://doi.org/10.2172/6515184

Hwang, Y., Cremaschi, L., Radermacher, R., Hirata, T., Ozaki, Y., Hotta, T., 2003. Oil Circulation Ratio in CO2 Climate Control Systems. https://doi.org/10.4271/2003-01-0730

Hwang, Y., Lee, J.-P., Radermacher, R., Pereira, R.H., 2000. An Experimental Investigation on Flow Characteristics of Refrigeration / Oil Mixture in Vertical Upward Flow. Purdue University Purdue e-Pubs International Refrigeration and Air Conditioning Conference, p. 7.

Hwang, Y., Radermacher, R., Hirata, T., 2008. Oil mass fraction measurement of CO2/PAG mixture. Int. J. Refrig. 31, 256–261. https://doi.org/10.1016/J.IJREFRIG.2007.05.011

Jacobs, M.L., Scheideman, F.C., Kazem, S.M., Macken, N.A., 1976. Oil Transport By Refrigerant Vapor. ASHRAE Trans. 82, 318–329.

Jia, X., Wang, J., Wang, X., Hu, Y., Sun, Y., 2020. Phase equilibrium of R1234yf and R1234ze(E) with POE lubricant and thermodynamic performance on the evaporator. Fluid Phase Equilib. 514, 112562. https://doi.org/10.1016/j.fluid.2020.112562

Kesim, S.C., Albayrak, K., İleri, A., 2000. Oil entrainment in vertical refrigerant piping. Int. J. Refrig. 23, 626–631. https://doi.org/10.1016/S0140-7007(99)00085-7

Klein, S., 2018. Engineering Equation Solver.

Kowalski, J., 1987. Wall and interfacial shear stress in stratified flow in a horizontal pipe. AICHE J. 33, 274–281.

Kutsuna, K., Inoue, Y., Mizutani, T., Sudo, E., Araga, T., 1991. Real time oil concentration measurement in automotive air conditioning by ultraviolet light absorption. SAE Tech. Pap. 100, 315–322. https://doi.org/10.4271/910222

Lebreton, J.M., Vuillame, L., 2001. Oil concentration measurement in saturated liquid refrigerant flowing inside a refrigeration machine. Int. J. Appl. Thermodyn. 4, 53–60. https://doi.org/10.5541/ijot.1034000061

Lee, J., Hwang, Y., Ph, D., Radermacher, R., Ph, D., 2002. An Experimental Investigation of Oil Retention Characteristics in Co 2 Air-Conditioning Systems. Purdue University Purdue e-Pubs International Refrigeration and Air Conditioning Conference.

Li, K., Luo, S., Wang, Z., Zhang, Hua, Su, L., Fang, Y., Zhou, X., Zhang, Huiqi, Tu, R., 2020. An experimental investigation of oil circulation ratio influence on heating performance in an air condition heat pump system for electrical vehicles. Int. J. Refrig. 122, 220–231. https://doi.org/10.1016/j.ijrefrig.2020.11.007

Mehendale, S.S., Radermacher, R., 2000. Experimental and Theoretical Investigation of Annular Film Flow Reversal In a Vertical Pipe: Application To Oil Return In Refrigeration Systems. HVAC&R Res. 6, 55–74. https://doi.org/10.1080/10789669.2000.10391250

Meyer, J.., Saiz Jabardo, J.., 1994. An ultrasonic device for measuring the oil concentration in flowing liquid refrigerant. Int. J. Refrig. 17, 481–486. https://doi.org/10.1016/0140-7007(94)90009-4

Min, K., Hwang, I., 2000. Oil circulation rate in rotary compressor: its measurement and factors affecting the rate. 15th International Compressor Engineering Conference.

Navarro de Andrade, E., Skowron, E., Goldschmidt, V.W., Groll, E.A., 1999. Oil concentration in liquid refrigerants: in situ measurement. Int. J. Refrig. 22, 499–508. https://doi.org/10.1016/S0140-7007(99)00008-0

Newell, T.A., 1996. In Situ Refractometry for Concentration Measurements in Refrigeration Systems. HVAC&R Res. 2, 247–255. https://doi.org/10.1080/10789669.1996.10391347

Ossorio, R., Navarro-Peris, E., 2020. Study of oil circulation rate in variable speed scroll compressor working with propane. Int. J. Refrig. 123, 63–71. https://doi.org/10.1016/j.ijrefrig.2020.12.002

Radermacher, R., Cremaschi, L., Schwentker, R.A., 2006. Modeling of oil retention in the suction line and evaporator of air-conditioning systems. HVAC&R Res. 12, 35–56.

Ramakrishnan, A., 2012. Investigation of oil retention and pressure drop in suction lines using R1234yf, R134a and R410A with POE ISO 100. University of Illinois at Urbana-Champaign.

Ramakrishnan, A., Hrnjak, P.S., 2012. Oil Retention and Pressure Drop of R134a, R1234yf and R410A with POE 100 in Suction Lines. Purdue University Purdue e-Pubs International Refrigeration and Air Conditioning Conference, p. 10. https://doi.org/10.1080/10789669.2014.930304

Scheideman, F.C., Jacobs, M.L., Kazem, S., Macken, N.A., 1977. PRESSURE LOSS OF OIL-REFRIGERANT MIXTURES IN SUCTION AND DISCHARGE LINES. ASHRAE Trans. 83, 203–221.

Sethi, A., 2011. Oil Retention And Pressure Drop Of R1234yf And R134a With Poe Iso 32 In Suction Lines. University of Illinois at Urbana-Champaign.

Sundaresan, S.G. (Copeland C.., Radermacher, R., 1996. Oil-return characteristics of refrigerant oils in split heat pump system. ASHRAE Journal; 38.

Suzuki, S., Fujisawa, Y., Nakazawa, S., Matsuoka, M., 1993. Measuring method of oil circulation ratio using light absorption. Trans. Soc. Heat. Refrig. AIR Cond. Eng. 99, 413.

Taitel, Y., Dukler, A.E., 1976. A model for predicting flow regime transitions in horizontal and near horizontal gas-liquid flow. AIChE J. 22, 47–55. https://doi.org/10.1002/aic.690220105

Thome, J.R., 1995. Comprehensive Thermodynamic Approach to Modeling Refrigerant-Lubricating Oil Mixtures. HVAC&R Res. 1, 110–125. https://doi.org/10.1080/10789669.1995.10391313

Tzotzi, C., Andritsos, N., 2013. Interfacial shear stress in wavy stratified gas–liquid flow in horizontal pipes. Int. J. Multiph. Flow 54, 43–54. https://doi.org/10.1016/J.IJMULTIPHASEFLOW.2013.03.003

Wada, A., Nomura, M., Tsuboi, K., Kutsuna, K., Nabeta, T., 1992. A novel approach to instrumentation and application for OCR measurement in refrigeration system, in: International Compressor Engineering Conference.

Wujek, S.S., Hrnjak, P.S., 2009. Using density to calculate the oil circulation ratio of a PAG oil in R134a. SAE Int. J. Mater. Manuf. 1, 362–368. https://doi.org/10.4271/2008-01-0833

Wujek, S.S., Hrnjak, P.S., Seeton, C.J., 2007. Online measurement techniques for determining oil circulation rate, in: 2007 Proceedings of the 5th Joint ASME/JSME Fluids Engineering Summer Conference, FEDSM 2007. 5th Joint ASME/JSME Fluids Engineering Conference, pp. 181–186. https://doi.org/10.1115/FEDSM2007-37640

Xu, J., Hrnjak, P., 2017. Quantification of flow and retention of oil in compressor discharge pipe. Int. J. Refrig. 80, 252–263. https://doi.org/10.1016/j.ijrefrig.2017.05.004

Xu, J., Hrnjak, P., 2016. Refrigerant-Oil Flow at the Compressor Discharge, in: SAE Technical Papers. https://doi.org/10.4271/2016-01-0247

Yan, G., Peng, L., Wu, S., 2015. A study on an online measurement method to determine the oil discharge ratio by utilizing Coriolis mass flow meter in a calorimeter. Int. J. Refrig. 52, 42–50. https://doi.org/10.1016/j.ijrefrig.2014.11.017

Yatim, A.S., Cremaschi, L., Fisher, D.E., 2014. Measurements of Oil Retention in a Microchannel Condenser for AC Systems. Purdue University Purdue e-Pubs International Refrigeration and Air Conditioning Conference, pp. 1–10.

Yoon, P., Kang, D., Kim, C., Ahn, S., Chung, B., Kim, B., Lee, J., Hwang, Y., 2011. An experimental study on oil discharge ratio at inverter-driven high shell pressure scroll compressor using R410A/PVE. Int. J. Refrig. 34, 105–112. https://doi.org/10.1016/J.IJREFRIG.2010.08.019

Zoellick, K.F., 2010. Oil Retention And Pressure Drop In Horizontal And Vertical Suction Lines With R410a / POE ISO 32. University of Illinois at Urbana-Champaig.

PUBLICATIONS

- ASHRAE Transaction
    - Shah, V.M.; Kurtulus, O.; Horton, W.T.; Groll, E.A.; and Braun, J.E., "In-situ Oil Circulation Ratio (OCR) Measurement using Separation Method in a Transport Refrigeration System with R404A and POE32," accepted for publication in 2021 ASHRAE Transactions, Vol. 127, Part 2
- 2021 ASHRAE Virtual Winter Conference
    - Shah, V.M.; Braun, J.E.; Groll, E.A., “Measuring Oil Retention in Unitary Split Systems Gas Lines”, accepted for publication in ASHRAE Conference
- 202One Purdue Conferences
    - Shah, V.M.; Braun, J.E.; Groll, E.A., “Stratified Flow Model to Predict Oil Retention in Horizontal Refrigerant Gas Lines of Unitary Split Systems Running R410A and POE32” accepted for publication in 18th International Refrigeration and Air Conditioning Conference at Purdue
- HFO 2021
    - Shah, V.M.; Braun, J.E.; Groll, E.A., “Study of Oil Retention in Suction Lines with R1234ze(E) and POE32” accepted for publication in 2nd IIR Conference on HFOs and Low GWP blends